

THE NATURE OF MOLECULES ADSORBED ON
CATALYTIC SURFACES: PULSED NUCLEAR MAGNETIC
RESONANCE AND INFRARED ABSORBANCE STUDIES

Thesis by
T. Michael Duncan

In Partial Fulfillment of the Requirements
for the Degree of
Doctor of Philosophy

California Institute of Technology

Pasadena, California

1980

(Submitted February 25, 1980)

Dedication

This thesis is dedicated to Professor Robert Walton Vaughan, who perished in a commercial airline accident on May 25, 1979. Bob's contribution to the field of high resolution solid state nuclear magnetic resonance included the development of multiple pulse schemes, dipolar modulation techniques, double resonance interferometry, and NMR instrumentation. Bob successfully applied these techniques to the study of a diverse group of materials including metal hydrides, metal carbonyls, hydrogen-bonded solids, superionic conductors, amorphous semiconductors, catalytic oxide surfaces, and molecules adsorbed on surfaces.

Bob's death leaves a large void in every scientific field he was involved with, but an even larger void was created in the lives of those who had the privilege of his personal contact; his family, his fellow faculty members, and his students. Though Bob's contributions were many, he always placed the development of the student above any material goals. He gave unselfishly of his time and of himself to the scientific training of the students, but more important, he also gave students encouragement, emotional support, understanding, and character. Bob's enthusiasm was as boundless as it was contagious. Indeed, he will be long remembered for his high speed delivery of the English language, modified with his own trademarked contributions to Webster's dictionary. Though Bob is missed greatly by us all, the greatest loss is to those students and colleagues yet to come, who will never have the honor and pleasure of studying with Robert W. Vaughan.

Acknowledgements

I wish to thank Professor W. Henry Weinberg and Professor Sunney I. Chan for their advice and guidance during the final eight months of my graduate study. In addition to the intense research programs each was already directing, they generously volunteered their time and energy to assure my completion of this thesis. I also wish to thank Dr. John T. Yates, Jr. for the enthusiasm and direction he generated during my third year of graduate study.

I wish to express my appreciation to Professor Cecil R. Dybowski, Dr. Alexander J. Vega, and Dr. Michael E. Stoll for the numerous hours they donated to introduce me to the field of solid state nuclear magnetic resonance. Much of the equipment used in this study was constructed and serviced by the competent members of the mechanical and electrical staffs; George Griffith, Seichi Nakawatase, John Yehle, Tony Stark, and Ray Reed. Many of the original manuscripts were typed by Sharon Vigario, whose dedication and interest in the final product are unsurpassed. Professor George R. Rossman generously made his infrared spectrometer available for all of the vibrational studies in this thesis. My residence in graduate school was enriched through the companionship and comradery of my fellow graduate students, including Jeff Reimer, Bill Olbricht, Gerry Fuller, Pat Thiel, and Gary Whatley.

I am forever grateful to my parents, Thomas and JoAnne Duncan for their assistance and encouragement throughout my education. Their hard work and dedication gave me the opportunities to pursue the career of my choice, and their discipline, foresight, and integrity prepared my mind to take full advantage of the training that I received. But most important,

they taught me how to enjoy what I have while striving for yet higher standards.

My wife, Deborah Lynne Duncan, provided support in all areas of this thesis. Psychologically, she gave me a life away from Caltech when I needed it the most, and gave me encouragement, understanding, and interest in my work when I practically disappeared into the laboratory for weeks at a time. She also graciously and competently undertook the task of typing the final drafts of this thesis.

I was supported financially in part by the National Science Foundation through its Energy Trainee Program and by the Office of Naval Research. Finally, I thank the Institute for its support and the environment it has created for the study of the sciences and the education of students.

Abstract

The nature of molecules adsorbed on high surface catalysts have been studied with infrared absorbance and nuclear magnetic resonance (NMR) techniques. The well-separated infrared vibrational spectra have been used mainly to identify the various surface species by comparison with known compounds. The frequency shifts in the molecular stretching modes indicate the strengthening or weakening of the bonds of the molecules upon adsorption. The NMR spectra have been used to quantify the distributions among the surface states and to describe the motional properties of the adsorbed molecules. The NMR data were obtained through the application of several recently developed multiple-pulse techniques. By analyzing the spin-lattice relaxation times, the dipolar interactions, and the chemical shift anisotropies, it has been possible to separate the overlapping NMR spectra and determine the molecular symmetries, bond lengths, and the nature of the adsorption site. The results of these two techniques were combined to describe the adsorbed states of CO on Rh dispersed on Al_2O_3 , and the distribution of formic acid on zeolite surfaces. The infrared spectroscopy confirmed the previous identification of three surface CO states; linear and bridged sites that form on Rh atoms in clusters on the Al_2O_3 , and dicarbonyl species on isolated Rh atoms. The desorption rate at 295 K is very slow. All three states readily exchange with CO(g) at 295 K, but only the dicarbonyl species exchanges at temperatures below 200 K. H_2CO decomposed on the dispersed Rh into adsorbed CO states, with no evidence of any H_xCO surface states, though there was further demonstration of isolated Rh atom sites. The ^{13}C NMR results quantified the distribution of the three surface sites, and thus calibrated

the infrared absorbances, as well as the local motions on the three sites. The infrared spectra of formic acid on the Y zeolites suggested the presence of unidentate and bidentate formate species on the surface. The bidentate structure was the dominant species on the more catalytically active zeolite. The combination of the results of several multiple-pulse NMR techniques are analyzed to measure the site distribution between the unidentate and bidentate species, as well as to further describe the bidentate formate ion. The bidentate structure is bonded to the Al atoms, rather than the Si atoms, has a structure similar to formate salts, and a more acidic carbonyl hydrogen, relative to formic acid.

TABLE OF CONTENTS

	<u>Page</u>
Dedication	ii
Acknowledgements	iii
Abstract	v
Chapter I: Introduction	1
Chapter II: An Infrared Study of the Adsorption of CO on Rh dispersed on Al_2O_3	14
Chapter III: An Infrared Study of the Adsorption of CO on Rh dispersed on Al_2O_3 ; Low Temperature Interactions	47
Chapter IV: An Infrared Study of the Adsorption of Formaldehyde on Rh dispersed on Al_2O_3	78
Chapter V: A ^{13}C Nuclear Magnetic Resonance Study of the Adsorption of CO on Rh dispersed on Al_2O_3	103
Chapter VI: An Infrared Study of the Adsorption of Formic Acid on Ammonium-Y and Ultrastable Hydrogen-Y Zeolites	147
Chapter VII: A Solid-State Nuclear Magnetic Resonance Study of the Adsorption of Formic Acid on Ammonium-Y and Ultrastable-Y Zeolites	173
Chapter VIII: Conclusions	230
Appendix A: Combined Nuclear Magnetic Resonance and Infrared Studies of CO Adsorbed on Rh Dispersed on Al_2O_3 ; Desorption and Elevated Temperature Experiments . . .	237

CHAPTER I

Introduction

The catalytic enhancement of chemical reactions, for improvements in product yields or selectivity, is an integral step in many commercial processes. It is estimated that the gross value of all manufactured goods involving at least one catalyzed reaction is of the order of hundreds of billions of dollars annually in the United States. Thus, the improvement in the yield of a catalytic reaction of only a few percent may result potentially in millions of dollars annually, as well as the conservation of natural resources. Since, in general, very few catalytic processes are understood, most improvements have been the result of optimizations of existing processes, by varying the parameters such as reactant concentrations, temperature, pressure, and the catalyst composition. However, it is possible that the optimization is only a local maximum in the multi-parameter space of the process, and there may exist dramatically improved processes for the reaction that involve radically different reaction conditions. An alternate approach is to understand the catalytic process on the molecular level, and then predict modifications to improve the existing systems and design catalytic systems for new reactions.

The primary objective of most investigations of heterogeneous catalytic process is to determine the nature of the reactive intermediate(s) and the active site(s). However, by nature, the lifetime of the reactive intermediate is extremely short. Because of the low concentrations of these intermediates, the catalytic system is studied at reduced temperatures and pressures which allow the formation of more stable surface species. It is then proposed that these relatively stable adsorbates, formed by the adsorption of reactants, products, or related compounds, are actually the reaction intermediates in the catalytic mechanism. In

order to describe the nature of the adsorbed state it is proposed that at least three properties must be characterized (1,2); 1. the nature of the active site (e.g. the bonding of the site to the substrate, its electronic properties, and the local environment), 2. the structure of the surface adsorbed species (e.g. bond angles, lengths, and strengths), and 3. the dynamic properties of the adsorbed state (e.g. the rate of diffusion or desorption on the surface, local reorientations at a site).

There is at present a vast armory of spectroscopic techniques available to study adsorbed species. The majority of these techniques involve the scattering of electrons, ions, or photons from single crystal faces at ultrahigh vacuum conditions. Examples include Low Energy Electron Diffraction, and numerous spectroscopies including Auger Electron, X-ray, Ultraviolet Photoelectron, Electron Energy Loss, Secondary Ion Mass, and many others (3), each of which is commonly known by its acronym. The advantages of these techniques include their sensitivity (most can detect as little as 0.01 monolayer) and that they may be applied in concert to the study of a single system, thus yielding a very complete description of the adsorbed state. However, the application of these results to the analysis of actual commercial processes has been somewhat lacking. Most commercial catalysts are high surface area oxides (over $100 \text{ m}^2 \text{g}^{-1}$), or transition metals dispersed on oxides. The high surface areas and large dispersions necessarily create crystal imperfections such as dislocations, corners, and end effects not present on single crystal faces. Also, the single crystal studies are generally performed at less than 10^{-6} Torr to prevent the rapid contamination of the substrate and to allow the charged particles to travel to and from the sample. Thus, effects which occur at

non-negligible rates at higher pressures, such as large site reconstruction or activated adsorption and exchange, are not observed.

The work presented in this thesis combines two spectroscopic techniques; nuclear magnetic resonance (NMR) and infrared absorbance, to study the adsorption of molecules on commercial-like catalysts. The infrared technique has been an important tool for the investigation of adsorbed molecules since its first application almost thirty years ago (4,5,6). On the other hand, though the phenomenon of NMR has been known since 1946 (7,8), only through recent advances in NMR instrumentation and techniques (9,10,11) has it been possible to obtain high-resolution spectra of chemically adsorbed molecules. The NMR and infrared techniques are highly compatible with respect to the types of catalytic systems each may analyze. However, the two phenomena observed, nuclear and vibrational spectra, are susceptible to different interactions and properties of the adsorbed molecules. The synergism of the combination of the results of NMR and infrared experiments creates a unique tool for the characterization of the adsorbed state.

The infrared absorbance spectrum of polycrystalline, high surface area catalysts is limited to the range 4000 cm^{-1} to 1000 cm^{-1} , which includes most of the fundamental modes of organic compounds. The region below 1000 cm^{-1} is unobservable due to the strong absorbance of the oxide support, thus masking some important low frequency vibrations, such as metal-carbon stretches. However, the vibrational spectrum below 1000 cm^{-1} of oxide catalysts may be measured with inelastic electron tunneling spectroscopy (12). The sensitivity of the infrared spectroscopy is generally limited to about 0.1 monolayer. The spectral resolution of the

infrared spectrometer is very good, typically less than 1 cm^{-1} , which is much less than the vibrational linewidths of most adsorbed species. Finally, with infrared spectroscopy, the catalytic system may be studied under relatively high pressures (about 10^4 Torr) and at high temperatures (700 K), thus approximating actual reaction conditions (13,14).

The analysis of vibrational spectra of adsorbed species is rather straightforward and will usually be similar to that of the pure compounds, with a few changes. Upon adsorption of a molecule, changes in symmetry and bonding may cause previously inactive modes to become active. Or, the intensity of other modes may be weakened severely or totally masked by the imaging effects of the substrate. The vibrational spectrum of an unknown surface species is usually interpreted by reference to the fundamental frequencies of common modes, such as C-H, C=O, and C-O stretches. These assignments may be aided by the substitution of isotopic molecules (^2D , ^{13}C , or ^{18}O enriched) to cause predictable shifts in the spectrum. In some cases, the structure of the surface compound may be elucidated through analogies with model compounds such as the similarity between the $\text{Rh}(\text{CO})_2$ surface species and $(\text{Rh}(\text{CO})_2\text{Cl})_2$ (15) and the correspondence between Rh_2CHCH_3 and Br_2CHCH_3 and Cl_2CHCH_3 (16).

The peaks in the infrared spectrum are usually sufficiently separated to allow an identification of the relevant features and thus propose the nature of the adsorbed species. However, the molar infrared absorbances may change dramatically for the adsorbed species (as much as a factor of 20 for CO) and thus the infrared peak intensities cannot be used to determine the quantitative distribution of the surface states. Also, the infrared techniques will not observe infrared-inactive states or states with absorbances below the lower limit of about 1000 cm^{-1} , such as

surface carbide species.

NMR techniques have been applied to the study of multi-layer coverages of molecules on surfaces since the mid-1950's (17,18,19). These early studies observed small changes in the isotropic chemical shifts and the spin-lattice relaxation times of physically adsorbed species. Since these molecules were in contact with chemically adsorbed state, by spin-spin couplings or chemical exchange, it was argued that these observed quantities were indicative of the nature of the chemically adsorbed state. Such analyses were rather limited and the conclusions rarely achieved any of the objectives outlined earlier.

Until recently, the NMR study of chemically adsorbed species was not possible because the low concentrations of surface species had prohibitively weak NMR signals, which were compounded with the problem of excessive line broadening, by a factor as large as 10^3 , relative to the physically adsorbed species. Both complications were removed to an acceptable level with the advent of pulsed Fourier transform NMR techniques. Whereas previously a single scan obtained by sweeping the magnetic field over the resonance of interest required about 20 minutes, the simple one-pulse technique could obtain the same information in about 0.3 sec. Thus, it became conceivable to accumulate as many as 500,000 averages, yielding a factor of 700 improvement in the signal-to-noise ratio.

The development of various pulse sequences and cycles made it possible to manipulate the dipolar broadening, so as to quantify it for structural analysis, remove it, or utilize it to enhance the NMR signal. The simplest and one of the first sequences was the spin echo devised by Hahn (20) to measure the transverse relaxation time in the presence of dipolar broaden-

ing and sample inhomogeneity to calculate the rate of diffusion. The echo technique was combined into a pulse cycle by Carr and Purcell (21). Since then, a series of pulse cycles have been developed to overcome the various interactions in the solid state. The principle of the solid echo ($90^\circ x - \tau - 90^\circ y$) (20) was incorporated into the theory of the four-pulse cycle to remove homonuclear dipolar couplings (22) which was later improved by the eight-pulse cycle (23), and recently by the 24- and 52-pulse cycles (24). Heteronuclear dipolar couplings, such as $^{13}\text{C}-^1\text{H}$ interactions, may be removed by the continuous irradiation of the undesired nucleus (25) or by pulsed irradiation (26). Or, the heteronuclear dipolar coupling may be utilized to enhance the spectral resolution with the cross-polarization technique (27), or to selectively differentiate between various species, such as with the dipolar-difference technique (28).

When the dipolar interactions are suppressed, the residual linewidth is primarily due to the chemical shift anisotropies of the adsorbed species. In the polycrystalline sample, the chemical shift spectrum will form a characteristic powder pattern. The principal components of this powder pattern are indicative of the symmetry of the electron distribution about the nucleus. The center of mass of the chemical shift pattern, which reflects the average electron density, may change only slightly upon adsorption, especially if the fundamental structure of the compound remains intact. However, the symmetry of the structure may change, which is readily detected in the relative positions of the principal chemical shift components.

The ^{13}C nuclear environment is usually the most sensitive probe in NMR studies of adsorbed species. In dilute surface samples, there is very little $^{13}\text{C}-^{13}\text{C}$ homonuclear broadening. The isotropic carbon chemical

shifts may vary as much as 200 ppm, with anisotropies over 400 ppm. Compared to the proton chemical shifts of about 20 ppm, the carbon chemical shift is much larger and may still be detectable even in the presence of substantial residual broadening. Because of the extremely low concentrations of surface species, it is necessary to enrich the natural abundance (1.1% ^{13}C) compounds. However, the selective ^{13}C enrichment in a complex molecule allows one to localize on the environment of a specific portion of the surface species.

This thesis concerns the study of two catalytic systems; CO adsorbed on Rh dispersed on Al_2O_3 and formic acid adsorbed on two molecular sieves, through the combined results of NMR and infrared absorbance spectroscopic techniques. Both CO and formic acid are chemically adsorbed on the respective substrates in multiple states. The substrates are typical high surface area catalysts, relevant to commercial processes.

Oxide-supported Rh is an active catalyst for both methanation and Fischer-Tropsch reactions. The Rh atoms are dispersed on the Al_2O_3 as small metal clusters or rafts containing about 20 atoms, and as isolated, single Rh atoms (15). In addition, Rh is capable of adsorbing two CO molecules per metal atom. The formation of surface dicarbonyls is rare and only Ru has been shown to also have this property(28). There are at least two fundamental proposed mechanisms for the methanation of CO (29,30,31). The carbide mechanism involves the reaction of a surface carbon formed by the dissociation of CO, or by disproportionation to C and CO_2 . The carbide species, which is present in both active and inactive forms, then reacts with H_2 to form methane or adsorbed methylene radicals which polymerize to form larger hydrocarbons. The other mechanism proposes a reaction path via a surface intermediate composed of C, O, and

H, such as surface aldehydes or alcohols.

The study of CO on Rh dispersed on Al_2O_3 is reported in chapters II through V. The infrared investigations are presented in chapters II and III. Chapter II confirms the existence of three surface CO species, a dicarbonyl on isolated Rh atoms, and linearly and bridged-bonded states on Rh rafts. The rate of exchange of CO(ads) with CO(g), and the desorption rate from the surface are also measured. Chapter III is an infrared study at cryogenic temperatures to differentiate between the surface states by the rate of exchange with CO(g) and the reduced rate of activated adsorption. To investigate the possibility of the existence of hydrogenated carbonyl surface species, the adsorption of H_2CO was studied with infrared techniques in chapter IV. The results of the NMR study, reported in chapter V, are used to quantify the distribution of the surface states of CO and the dispersion of the Rh on the Al_2O_3 , as well as to describe the motional properties of the adsorbed CO.

The decomposition of formic acid is often studied as a prototype reaction for the dehydration and dehydrogenation reactions of organic acids. On the ammonium-Y ($\text{NH}_4\text{-Y}$) and ultrastable hydrogen-Y (H-Y) zeolites, formic acid decomposes exclusively by the dehydration path to CO and H_2O . It has been proposed that this reaction proceeds by either the direct decomposition of the adsorbed formate species (32) or by the reaction of the gaseous formic acid with the hydrogen ions of the substrate (33). The ultrastable H-Y zeolite is catalytically more active for the formic acid decomposition reaction than the $\text{NH}_4\text{-Y}$ zeolite. The reason for the enhanced activity may be either the result of higher concentrations of Brönsted acid sites or the increased concentration of hydrogen ions. The goal in this study was to describe the different states on the two

zeolites to determine why one is more reactive.

The results of the formic acid study are reported in chapters VI and VII. The infrared spectra in chapter VI suggest that the formic acid is dissociatively adsorbed through the loss of the acidic proton and is present as unidentate and bidentate formate species on both zeolites. The bidentate species is in the majority on the ultrastable H-Y zeolite, whereas the $\text{NH}_4\text{-Y}$ contains approximately equal numbers in each state. The results on the NMR study in chapter VII quantify the distribution of the two surface species and describe the symmetry and motional properties of the bidentate formate ion.

The following chapters were prepared for publication. Thus, the references, tables, and figures are local to each chapter.

References

1. J. B. Butt, AICHE Journal 22, 1 (1976).
2. M. L. Poutsma, Zeolite Chemistry and Catalysis, J. A. Rabo, ed., (ACS Monograph 171, Washington D.C., 1976), p. 437.
3. C. B. Duke, CRC Critical Reviews in Solid State Sci., 541 (1974).
4. R. P. Eischens and W. A. Pliskin, Adv. in Catalysis 10, 1 (1958).
5. L. H. Little, Infrared Spectra of Adsorbed Species, (Academic Press, New York, 1966).
6. M. L. Hair, Infrared Spectroscopy in Surface Chemistry, (Dekker, New York, 1967).
7. A. Abragam, The Principles of Nuclear Magnetism, (Oxford University Press, London, 1961).
8. C. P. Slichter, Principles of Magnetic Resonance, (Springer-Verlag, New York, 1978).
9. R. W. Vaughan, Ann. Rev. Phys. Chem. 29, 397 (1978).
10. M. Mehring, High Resolution NMR Spectroscopy in Solids, (Springer-Verlag, New York, 1976).
11. U. Haeberlin, High Resolution in Solids - Selective Averaging, (Academic Press, New York, 1976).
12. W. H. Weinberg, Ann. Rev. Phys. Chem. 29, 115 (1978).
13. J. B. Peri, Symp. on New Tools in Catalysis, Div. of Petroleum Research, ACS, Miami, Sept 10-15, 1978.
14. R. Bouwman and I. L. C. Freliks, Appl. Surf. Sci. 4, 11 (1980).
15. A.C. Yang and C. W. Garland, J. Phys. Chem. 61, 1504 (1957).
16. R. M. Kroeker, W. C. Kaska, and P. K. Hansma, J. Catalysis 61, 87 (1980).
17. H. Winkler, Bull. Ampere, 10th Year Special Ed., (1961), p. 219.

18. D. E. O'Reilly, *Adv. Catalysis* 12, 31 (1960).
19. E. G. Derouane, J. Fraissard, J. J. Fripiat, and W. E. E. Stone, *Catalysis Rev.* 7, 121 (1972).
20. E.L. Hahn, *Phys. Rev.* 80, 580 (1950).
21. H. Y. Carr and E. M. Purcell, *Phys. Rev.* 94, 630 (1954).
22. (a) J. S. Waugh, L. M. Huber, and U. Haeberlin, *Phys. Rev. Lett.* 20 180 (1968); (b) U. Haeberlin and J. S. Waugh, *Phys. Rev.* 175, 453 (1968).
23. (a) W. K. Rhim, D. D. Elleman and R. W. Vaughan, *J. Chem. Phys.* 59 3740 (1973); (b) W. K. Rhim, D. D. Elleman, L. B. Schreiber, and R. W. Vaughan, *J. Chem. Phys.* 60, 4595 (1974).
24. (a) D. P. Burum, Ph.D. Thesis, Caltech, 1979; (b) W. K. Rhim, D. P. Burum, and D. D. Elleman, *J. Chem. Phys.* 71, 3139 (1979).
25. (a) A. Pines, M. G. Gibby, and J. S. Waugh, *J. Chem. Phys.* 56, 1776 (1972); (b) A. Pines, M. G. Gibby, and J. S. Waugh, *J. Chem. Phys.* 59, 569 (1973).
26. M. Mehring, A. Pines, W. K. Rhim, and J. S. Waugh, *J. Chem. Phys.* 54, 3239 (1971).
27. (a) S. R. Hartman and E. L. Hahn, *Phys. Rev.* 128, 2042 (1962); (b) D. E. Demco, J. Tegenfeldt, and J. S. Waugh, *Phys. Rev. B* 11, 4133, (1975).
28. M. Kobayashi and T. Shirasaki, *J. Catalysis* 32, 254 (1974); R.A. Dalla Betta, *J. Phys. Chem.* 79, 2519 (1975).
29. G. A. Mills and F. W. Steffgen, *Catalysis Rev.* 8, 159 (1974).
30. M. A. Vannice, *Catal. Rev. - Sci. Eng.* 14, 153 (1976).
31. V. Ponec, *Catal. Rev. - Sci. Eng.* 18, 151 (1978).
32. J. J. F. Scholten, P. Mars, P. G. Menon, and R. Van Hardeveld,

Proc. Intern. Cong. Catalysis, 3rd, Amsterdam, 1964, p. 881.

33. Y. Noto, K. Fukuda, T. Onishi, and K. Tamaru, *Trans. Far. Soc.* 63, 2300 (1967).

CHAPTER II

AN INFRARED STUDY OF THE ADSORPTION
OF CO ON Rh DISPERSED ON Al₂O₃

(Chapter II is essentially an article by J.T. Yates, Jr., T.M. Duncan, S.D. Worley, and R.W. Vaughan, entitled "Infrared Spectra of Chemisorbed CO on Rh." This article was published in The Journal of Chemical Physics, Vol. 70, No. 3, p. 1219, February 1, 1979.)

ABSTRACT

The infrared spectrum of CO chemisorbed on alumina-supported Rh atoms has been investigated. In agreement with previous work, three types of adsorbed species have been clearly distinguished on the basis of their C-O stretching frequencies. Species I, assigned as $\text{Rh}(\text{CO})_2$, is formed only with Rh atoms which are isolated from each other. Species II, assigned as $\text{Rh}-\text{CO}$, and III, assigned as Rh_2CO , are formed on Rh clusters having two or more Rh atoms. CO-species II and III undergo interactions with neighbor CO species causing an increase in wavenumber as coverage increases. Based on infrared intensity measurements for species I, the OC-Rh-CO angle is 103^0 . Chemisorbed ^{13}CO yields the expected infrared spectrum on Rh, and rapid isotopic exchange between $^{13}\text{CO}(\text{ads})$ and $^{12}\text{CO}(\text{g})$ is observed which cannot be explained by the observed rate of desorption of CO from the supported Rh surface.

I. INTRODUCTION

The chemisorption of CO on transition metals has been studied by many physical techniques in an effort to understand the molecular and electronic character of the adsorbed species. The surface measurement techniques at our disposal range from those useful for studying adsorbed layers on single crystal surfaces to other techniques which may be more readily applied to metal adsorbents which are highly dispersed on inert, high area, supports. It is the latter class of surfaces which more closely resemble heterogeneous catalysts used in practice, and in fact the ability to disperse precious metals has been of major importance in enhancing their usefulness as catalysts.

While the study of single crystal adsorbents represents a limit of refinement in one direction (e.g., high-purity substrates, well-defined atomic periodicity and electronic character, etc.), dispersed metal catalysts can in principle achieve a limiting case in the opposite direction (atomic dispersal to the limit of single isolated metal atoms). Comparisons between chemisorbed CO on single metal atoms (or small metal clusters) and the vast literature of metal carbonyl chemistry have often been made (1). Such comparisons are often extended to single crystals containing chemisorbed CO (2,3).

One of the best ways to study the structure of chemisorbed species involves the use of vibrational spectroscopy. This has been effectively carried out on single crystals using electron energy loss

spectroscopy (EELS) (3-6) as well as reflection-absorption infrared spectroscopy (RAIS) (7-9). On dispersed metals, inelastic electron tunneling spectroscopy (IETS) has recently been employed (10). However, most vibrational work to date on dispersed metals has been done using transmission infrared spectroscopy (11,12). For both single crystals and dispersed metals, the infrared techniques currently offer the highest frequency resolution, and this technique is therefore more suitable for work involving isotopic labeling where small spectral shifts may be involved.

The chemisorption of CO by supported Rh has been well studied in the past, using infrared spectroscopy. For Al_2O_3 -supported Rh, Yang and Garland (13) first postulated that at low Rh concentrations, where sintering did not occur at reduction temperatures below 200^0 C , Rh existed in a condition closely approaching atomic dispersion (i.e. isolated Rh atoms). This picture has been confirmed by others on Al_2O_3 (14-17) although there are differences in interpretation regarding the degree of dispersion. Yao and Rothschild (17) regard the Rh as existing as isolated atoms on Al_2O_3 at 0.9 wt.% Rh on $\gamma\text{-Al}_2\text{O}_3$. D.J.C. Yates (16) regards the Rh to exist as tiny "rafts," containing about 7 atoms, with 6 atoms being edge atoms and behaving as if they are isolated. It has been shown in several laboratories that these highly dispersed Rh atoms are able to adsorb 2 CO molecules each, yielding a doublet in the infrared spectrum corresponding to symmetric and antisymmetric coupling between pairs of CO molecules adsorbed on the same Rh atom(13-17).

The close correspondence between the doublet frequencies and the spectrum of $\text{Rh}_2(\text{CO})_4\text{Cl}_2$ and $\text{Rh}_2(\text{CO})_4\text{Br}_2$ (which contain pairs of linear CO molecules on each Rh atom (13,18,19)) leaves little doubt regarding this assignment.

In this paper, we reinvestigate the CO/Rh system using infrared spectroscopy, volumetric uptake and isotopic substitution.

II. EXPERIMENTAL

The infrared cell used in these experiments is shown in Figure 1. It consists of two stainless steel "conflat" flanges containing 33 mm diameter CaF_2 single crystal windows which are sealed to a Ag ring using AgCl cement. Such windows are commercially available(20). The cell may be assembled using Cu gaskets and a double-sided flange which serves as the central section of the cell.

The vacuum system used in this work is a small bakeable all-metal system capable of being pumped below 10^{-8} Torr with a 20 l sec^{-1} ion pump. In addition, for handling higher pressure gases, the system may be evacuated with a N_2 trapped forepump. Pressure may be measured with a bakeable Baratron capacitance manometer to ± 0.001 Torr. A Bayard-Alpert gauge is used for background pressure measurements below 10^{-4} Torr.

The Rh samples are supported on Al_2O_3 (21) and are prepared as described by Yang and Garland (13). Briefly, an aqueous solution of RhCl_3 is diluted 10:1 with reagent-grade acetone and high-area Al_2O_3 is added with stirring. This slurry is continuously mixed

while being sprayed with an atomizer onto the CaF_2 window maintained at 80°C . Flash evaporation of the solvent during spraying leaves an adherent coating on the window. The weight of these deposits is $\sim 11 \text{ mg/cm}^2$ and the Rh content is 2.2% by weight. The cell is then assembled and the deposit is degassed by pumping at room temperature. Following this, the deposit and the cell are heated in a circulating-air oven to 150°C for 4 hours while degassing with the ion pump. Reduction to Rh metal is achieved using $\text{H}_2(\text{g})$ (Matheson grade 99.9995% pure) which has been stored at 1.3 atmospheres in a stainless steel tube immersed in l-N_2 . Three sequential 400 cm^3 charges of H_2 at ~ 180 Torr are used during reduction at 150°C , with the final reduction being carried out for 1 hour. Following reduction, the $\text{Rh}/\text{Al}_2\text{O}_3$ is outgassed at 175°C for ~ 8 hours until the background pressure falls below 1×10^{-6} Torr. Following cooling, a background IR spectrum from 4000 cm^{-1} to 1000 cm^{-1} is recorded. The sample is then ready for adsorption experiments. All spectra reported have been obtained by subtraction of the smooth background.

The infrared spectrometer is a Perkin-Elmer Model 180 grating spectrometer operated in the 2000 cm^{-1} region with a spectral resolution of 2.6 cm^{-1} . Spectra are recorded in the absorbance mode using the double beam facility. Calibration of the instrument's absorbance scale is carried out using standard density grids. The wavenumber scale was calibrated (22) above 2000 cm^{-1} with a gas cell containing $\text{CO}(\text{g})$ at ~ 150 Torr. Below 2000 cm^{-1} the branch of $\text{H}_2\text{CO}(\text{g})$ at 1750 cm^{-1} (23) was used as a calibration point. A 5 cm^{-1} shift in

the two scales occurs at 2000 cm^{-1} due to a grating change in the spectrometer. The reported spectral features in this paper are accurate to 1 cm^{-1} .

Spectroscopic grade CO from a glass breakseal bulb was used for adsorption without further purification. ^{13}CO was obtained from Merck Isotopes at 90% enrichment and was used without purification.

III. RESULTS

A. Adsorption and Desorption Isotherm

By means of pressure measurements in the vacuum system of known volume, it was possible to measure accurately the number of CO molecules adsorbed by the Rh samples. A plot of typical results is shown in Figure 2. It was found that the final equilibrium pressure was approached very slowly in these measurements so that small positive errors in the pressure corresponding to each point may exist. This does not affect the measurement of the quantity of CO adsorbed. The data in Figure 2 were measured on approximately 0.5g of a 2.2% Rh on Al_2O_3 substrate. This sample is sufficiently large relative to the dead volume of the gas dosing system to allow an accurate calculation of the amount of adsorbed CO to pressures of 10 Torr. On this sample, for CO-to-Rh ratios below about 0.45, the equilibrium pressure of CO is less than 0.02 Torr. However, as the pressure is increased, the samples continue to adsorb CO, yielding a CO-to-Rh ratio of about 0.65 at 9.4 Torr. The desorption isotherm exhibits a pronounced hysteresis. The CO does not begin to desorb from the Rh on Al_2O_3 substrate until the pressure is decreased below about 0.02 Torr. The points (a) to

(f) on the isotherm in Figure 2 correspond to the labeled spectra in Figure 3. It was found that the overall integrated IR intensity in spectra (a) to (f) increased in an approximate linear fashion with the number of CO molecules chemisorbed. Thus, assuming this relationship to hold for the entire range of coverage, we may calculate the approximate number of CO molecules adsorbed per Rh atom at high CO pressure from the integrated intensity of the spectra. At a final $P_{CO} \approx 50$ Torr, $N_{CO}/N_{Rh} = 0.92$ using this method.

B. Infrared Spectra of ^{12}CO Adsorbed on Rh

Following each adsorption point in Figure 2, the infrared spectra shown in Figure 3 were recorded. Four spectral features are clearly evident at all coverages of CO. A broad band at 1855 cm^{-1} develops and shifts to 1870 cm^{-1} as coverage increases. This band is assigned to CO bonded to more than one Rh atom and is termed "bridged-CO," $Rh_2(CO)(13)$. A second band of low relative intensity is observed at 2056 cm^{-1} at lowest CO coverage and shifts upward to 2070 cm^{-1} as coverage increases. This is assigned as a linear-CO species bonded to a single Rh atom which exists in coordination with other Rh atoms, $Rh(CO)(13)$. It has been shown previously that as the concentration of Rh on the Al_2O_3 support is increased, both the linear and bridged-CO species are enhanced in relative intensity(13). The most pronounced spectral feature in Figure 3 is a doublet with components at 2101 cm^{-1} and 2031 cm^{-1} . This doublet increases in intensity during the entire course of adsorption without change in wavenumber, as reported previously by Yang and Garland(13). The doublet is assigned to a pair

of CO molecules adsorbed on isolated Rh atoms, $\text{Rh}(\text{CO})_2$ (13). Spectrum (g) of Figure 1 was taken with ~50 Torr ^{12}CO above the Rh surface, and on the leading edge of the highest wavenumber peak one can see the fine structure of the $\text{CO}(\text{g})$ superimposed on the spectrum. These spectra correspond almost exactly to those obtained by Yang and Garland(13), except that a bridged-CO bond was not observed in their work on 2% Rh samples prepared in similar fashion to ours. Comparisons with the literature are summarized below in Table I.

The rate of growth of each of the three surface-CO species can be studied by plotting the background-corrected heights of the infrared peaks as a function of the CO-to-Rh ratio. The contribution of the peak at 2060 cm^{-1} is calculated by extending trailing edges of the large peaks at 2101 and 2031 cm^{-1} and subtracting the baseline in the middle. The adsorption isotherm of this sample is similar to that of Figure 2. The data are plotted in Figure 4. These data indicate that the $\text{Rh}(\text{CO})_2$ and bridged-CO states (2101, 2031, and 1870 cm^{-1} bands) are populated at an approximate linear rate with the CO-to-Rh ratio. However, the linearly-bonded species (2070 cm^{-1}) experiences an initial rapid growth, levels off, and then grows again after the first bend in the adsorption isotherm, at $N_{\text{CO}}/N_{\text{Rh}}$ equal to about 0.45.

C. Infrared Spectra of the Desorption of ^{12}CO from Rh

It was found that CO could be reversibly desorbed thermally at $T \leq 336 \text{ K}$. Representative desorption spectra are shown in Figure 5. It was found that rapid desorption occurs initially at 295 K for the $\text{Rh}(\text{CO})_2$ species and that both $\text{Rh}_2(\text{CO})$ and $\text{Rh}(\text{CO})$ appear to desorb less rapidly than $\text{Rh}(\text{CO})_2$, as reported by others (13,17). However, at 295 K

the rate of loss of infrared intensity decreases significantly following the first desorption stage, and the surface must be warmed slightly to promote more rapid removal of chemisorbed CO.

It should be noted that the wavenumber of the components of the $\text{Rh}(\text{CO})_2$ doublet is invariant at all stages of desorption whereas both the $\text{Rh}(\text{CO})$ and $\text{Rh}_2(\text{CO})$ features shift to slightly lower wavenumber as desorption progresses.

Following spectrum (d), CO was readSORBED at ~50 Torr and spectrum (a) was reproduced almost exactly. The reversible behavior for CO adsorption and desorption below 336 K suggests that CO dissociation (or disproportionation), leaving a carbon residue on the surface, does not occur below 336 K. Carbonization of bulk Rh by CO has been reported at 573 K(24).

D. Infrared Spectrum of ^{13}CO Adsorbed on Rh

Adsorption experiments were repeated on a freshly prepared $\text{Rh}/\text{Al}_2\text{O}_3$ surface using 90% ^{13}CO as the adsorbate. The spectra for increasing exposure to CO are shown in Figure 6. The general behavior observed for ^{12}CO is reproduced for ^{13}CO , and a comparison of wavenumbers for each isotopic species is given in Table II. An unusual and reproducible effect may be seen in comparison of ^{12}CO spectra and ^{13}CO spectra (Figures 3 and 6). The intensities for the two components of the doublet invert when the different CO isotopes are adsorbed.

E. Infrared Spectrum of $\text{Rh}(\text{CO})$ (^{12}CO)

Since the ^{13}CO used above contains 10% ^{12}CO , a doublet feature due to $\text{Rh}(\text{CO})(^{12}\text{CO})$ is expected. The high wavenumber component of

this doublet is seen in Figure 6 at 2086 cm^{-1} . The low wavenumber component is unfortunately hidden under the ^{13}CO features near 2000 cm^{-1} . The statistical fraction, X , of $\text{Rh}(\text{CO})_2$ on this surface is 0.18. Using the maximum absorbance peak heights, A , for the two high wavenumber bands, we see that the ratio of absorbances, R_A is

$$R_A = \frac{A_{12,13}}{A_{12,12} + A_{12,13} + A_{13,13}} = \frac{0.01}{0.01 + 0.01 + 0.93} = 0.096 \quad (1)$$

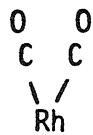
where $A_{12,12}$ was not measured but assumed to be 0.01 from the statistics of mixing.

F. Exchange of $^{13}\text{CO}(\text{ads})$ with $^{12}\text{CO}(\text{g})$

Following the observation of the spectrum for ^{13}CO in Figure 5, 50 Torr of $^{12}\text{CO}(\text{g})$ was introduced into the infrared cell, and the spectrum shown in Figure 7 was measured within 11 minutes. Almost complete exchange of all isotopic CO-adsorbed species was observed in this short time, and the rapidity of this exchange process sharply contrasts with the slow rate of desorption observed in Figure 5. In addition, following exchange, a shoulder due to the low-frequency component of the $\text{Rh}(\text{CO})_2$ doublet is now seen near $\sim 2012 \text{ cm}^{-1}$. Unfortunately, it is not possible to determine the exact frequency of the $\text{Rh}(\text{CO})_2$ low wavenumber component because the shoulder at $\sim 2012 \text{ cm}^{-1}$ contains contributions from an unknown ratio of $\text{Rh}(\text{CO})_2$, $\text{Rh}(\text{CO})(^{12}\text{CO})$, and $\text{Rh}(\text{CO})_2$.

IV. DISCUSSIONA. Assignment of IR Spectral Features

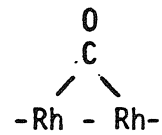
Three infrared-active adsorbed species are clearly seen from the spectra of chemisorbed CO on Rh. They are:



I



II



III

The assignment of species I is made on the basis of the doublet in the infrared spectrum and its close correspondence with the spectrum of $\text{Rh}_2(\text{CO})_4\text{X}_2$ where $\text{X} = \text{Cl}$ or Br (19). This comparison is tabulated in Table III and was originally proposed by Yang and Garland (13) as evidence for species I.

The striking feature to be noted regarding the infrared spectrum of species I is that both the CO stretching frequencies are invariant to within 1 cm^{-1} over the entire coverage range studied here (a 30-fold range of infrared intensity). This may be regarded as strongly indicative that the Rh atoms associated with species I are in fact isolated Rh atoms on the Al_2O_3 support. For Rh atoms within a Rh cluster, CO adsorption on neighboring Rh atoms should lead to interactions producing an increase in wavenumber as CO coverage increases. This behavior is generally observed for interacting CO molecules on bulk metals and may lead at full CO coverage to shifts of $\sim 100 \text{ cm}^{-1}$ in the C-O vibration. It is now generally accepted that interactional effects between CO molecules can occur via three

mechanisms, namely dipole-dipole coupling, direct intermolecular repulsion, and indirect effects through the metal(9,3). The suggestion that the lack of a coverage-dependent shift for species I was indicative of isolated Rh atoms was first made by Yang and Garland (13). This view is confirmed by Yao and Rothschild(17), who suggest that on their Rh/Al₂O₃ surfaces Rh...Rh distances of order 8 Å are necessary for Rh(CO)₂ formation. The results of this study are in agreement with this general view that isolated Rh atoms are present.

Both species II and III are associated with infrared bands which shift upwards by ~15 cm⁻¹ as CO coverage rises to saturation. These bands also exhibit reversible wavenumber behavior upon desorption. On this basis, both species are thought to exist on Rh sites which are coordinated to other Rh atoms. The first site of this type would be Rh₂. Multiple Rh coordination would permit interactional effects between neighbor CO molecules on neighbor Rh atoms.

B. Estimate of the Fraction of Rh Present as Isolated Atoms

A qualitative model involving only Rh and Rh_x sites is presented in this section. In this model we assume that all Rh_x sites adsorb only the bridged-CO species, III. The amount of species II is assumed to be zero in conformance with the low intensity associated with this species (Figure 2)

Let N_S = number of single Rh atoms.

N_B = number of Rh_x sites.

Then,

$$N_S + xN_B = N_{Rh}$$

$$2N_S + N_B = N_{CO}$$

From our volumetric uptake and infrared measurements, $N_{CO}/N_{Rh} = 0.92$ at saturation. For $x = 2$, $N_s/N_B = 0.8$. For $x = 3$, $N_s/N_B = 1.62$. These ratios correspond to ~40% or ~60% isolated Rh atom sites, respectively. A comparison of the integrated intensity of the doublet feature to the integrated intensity of the bridged-CO feature indicates that ~60% of the total integrated intensity is within the doublet feature. Based on the assumption of equivalent extinction coefficients per CO moiety for the two structures I and III, this measurement would suggest that ~30% of the sites are isolated Rh atom sites. While these two methods of calculation both suffer from the approximations made, it is clear that an appreciable fraction of the adsorption sites (30-60%) is capable of adsorbing 2-CO molecules and should be considered as isolated Rh atoms. A much better estimate of this quantity is determined by nuclear magnetic resonance techniques, in Chapter 5.

C. Carbonyl Bonding in $Rh(CO)_2$

The high wavenumber component in the doublet feature of $Rh(CO)_2$ corresponds to the symmetric CO-stretching mode and is assigned in this fashion in metal carbonyl spectra(26-28). The low wavenumber component is the result of antisymmetric coupling between CO oscillators. It has been demonstrated in metal carbonyls(27) that the ratio of integrated absorbance, (A_{asym}/A_{sym}) , is related to the angle, (2α) , between carbonyl groups as follows:

$$\frac{A_{asym}}{A_{sym}} = \tan^2 \alpha \quad (2)$$

As an example of the application of this equation, in the compound $(\pi\text{-C}_5\text{H}_5)\text{Fe}(\text{CO})_2\text{Sn}(\text{Ph})_3$, the measured intensity ratio gives a value of $2\alpha = 93^\circ$ whereas x-ray studies give $2\alpha = 95^\circ$ (28).

From the spectra in Figure 2, for peaks above an absorbance of about 0.5, the ratio $A_{\text{asym}}/A_{\text{sym}}$ ($\nu(2031 \text{ cm}^{-1})/\nu(2101 \text{ cm}^{-1})$) is about 1.6 ± 0.1 . This yields a OC-Rh-CO bond angle of $103 \pm 2^\circ$. This is in good agreement with the bond angle (91°) between carbonyl groups in $\text{Rh}_2(\text{CO})_4\text{Cl}_2$ (18) and with the ratio ($A_{\text{asym}}/A_{\text{sym}}$) = 1.0 ± 0.1 measured for this compound (13). Recently, Knözinger, *et al.* (29) have made the same calculation of the bond angle of the $\text{Rh}(\text{CO})_2$ specie formed by the decomposition of $\text{Rh}_6(\text{CO})_{16}$ onto ligand-modified silicas. They report bond angles of 98.6° and 100.2° for $\text{Rh}(\text{CO})_2$ on silicas with $(\text{CH}_2)_3\text{NHC}_6\text{H}_{11}$ and $(\text{CH}_2)_3\text{NH}(\text{CH}_2)_2\text{NH}_2$ ligands.

D. Isotopic Shift for ^{13}CO -Labeled Species

For completely labeled carbonyl species, the isotopic wavenumber ratio is given by

$$\frac{\tilde{\nu}^*}{\tilde{\nu}} = \left(\frac{\mu_{\text{CO}}}{\mu_{\text{CO}}^*} \right)^{\frac{1}{2}} \quad (3)$$

where μ_{CO} or μ_{CO}^* are the reduced masses of the unlabeled and labeled CO molecule (26). In Table II, the observed wavenumbers and their isotopic shifts are shown from our experimental measurements and from the calculation based on Equation (3). All wavenumber shifts calculated are in agreement with measured shifts within the experimental error of locating band centers.

An explanation for the intensity inversion of the symmetric and antisymmetric bands for species I following ^{13}CO isotopic substitution is currently under investigation.

E. Comparison of Isotopic Exchange with Desorption Measurements

All of the adsorbed CO species, I, II, and III, undergo rapid isotopic exchange with CO(g) at 295 K, as shown in Figure 7. It was noted that the exchange of $^{13}\text{CO(ads)}$ with $^{12}\text{CO(g)}$ at 50 Torr was much faster than the CO desorption rate (Figure 4) in vacuum at 295 K.

Two possible explanations can be offered to explain the rapidity and completeness of CO exchange at high CO pressures:

1. High pressure CO above a surface containing species I, II, and III is able to produce transient adsorbed species containing extra CO moieties. Isotopic exchange with CO(g) takes place readily via these intermediate species.

2. A fraction of the Rh and Rh_x sites is buried in pores within the support and is rapidly accessible only at high CO pressures.

Because of readorption processes during desorption from these buried sites, the rate of desorption is slow. However, at high CO pressures (~50 Torr) both adsorption and isotopic exchange occur readily.

After completing an infrared study, one of the 2.2% Rh on Al_2O_3 samples was analyzed for N_2 BET surface area and pore size distribution. The specific surface area was $55\text{m}^2/\text{g}$, significantly lower than the $90\text{ m}^2/\text{g}$ of the Alon-C powder. The computed cylindrical pore size diameter distribution ranged from about 200 \AA to over 1000 \AA , with a maximum at about 550 \AA . These pores should be readily accessible

at all CO pressures. However, if the ratio of the pore length to the pore diameter is large, about 100, the desorption process would be expected to be slow.

We believe that both explanations may be involved here. The rapidity and completeness of exchange suggest that model (1) above is operative. The very great decrease observed for the desorption rate of spectroscopically similar CO (i.e., species I) suggests that model (2) applies to a fraction of the Rh on the supported surface.

V. SUMMARY

The following features of CO adsorption on Rh/Al₂O₃ have been determined or verified:

1. Three CO species, I, II, and III, are distinguished on Rh/Al₂O₃ surfaces.
2. Species I, Rh(CO)₂, is produced on isolated Rh atoms as judged from lack of evidence for interaction with neighboring CO molecules as coverage is increased.
3. Species II and III are able to undergo interaction with neighboring CO molecules adsorbed on neighbor Rh atoms. This suggests the presence of some Rh_x species.
4. An estimate of a surface population of 30-60% isolated Rh atom sites is made, based on spectral band development and volumetric uptake measurements.
5. Species I exists with an angle about 103° between CO groups.
6. ¹³CO substitution for ¹²CO yields the expected isotopic

shifts.

7. One feature in the spectrum of $\text{Rh}(\text{¹²CO})(\text{¹³CO})$ has been observed at 2086 cm^{-1} , lending further confirmation to the structure postulated for species I.

8. Rapid isotopic exchange of ¹²CO with ¹³CO(ads) occurs for all of the adsorbed CO species. This suggests the existence of transient adsorbed species containing more CO moieties than species I, II, and III.

VI. ACKNOWLEDGMENT

The authors gratefully acknowledge support from ONR under contract N00014-77-F-0008 and N00014-75-C-0960. We also acknowledge valuable discussions with Dr. Ben Huie. We thank Professor George F. Rossman for his kindness in allowing us to use the infrared spectrometer and Dr. D.W. Blakely for measuring the pore size distribution.

References

1. T. L. Brown and D. J. Darensbourg, Inorg. Chem. 6, 971 (1967).
R. P. Eischens, S. A. Francis, and W. A. Pliskin, J. Phys. Chem. 60, 194 (1956); G. Blyholder, J. Phys. Chem. 68, 2772 (1968).
2. H. Conrad, G. Ertl, H. Knözinger, J. Küppers and E. E. Latta, Chem. Phys. Lett. 42, 115 (1976).
3. G. E. Thomas and W. H. Weinberg, J. Chem. Phys. 70, 954 (1979)
4. H. Ibach, M. Hopster, and B. Sexton, Application of Surface Science 1, 1 (1977).
5. G. Dalmai-Imelik, J. C. Bertolini, and J. Rousseau, Surface Sci. 63, 67 (1977).
6. S. Anderson, Solid State Comm. 20, 229 (1976); 21, 75 (1977).
7. (a) J. Pritchard, M. L. Sims, Trans. Far. Soc. 66, 427 (1970);
(b) J. Pritchard, T. Catterick, and R. K. Gupta, Surface Sci. 53, 1 (1975).
8. (a) J. T. Yates, Jr. and D. A. King, Surface Sci. 30, 601 (1972);
(b) J. T. Yates, Jr., R. G. Greenler, I. Rataczykowa, and D. A. King, Surface Sci. 36, 739 (1973).
9. A. M. Bradshaw and F. M. Hoffman, Surface Sci. 72, 513 (1978).
10. P. K. Hansma, W. C. Koska, and R. M. Laine, J. Amer. Chem. Soc. 98, 6064 (1976).
11. L. H. Little, Infrared Spectra of Adsorbed Species (Academic Press, London, 1966).
12. M. L. Hair, Infrared Spectroscopy in Surface Chemistry (Marcel Dekker, New York, 1967).

13. A. C. Yang and C. W. Garland, *J. Phys. Chem.* 61, 1504 (1957).
14. C. W. Garland, R. C. Lord, and P. F. Troiano, *J. Phys. Chem.* 69, 1188 (1965).
15. H. Arai and H. Tominaga, *J. Catalysis* 43, 131 (1976).
16. D. J. C. Yates, Conference on Catalyst Deactivation and Poisoning, May 24-28, 1978, Lawrence Berkeley, Calif. 94720, Pub. 238.
17. H. C. Yao and W. G. Rothschild, *J. Chem. Phys.* 68, 4774 (1978).
18. L. F. Dahl, C. Martell, and D. L. Wampler, *J. Amer. Chem. Soc.* 83, 1761 (1961).
19. C. W. Garland and J. R. Wilt, *J. Chem. Phys.* 36, 1094 (1962).
20. Obtainable from the Harshaw Chemical Company, Crystal and Electronic Products Department, 6801 Cochran Road, Solon, Ohio 44139.
21. Alon C is a high-area alumina supplied by Godfrey L. Cabot, Inc., Boston, Massachusetts 02110. The specific surface area of this lot, produced in 1958, is $90 \text{ m}^2 \text{g}^{-1}$.
22. E K. Plyler, A. Danti, L. R. Blaine, and E. D. Tidwell, *J. Res. N.B.S.*, A, 64, 29 (1960).
23. E S. Ebers and H. H. Nielsen, *J. Chem. Phys.* 6, 311 (1938).
24. B. A. Sexton and G. A. Somorjai, *J. Catalysis* 46, 167 (1977).
25. E. R. Corey, L. F. Dahl, and W. Beck, *J. Amer. Chem. Soc.* 85, 1202 (1963).
26. G. Bor, *J. Organometallic Chemistry* 10, 343 (1967).
27. (a) S. F. A. Kettle and I. Paul, *Advances in Organometallic*

Chemistry 10, 199 (1972); (b) P. S. Braterman, Metal Carbonyl Spectra (Academic Press, New York, 1975).

28. J. Dalton, I. Paul, and F. G. A. Stone, J. Chem. Soc. A, 2744 (1969).

29. H. Knözinger, E. W. Thornton, and M. Wolf, J. Chem. Soc. Far. Trans, I, 75, 1888 (1979).

TABLE I

Comparison of Full-Coverage Infrared Spectrum of CO on Rh/Al₂O₃ at 300 K

<u>%Rh/Al₂O₃</u>	<u>Rh-CO</u>	<u>Species (v) - (cm⁻¹)</u>		<u>Reference</u>
		<u>Rh(CO)₂</u>	<u>Rh₂(CO)</u>	
2.2%	2070	2101 ; 2031	1870	This work
2.0%	~2068	2095 ; 2027	--	(13)
0.92%	~2069	2100 ; 2030	1850	(17)
?	Unresolved	2108 ; 2040	1360	(15)

TABLE II

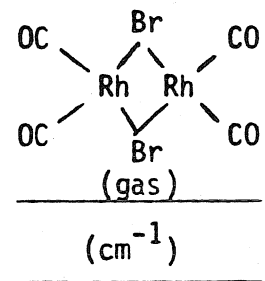
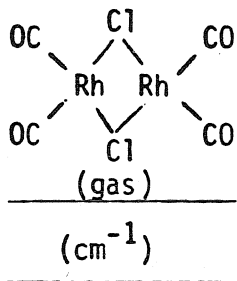
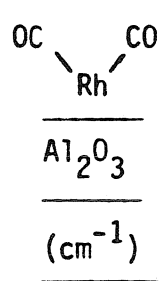
Comparison of Full-Coverage ^{12}CO and ^{13}CO Stretching Frequencies on Rh/ Al_2O_3

	<u>Species ($\tilde{\nu}$) - (cm$^{-1}$)</u>		
	<u>Rh-CO</u>	<u>Rh(CO)₂</u>	<u>Rh₂(CO)</u>
^{12}CO	2070	2101;2031	1870
^{13}CO	2024	2056;1987	1832
$\Delta\tilde{\nu}$	46	45;44	38
$\Delta\tilde{\nu}_{\text{calc.}}$	46	47;45	42

TABLE III

Comparison of Symmetric and Antisymmetric
Carbonyl Stretching Frequencies

Species



$\tilde{\nu}_{\text{sym}}$ 2101 2095 2092

$\tilde{\nu}_{\text{asym}}$ 2031 2043 2042

Reference: this work (19) (19)

Figure Captions

Figure 1. Side view of vacuum cell used for transmission infrared spectroscopy of supported metals.

Figure 2. Typical adsorption/desorption isotherm for CO chemisorption on supported Rh. T = 295 K. (The labeled points correspond to spectra shown in Figure 3.)

Figure 3. Infrared spectra for ^{12}CO adsorbed on Rh for increasing CO coverage. T = 295 K.

Spectrum (a). $P_{\text{CO}} = 2.9 \times 10^{-3}$ Torr.

Spectrum (b). $P_{\text{CO}} = 4.3 \times 10^{-3}$ Torr.

Spectrum (c). $P_{\text{CO}} = 5.0 \times 10^{-3}$ Torr.

Spectrum (d). $P_{\text{CO}} = 8.3 \times 10^{-3}$ Torr.

Spectrum (e). $P_{\text{CO}} = 0.76$ Torr.

Spectrum (f). $P_{\text{CO}} = 9.4$ Torr.

Spectrum (g). $P_{\text{CO}} \approx 50$ Torr.

Figure 4. Background - corrected peak intensities of the four infrared peaks as a function of the overall CO-to-Rh ratio, as determined by volumetric uptake.

Figure 5. Infrared spectra for ^{12}CO on Rh following desorption.

Spectrum (a). Full coverage at ~ 50 Torr, 295 K.

Spectrum (b). Desorption time, 150 s, 295 K.

Spectrum (c). Desorption time, 3.6×10^4 s, 321 K.

Spectrum (d). Desorption time, 2.2×10^4 s, 336 K.

Figure 6. Infrared spectra for 90% ^{13}CO adsorbed on Rh for increasing

CO coverage. T = 295 K.

Spectrum (a). $P_{CO} = 7 \times 10^{-3}$ Torr.

Spectrum (b). $P_{CO} = 0.69$ Torr.

Spectrum (c). $P_{CO} = 7.5$ Torr.

Spectrum (d). $P_{CO} \approx 50$ Torr.

Figure 7. Spectral changes during isotopic exchange of $^{13}CO(ads)$ with $^{12}CO(g)$. T= 295 K.

Spectrum (a). Full coverage ^{13}CO (90%) achieved at ~50 Torr.

Spectrum (b). Following 660 sec. exchange with ^{12}CO at 50 Torr.

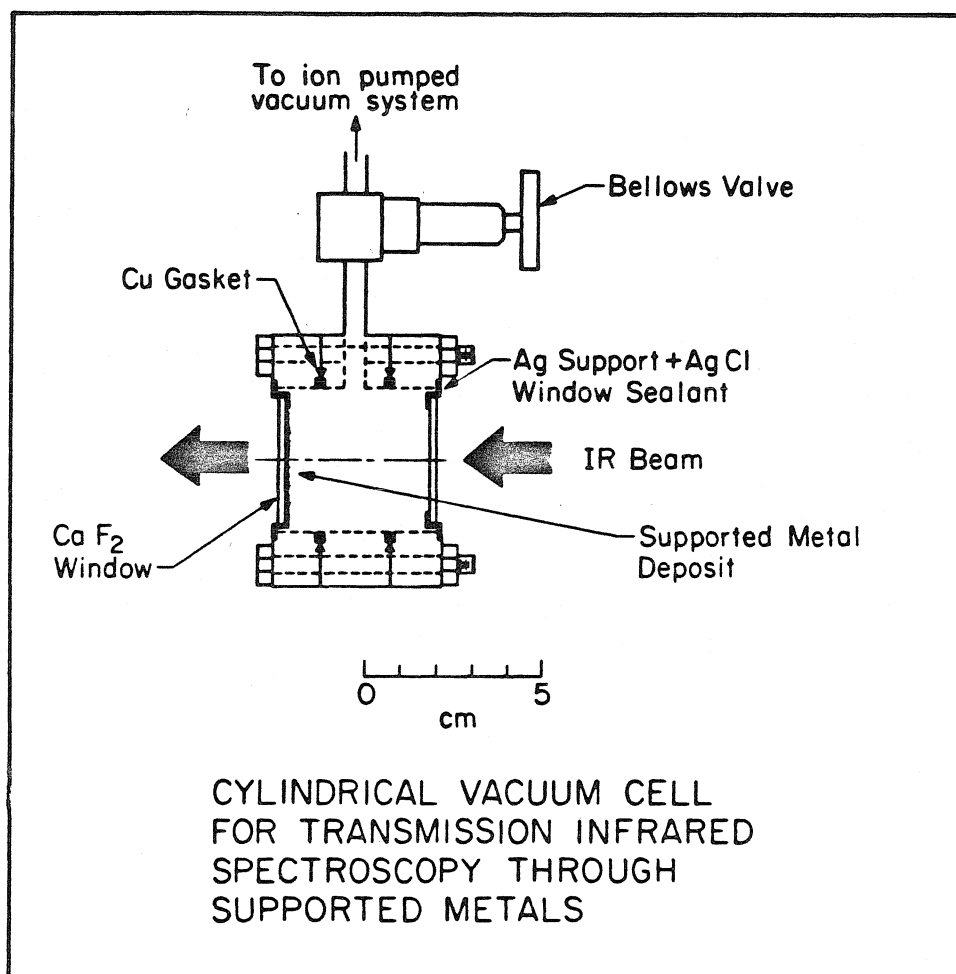


Figure 1

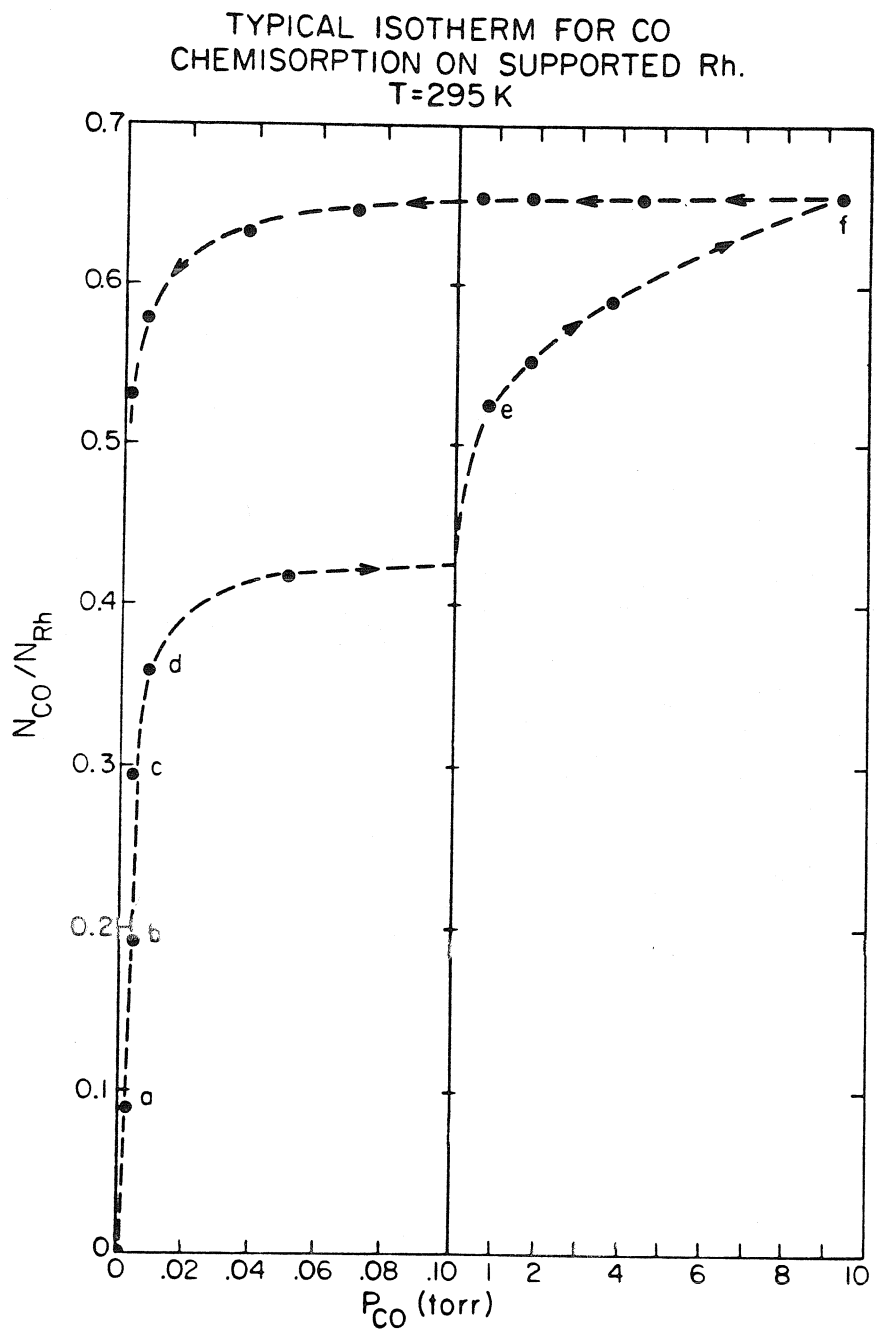


Figure 2

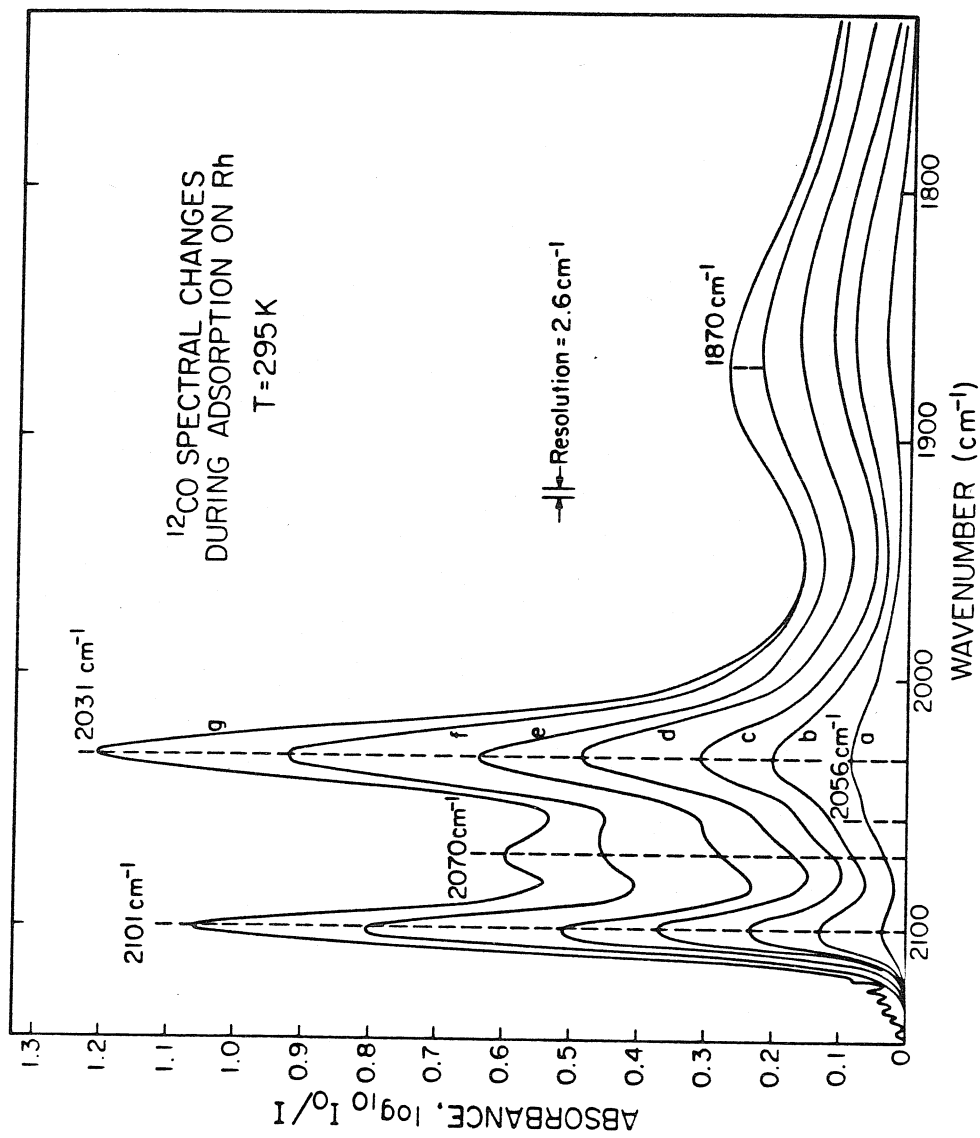


Figure 3

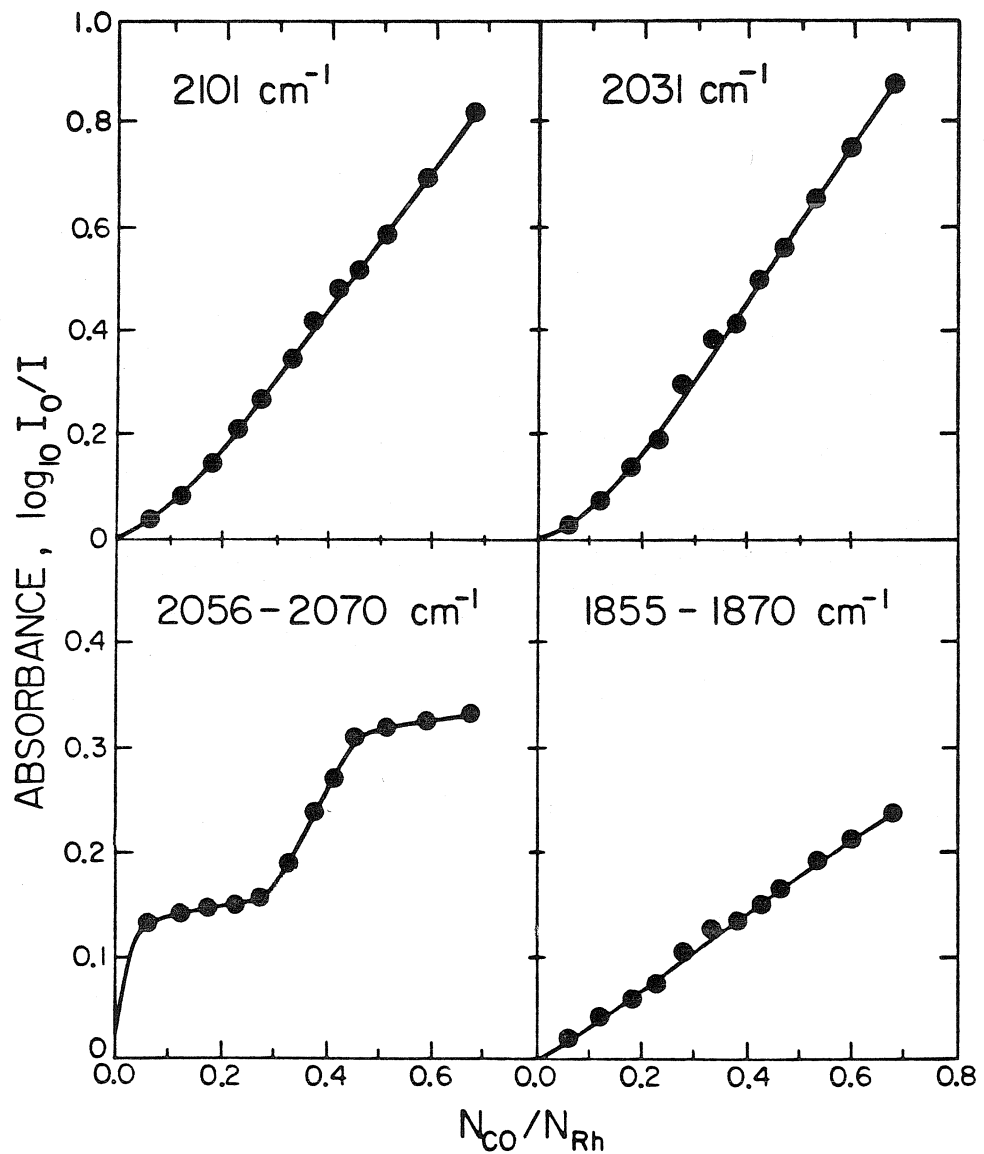


Figure 4

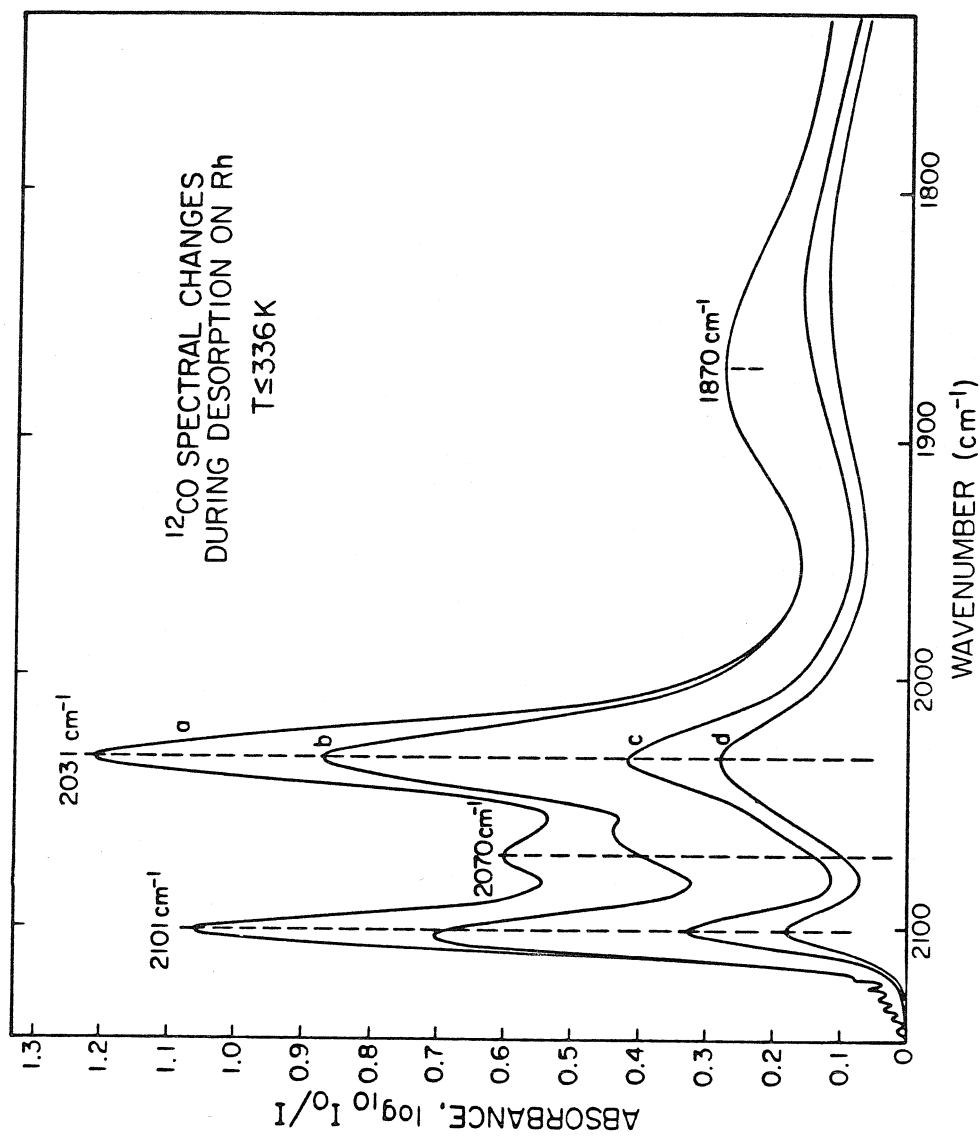


Figure 5

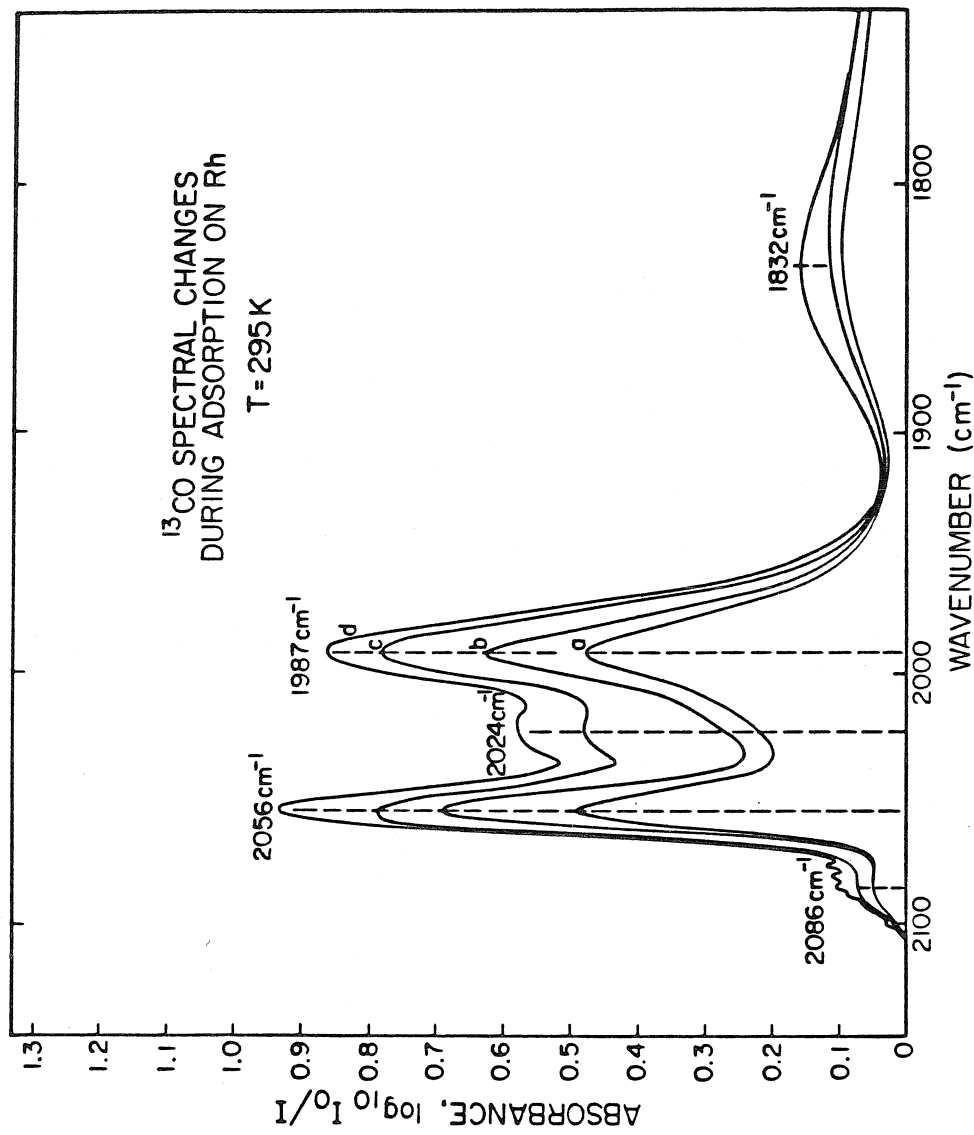


Figure 6

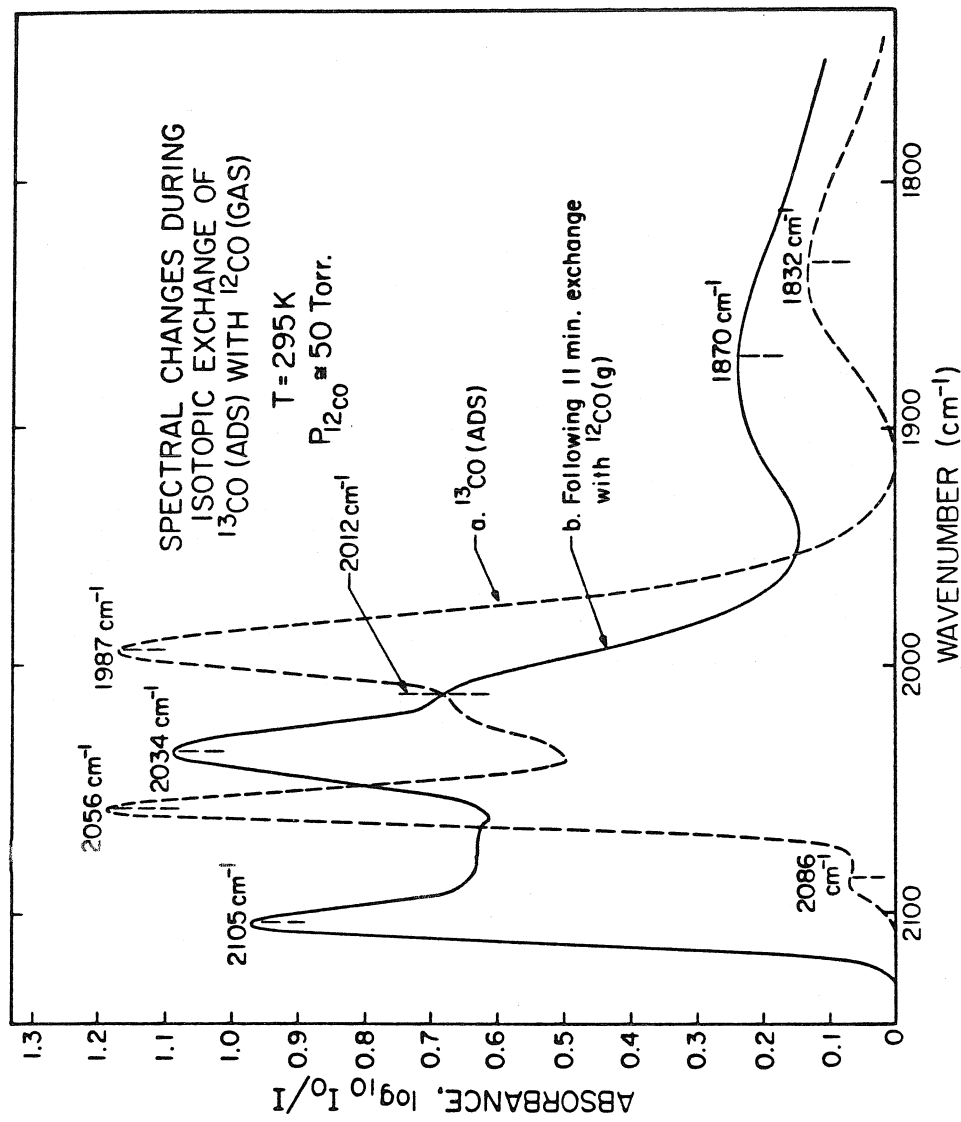


Figure 7

CHAPTER III

AN INFRARED STUDY OF THE ADSORPTION
OF CO ON Rh DISPERSED ON Al_2O_3 :
LOW TEMPERATURE INTERACTIONS

(Chapter III is essentially an article by J.T. Yates, Jr., T.M. Duncan, and R.W. Vaughan, entitled "Infrared Spectroscopic Study of Activated Surface Processes: CO Chemisorption on Supported Rh." This article was published in The Journal of Chemical Physics, Vol. 71, No. 10, p. 3908, November 15, 1979.)

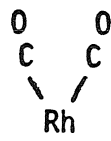
ABSTRACT

The infrared spectrum of CO chemisorbed on alumina-supported Rh surfaces has been studied following chemisorption at cryogenic temperatures. Major differences are observed in the distribution and spectroscopic character of chemisorbed CO species produced at low temperatures (110-170K) compared to chemisorbed CO species produced on Rh at 295 K. It has been found that the species $\text{Rh}(\text{CO})_2$, formed on isolated Rh sites, is produced rapidly via an activated chemisorption process above ~ 200 K. On more "crystalline" Rh_x sites, containing chemisorbed CO, an activated CO adsorbate-conversion process has been detected in which $\tilde{\nu}_{\text{CO}}$ decreases by $\sim 50 \text{ cm}^{-1}$ on warming the adsorbed layer above ~ 265 K. Isotopic exchange between $^{13}\text{CO(g)}$ and $^{12}\text{CO(ads)}$ has been shown to occur rapidly at low temperature (~ 200 K) for $\text{Rh}(\text{CO})_2$ species, whereas $\text{Rh}_x(\text{CO})$ species exchange rapidly only at higher temperatures ($\gtrsim 250$ K). These results, taken together, serve to confirm a model in which isolated Rh sites coexist on the alumina support with crystalline Rh_x sites; the two kinds of sites are separable on the basis of the spectroscopic character of the chemisorbed CO species they adsorb as well as by means of their chemical properties.

I. Introduction

The method of transmission infrared spectroscopy for the study of adsorbed molecules on high-area surfaces has been shown to be useful in a wide variety of studies related to adsorption and heterogeneous catalysis (1,2). Through the observation of characteristic stretching frequencies, it is often possible to assign the structure of chemisorbed species. This is usually done by employing analogies between the observed vibrational frequencies and the frequencies observed in molecules of known structure. At the present time, optical spectroscopy techniques offer the highest resolution of any of the vibrational spectroscopy methods employed for surface studies. Infrared spectroscopy is therefore most suitable for the study of isotopic effects and other effects where small vibrational spectral shifts may be involved.

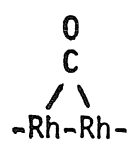
The chemisorption of CO by supported Rh has been studied extensively in the past by a number of workers, and infrared results for this system are briefly reviewed in a previous paper (3). It is believed that three generalized types of chemisorbed CO are produced on dispersed Rh surfaces at ~300K. They are:



I



II



III .

$$\tilde{\nu}_{\text{CO}} = 2104 \text{ cm}^{-1} (\text{sym})$$

$$\tilde{\nu}_{\text{CO}} = 2070 \text{ cm}^{-1}$$

$$\tilde{\nu}_{\text{CO}} = 1870 \text{ cm}^{-1}$$

$$\tilde{\nu}_{\text{CO}} = 2034 \text{ cm}^{-1} (\text{asym})$$

There is some controversy (3) regarding the degree of Rh dispersion required to allow the formation of species I. The question of the oxidation state of the Rh in species I has also been raised (4). D. J. C. Yates (5) suggests that the species I may form on the edge atoms of supported Rh "rafts" containing ~7 Rh atoms as seen in electron microscope photographs. The observed invariance of the wavenumber of the symmetric and antisymmetric stretching motion as CO coverage increases (3,6,7,8) indicates, however, that appreciable intermolecular interactions through space and through the metal do not occur for species I. This suggests that species I is formed at isolated sites (3,6,8). CO-CO interactions on bulk metal surfaces are known to produce increases of as much as 100 cm^{-1} in $\tilde{\nu}_{\text{CO}}$ as coverage increases (9). With regard to the question of the oxidation state of Rh, Primet (4) has recently suggested that CO dissociation at 200 K on Rh, producing chemisorbed oxygen, leads to the formation of Rh^+ which then adsorbs 2 CO molecules, giving the infrared doublet. The basis for this suggestion is founded on the observation of a slight intensification of the doublet when the Rh surface is treated prior to CO chemisorption with oxygen (4), as well as the need for thermal activation to produce the doublet feature during pure CO adsorption.

In contrast to species I, species II and III are thought to be associated with CO adsorption on more "crystalline" Rh sites. The observed shift of the CO stretching vibrational frequency to higher wavenumber as CO coverage is increased as interactions between neighboring CO species occur is consistent with this assignment. The

chemical reactivity of sites responsible for species II and III has been shown to differ from the behavior of sites responsible for species I (3,4,7).

In this paper we employ an infrared cell which can be operated at cryogenic temperatures. It has been possible to observe new adsorption states of CO on Rh at low temperatures and to investigate activated adsorption and activated isotopic exchange processes for CO in the various states described above. In addition, small reversible thermal effects on infrared lineshapes have been detected.

II. Experimental Methods

The low temperature infrared cell used in this work is shown in Figure 1. It contains a recessed Cu ring in which a 2.5 cm diameter CaF_2 single crystal disk holding the Al_2O_3 -supported Rh adsorbent is snugly mounted. The Cu ring may be cooled in vacuo to ~100 K by conduction to a $\lambda\text{-N}_2$ reservoir which is attached to the ring in the center of the cell. The infrared transmitting windows are 3.3 cm-diameter CaF_2 single crystals mounted in stainless steel "conflat" flanges (3), and sealed to the body of the cell (a double-sided stainless steel flange) using Cu gaskets. The temperature of the Cu sample holder ring may be monitored by means of a 0.025 cm diameter Fe-constantan thermocouple. It is likely that the temperature of the Rh surface may be slightly higher than the indicated thermocouple temperature during spectral measurements due to heating of the sample by the infrared beam, as discussed by Little (1). In addition, when the cell is filled above a few microns pressure with CO(g), thermal

conduction to the cooled sample causes some increase in measured temperature.

The vacuum system used in this work is a small, bakeable, all-metal, grease-free system described previously (3) capable of being pumped below 10^{-8} Torr with a 20 l sec⁻¹ ion pump. Provisions within the vacuum system are available for accurate volumetric measurement of the adsorption of CO by the sample.

The supported Rh samples (2.2% Rh by weight) are prepared by RhCl₃ dispersion on Alon-C alumina (3). Reduction to Rh⁰ is achieved in high-purity hydrogen gas at 425 K, followed by outgassing at 450 K. The Perkin-Elmer Model 180 infrared spectrometer was used in the double beam mode at 2.6 cm⁻¹ resolution (at 2000 cm⁻¹). The absorbance scale was calibrated using standard density grids. The wavenumber scale was calibrated using the P and R branches for CO(g) when present above the sample in the IR cell. In certain cases, subtraction of related infrared spectra has been carried out, yielding difference spectra which illustrate various effects. Other experimental details are described elsewhere (3).

III. Results

A. Temperature Effects in CO Adsorption

Figure 2 shows a comparison of the spectral development for CO adsorption at low temperatures ($T \leq 173$ K) and at room temperature ($T = 295$ K). It can be seen in the carbonyl stretching region that the infrared spectra differ significantly at these two adsorption

temperatures for similar exposures to CO. Three differences are noted:

- (a) The doublet at 2104 cm^{-1} and 2034 cm^{-1} is less developed at the low adsorption temperature.
- (b) The spectral feature observed between the components of the doublet is seen to shift upward in a higher wavenumber range (2065 cm^{-1} - 2082 cm^{-1}) as CO coverage increases at 173 K compared to the spectral range observed for this feature for CO adsorption at 295 K (2056 cm^{-1} - 2066 cm^{-1}) (3).
- (c) For low temperature CO adsorption the broad "bridging-CO" band occurs at slightly higher wavenumber ($\sim 1900\text{ cm}^{-1}$) than the comparable band produced at 295 K ($\sim 1870\text{ cm}^{-1}$).

Similar spectral differences are present in the spectra reported at 103 K by Primet (4) compared to his spectra obtained at 300 K for CO on Rh supported on Al_2O_3 .

In order to investigate the possibility that the chemisorption of CO on Rh is an activated process, the following experiment was performed, the results of which are shown in Figure 3. A clean Rh surface was exposed to CO (7.1 Torr) at temperatures below 178 K. The spectrum shown in Figure 3A (a;b) was obtained, and the adsorbed species were shown to be stable by repeating the spectral scan at this temperature. The spectrum 3A (a;b) agrees well with spectrum 2A (d) and demonstrates again that the carbonyl-doublet is retarded in its development during CO chemisorption at low temperature.

The Rh surface was then slowly warmed in the presence of CO(g) and the infrared spectrum was continuously rescanned as shown for

spectra 3A (c,d, and e). Three effects are prominent:

- (a) The doublet at 2104 cm^{-1} and 2034 cm^{-1} develops extensively above 200 K.
- (b) The single band at 2082 cm^{-1} shifts to lower wavenumber as temperature and coverage increase. This wavenumber shift is opposite to the behavior seen for increasing coverage at $T \lesssim 173 \text{ K}$ (Figure 2A) or at $T = 295 \text{ K}$ (3).
- (c) Enhanced infrared absorption below 2000 cm^{-1} is observed.

All of these features are best visualized in the difference spectrum in Figure 3B. The slight negative feature near 2022 cm^{-1} is due to a small reversible temperature-dependent lineshape effect to be discussed later.

B. Low Temperature Adsorption on a CO-pretreated Rh Substrate

The slow formation of the $\text{Rh}(\text{CO})_2$ dicarbonyl sites is also observed at 295 K. For example, on samples aged for one year or more, the population of the dicarbonyl sites increases in the presence of CO at pressures of about 50 Torr, as discussed in chapter 5 of this thesis. One possibility is that surface reconstruction is responsible for the formation of $\text{Rh}(\text{CO})_2$ at high CO pressures and at room temperature. One such mechanism could be that single Rh atoms are formed by the migration of Rh atoms from the Rh rafts. One could envision a process in which the Rh atom breaks one or more Rh-Rh bonds at the raft edge, forms a second Rh-CO bond, and then migrates across the Al_2O_3 surface to an adsorption site away from the parent raft. If the activation energy for this process is sufficient to limit the

separation and migration at temperatures on the order of 200 K, there would be a reduced development of the doublet at 2104 and 2034 cm^{-1} .

To test the hypothesis of surface reconstruction, a fresh 2.2% Rh on Al_2O_3 sample was prepared and cooled to a temperature of about 200 K. The surface was then exposed to 7.0 Torr and again, the inhibited formation of the dicarbonyl species was observed, as revealed by the reduced height of the peaks at 2104 and 2034 cm^{-1} . Upon warming the sample to 295 K, the doublet intensity increased to typical levels, as before. The infrared intensity of the peak at 2034 cm^{-1} , the asymmetric stretch of the $\text{Rh}(\text{CO})_2$ species, and the corresponding sample temperature are plotted as a function of time in Figure 4. The peak grows exponentially to an absorbance of about 0.24 at 200 K, then levels off. When the cell is allowed to warm to 295 K, the intensity develops further to an absorption of 0.64.

This sample was then outgassed at 295 K with an ion pump for about 340 hours to an equilibrium CO pressure of about 3×10^{-6} Torr. The desorption reduced the intensity of the 2034 cm^{-1} peak from 0.64 to 0.29. The sample was then re-cooled to about 200 K, re-exposed to 7.0 Torr of CO, and then again allowed to warm to 295 K. The development of the 2034 cm^{-1} peak is plotted in Figure 4. Once again, the low temperature formation of the $\text{Rh}(\text{CO})_2$ species is inhibited and the peak grows to its full height only after warming to 295 K. Thus, the activation barrier to the adsorption of CO on the dicarbonyl site is also present on a CO-pretreated Rh substrate.

C. Temperature Effects Causing CO Adsorbate State Conversion at Constant Coverage

In order to investigate the possibility that activated processes may occur at constant coverage in the chemisorbed CO layer upon heating, the following experiment, yielding the infrared spectra shown in Figure 5, was carried out. A partial coverage of CO was produced by means of exposure of CO to a Rh surface at 200 K. The cell was evacuated to prevent further CO adsorption, and the surface cooled to 110 K where spectrum 5A (a) was recorded. The Rh surface was then allowed to warm in vacuo and the spectral changes were observed as shown in spectra 5A (b,c and d). The processes which occur upon the warming of a CO layer in the absence of further CO adsorption are well illustrated in the difference spectrum, Figure 5B. Here it can be seen that an activated state conversion process takes place in which the 2082 cm^{-1} infrared feature converts into an asymmetric feature with peak maximum near 2030 cm^{-1} . In addition, some evidence for the production of a broad "bridged-CO" feature centered near 1828 cm^{-1} is seen. Little or no change occurs in the intensity of the high wavenumber component of the doublet at 2104 cm^{-1} , suggesting that the $\text{Rh}(\text{CO})_2$ species is stable in vacuum on warming from 100-314 K. Finally, a reversible temperature effect is seen for the 2104 cm^{-1} component of the doublet and possibly also for the 2034 cm^{-1} component of the doublet. This reversible phenomenon will be discussed later.

D. Kinetic Studies of Isotopic CO Exchange between Adsorbate States and the Gas Phase

We have carried out systematic spectroscopic studies of the exchange between adsorbed $^{12}\text{C}^{16}\text{O}$ species and $^{13}\text{C}^{16}\text{O(g)}$ as a function of sample temperature to determine whether differences exist in the degree of lability for the different adsorbate states detected by infrared spectroscopy.

The infrared spectrum (a) shown in Figure 6A is the result of $^{12}\text{C}^{16}\text{O}$ saturation of the Rh surface at 295 K. Following spectrum 6A (a), the surface was cooled to ~ 200 K and $^{13}\text{C}^{16}\text{O(g)}$ was admitted at ~ 50 Torr pressure. From earlier experiments (3) at 295 K, this procedure was shown to result in extensive isotopic exchange within minutes (3). However, as seen from spectrum 6A (b), and as more clearly demonstrated from the difference spectrum 6B, only species I, $\text{Rh}(\text{CO})_2$, appears to exchange readily below ~ 220 K. We see that above $\sim 1960 \text{ cm}^{-1}$ loss of the $\text{Rh}(\text{CO})_2$ doublet feature occurs with the production of doublet intensity for $\text{Rh}(\text{CO})_2$. The wavenumber of the two interconverting doublets agrees well with that measured for pure isotopic CO species (3). There is also a fairly featureless loss of intensity below $\sim 1960 \text{ cm}^{-1}$ (species III). This effect was determined to be due to a reversible shift in the background spectrum, and not the exchange of species III. As the Rh surface is warmed above ~ 220 K, further isotopic exchange occurs as shown in Figure 7. Here from the difference spectrum 7B, it can be seen that a small amount of exchange in the doublet region (species I) continues, but the dominant process is

exchange of CO species II in the 2070 cm^{-1} region, with production of an exchanged broad asymmetric feature maximized near 2008 cm^{-1} . Thus, as shown by comparison of Figure 6B and 7B, this method has discriminated between the various types of chemisorbed CO species on the basis of the temperature required for rapid isotopic exchange between the gas phase and the adsorbate species.

E. Reversible Temperature Effects on Infrared Frequencies

A Rh surface fully covered with $^{12}\text{C}^{16}\text{O}$ at 295 K was cooled slowly to various temperatures, and the infrared spectrum was carefully measured as shown in Figure 8. The peak maxima for the two sharp components of the doublet (originating from species I) are both seen to shift slightly to higher wavenumber in a monotonic fashion as the surface cools. The shift is $\sim 3\text{ cm}^{-1}/200\text{ K}$. The reversible temperature effect clearly seen in Figure 5B is therefore a consequence of temperature-dependent frequency changes.

At the present time we believe that reversible temperature-dependent frequency changes observed in Figure 8 (and Figure 5) are related to coupling of the C-O oscillators in $\text{Rh}(\text{CO})_2$ to phonon modes in the Al_2O_3 support. Our data at present do not permit a quantitative analysis of this effect.

IV. Discussion

A. Activated Adsorption of CO by Rh

Let us consider for simplicity that two general kinds of adsorption sites exist for CO chemisorption on Al_2O_3 -supported Rh.

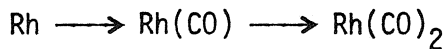
These are isolated Rh sites, designated Rh, and more compact arrangements of Rh atoms designated Rh_x (3). The Rh sites form $\text{Rh}(\text{CO})_2$ (species I) upon chemisorption while the Rh_x sites yield linear and bridge-bonded CO (species II and III).

One possibility for the retardation of filling of the Rh sites to yield $\text{Rh}(\text{CO})_2$ at low temperatures ($T \leq 173$ K), as shown in Figures 2 and 3, is that an activated process is involved for chemisorption on these sites. As was experimentally observed in part B of the results section, this activated process is present on CO-pretreated Rh samples, in which CO was first adsorbed on the substrate and then removed by extended outgassing at 295 K. Thus, if a reconstruction of the surface is responsible for the activation barrier to adsorption of CO, such reconstruction must relax upon the desorption of CO. If the formation of $\text{Rh}(\text{CO})_2$ is due to the separation and migration of Rh atoms from the Rh rafts, the infrared spectra suggest that the Rh atoms re-migrate to the rafts upon the loss of CO.

This activation energy could be related to the need for rehybridization of the supported Rh atoms to accommodate two CO ligands. The activated process leading to $\text{Rh}(\text{CO})_2$ was previously attributed by Primet (4) to CO decomposition, leading to the production of Rh^+ sites which were postulated to then adsorb two CO molecules. The low temperature associated with this activated process seems to argue against a model involving CO dissociation on Rh sites. In addition, Ozin, et al. (13) has reported that at 15 K Rh + CO produces $\text{Rh}(\text{CO})_4$ species in CO matrices; this observation strongly suggests that

activated CO dissociation is not the cause of multiple CO bonding to Rh. Furthermore, recent studies of CO interaction with Rh(111) crystals have shown that isotopic mixing does not occur between $^{12}\text{C}^{18}\text{O}$ and $^{13}\text{C}^{16}\text{O}$ in temperature range 300 K to 800 K (14). This observation further excludes CO dissociation on Rh as being operative for the production of an adsorption site yielding $\text{Rh}(\text{CO})_2$.

Another possibility for the inhibited formation of the $\text{Rh}(\text{CO})_2$ species at temperatures below 200 K is that the adsorption process on isolated Rh atoms;



is terminated after the formation of the $\text{Rh}(\text{CO})$ species. Thus, the low temperature infrared band at 2082 cm^{-1} may be the combination of linearly bonded species on the Rh rafts (normally occurring at 2070 cm^{-1} at 295 K) and a linear species on an isolated Rh atom (which may appear at a frequency closer to 2082 cm^{-1}). The shift in the band from 2082 to 2070 cm^{-1} upon warming may be partially due to the conversion of $\text{Rh}(\text{CO})$ to $\text{Rh}(\text{CO})_2$.

The thermal ($T \gtrsim 265 \text{ K}$) conversion of the 2082 cm^{-1} - CO state to a state exhibiting $\tilde{\nu}_{\text{CO}} \approx 2030 \text{ cm}^{-1}$, (Figure 5), suggests that an activated CO state-conversion process is involved on the Rh_X sites, and that the 2082 cm^{-1} CO species produced at low temperature is metastable with respect to the final CO bonding state. The downward shift of $\sim 50 \text{ cm}^{-1}$ in $\tilde{\nu}_{\text{CO}}$ during this conversion is consistent with stronger $\text{Rh}_X\text{-CO}$ bonding for the lower wavenumber CO state(s) produced above 265 K. Similar state conversion processes, induced by heating, have been

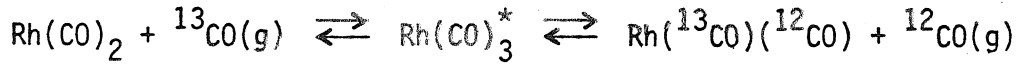
observed for CO chemisorbed on tungsten. Here the "virgin-CO" state, stable at low temperatures, converts into α -CO and β -CO upon heating (10,11). β -CO is thought to be dissociated on tungsten.

The presence of independent activated processes involving $\text{Rh}(\text{CO})_2$ formation and $\text{Rh}_x(\text{CO})$ conversion processes is consistent with the contention that Rh sites are isolated from Rh_x sites. This view was previously suggested (3) on the basis of the invariance of $\tilde{\nu}_{\text{CO}}$ (sym) and $\tilde{\nu}_{\text{CO}}$ (asym) for species I as CO coverage is increased. In addition, specific effects for H_2CO decomposition on Rh sites support this conclusion (3).

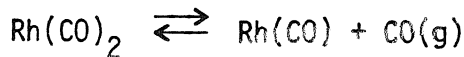
B. Activated Exchange Processes between $\text{CO}(\text{ads})$ and $\text{CO}(\text{g})$

We have previously demonstrated that exchange between $\text{CO}(\text{g})$ and $\text{CO}(\text{ads})$ is very rapid at 295 K compared to desorption at this temperature (3). It was proposed that the rapid exchange occurred via the formation of transient adsorbed species containing extra CO moieties.

Thus, a process such as



appears to be occurring at a rapid rate compared to isotopic exchange at a rate controlled by the desorption-limited process:



As seen by comparison of Figure 6 and Figure 7, it has in fact been found that $\text{CO}(\text{g})$ exchanges with $\text{Rh}(\text{CO})_2$ at a lower temperature than with $\text{Rh}_x(\text{CO})$. Slow warming of the surface in $\text{CO}(\text{g})$ results in sequential isotopic exchange of species II and III.

C. Qualitative Thermodynamic Model

Although it has not been possible to measure activation energies directly for any of the processes studied in this work, it is possible to suggest general features about the energetics of various surface processes as shown in Figure 9. Here it is postulated that the energetic features differ significantly for Rh and Rh_x sites. In particular, the activation energy E_a (or possibly E_b) for CO adsorption on Rh to yield $Rh(CO)_2$ is higher than E_c for adsorption on Rh_x . There is an activation energy, E_d , for conversion from the metastable $Rh_x(CO)^*$ to $Rh_x(CO)$, whereas no metastable $Rh(CO)_2$ was detected. There also seem to be small differences in the activation energy for CO exchange with the exchange process on isolated Rh sites occurring more readily. The activation energy for CO desorption from Rh_x sites may be estimated from the measured activation energy for CO desorption from Rh (111): in the limit of zero coverage, $32 \text{ kcal/mole}^{-1}$ (12). This value is probably greater than $(E_2 + E_a)$ since species I, $Rh(CO)_2$, desorbs more rapidly than species II (7,8,3) near 300 K.

The origin of several irreversible activated processes involving CO adsorption and CO adsorbate state conversion is not understood at present. One possible view is that the final structural state achieved for CO chemisorbed at elevated temperature is the result of passage through higher energy intermediate states of chemisorbed CO. In this view, rehybridization of the Rh atoms in both isolated and "crystalline" sites may be responsible for the observed activated processes as seen by means of the infrared spectrum of the bound CO.

A second model would involve activated structural rearrangements within the Rh substrate itself, caused by chemisorptive interaction with CO, as discussed earlier, such as the migration of single Rh atoms from the Rh rafts. Similar reconstruction processes on Rh_x sites could lead to the conversion of $\text{Rh}_x(\text{CO})^*$ (2082 cm^{-1}) to a more strongly bound $\text{Rh}_x(\text{CO})(2030 \text{ cm}^{-1})$.

Structural rearrangements of single crystal surfaces due to chemisorption are now being recognized from LEED studies (15). In addition, alloy surface segregation processes induced by adsorption on the alloy surface have been observed in which the driving force is related to the formation of the chemisorption bond with one component of the alloy (16). By analogy, it is possible that the activated processes observed here may be due at least in part to structural rearrangements of the Rh substrate caused by CO chemisorption.

V. Summary

The following features related to the chemisorption of CO on Al_2O_3 -supported Rh have been observed:

1. The adsorption of CO on isolated Rh sites to form $\text{Rh}(\text{CO})_2$ species is an activated process which occurs rapidly above ~ 170 K. This activated process for CO adsorption was present on a sample in which CO was adsorbed and then desorbed from the Rh sites. No evidence for oxidation of Rh via CO dissociation has been found, contrary to the conclusions of Primet (4).
2. For CO adsorption on Rh_x sites as linear species, an

activated state-conversion process is observed above 265 K, causing a shift in $\tilde{\nu}_{CO}$ from $\sim 2082 \text{ cm}^{-1}$ to $\sim 2030 \text{ cm}^{-1}$. This presence of the feature at $\sim 2030 \text{ cm}^{-1}$ overlaps directly with the low frequency component of the $\text{Rh}(\text{CO})_2$ doublet, a fact which was not recognized in earlier work done at 295 K (3, 4, 5, 6, 7, 8). This large irreversible shift implies that a major strengthening of the Rh-CO bond occurs as some type of structural rearrangement takes place on these sites.

3. Selective isotopic exchange of $^{*}\text{CO(g)}$ with $\text{Rh}(\text{CO})_2$ species may be achieved at 200 K while higher temperatures are required for rapid exchange of linear CO species on Rh_x sites.

4. These results, when considered along with previous information regarding the Rh-Al₂O₃ system (3), suggest that the Rh sites responsible for $\text{Rh}(\text{CO})_2$ species are single atom sites distinct from the Rh_x sites associated with linear and bridged-CO bonding.

VI. Acknowledgment

The authors gratefully acknowledge support from ONR under contracts N00014-77-F-0008 and N00014-75-C-0960. We thank Professor George F. Rossman for his kindness in allowing us to use the infrared spectrometer. We thank Dr. Richard Cavanagh and Dr. James Hall for helpful comments.

References

1. L. H. Little, Infrared Spectra of Adsorbed Species (Academic Press, London, 1966).
2. M. L. Hair, Infrared Spectroscopy in Surface Chemistry (Marcel Dekker, New York, 1967).
3. J. T. Yates, Jr., T. M. Duncan, S. D. Worley, and R. W. Vaughan, *J. Chem. Phys.* 70, 1219 (1979); see also, J. T. Yates, Jr., S. D. Worley, T. M. Duncan, and R. W. Vaughan, *J. Chem. Phys.* 70, 1225 (1979).
4. M. Primet, *J. Chem. Soc. Far. Trans. I* 74, 2570 (1978).
5. D. J. C. Yates, private communication.
6. A. C. Yang and C. N. Garland, *J. Phys. Chem.* 61, 1504 (1957).
7. H. Arai and H. Tominaga, *J. Catalysis* 43, 131 (1976).
8. H. C. Yao and W. G. Rothschild, *J. Chem. Phys.* 68, 4774 (1978).
9. G. E. Thomas and W. H. Weinberg, *J. Chem. Phys.* 70, 954 (1979). See also A. M. Bradshaw and F. M. Hoffman, *Surface Sci.* 72, 513 (1978).
10. R. Gomer, Proc. 2nd Internl. Conf. on Solid Surfaces, 1974, Japan *J. Appl. Phys.*, Suppl. 2, Pt. 2, p. 213 (1974).
11. J. T. Yates, Jr., T. E. Madey, and N. E. Erickson, *Surface Sci.* 43, 257 (1974); J. T. Yates, Jr., N. E. Erickson, S. D. Worley, and T. E. Madey, "The Physical Basis of Heterogeneous Catalysis," ed. E. Drauglis and R. I. Jaffee, Plenum Press, p. 75 (1975).
12. P. A. Thiel, E. D. Williams, J. T. Yates, Jr., and W. H. Weinberg, *Surface Sci.* 84, 54 (1979).
13. L. A. Hanlan and G. Ozin, *J. Amer. Chem. Soc.* 96, 6324 (1974).

14. J. T. Yates, Jr., E. D. Williams, and W. H. Weinberg, Surface Science, submitted.
15. R. A. Baker and P. J. Estrup, Phys. Rev. Lett. 41, 1307 (1978).
16. R. Bouwman and W. M. H. Sachtler, J. Catal. 19, 127 (1970).

Figure Captions

Figure 1. Infrared cell for low temperature adsorption studies.

Figure 2. Comparison of $^{12}\text{C}^{16}\text{O}$ adsorption on Rh at low temperature and high temperature. The infrared spectra correspond to approximately equivalent amounts of CO admitted to the IR cell.

Figure 3. Activated $^{12}\text{C}^{16}\text{O}$ adsorption on Rh for increasing Rh temperature.

Figure 4. The infrared absorbance of the 2034 cm^{-1} peak of CO on Rh on Al_2O_3 plotted concurrently with the sample temperature as a function of time. Line (a) occurs upon the exposure of CO to a freshly prepared substrate. Line (b) is observed when the experiment is repeated after the CO was partially desorbed from the sample. In both experiments, 7.0 Torr of CO was dosed to the sample at time zero.

Figure 5. Activated adsorbate conversion processes - $^{12}\text{C}^{16}\text{O}$ on Rh. Spectrum (a) was measured at 110 K after CO adsorption at ~ 200 K. All changes occur upon heating CO on Rh surface in vacuum.

Figure 6. Low temperature isotopic exchange of chemisorbed CO on Rh.

Figure 7. High temperature isotopic exchange of chemisorbed CO on Rh.

Figure 8. Reversible temperature effects on infrared spectrum - $^{12}\text{C}^{16}\text{O} + \text{Rh}$. The adsorbed layer produced at 314 K was cooled to various temperatures and the infrared spectrum was measured.

Figure 9. Qualitative free energy diagram for the adsorption of CO on Rh sites. For the isolated Rh sites, the most stable species, $\text{Rh}(\text{CO})_2$, is inhibited from forming at low temperatures because E_a (or E_b) is larger than kT at $T \lesssim 200$ K. For the crystalline Rh sites, adsorption of CO at low temperatures results in the formation of a metastable species $\text{Rh}_x(\text{CO})^*$, since $E_c < kT < E_d$ for $T \lesssim 200$ K. At higher temperatures, the reaction proceeds over the activation barrier E_d to the more stable $\text{Rh}_x(\text{CO})$. At both sites, exchange proceeds via the proposed activated complexes $\text{Rh}(\text{CO})_3^*$ and $\text{Rh}_x(\text{CO})_2^*$, rather than by desorption, then re-adsorption.

INFRARED CELL FOR LOW TEMPERATURE ADSORPTION STUDIES

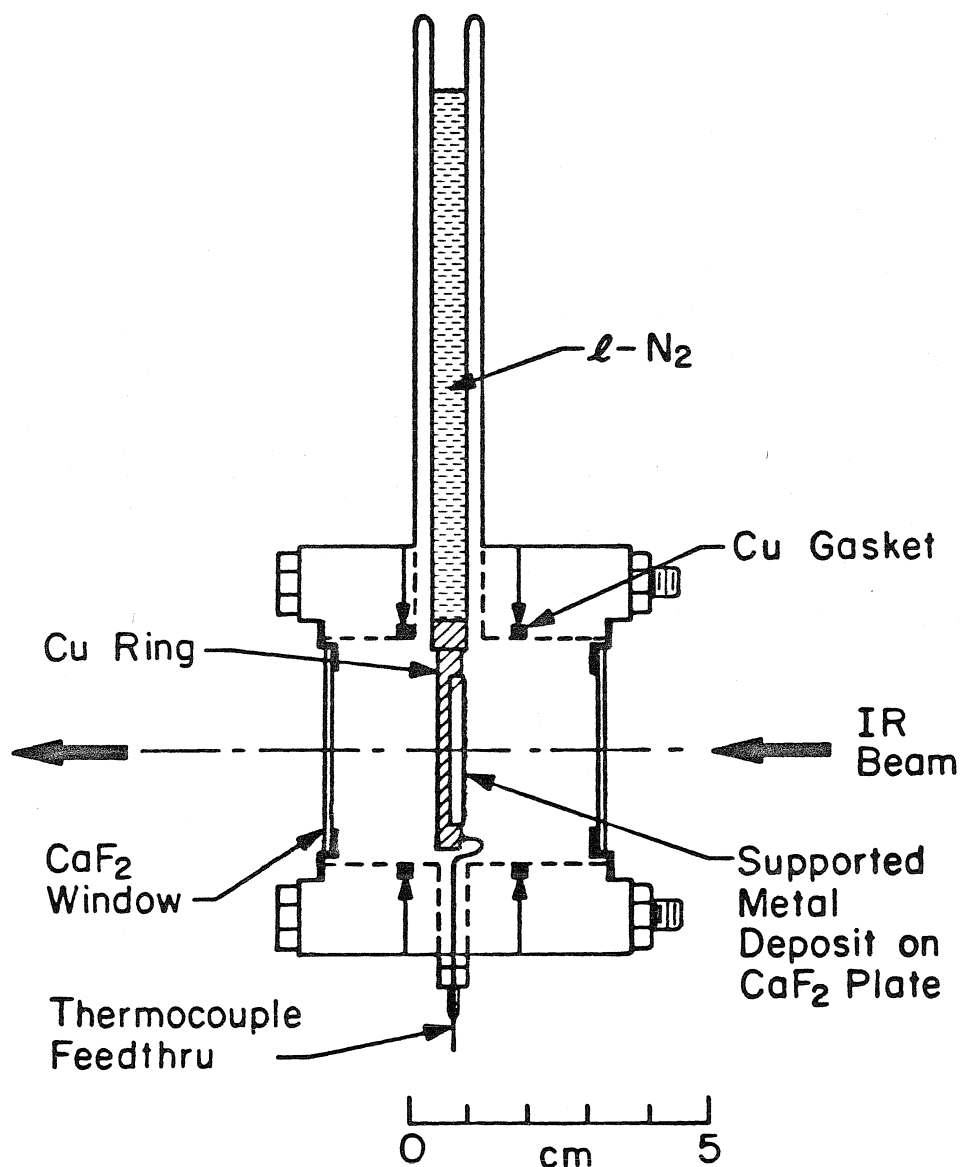


Figure 1

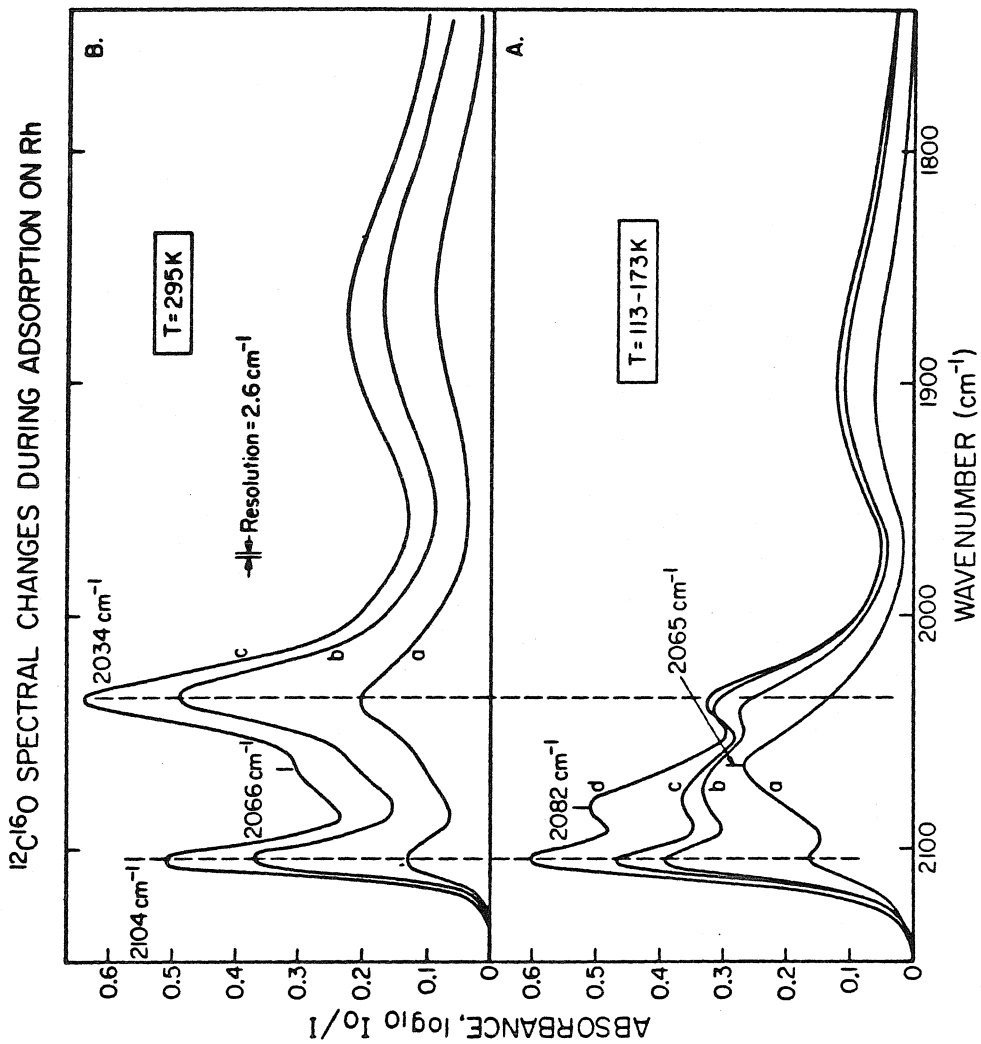


Figure 2

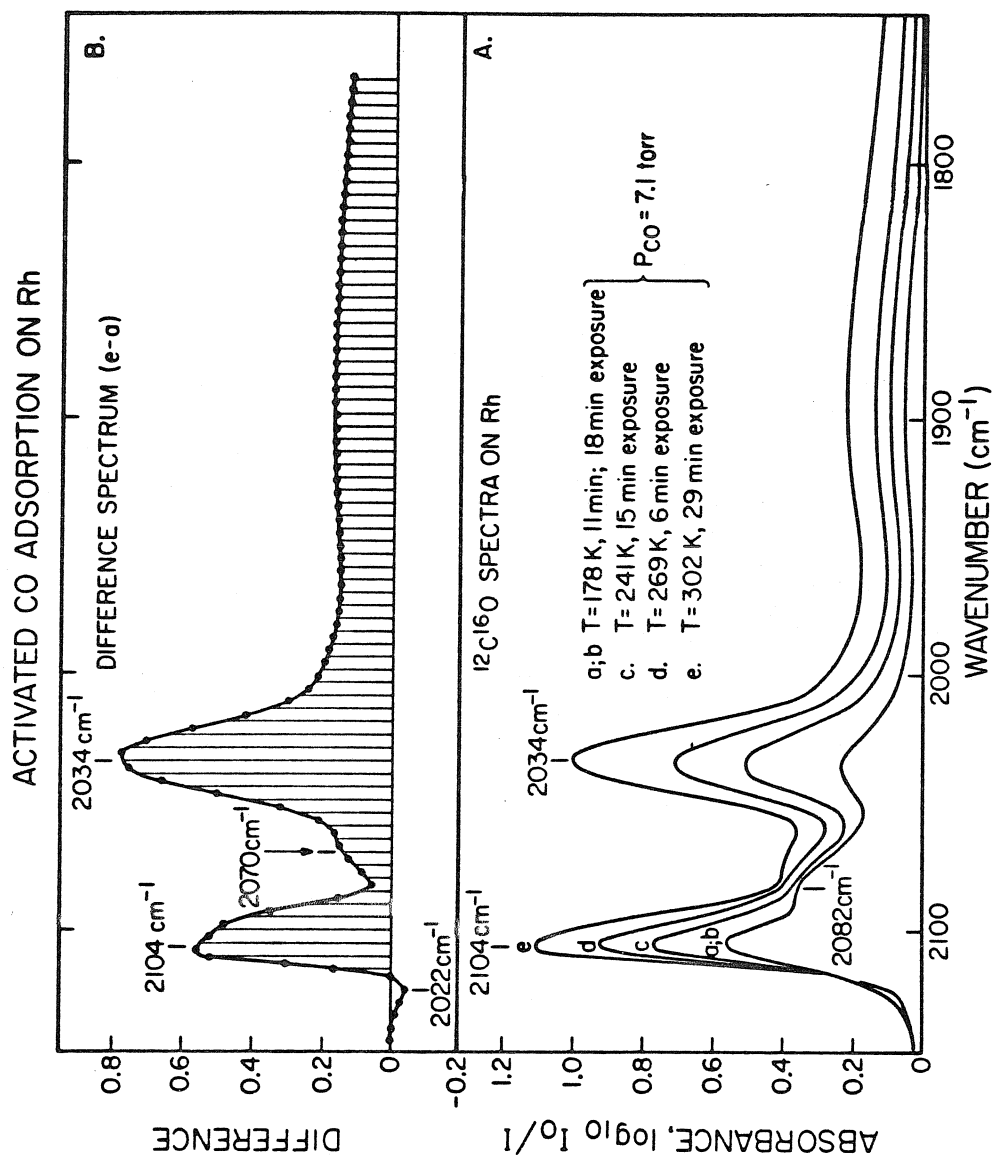


Figure 3

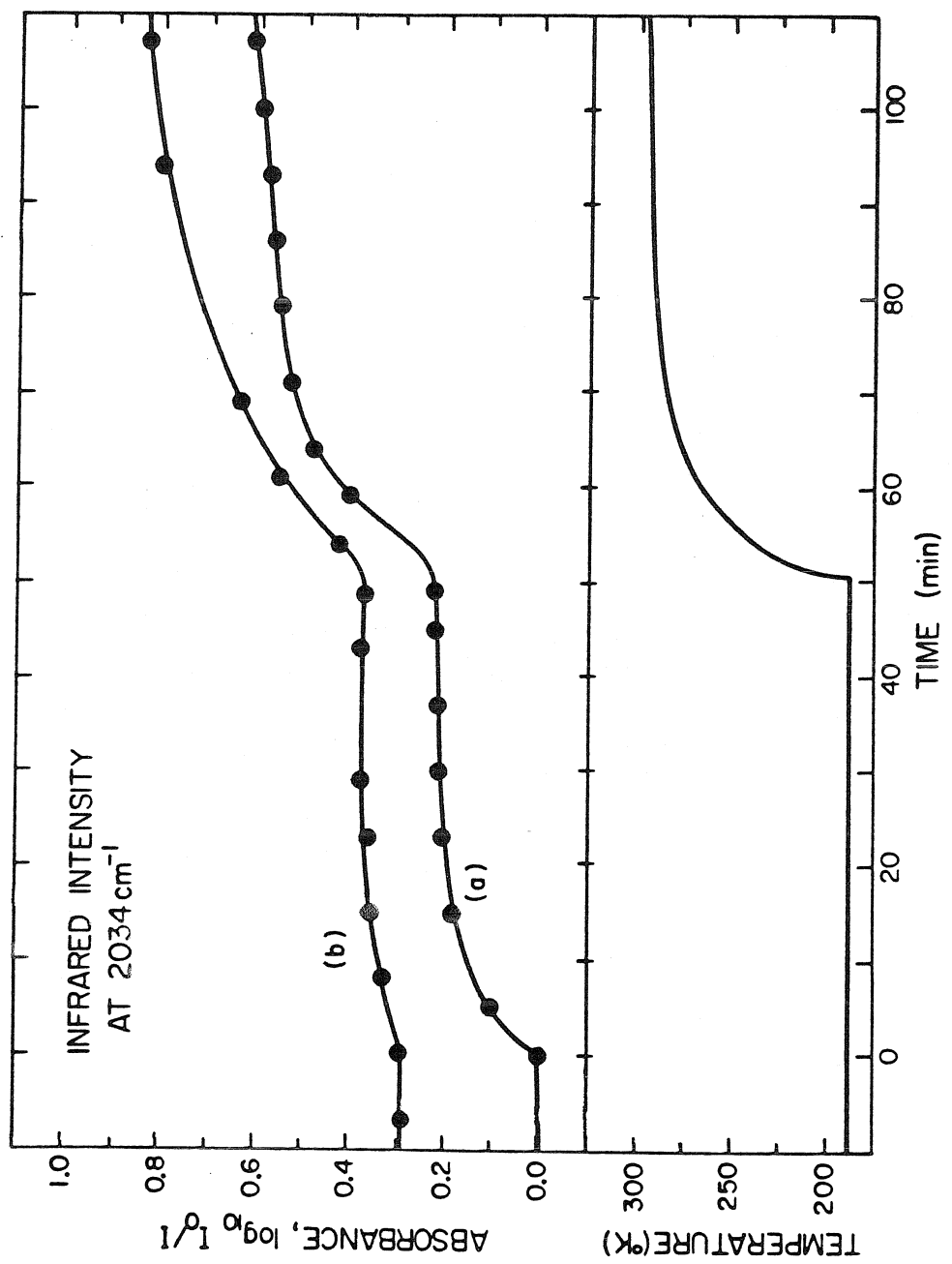


Figure 4.

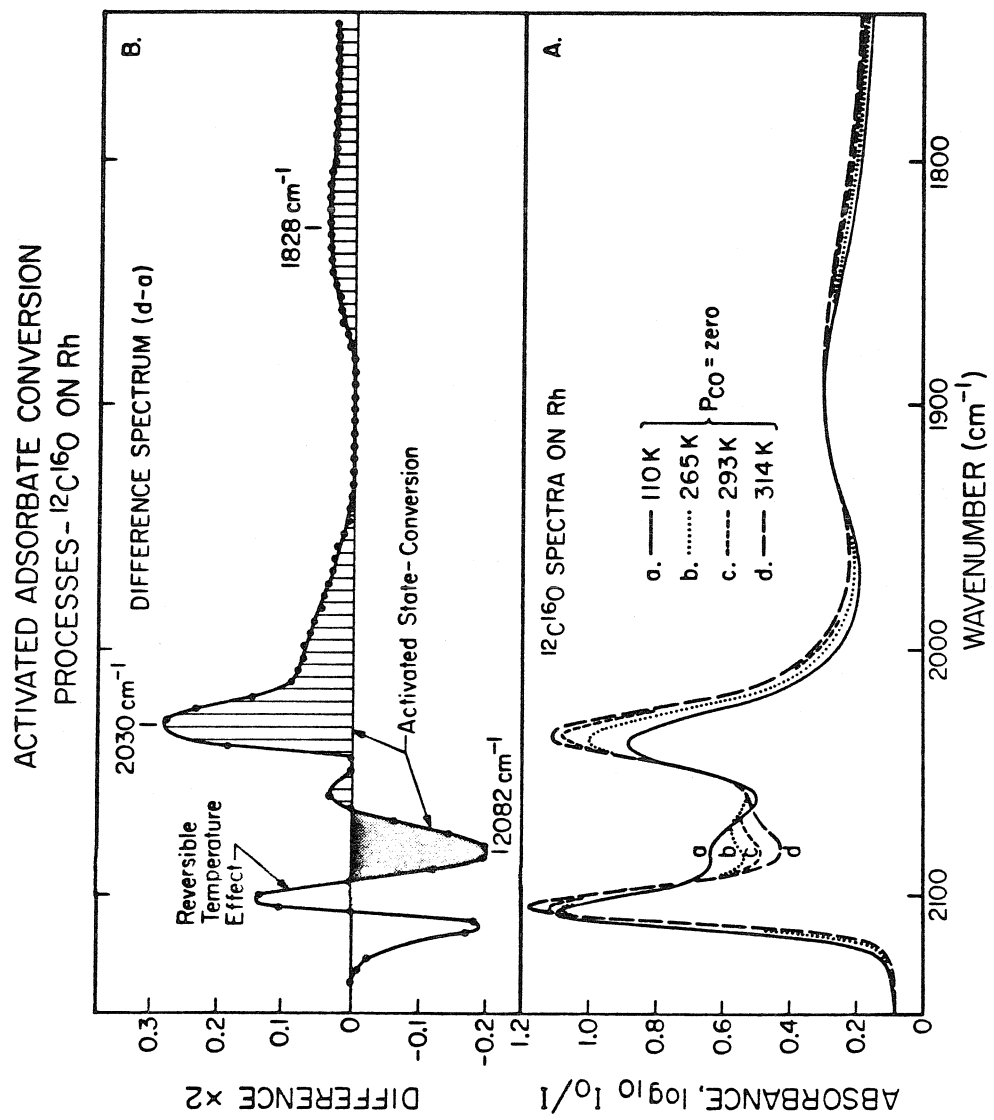


Figure 5

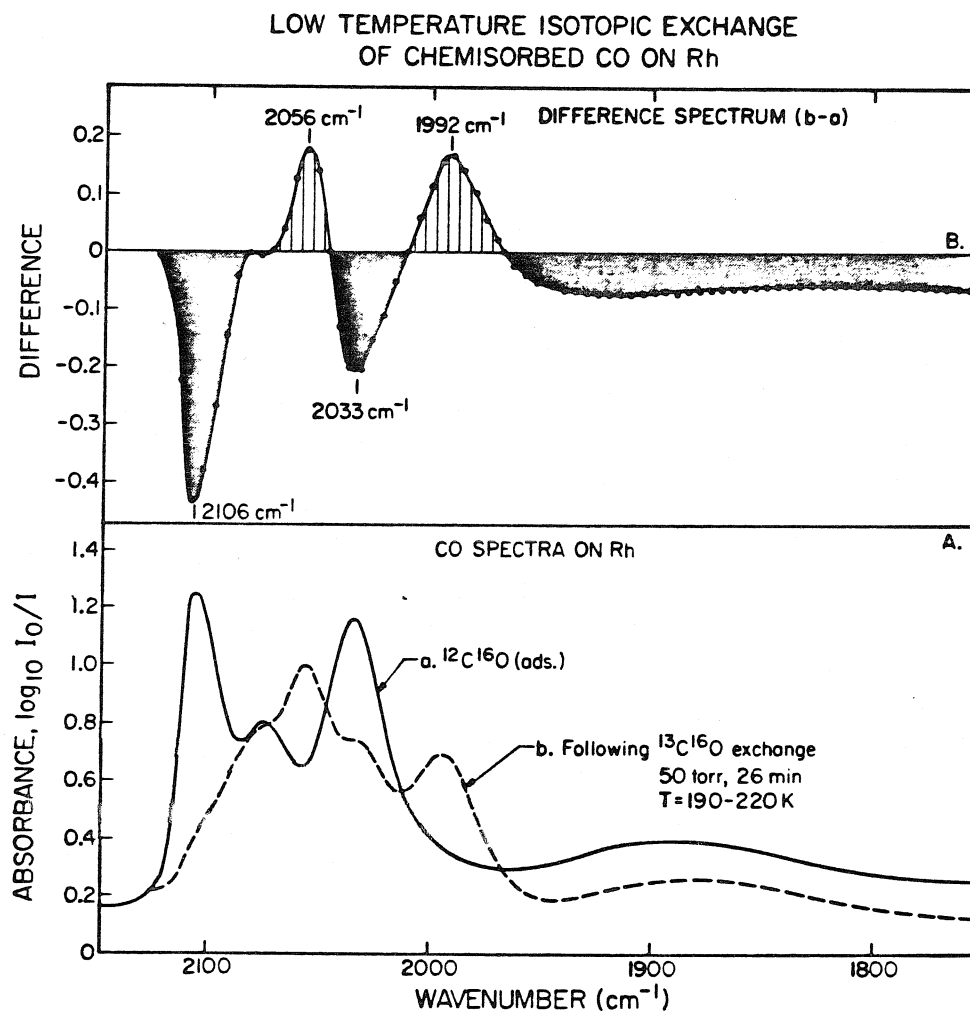


Figure 6

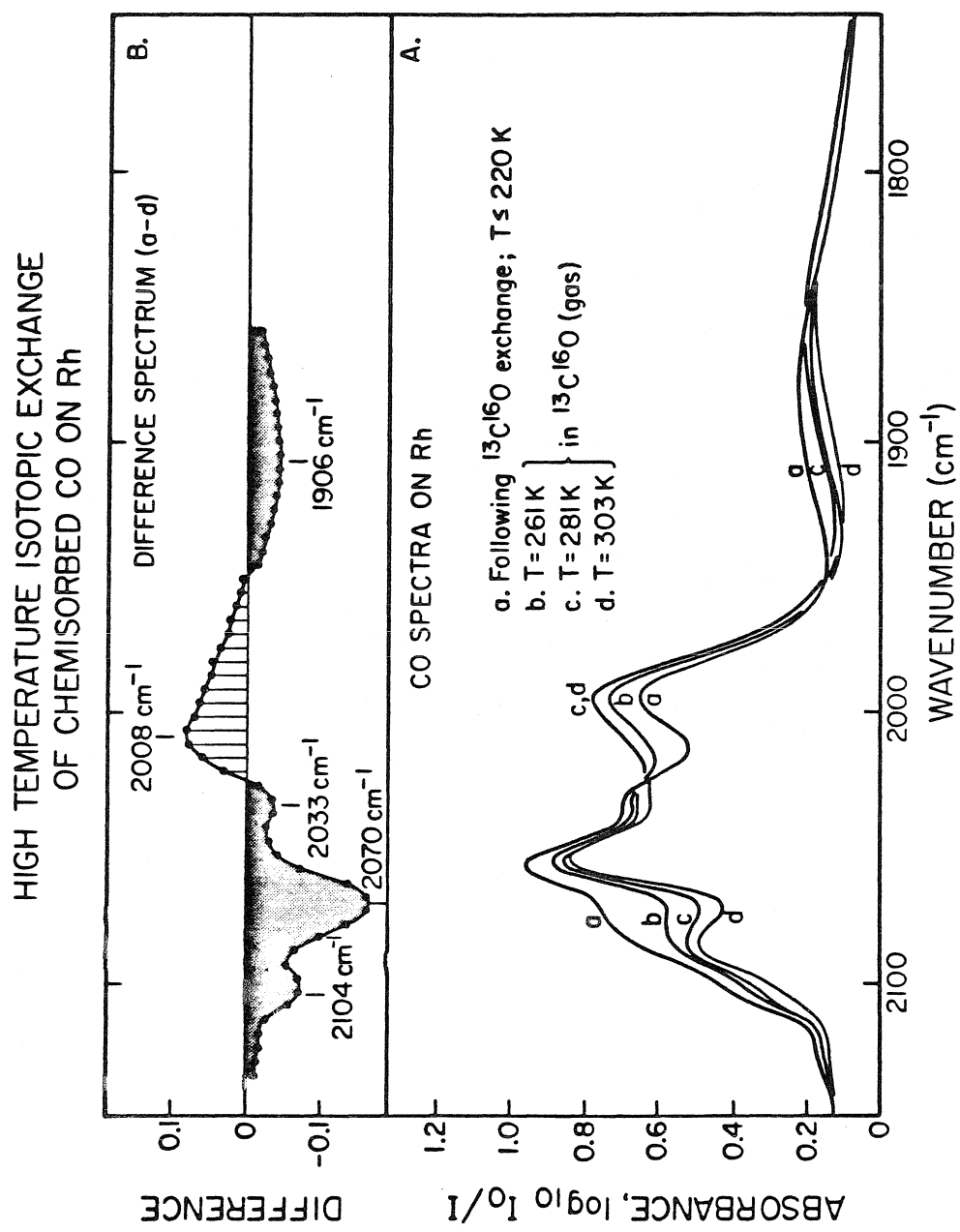


Figure 7

REVERSIBLE TEMPERATURE EFFECTS
ON INFRARED SPECTRUM- $^{12}\text{C}^{16}\text{O} + \text{Rh}$

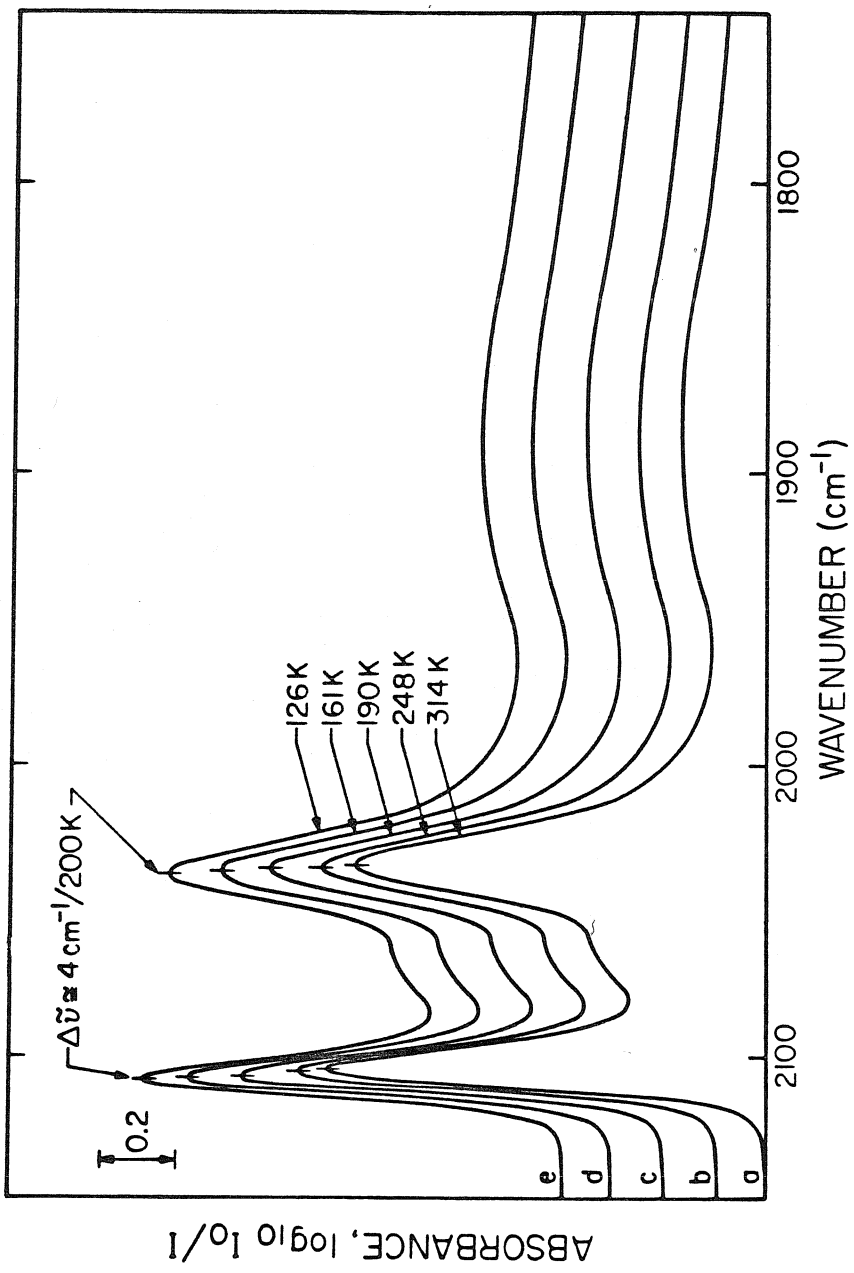


Figure 8

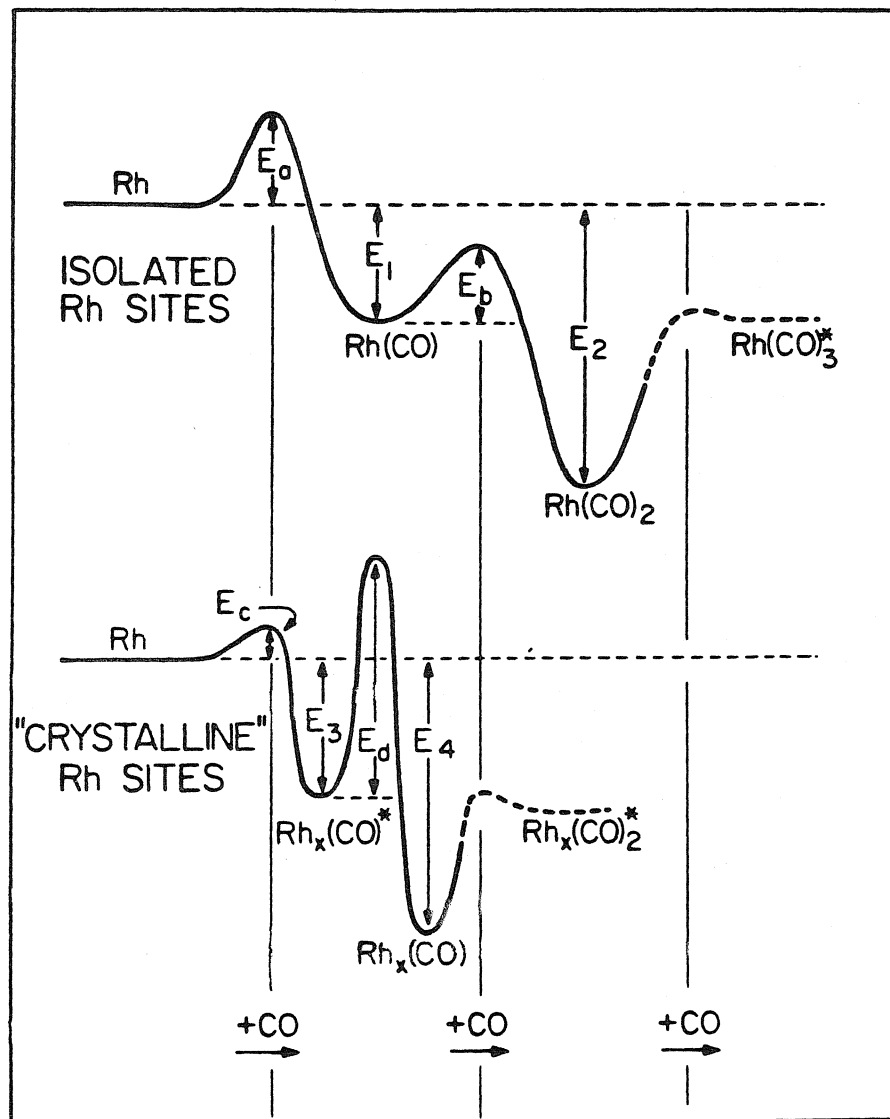


Figure 9

CHAPTER IV

AN INFRARED STUDY OF
THE DECOMPOSITION OF FORMALDEHYDE
ON Rh DISPERSED ON Al_2O_3

(Chapter IV is essentially an article by J. T. Yates, Jr., S. D. Worley, T. M. Duncan, and R. W. Vaughan, entitled "Catalytic Decomposition of Formaldehyde on Single Rhodium Atoms." This article was published in The Journal of Chemical Physics, Vol 70, No. 3, p. 1225, 1979.)

Abstract

The interaction of H_2CO with alumina-supported Rh has been studied by transmission infrared spectroscopy. It has been shown that isolated Rh atoms catalyze the decomposition of H_2CO to produce carbonyl hydride species H_xRh-CO ($x = 1,2$). Species of the type $Rh(HCO)$ and $Rh(HCOH)$ are not observed to form in detectable amounts. Hydride bonding to rhodium carbonyl species is associated with electron donation to Rh causing a decrease in $\tilde{\nu}_{CO}$ due to electron donation into $2\pi^*-CO$ orbitals. Hydride displacement by CO may occur on exposure to $CO(g)$. The conversion of the species $H-Rh(CO)_2$ to $H-Rh(CO)$ has been followed spectroscopically during desorption.

I. Introduction

The previous two chapters (1) have discussed the use of infrared spectroscopy to characterize the chemisorption of CO on highly dispersed Rh atoms supported on high-area Al_2O_3 . This work forms a foundation for the present study of formaldehyde chemisorption on similar Rh surfaces.

Rh is a very active catalyst for the production of CH_4 from $\text{H}_2 + \text{CO}$, the catalytic methanation reaction (2-4). It has been postulated (2) that intermediates such as $\text{HCO}(\text{ads})$ or $\text{HCOH}(\text{ads})$ may be involved in catalytic methanation. Therefore, in this work a spectroscopic search for these species was undertaken using H_2CO as the adsorbate. In related work on single crystals of W and Ru, it has been observed that small quantities of CH_4 are produced by thermal desorption following adsorption of H_2CO (5-10). Both W and Ru are active catalysts for the methanation reaction (11,2), and the observation of CH_4 production from H_2CO has given support to the hypothesis that intermediates derived from H_2CO may also be present in the reaction of $\text{H}_2 + \text{CO}$ to yield CH_4 .

The chemisorption of H_2CO by metals has been previously studied (5-14), but no definitive vibrational spectroscopic work has been reported for surface species derived from this molecule.

II. Experimental Procedure

The experimental apparatus and the infrared spectrometer have been described previously (1). Highly dispersed Rh supported on

Al_2O_3 was prepared as described earlier (1,4) by reduction of highly dispersed RhCl_3 on Al_2O_3 using H_2 at 425 K. $\text{H}_2\text{CO(g)}$ was prepared (5) by heating paraformaldehyde in a glass generator at 355 K, passing the gas through a glass trap at 195 K, and directly admitting the $\text{H}_2\text{CO(g)}$ to the stainless steel manifold. At H_2CO pressures as high as 5 Torr, little difficulty was encountered with polymerization loss at the vacuum system walls as judged by the constancy (~2%) of $\text{H}_2\text{CO(g)}$ pressure in the isolated manifold for times of the order of minutes. This method of producing $\text{H}_2\text{CO(g)}$ from paraformaldehyde has been checked mass-spectrometrically and was found to produce pure H_2CO (5). $\text{D}_2\text{CO(g)}$ was prepared as above from completely deuterated paraformaldehyde obtained from Merck Isotopes.

III. Experimental Results

A. H_2CO Adsorption of Rh

Figure 1A shows the spectral developments which occur as successive quantities of H_2CO are adsorbed on Rh. It may be seen that at lowest H_2CO exposures a band near 1860 cm^{-1} and a band near 2038 cm^{-1} develop. As the H_2CO exposure is increased, there is an indication of three overlapping features at 2026 cm^{-1} , 2048 cm^{-1} , and 2066 cm^{-1} , as well as a small sharp band near 2100 cm^{-1} . This spectrum is distinctly different from the spectrum of ^{12}CO on Rh (see reference 1, Figure 3), where a strong doublet feature at 2101 cm^{-1} and 2031 cm^{-1} is dominant at comparable levels of CO exposure.

It was important to determine whether Rh was acting as a

catalyst for decomposition of $H_2CO(g)$ into $H_2(g)$ and $CO(g)$. If this were true, then the spectra of Figure 1A could be attributed to competition between $H_2(g)$ and $CO(g)$ for adsorption sites, and the absence of the doublet feature obtained with pure CO could be attributed to this competition. Therefore, the experiment shown in Figure 1A was repeated on a freshly prepared Rh surface using an equimolar $H_2 + CO$ mixture instead of $H_2CO(g)$ as the adsorbate. The results are shown in Figure 1B where the dosage of the $H_2 + CO$ mixture has been made equivalent to the $H_2CO(g)$ dosage used in Figure 1A for each spectrum, a through e. Spectral developments using the $H_2 + CO$ mixture are very similar to those observed for pure CO adsorption. The major differences observed in comparison of the spectral in Figures 1A and 1B indicate that $H_2CO(g)$ does not behave in a fashion resembling $H_2(g) + CO(g)$ during chemisorption on Rh.

Since the doublet feature characteristic of pure CO adsorption on Rh was strongly retarded in its development with H_2CO as the adsorbing species, we attempted to see whether the doublet would develop by adsorbing CO following high exposures of H_2CO on Rh. This procedure caused the development of new spectral features as shown in Figure 2. Extensive development of the doublet occurs as well as some growth of features at $\sim 2060\text{ cm}^{-1}$ and 1880 cm^{-1} .

B. D_2CO Adsorption on Rh

In order to determine whether hydrogen motions exist in any of the vibrational features observed as a result of H_2CO adsorption, the adsorption of D_2CO was undertaken. These results are given in Figure 3

where the D_2CO dosages are equivalent to those used for H_2CO in Figure 1A. There is no difference in the D_2CO and the H_2CO -derived spectra. The agreement between the frequencies for H_2CO and D_2CO -derived species proves that the adsorbed species observed here do not involve hydrogen bonded to either C or O.

C. Desorption from Rh Exposed to D_2CO

Previous studies have shown that thermal desorption from pure CO layers on Rh is entirely reversible at $T \leq 336$ K (1). A similar study was performed on a Rh surface which had been exposed to D_2CO . The results shown in Figure 4 are strikingly different from the pure CO results since an interconversion between difference adsorbed species is indicated by the significant increase in absorbance near 2048 cm^{-1} as the doublet features at $\sim 2090\text{ cm}^{-1}$ and $\sim 2018\text{ cm}^{-1}$ disappear during desorption. In the lower portion of Figure 4, difference spectra are presented which clearly show this interconversion effect.

D. General Observations of H_2CO Adsorption

The infrared spectra were examined for the presence of other complexes adsorbed on the Rh on Al_2O_3 . A comparison of the adsorption of H_2CO on Rh on Al_2O_3 and on Al_2O_3 was made in the 4000 cm^{-1} to 1000 cm^{-1} region. A number of new spectral features were detected upon exposure to H_2CO but in each case the new feature was associated with H_2CO adsorption on Al_2O_3 except for those features shown in Figure 1A.

As the H_2CO was adsorbed on the substrate, there was evidence that H_2 was evolved. During the H_2CO exposures which produced the spectra a - e in Figure 1A, it was noted that the pressure within the

adsorption cell and the manifold did not decrease below ~20-30% of its initial value. Similar dosages of CO would have been accompanied by a pressure drop to ~5% of the initial pressure. It is suspected that this behavior is due to $H_2(g)$ evolution as H_2CO is decomposed on Rh.

Infrared spectra were measured in the 4000 cm^{-1} to 1000 cm^{-1} region with both ~50 Torr and ~500 Torr of H_2 above the Rh surface at 295 K. No spectral bands due to H_2 chemisorption were detected. The accuracy of these measurements is such that an absorbance change of <0.02 could have been detected easily.

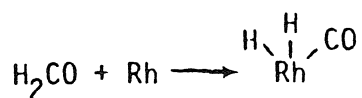
IV. Discussion

A. Assignment of IR Spectral Features - Interaction of H_2CO with Rh

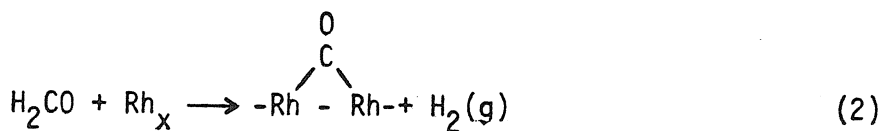
By virtue of the observation of several spectral features in the CO stretching region (and the lack of CH and OH bands) a tentative assignment of H_2CO -derived adsorbed species and their vibrational frequencies may be made (Table I).

It is proposed here that the following surface processes occur when H_2CO adsorbs on various Rh sites which are present together on the supported catalyst (1).

Isolated Rh Atom Sites

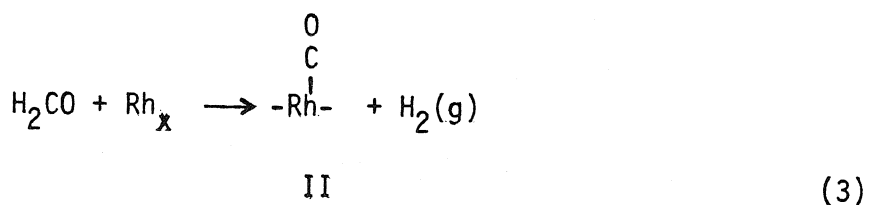


B

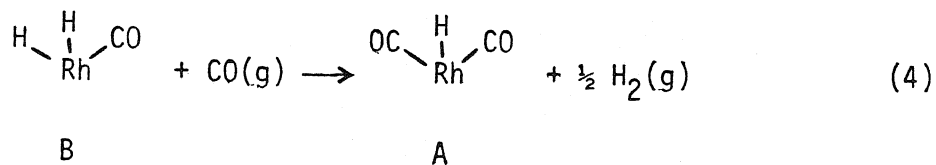
Rh_x Sites

III

and



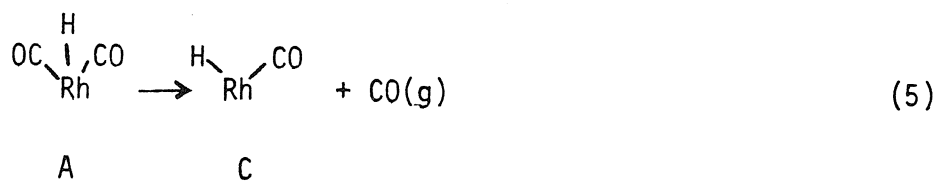
When additional CO is adsorbed on the Rh surface following H₂CO adsorption, the following hydrogen-displacement process takes place:



B

A

Finally, when thermal desorption occurs, the first step is:



A

C

This scheme of reactions will explain all of the effects observed in the experiments reported above. In particular, the observations tabulated in Table II are consistent with the above processes.

Several transition metal complexes of Rh containing the hydride and CO functional groups simultaneously, as well as other ligands, have been prepared. Thus, the proposed intermediate species A, B, and C would seem to be reasonable from a bonding point of view. It is notable that the stretching frequencies for the CO ligands and the Rh-H moiety are in the same region (ca. 2000 cm^{-1}) for these transition metal complexes (14).

It is likely that the small doublet -CO feature at 2096 cm^{-1} and 2026 cm^{-1} which was seen following exposure to $\text{H}_2\text{CO(g)}$ at ~ 5 Torr is due to traces of CO impurity produced from the H_2CO in the vacuum system or on the Rh catalyst. This CO adsorbs via process (4) converting species B to species A. Based on control studies of CO adsorption (1), approximately 3% decomposition of H_2CO at ~ 5 Torr would yield the doublet feature of comparable intensity to that measured in Figure 1A, spectrum e.

B. Absence of Detectable Surface Coverages of HCO(ads) or HCOH(ads)

The infrared spectra of HCO and DCO (the formyl radical) have been studied by others using matrix-isolation infrared spectroscopy (15). For HCO, a very intense CO stretching vibration at 1861 cm^{-1} was observed, whereas DCO gave a feature shifted to 1800 cm^{-1} . HCO also exhibited an abnormally low C-H stretching vibration at 2488 cm^{-1} (15).

We can eliminate HCO(ads) and HCOH(ads) as being present on Rh at 295 K in concentrations measurable by infrared spectroscopy on the following basis:

1. Evidence against HCO(ads) on Rh

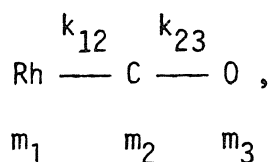
- i. No new spectral features near or below 1861 cm^{-1} were observed in comparing H_2CO with CO adsorption on Rh.
- ii. No shift in any C-O stretching vibration due to deuterium labeling of formaldehyde was observed.

2. Evidence against HCOH(ads) on Rh

- i. No new C-H or O-H stretching vibrations were observed following H_2CO adsorption on Rh.
- ii. No shift in any C-O stretching vibration due to deuterium labeling of formaldehyde was observed.

C. Vibration of the H-Rh-CO Species - Evidence for RhodiumCarbonyl Hydride Species Derived from H_2CO

Two factors must be considered in discussing the variation of $\tilde{\nu}$ -CO following the introduction of hydrogen ligands to Rh. The first of these is the mechanical effect on $\tilde{\nu}$ -CO caused by bonding of hydrogen to Rh. Effects of this kind have been considered formally by Adel (16). For the linear oscillator,



the addition of a hydrogen atom to m_1 may be considered to cause a change of $\Delta m_1 = 1 \text{ amu}$ at m_1 . For the two stretching frequencies ω_{23} and ω_{12} , the fractional shifts in frequency are given by :

$$\frac{d\omega_{23}}{\omega_{23}} = \frac{\left[\frac{-k_{12} k_{23}}{\mu_{23}} \left(\frac{dm_1}{m_1^2} \right) - \left\{ (2\pi\omega_{23})^2 + (2\pi\omega_3)^2 \right\} \left\{ -k_{12} \left(\frac{dm_1}{m_1^2} \right) \right\} \right]}{2(2\pi\omega_{23})^2 \left[(2\pi\omega_{23})^2 - (2\pi\omega_{12})^2 \right]} \quad (6)$$

and,

$$\frac{d\omega_{12}}{\omega_{12}} = \frac{\left[\frac{-k_{12} k_{23}}{\mu_{23}} \left(\frac{dm_1}{m_1^2} \right) - \left\{ (2\pi\omega_{12})^2 + (2\pi\omega_3)^2 \right\} \left\{ -k_{12} \left(\frac{dm_1}{m_1^2} \right) \right\} \right]}{2(2\pi\omega_{12})^2 \left[(2\pi\omega_{12})^2 - (2\pi\omega_{23})^2 \right]} \quad (7)$$

where k_{ij} = force constant for bond stretching (dynes cm^{-1}).

ω_{12} = "metal-carbon" stretching frequency (sec^{-1}).

ω_{23} = "carbon-oxygen" stretching frequency (sec^{-1}).

ω_3 = "bending" frequency (sec^{-1}).

$$\mu_{ij} = \frac{m_i m_j}{m_i + m_j}$$

Typical values of ω_{12} , ω_{23} , ω_3 , and k_{ij} as found for metal carbonyls (17) will be assumed. For $\tilde{\nu}_{23} \approx 2000 \text{ cm}^{-1}$, $\omega_{23} \approx 6 \times 10^{13} \text{ sec}^{-1}$; for $\tilde{\nu}_{12} \approx \tilde{\nu}_3 \approx 400 \text{ cm}^{-1}$, $\omega_{12} \approx \omega_3 \approx 1.2 \times 10^{13} \text{ sec}^{-1}$. Also, $k_{23} \approx 17 \times 10^5 \text{ dynes cm}^{-1}$, and $k_{12} \approx 3 \times 10^5 \text{ dynes cm}^{-1}$.

For $\Delta m_1 = 1 \text{ amu}$, equations (6) and (7) yield $\frac{d\omega_{23}}{\omega_{23}} = -6 \times 10^{-6}$ and $\frac{d\omega_{12}}{\omega_{12}} = +8 \times 10^{-4}$. Thus, for the addition of a single H to Rh,

$d\tilde{\nu}_{23} \approx -0.012 \text{ cm}^{-1}$ and $d\tilde{\nu}_{12} \approx 0.32 \text{ cm}^{-1}$. The mechanical effect of

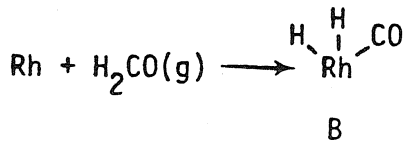
hydrogen substitution on $\tilde{\nu}_{CO}$ is therefore entirely negligible and would not be observable. Also, a deuterium isotope effect would not be seen.

The second factor concerning hydrogen addition to Rh and the resultant changes in $\tilde{\nu}_{CO}$ is the electronic influence of H ligand(s) on Rh and hence on the CO ligand. It is generally accepted that hydrogen bound to the metal atom of a carbonyl will be electron donating (18,19). This will reduce carbonyl stretching parameters. Thus, σ -donation of electrons from H to Rh would be expected to increase π -donation from the metal into the antibonding $2\pi^*$ -CO orbitals leading to a decrease in k_{23} and $\tilde{\nu}_{CO}$. Such effects might be expected to yield $\sim 10 \text{ cm}^{-1}$ downward shifts in $\tilde{\nu}_{CO}$ based on comparison of metal carbonyls containing ligands of varying electron donating ability (20). In each case in Table I where a Rh-carbonyl-hydride species is compared with its non-hydride counterpart, it is seen that $\tilde{\nu}_{CO}$ decreases by 5-10 cm^{-1} for each hydrogen ligand added. These significantly lower $\tilde{\nu}_{CO}$ values measured for H_2CO -derived species on Rh compared to CO-derived species on Rh leave little doubt that H_2CO adsorption on Rh yields carbonyl hydride species A, B, and C. There are many examples of analogous metal carbonyl hydride molecules of known structure (21).

D. Thermodynamic Estimate of the Energetics of the Reaction of H_2CO with a Rh Atom

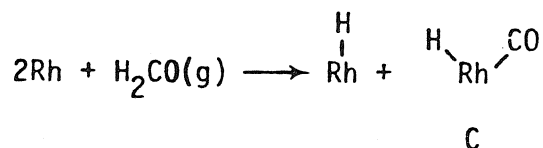
An estimate of the Rh-CO and the Rh-H bond strength can be made using desorption activation energies, E_d , from Rh single crystal surfaces. For $H_2(g)$ desorption from Rh (111), $E_d^{H_2} \approx \Delta H \approx 19 \text{ kcal}$

mole⁻¹ (22). For CO desorption from Rh(111), $E_d^{CO} \approx \Delta H \approx 32 \text{ kcal mole}^{-1}$ (23). On this basis, the bond strengths are estimated to be $E_{Rh-H} = 61.6 \text{ kcal mole}^{-1}$ and $E_{Rh-CO} = 32 \text{ kcal mole}^{-1}$. Therefore, for the reaction:



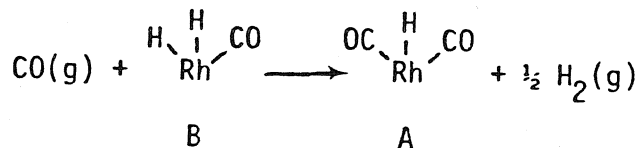
$$\Delta H_{(8)} \approx -2E_{Rh-H} - E_{Rh-CO} + D_{H_2}^0 - \Delta H_{H_2\text{CO(g)}}^f = -23 \text{ kcal mole}^{-1}$$

For the reaction:



$$\Delta H_{(9)} \approx -23 \text{ kcal mole}^{-1}.$$

For the ligand exchange process:



$$\Delta H_{(10)} \approx E_{Rh-H} - E_{Rh-CO} - \frac{1}{2} D_{H_2}^0 = -23 \text{ kcal mole}^{-1}$$

Thus, all of the spontaneous processes observed in this work are expected to be exothermic and probably irreversible at 295 K and at the pressures employed here.

These thermodynamic estimates are inexact for two reasons:

- (1) an isolated Rh atom will differ in its energetics from a

Rh atom in a single crystal; and

(2) additivity of bond energies is an inexact approximation.

However, for the higher values of $E_{\text{Rh-H}}$ and $E_{\text{Rh-CO}}$ expected for an isolated Rh atom compared to a Rh atom in a crystal, the exothermicity of processes 8, 9, and possibly 10 will increase.

V. Summary

The following features of H_2CO dissociative chemisorption on isolated Rh atoms have been found:

1. H_2CO chemisorbs dissociatively on isolated Rh atoms to produce carbonyl-hydride species containing a single CO ligand and one or two H ligands.
2. $\text{HCOH}(\text{ads})$ and $\text{HCO}(\text{ads})$ species are not observed to form from H_2CO on Rh at 295 K.
3. Hydride bonding to Rh-carbonyl species is associated with electron donation to the Rh causing a decrease in $\tilde{\nu}_{\text{CO}}$ in accordance with expectations for electron donation into $2\pi^*-\text{CO}$ orbitals.
4. Hydride displacement by CO ligands may occur on Rh-carbonyl-hydride species by exposure to $\text{CO}(\text{g})$ at 295 K.
5. Thermal desorption from $\text{OC}-\begin{smallmatrix} \text{H} \\ \diagup \\ \text{Rh} \\ \diagdown \\ \text{CO} \end{smallmatrix}$ involves loss of CO to yield $\begin{smallmatrix} \text{H} \\ \diagup \\ \text{Rh} \\ \diagdown \\ \text{CO} \end{smallmatrix}$.
6. H_2CO interaction with supported Rh atoms involves specific bond-breaking and new bond formation which cannot be achieved by coadsorption of equimolar mixtures of H_2 and CO.

VI. Acknowledgment

The authors gratefully acknowledge support from QNR under contract N00014-77-F-0008 and N00014-75-C-0960. We thank Professor George R. Rossman for his kindness in allowing us to use his infrared spectrometer.

References

1. (a) J. T. Yates, Jr., T. M. Duncan, S. D. Worley, and R. W. Vaughan, J. Chem. Phys. 70, 1219 (1979); (b) J. T. Yates, Jr., T. M. Duncan, and R. W. Vaughan, J. Chem. Phys. 71, 3908 (1979).
2. G. A. Mills and F. W. Steffan, Catalysis Rev. - Sci. Eng. 8, 159 (1973).
3. B. Sexton and G. A. Somorjai, J. Catalysis 44, 439 (1976).
4. A. C. Yang and C. W. Garland, J. Phys. Chem. 61, 1504 (1957).
5. J. T. Yates, Jr., T. E. Madey, and M. J. Dresser, J. Catalysis 30, 260 (1973).
6. J. T. Yates, Jr., N. E. Erickson, S. D. Worley, and T. E. Madey, in The Physical Basis for Heterogeneous Catalysis, eds. E. Drauglis and R. I. Jaffee (Plenum Press, 1975), p. 75.
7. S. D. Worley, N. E. Erickson, T. E. Madey, and J. T. Yates, Jr., J. Electron Spec. 9, 355 (1976).
8. J. T. Yates, Jr., T. E. Madey, N. E. Erickson, and S. D. Worley, Chem. Phys. Letters 39, 113 (1976).
9. S. D. Worley and J. T. Yates, Jr., J. Catalysis 48, 395 (1977).
10. D. W. Goodman, T. E. Madey, M. Ono, and J. T. Yates, Jr., J. Catalysis 50, 279 (1977).
11. R. D. Kelley, T. E. Madey, and J. T. Yates, Jr., J. Catalysis 50, 301 (1977).
12. J. F. Harrod, R. W. Roberts, and E. F. Rissman, J. Phys. Chem. 71, 343 (1967).
13. L. Kubelkova, P. Jiru, and P. Schurer, Collect. Czech. Chem. Comm.

34, 3942 (1969).

14. For example, see S. S. Bath and L. Vaska, *J. Amer. Chem. Soc.* 85, 3500 (1963); D. Evans, G. Yagupsky, and G. Wilkinson, *J. Chem. Soc. A* 2660, 2665 (1968); L. Vallarino, unpublished data.
15. D. Milligan and M. Jacox, *J. Chem. Phys.* 41, 3032 (1964).
16. A. Adel, *Phys. Rev.* 45, 56 (1934).
17. For an example, see R. S. McDowell, W. D. Horrocks, Jr., and J. T. Yates, Jr., *J. Chem. Phys.* 34, 530 (1961).
18. F. A. Cotton and G. Wilkinson, Advanced Inorganic Chemistry, Interscience Publishers, John Wiley (1962), pp.631-637.
19. P. S. Braterman in Structure and Bonding, Vol. 26, Eds. J. D. Dunitz, et al., Springer-Verlag, Berlin (1976), p.32.
20. For several examples of the effect of various substituents on metal carbonyl spectra, see T. L. Brown and D. J. Darensbourg, *Inorg. Chem.* 6, 971 (1967).
21. For example, see P. S. Braterman, R. W. Harrill, and H. D. Kaesz, *J. Amer. Chem. Soc.* 89, 2851 (1967).
22. J. T. Yates, Jr., P. A. Thiel, W. H. Weinberg, *Surface Sci.* 84, 427 (1979).
23. P. A. Thiel, E. D. Williams, J. T. Yates, Jr., and W. H. Weinberg, *Surface Sci.* 84, 54 (1979).

TABLE I

Assignment of IR Spectral Features for
 Species Produced by H_2CO or CO on Rh

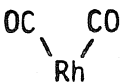
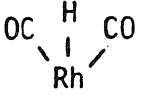
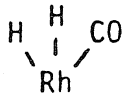
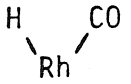
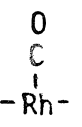
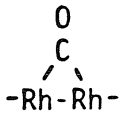
<u>Species</u>	<u>Wavenumber (cm^{-1})</u>	<u>Designation</u>
	2101 (sym) 2031 (asym)	I (ref. 1)
	~2092 (sym) ~2025 (asym)	A
	~2038	B
	~2048	C
	2058 - 2070	II (ref. 1)
	~1860	III (ref. 1)

TABLE II
Spectroscopic Observations for H_2CO Adsorption on Rh

<u>Observation</u>	<u>Rationale</u>
1. Lack of intense doublet-CO bands with H_2CO as adsorbate in contradistinction to pure CO adsorption.	1. Process (1) yields species B; CO adsorption yields species I.
2. Presence of species associated with lower $\bar{\nu}$ -CO-singlet-bands than pure CO will produce.	2. Process (1) yields species B; CO adsorption yields species II.
3. <u>Shifted</u> doublet produced by CO adsorption following H_2CO adsorption.	3. Process (4) yields species A; CO adsorption yields species I.
4. Interconversion of doublet-CO species to species with $\bar{\nu}$ -CO near 2048 cm^{-1} as desorption occurs	4. Process (5) yields species C as species A loses a CO ligand.
5. Presence of an 1860 cm^{-1} species following H_2CO adsorption.	5. Process (2) occurs for both H_2CO and CO adsorption.
6. Evolution of H_2 during H_2CO adsorption/decomposition on Rh.	6. Processes (2), (3), and (4) occur for H_2CO adsorption, yielding $H_2(g)$.

Figure Captions

Figure 1: Comparison of adsorption from H_2CO and equimolar $H_2 + CO$ on Rh.
 $T = 295$ K.

A. H_2CO Adsorption

Spectrum (a). 1.04×10^{18} H_2CO molecules added
 Spectrum (b). 1.05×10^{18} H_2CO molecules added
 Spectrum (c). 2.12×10^{18} H_2CO molecules added
 Spectrum (d). 2.63×10^{18} H_2CO molecules added
 Spectrum (e). 5.21×10^{18} H_2CO molecules added.

B. Equimolar $H_2 + CO$ Adsorption

Spectrum (a). 1.11×10^{18} $H_2 + CO$ molecules added
 Spectrum (b). 1.09×10^{18} $H_2 + CO$ molecules added
 Spectrum (c). 2.36×10^{18} $H_2 + CO$ molecules added
 Spectrum (d). 2.75×10^{18} $H_2 + CO$ molecules added
 Spectrum (e). 5.19×10^{18} $H_2 + CO$ molecules added

Figure 2. Site filling by CO following full coverage from H_2CO . $T = 295$ K.

Spectrum (a). Full coverage H_2CO followed by 60 minutes pumping.
 Spectrum (b). Addition of ~50 torr CO to (a).

Figure 3. D_2CO adsorption on Rh. $T = 295$ K.

Spectrum (a). 1.02×10^{18} D_2CO molecules added
 Spectrum (b). 1.08×10^{18} D_2CO molecules added
 Spectrum (c). 2.08×10^{18} D_2CO molecules added
 Spectrum (d). 2.62×10^{18} D_2CO molecules added
 Spectrum (e). 5.25×10^{18} D_2CO molecules added

Figure 4. Desorption from Rh exposed to D_2CO

Spectrum (a). Full coverage of D_2CO

Spectrum (b). Follows 120 hours desorption at 295 K

Spectrum (c). Follows additional 9 hours desorption at 316 K

Lower section. Difference spectra obtained by spectrum subtraction as shown

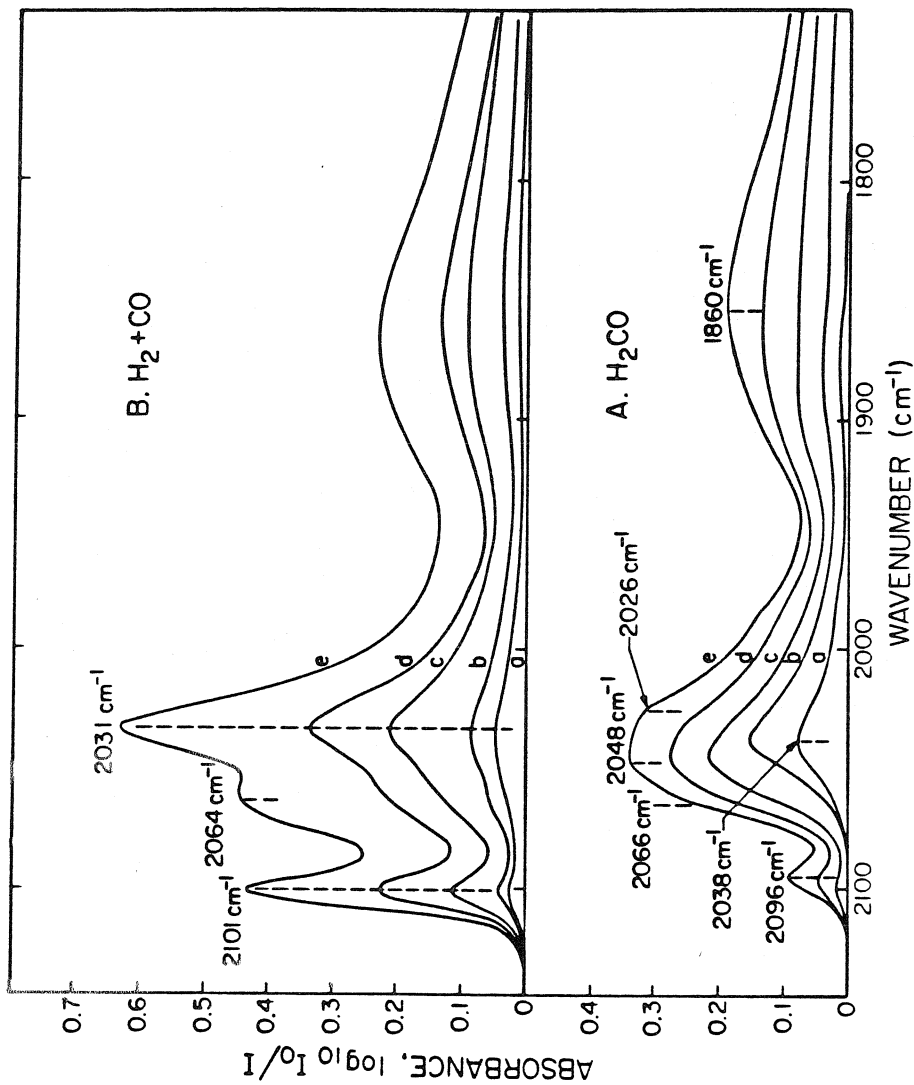
COMPARISON OF ABSORPTION FROM H_2CO AND EQUIMOLAR $\text{H}_2\text{+CO}$ ON Rh.

Figure 1

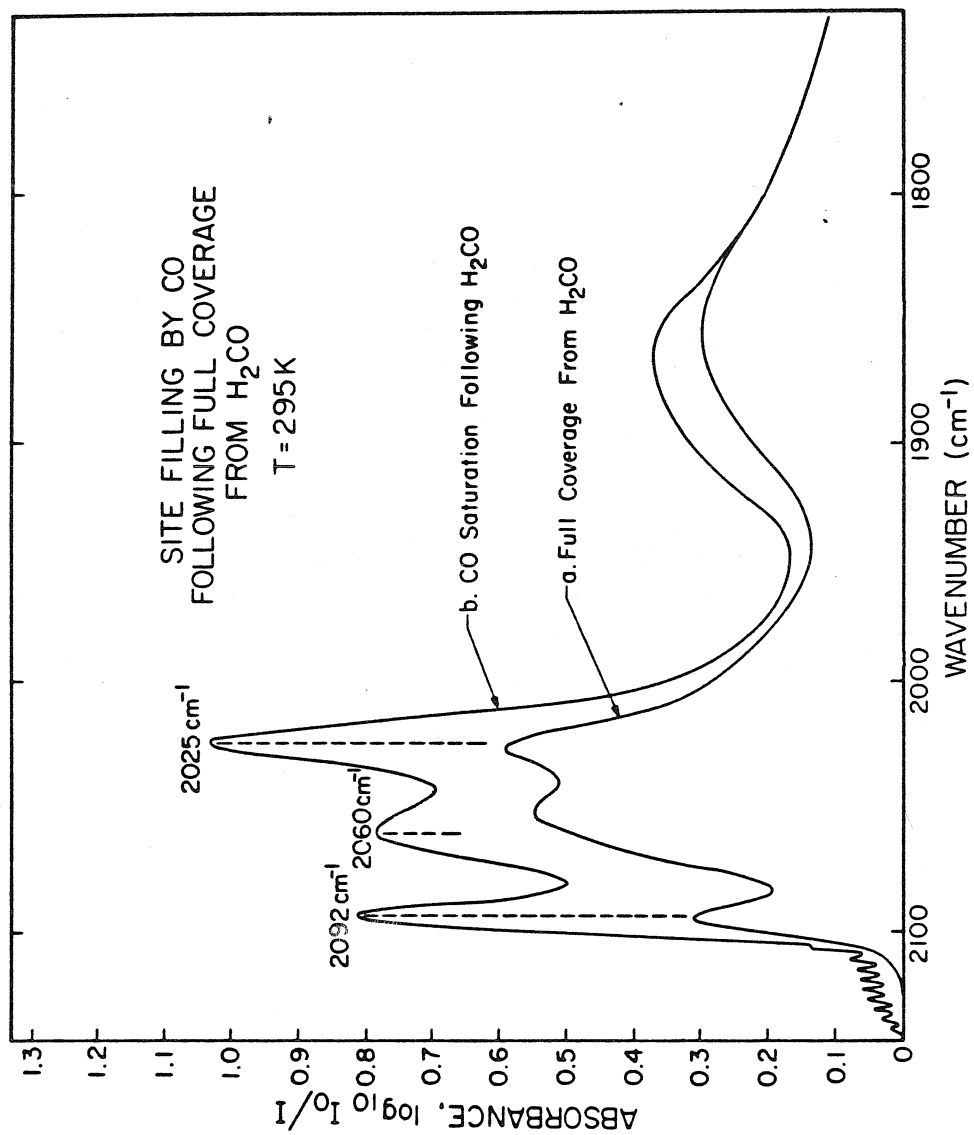


Figure 2

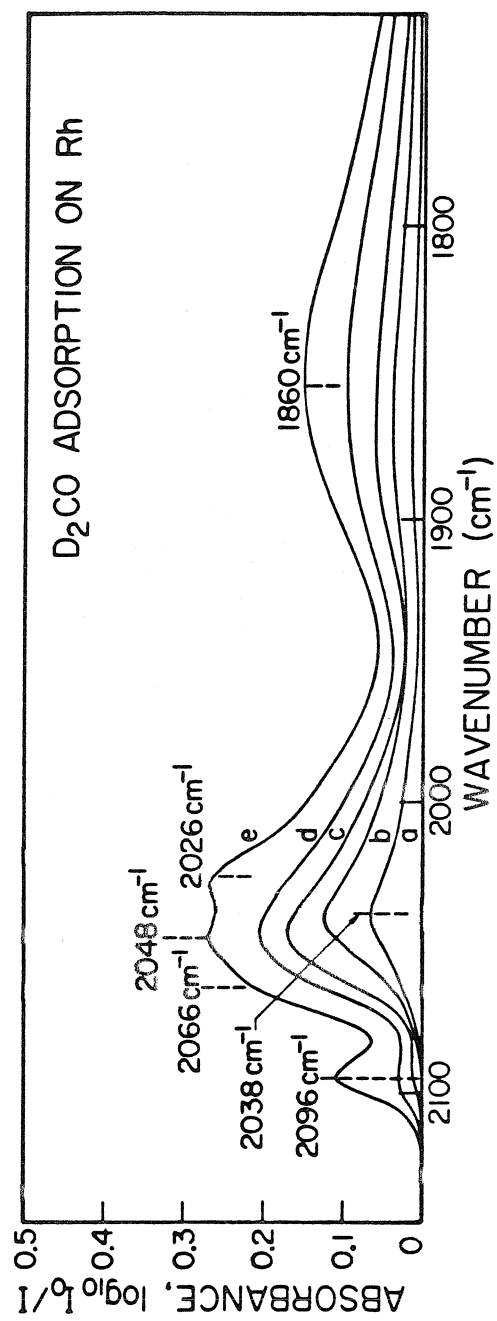


Figure 3

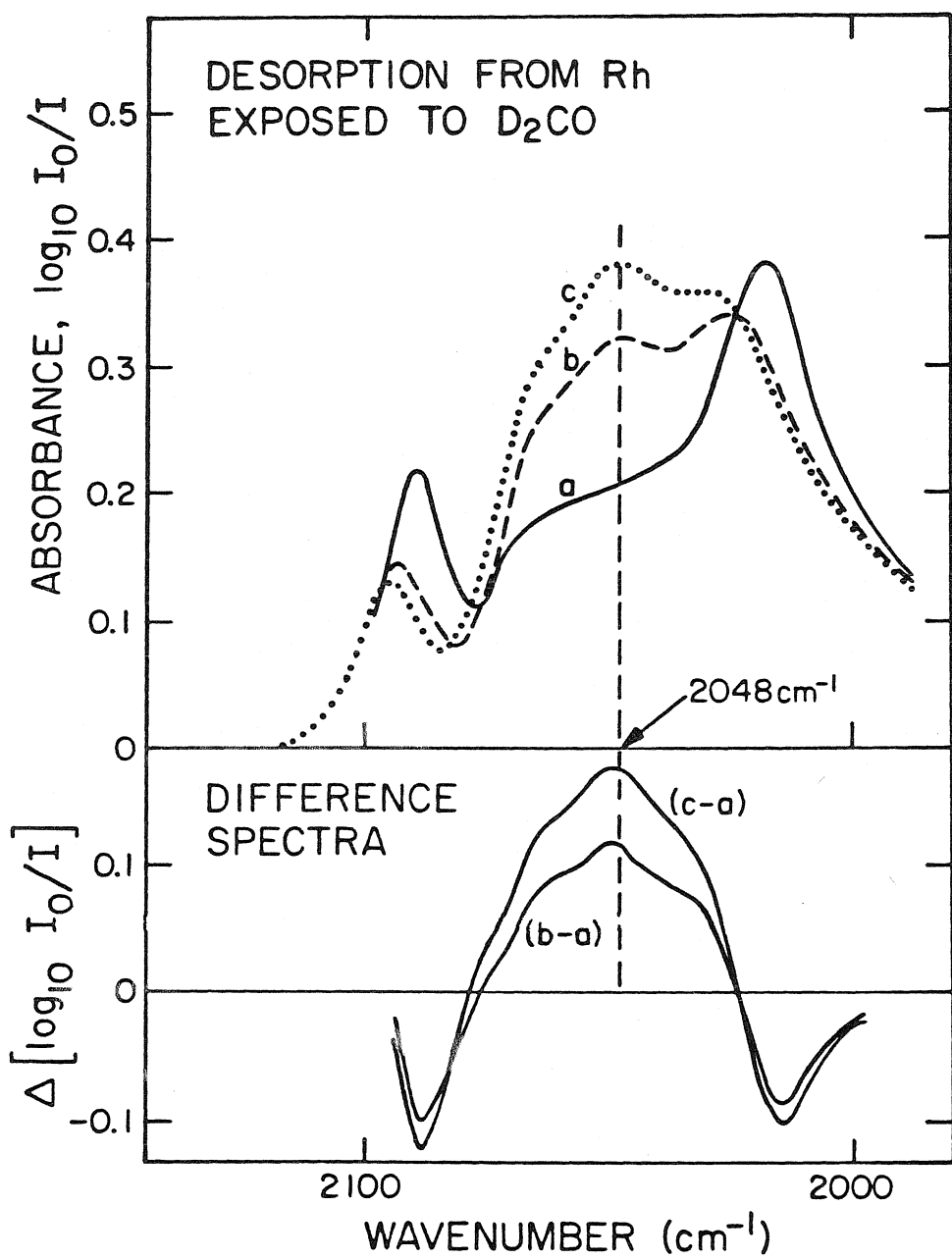


Figure 4

CHAPTER V

A ^{13}C NUCLEAR MAGNETIC RESONANCE STUDY
OF THE ADSORPTION OF CO
ON Rh DISPERSED ON Al_2O_3

(Chapter V is essentially an article by T. M. Duncan, J. T. Yates, Jr., and R. W. Vaughan, entitled "A ^{13}C NMR Study of the Adsorbed States of CO on Rh Dispersed on Al_2O_3 ." This article has been submitted for publication in The Journal of Chemical Physics.)

ABSTRACT

The results of nuclear magnetic resonance (NMR) spectroscopy have been analyzed with respect to previous infrared studies of CO adsorbed on Rh dispersed on Al_2O_3 to quantify the site distribution and to describe the adsorbed state. The ^{13}C NMR spectra account for all the ^{13}CO adsorbed on a 2.2% Rh on Al_2O_3 substrate. Although the spectra from the different adsorbed states of CO overlap, the lineshapes may be separated into two components based on differences in the ^{13}C spin-lattice relaxation times. These two components have been assigned to the ^{13}CO dicarbonyl formed on single Rh atoms and to ^{13}CO adsorbed on Rh rafts. The component attributed to the CO adsorbed on the raft sites is further separated into linear and bridged CO state contributions based on chemical shift information, yielding a quantitative distribution of the three adsorbed states of CO on Rh. The ^{13}CO distribution is used to estimate the molar integrated intensities of the infrared spectrum of ^{13}CO on Rh at high coverage and to determine the degree of dispersion of Rh on the Al_2O_3 . The ^{13}C NMR lineshapes of CO adsorbed on Rh are different from the powder pattern of $\text{Rh}_2\text{Cl}_2(\text{CO})_4$. The lineshapes of the dicarbonyl surface species is narrowed to a Lorentzian curve by reorientation at the site and the lineshape of CO on the Rh rafts is modulated by exchange between sites on a single raft. The ^{13}C relaxation time distribution provides further evidence for the existence of isolated Rh atoms on the Al_2O_3 surface.

I. INTRODUCTION

The adsorption of molecules on transition metals dispersed on oxide supports has been studied extensively by transmission infrared spectroscopy (1,2). More recently, inelastic electron tunneling spectroscopy has improved the sensitivity and extended the spectral range of the vibrational studies (3). High resolution solid state nuclear magnetic resonance (NMR) spectroscopy (4-6) has been applied to the study of molecules adsorbed on high area surfaces (7,8). NMR spectra are sensitive to molecular motions on the order of the linewidth, which is typically 10 to 10^4 Hz for chemisorbed molecules. Motions such as surface diffusion or hindered rotation are usually in this frequency range. Since the integrated intensity of the NMR spectrum is linearly proportional to the concentration, it is possible to calculate absolute site populations. The synergistic combination of vibrational and NMR spectroscopies provides a unique tool for the characterization of the nature of the adsorbed molecule. The ^{13}C NMR study of CO adsorbed on supported Rh has only recently been reported (9) and represents the first example of the use of this technique to study chemisorption on dispersed metals. Such systems are difficult to study mainly because the dilute spins yield an extremely weak resonance signal. We report here a more detailed ^{13}C NMR study of the adsorbed states of CO on Rh dispersed on Al_2O_3 .

In dilute ^{13}C spin systems, the homonuclear dipolar broadening is weak; thus, the major effects observed in the NMR spectra are the chemical shift interaction and the heteronuclear broadening. Two

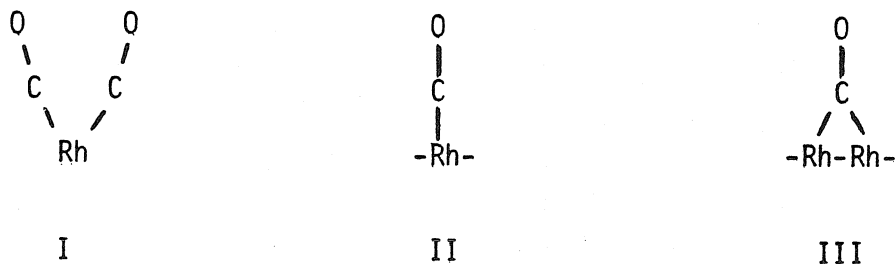
features of the chemical shift interaction are most useful in characterizing the ^{13}C electronic environment. The average resonant frequency, or the center of mass, of the lineshape can be compared with the chemical shifts of known compounds for identification in a finger-printing fashion. The center of mass of a species is independent of the motional properties of the molecule; thus, the broad line of a solid has the same center of mass as a rapidly reorienting liquid, provided there are no chemical changes in the phase transition. Second, the principal components of the second rank chemical shift tensor are good indicators of the molecular symmetry and the degree of anisotropy of the electron distribution. Various molecular motions, such as wagging, rotation, or diffusion, will uniquely modulate the rigid chemical shift powder pattern. Although there exist reasonable calculations to predict trends in isotropic chemical shifts within a group, such as alkanes, alkenes, or carbonyls, there is at present no general theory to cover the entire range of carbon compounds (10-12). Thus, to date the chemical shift data has been analyzed in a correlative fashion. To investigate the nature of an unknown surface species, it is necessary to study the chemical shift powder pattern of a number of related, well-defined compounds. In addition, the specific modulation of the characteristic chemical shift tensor by molecular reorientation provides information on the frequency and the nature of the motion (5). The major heteronuclear dipolar interactions for the ^{13}C nuclei in the Rh on Al_2O_3 system are with the ^{27}Al of the support, the ^1H of the hydroxyls and adsorbed water, and the ^{103}Rh . However, because of large internuclear distances

between ^{13}C and ^{27}Al or ^1H and the low gyromagnetic ratio of ^{103}Rh , each of these interactions is predicted to be much less than the chemical shift anisotropy.

The spin-lattice relaxation time, T_1 , of surface adsorbed molecules may also be used to characterize the local environment on the substrate (7,8). In general, the relaxation is determined by local magnetic fields fluctuating at rates near the Larmor frequency of the nucleus of interest. Thus, the T_1 of the nucleus of interest is affected by dipolar interactions with neighboring unpaired electrons or other nuclei with magnetic moments, exchange between adsorption sites with different anisotropic shieldings, or librations through chemical shift orientational anisotropy. Under certain conditions (8), a measurement of the T_1 as a function of temperature can be used to determine the correlation time for molecular reorientation or diffusion, average internuclear distances, and the heterogeneity of the distribution of adsorption sites on the surface, i.e., isolated or clustered. In some dilute spin systems, less than $\sim 10^{20}$ spins/cm³, there may exist a nonuniform distribution of T_1 's, resulting from an angular distribution of axes of reorientation or local concentration of adsorbates and paramagnetic centers. In these cases, it may be possible to use the T_1 distribution to differentiate between dissimilar adsorbed species.

The adsorption of CO on Rh dispersed on Al_2O_3 has been studied extensively by infrared spectroscopy (13-17) combined with electron microscopy (18), and by inelastic electron tunneling spectroscopy (19). The infrared results were reviewed briefly in previous papers (14,15),

The three generally accepted states of CO on Rh dispersed on Al_2O_3 , originally proposed by Yang and Garland (13), are a dicarbonyl site (species I), a linearly bonded CO (species II), and a multi-bonded bridging CO (species III).



Species II and III are believed to form on Rh atoms congregated into small rafts or islands on the Al_2O_3 support (13,14,17,18). There is some controversy as to the nature of species I. It is maintained by some workers (18) that the dicarbonyl species form on the edge atoms of Rh rafts, while others (13,14,17) suggest that these Rh sites exist as isolated atoms on the surface. This topic will be addressed later in this work. It has been found that the rate of isotopic exchange (15) and the chemical reactivity and selectivity of the Rh responsible for sites II and III are different from the Rh in species I (16,20,21). Thus, it would be useful to know the absolute populations of the two states.

II. EXPERIMENTAL PROCEDURES

The samples of Rh dispersed on Al_2O_3 were treated and analyzed

in a combined infrared/NMR cell. The infrared cell, a stainless steel body with single-crystal CaF_2 windows, as well as the all-metal 10^{-8} Torr vacuum system have been described previously (14). The infrared cell was modified to accommodate NMR samples by welding a $\frac{1}{4}$ in. I.D. stainless steel fitting to a port drilled in a central section of the cell. The NMR sample tubes attached to this port consist of a stainless steel Cajon VCR fitting welded to a copper tube fused to 10 mm O.D. pyrex glass. The NMR tube may be permanently detached from the cell by pinching off the copper section to form an ultrahigh-vacuum cold-welded seal. This separation does not perturb the vacuum integrity in either section. The total dead volume of the cell is $\sim 50 \text{ cm}^3$.

The infrared scans were recorded in the absorbance mode on a Perkin-Elmer 180 grating spectrometer operated in the double beam option. Calibration procedures using CO(g) and $\text{H}_2\text{CO(g)}$ were described previously (14). The spectral resolution in the 2000 cm^{-1} region was set at 2.6 cm^{-1} .

The NMR spectra were taken on a 1.32 Tesla spectrometer described previously (22), stabilized with an external pulsed lock system to drifts of less than 1 ppm over an 8-hour period. The single resonance probe is tuned to 14.175 MHz with a 10 mm I.D., 14 mm long coil. The coil is enclosed in a glass dewar, and the sample temperature is lowered by drawing LN_2 past the coil with a small roughing pump. The NMR spectra were obtained by Fourier transforming the free induction decay after 90° pulse. A 180° prepulse was applied at time τ before the

90° pulse to every other decay, and the transients were alternately added and subtracted to eliminate instrumental artifacts. Also, the longitudinal relaxation time, T_1 , of the sample may be determined by the intensity of the magnetization as a function of τ (23). The field strengths for the 90° and 180° pulses are 78 and 70 gauss, or 84 and 75 KHz for ^{13}C nuclei, respectively, sufficient to satisfy the criterion for nonselective pulses (24). The ^{13}C NMR spectra of the adsorbed CO reported here are the accumulation of at least 400 000 averages at 300 K and 100 000 at 80 K. The chemical shift scale was calibrated by the ^{13}C resonance in tetramethylsilane (TMS, 0 ppm), adamantane (-34.4 ppm) (10) and sodium formate dissolved in water (-168.7 ppm). Note that all features are reported on the σ scale for chemical shifts relative to TMS (5). The ^{13}C spin counts were calibrated at 300 K with natural abundance ^{13}C adamantane and at 80 K with 70% ^{13}C -enriched barium carbonate. With the number of averages taken, the error limits of the NMR spectra are $\pm 2\%$ of the ^{13}C spin count and ± 7 ppm (one channel) on the frequency scale.

The 2.2% by weight Rh on Al_2O_3 substrate was prepared as described previously (14). Briefly, $\text{RhCl}_3 \cdot 3\text{H}_2\text{O}$ is dissolved in a water; acetone (1:10) suspension of Al_2O_3 and then sprayed onto a CaF_2 window and simultaneously onto a pyrex glass plate, both at 355 K. The CaF_2 window, covered with $\sim 11 \text{ mg/cm}^2$ of sample, is mounted in the infrared cell. The deposit on the pyrex plate is scraped off and tamped into the bottom of the NMR tube. The NMR sample is $\sim 0.50 \text{ g}$ (5.9×10^{19} Rh atoms) with a void fraction of 75%, calculated from the bulk Al_2O_3 density.

The cell is assembled and both the infrared and NMR samples are outgassed, heated to 425 K at 15 K/hr, and reduced in H_2 as before (14). For each of the three charges of H_2 (Matheson grade 99.9995% pure) to the sample, the ratio of H_2 to Rh was 100:1. The Al_2O_3 -supported Rh substrate is outgassed at 450 K for 12 hours to a background pressure of $\sim 10^{-6}$ Torr, then slowly cooled (25 K/hr) to room temperature. A background infrared scan from 4000 to 1200 cm^{-1} is taken to assure that the sample is free of impurities observable by IR. The typical H/Rh ratios measured on freshly prepared substrates at 300 K was 0.90.

The Al_2O_3 , "Alon-C," was prepared by Cabot, Inc., Boston, Massachusetts. The powder has a specific surface area of $90\text{ m}^2/\text{g}$ and contains $0.21 \pm 0.01\%$ Fe and $0.38 \pm 0.05\%$ Cl by weight, as determined by atomic absorption and selective ion electrode analysis, respectively. The Al_2O_3 was commercially prepared by fuming $AlCl_3$ in a hydrogen/oxygen flame at ~ 2100 K; thus, one would expect that the Fe is incorporated into the Al_2O_3 framework during the oxidation by substituting for Al atoms. The electron paramagnetic spectrum of the Alon-C powder at 8 K and the microwave frequency at 9.25 GHz shows a sharp transition at $g = 4.25$. Thus, the iron is atomically dispersed throughout the sample and is not clustered in small particles. Also, the g value is typical of Fe^{++} in oxides, rather than Fe^{+++} which has a g value of 2.0 at levels of 0.02% in natural sapphire (Al_2O_3) (25). After reduction and outgassing, the Al_2O_3 -supported Rh samples contained 1.36 to 1.56% Cl by weight. Thus, 48 to 57% of the Cl introduced as $RhCl_3 \cdot 3H_2O$ was retained by the sample. The HCl formed

during the reduction of $\text{RhCl}_3 \cdot 3\text{H}_2\text{O}$ is most likely reacting with the Al_2O_3 surface. At room temperature, HCl reacts with Al_2O_3 to produce new hydroxyl groups and H_2O , as observed by infrared studies (26). The HCl is chemisorbed by inserting into an Al-O-Al bond to form Al-Cl and Al-OH or by exchanging with an Al-OH site to form Al-Cl and H_2O .

The ^{13}CO (90% enriched) obtained from Merck Isotopes and spectroscopic grade CO, both in glass breakseal bulbs, were used without further purification. The $\text{Rh}_2\text{Cl}_2(\text{CO})_4$, prepared by Alfa-Ventron, was enriched to ~20% ^{13}C in an all-glass closed vessel by exposing the crystals to $^{13}\text{CO(g)}$ for 7 days at 370 K, which is below the decomposition temperature (27).

III. RESULTS

A. ^{13}C NMR Spectrum of $\text{Rh}_2\text{Cl}_2(\text{CO})_4$

The ^{13}C T_1 of $\text{Rh}_2\text{Cl}_2(\text{CO})_4$ is ~30 minutes at 300 K, which prohibited extended averaging. The sum of 328 transients taken once every 45 minutes is shown in Figure 1. The center of mass, or average spectral frequency, of the spectrum is -186 ± 7 ppm, in close agreement with the observed isotropic chemical shift of the compound in solution, -180.4 ppm (28). The lineshape is fit with a nonlinear least-squares theoretical chemical shift powder pattern, convoluted with a Lorentzian broadening function (29). The principal components of the computed fit are $\sigma_{11} = 99$ ppm, $\sigma_{22} = -299$ ppm, and $\sigma_{33} = -306$ ppm, yielding an isotropic chemical shift of -169 ppm. The discrepancy between the isotropic value of the fit and the computed center of the line indicates that the data are not fully developed powder pattern. The most

probable cause is that the spin-lattice relaxation process, which is principally the result of librations through different chemical shift shieldings, has a pronounced angular dependence, as observed in other transition metal carbonyls (30,31). Thus, portions of the spectrum have relatively longer T_1 's, resulting in a lower intensity at these orientations and causing a slightly distorted pattern.

B. ^{13}C NMR Spectrum of ^{13}CO Adsorbed on Rh

A 2.2% Rh on Al_2O_3 substrate was exposed to ~50 Torr of ^{13}CO at 300 K. The integrated intensities of the infrared spectrum, calibrated against the CO uptake of previous samples (14), indicate that the ratio of adsorbed CO to Rh is ~0.9. The integrated intensity of the NMR spectrum, shown in Figure 2(a), yields a CO-to-Rh ratio of 0.87 ± 0.02 . When the sample is cooled to 80 K, after pumping out the excess CO(g) to 0.02 Torr to prevent the formation of any physisorbed CO at low temperatures, the NMR spectrum broadens, as illustrated in Figure 2(b), but the temperature-compensated integrated intensity remains constant. The center of mass of the ^{13}C NMR spectrum is constant with temperature change, at -191 ± 7 ppm.

When the pressure of the ^{13}CO is reduced from 50 Torr to 10^{-6} Torr, the ^{13}C NMR lineshape intensity at 300 K decreased uniformly by 15%, with no change in the linewidth or the center of mass. A sample of Al_2O_3 , with no Rh, dosed with 50 Torr of ^{13}CO gave no NMR signal, indicating no adsorption (chemical or physical) of CO on the support, consistent with adsorption isotherm measurements at 300 K.

C. ^{13}C Relaxation Times of CO Adsorbed on Rh

A second 2.2% Rh on Al_2O_3 sample was prepared and progressively charged with ^{13}CO to a pressure of ~ 50 Torr at 300 K. The infrared spectra for precisely this sample were reported in Figure 5 of Reference 14. The NMR tube was separated from the infrared cell under ~ 50 Torr of ^{13}CO and stored at 300 K for 13 months.

The observed ^{13}C magnetization of this aged sample versus τ , the delay between the 180° prepulse and the 90° pulse, is plotted in Figure 3. If the ^{13}C nuclei had a single, spatially uniform T_1 , the magnetization as a function of τ would form a straight line when plotted as in Figure 3. The data in Figure 3 can be fit within experimental error limits by assuming that the ^{13}C nuclei are separated into two types, with two distinct T_1 's. The theoretical equation describing the magnetization as a function of τ and the cycle time for this two-group model is:

$$M = M_0 \left[\alpha_a e^{-\tau/T_{1a}} \left(1 - e^{-t_c/T_{1a}} \right) + \alpha_b e^{-\tau/T_{1b}} \left(1 - e^{-t_c/T_{1b}} \right) \right]$$

where M is the magnetization observed with a delay τ for measurements repeated after time t_c ; α_a and α_b are the fractions of ^{13}C nuclei with spin-lattice relaxation times T_{1a} and T_{1b} , respectively; and M_0 is the equilibrium ^{13}C magnetization. A least-squares fit of this equation to the data in Figure 3 indicates that, for this sample at 300 K, $42 \pm 1\%$ of the ^{13}C nuclei have a T_1 of 5.6 ± 0.4 msec, $58 \pm 1\%$ have a T_1 of 64 ± 4 msec, and $M_0 = 4.44 \pm 0.04 \times 10^{19}$ ^{13}C nuclei, yielding a

CO-to-Rh ratio of 1.04. When the experiment is repeated at 80 K, a least least-squares fit of the data to the two-group model indicates that $43 \pm 1\%$ of the ^{13}C nuclei have a T_1 of 33 ± 3 msec and $57 \pm 1\%$ have a T_1 of 0.78 ± 0.08 sec. T_1 measurements on other 2.2% Rh on Al_2O_3 samples show that the relaxation times and site distributions are independent of the equilibrium pressure of ^{13}CO , in the range 50 to 10^{-3} Torr.

The lineshapes of the ^{13}C NMR spectra vary as τ increases, illustrated by representative spectra in Figure 4. One observes that the peak at ~ 165 ppm disappears relatively quickly, while the shoulder at ~ 280 ppm remains intact longer. With the relative proportions calculated from the T_1 data, the ten spectra associated with the data points in Figure 3 may be decomposed into the two basis spectra corresponding to the two different T_1 's. A least-squares deconvolution yields the two spectra shown in Figure 5. Although this aged sample is composed of a greater percentage of short T_1 ^{13}C nuclei than fresh samples, the spectrum for the species with $T_1 = 5.6$ msec, Figure 5(a), still contains a relatively high noise level because the signal decays rapidly with τ , and thus the computed spectrum is determined by relatively fewer experimental spectra. The data of Figure 5(a) are fit with a Lorentzian function with 1.85 KHz full width at half maximum. The centers of mass of the two generated spectra are -177 ± 7 ppm and -199 ± 7 ppm for the species with T_1 's of 5.6 msec and 64 msec, respectively. The signal-to-noise ratios for the spectra at 80 K prohibited a meaningful decomposition into the basis spectra at that temperature.

D. Exchange of $^{12}\text{CO(g)}$ with $^{13}\text{CO(ads)}$

Previous infrared studies have shown that adsorbed ^{13}CO exchanges readily and extensively with $^{12}\text{CO(g)}$ at 300 K (14). In addition, it is possible to exchange selectively only the $\text{Rh}(\text{CO})_2$ species by cooling the substrate to temperatures lower than 200 K and then exposing to ^{12}CO (15,32). Further studies on CO adsorbed on Rh on Al_2O_3 reveal that upon warming the selectively exchanged sample from 200 K to 300 K, complete isotopic mixing between CO adsorbed on all sites on the surface occurs on the order of hours, even at CO pressures below $\sim 10^{-3}$ Torr (33).

By studying these exchange phenomena with ^{13}C NMR, it is possible to determine quantitatively the site distribution of adsorbed CO. A freshly prepared sample of 2.2% Rh on Al_2O_3 was exposed to 50 Torr of ^{13}CO at 300 K and allowed to equilibrate for two days. After reducing the CO pressure to 10^{-2} Torr, the infrared scan of the sample was similar to spectra previously reported, e.g., Figure 5 of Reference 14. The integrated intensity of the NMR spectrum indicates a CO-to-Rh ratio of 0.82 ± 0.02 . The ^{13}C T_1 's of this sample were measured as before and, assuming a two-group model, were found to be distributed as $34 \pm 1\%$ with T_1 equal to 4.0 ± 0.2 msec and $66 \pm 1\%$ with T_1 equal to 34 ± 2 msec. The ratio of short to long T_1 's in the freshly prepared sample (34:66) was less than that of the 13-month-old sample (42:58). Concurrently, the overall CO-to-Rh ratio as measured by the NMR varied from 0.82 for the fresh sample to 1.04 for the aged sample.

The freshly prepared NMR sample was cooled to 195 K in a dry ice/acetone bath and then exposed to ~ 50 Torr ^{12}CO , such that the ratio

of $^{12}\text{CO(g)}$ to exchangeable (at 195 K) $^{13}\text{CO(ads)}$ was ~ 45 . (The present configuration of the equipment does not afford simultaneous low temperature experiments on the NMR and infrared samples.) After one hour, the CO pressure was reduced to 10^{-3} Torr over a 20 minute period; then the sample was allowed to warm while constantly pumping with a 20 liter/sec ion pump. After warming to 300 K, the sample was stored under an equilibrium CO pressure of 5×10^{-3} Torr.

After the low temperature exchange, the equilibrium magnetization of this sample had decreased by $33 \pm 1\%$. Thus, 33% of the ^{13}CO adsorbed on the Rh on Al_2O_3 exchanged with the $^{12}\text{CO(g)}$ at 200 K and was evacuated from the sample. After the exchange the ^{13}C T_1 's were distributed as $31 \pm 1\%$ with a T_1 of 2.4 ± 0.2 msec and $69 \pm 1\%$ with a T_1 of 43 ± 4 msec. Thus, decreasing the ^{13}C -isotopic enrichment of the adsorbed CO from 90% to 70% causes the rapidly relaxing group to relax more quickly and the relatively slower relaxing group to relax more slowly. In addition, the new distribution (31:69) is almost the same as the original distribution (34:66). This distribution was measured after the system had sufficient time to isotopically scramble from $\sim 100\%$ ^{12}CO on the dicarbonyl site and 10% ^{12}CO on the Rh rafts to a uniform $^{13}\text{CO}/^{12}\text{CO}$ ratio on both the dicarbonyl and raft sites, as observed by infrared spectroscopy. Because of the extended period of time required to measure the T_1 distribution, it was not possible to complete the NMR measurements at 300 K immediately after the exchange, nor was it feasible to maintain temperatures of 200 K for the duration of the experiment. Consequently, it was not possible to determine with

NMR spectroscopy if the exchange selectively removed ^{13}CO from one T_1 group (i.e., almost all the ^{13}CO of the short T_1 group or about half the longer T_1 group) which subsequently redistributed upon warming, or if the exchange was equally distributed among the two T_1 groups.

IV. DISCUSSION

A. ^{13}C Relaxation Mechanism for ^{13}CO Adsorbed on Rh

The ^{13}C T_1 's of the adsorbed CO on Rh dispersed on Al_2O_3 are between 2 and 64 msec in the two samples examined. These extremely short T_1 's are typical of relaxation from paramagnetic centers. Other relaxation processes, such as fluctuating dipolar interactions from neighboring ^{27}Al or ^1H spins of the substrate typically yield ^{13}C T_1 's of many seconds or more. The Al_2O_3 contains a relatively high level of Fe impurities, 0.2% by weight. The electron paramagnetic resonance spectrum indicates that the Fe is distributed throughout the sample, rather than clustered in metallic particles, and is present as Fe^{++} . The rapidly fluctuating magnetic fields from the unpaired electrons of these Fe ions can relax nuclei in the sample by three mechanisms, depending on the mobility of the unpaired electrons and the nuclei of interest. First, if the unpaired electron is confined to the metal atom and the ^{13}C nuclei are spatially fixed, the ^{13}C nuclei very close to the metal atoms will relax rapidly and then equilibrate with the other ^{13}C nuclei via ^{13}C - ^{13}C mutual spin flips. Second, if the molecules containing the ^{13}C diffuse rapidly through the sample, each ^{13}C nucleus may be individually relaxed by contacting the paramagnetic center. Third, the unpaired electrons may interact directly with each

^{13}C nucleus if the electrons are free to move through the lattice to the ^{13}C adsorption sites.

Although it is not possible at present to determine which mechanism or combination of mechanisms is causing the ^{13}C spin-lattice relaxation, one can eliminate some possibilities due to the nature of the sample or the consequences of the models invoked. For example, it is inconceivable that the unpaired electrons are able to translate freely through an insulator such as Al_2O_3 . Also, the desorption studies have shown that the CO does not diffuse through the sample by desorbing into the gas phase and then readsorbing onto a different site. (However, this does not rule out exchange between sites on a single raft.) Homonuclear ^{13}C - ^{13}C spin flips are too slow to account for the rapid dissemination of relaxation through the sample because of long internuclear distances between different rafts or carbonyl sites.

A random distribution of Fe^{++} in the Al_2O_3 lattice yields an average ^{13}C - Fe^{++} separation of $\sim 35 \text{ \AA}^0$, which is sufficient to allow direct relaxation between fixed sites. Such a random distribution of lengths and orientations relative to the external magnetic field of the ^{13}C - Fe^{++} internuclear vector could result in an inhomogeneous T_1 for the ^{13}C nuclei. If both the ^{13}C nuclei and the Fe^{++} paramagnetic centers are fixed, the ^{13}C T_1 is given by the following equation (34):

$$\frac{1}{T_1} = 6 \frac{\gamma_c^2 \gamma_e^2 \pi^2}{r^6} \sin^2 \theta \cos^2 \theta \left[\frac{T_{1e}}{1 + \omega_c^2 T_{1e}^2} \right]$$

for an internuclear vector of length r at an angle θ to the external magnetic field, γ_i is the respective gyromagnetic ratio, T_{1e} is the electron spin-lattice relaxation time, typically 10^{-6} to 10^{-7} s at 300 K, and ω_c is the carbon Larmor frequency. One can derive an expression for the number of spins as a function of T_1 , i.e., $N(T_1)$, from the above equation. The magnetization as a function of τ , the delay between 180° and 190° pulses, is given by the following equation:

$$M(\tau) = \int_0^{T_1, \text{max}} e^{-\tau/T_1} N(T_1) dT_1$$

This model for $N(T_1)$ yields an $M(\tau)$ that decreases approximately exponentially with τ , yielding a straight line with a slight concave downward shape when plotted as in Figure 3. Although not shown, this results in a very poor fit to the experimental data. In addition, the isotropic chemical shifts of the two T_1 -resolved spectra differ by 22 ppm. In an amorphous sample, the unpaired electron of one atom may cause the broadening of the NMR lineshape of the nucleus of a different atom but not a shift in the overall frequency (35). Thus, the difference in chemical shifts between rapidly and slowly relaxing nuclei indicates that the two T_1 types are chemically distinct and not the results of a random site formation near Fe^{++} paramagnetic centers. This does not rule out the possibility that the Rh preferentially congregates at the paramagnetic sites. Although it is possible to postulate a nonrandom distribution of paramagnetic impurities to fit the T_1 data, we believe it is very unlikely that the Rh would selectively distinguish

between the FeO and Al_2O_3 sites of the substrate when the Rh is deposited as RhCl_3 or when later reduced since there are only 2 atoms of Fe per 1000 Al atoms.

The current data do not allow one to deduce the principal NMR relaxation process and, more specifically, why there is a distribution of ^{13}C T_1 's. However, as introduced earlier in this paper, the T_1 data can be fit with a model that assumes there are two types of adsorbed ^{13}CO , each with distinct T_1 's. The interpretation and justification of this two-group model will be discussed in the next section. This model assumes that $N(T_1)$ is the sum of two delta functions at T_{1a} and T_{1b} , with relative areas α_a and α_b , which yields an $M(\tau)$ that is the sum of two exponentials (for adequately slow pulse rates). For negligible cross-relaxation and molecular exchange between groups, which is the case for this dilute ^{13}C system, α_a and α_b represent the relative populations of the two T_1 groups. The fit of this model is not improved within error limits by increasing the number of T_1 types to three or more. Also, this simple model assumes that ^{13}C nuclei have T_1 's of precisely T_{1a} or T_{1b} , which is probably not the case with this amorphous, inhomogeneous sample. Rather, there is more likely two distributions of T_1 's centered at T_{1a} and T_{1b} which would more accurately be modeled by two finite width Gaussian peaks rather than two delta functions.

B. Interpretation of the T_1 -resolved ^{13}C NMR Spectra

As discussed in the introduction, previous infrared studies have established three states of CO adsorbed on dispersed Rh. Of these three

states, the linear and bridged bonded CO (species II and III) would be expected to have the same ^{13}C T_1 's because of rapid interconversion and diffusion of CO states on the raft and the same exposure to nearby paramagnetic centers in the substrate lattice. Thus, in terms of the infrared-identified states, the two ^{13}C T_1 types would be assigned to CO on a single Rh (species I) and CO on the Rh rafts (species II and III). This interpretation of the two T_1 types as well as the assignment of the two T_1 -resolved NMR spectra in Figure 5 is supported by the chemical shift information, the results of the quantitative selective $^{12}\text{CO(g)}/^{13}\text{CO(ads)}$ exchange, and the T_1 distribution as a function of the overall ratio of CO(ads) to Rh.

The isotropic chemical shifts of the two T_1 -resolved spectra are -177 ppm for the 5.6 msec T_1 spectrum (Figure 5(a)) and -199 ppm for the 64 msec T_1 spectrum (Figure 5(b)). Recall that the difference of 22 ppm between the two T_1 types indicates that the two T_1 types are chemically distinct. The chemical shifts of various rhodium carbonyl compounds are given in Table I. The isotropic chemical shift of CO is -181.3 ppm. The model compound for the surface dicarbonyl species, $\text{Rh}_2\text{Cl}_2(\text{CO})_4$, has a chemical shift anisotropy comparable to the computed static value for CO (36) and a very slight shift in the center of mass to -180 ppm. The isotropic chemical shifts of CO bonded as a terminal group on various rhodium complexes range from -176 to -192 ppm, with an average at about -184 ppm. The bridged bonded state of CO has the largest change in chemical shift, ranging from -212 to -236 ppm, with an average at about -228 ppm.

The ^{13}C NMR lineshape of CO adsorbed on the Rh rafts will contain contributions from the linear and bridged sites. The isotropic chemical shift of the longer T_1 species, -199 ppm, lies in the range of shifts between the linear and bridged values. The isotropic chemical shift of the species with the 5.6 msec T_1 is 22 ppm upfield at -177 ppm, which is closer to that of the dicarbonyl state. Thus, based on the isotropic chemical shifts, we assign the lineshape with the T_1 of 5.6 msec to ^{13}CO adsorbed in the dicarbonyl state (species I) and the lineshape with the T_1 of 64 msec, Figure 5(b), to the ^{13}CO adsorbed on the Rh rafts (species II and III).

The isotropic chemical shift of the ^{13}C spectrum of CO on the rafts is a linear combination of the isotropic shifts of the linear and bridged states. Assuming that the chemical shifts of the linear and bridged species are similar to those of the model compounds, -184 and -228 ppm, respectively, the observed isotropic shift of Figure 5(b), -199 ppm, yields an estimated CO distribution of 66% linear states and 34% bridged states. Thus, based on the chemical shift data, the CO is distributed on this aged sample as 42% dicarbonyls (species I), 38% linear bonded (species II), and 20% bridged bonded (species III).

The results of the $^{12}\text{CO(g)}/^{13}\text{CO(ads)}$ exchange at 200 K support the assignment of the two T_1 types to CO adsorbed as a dicarbonyl and CO adsorbed on the Rh rafts. Recall that infrared studies have demonstrated that the $\text{Rh}(\text{CO})_2$ species exclusively and extensively exchanges with $^{12}\text{CO(g)}$ at temperatures below 200 K (15). The NMR revealed that for a sample in which 34% of the ^{13}CO was adsorbed in the

short T_1 state and 66% was adsorbed in the longer T_1 state, the low temperature ^{12}CO exchange removed 33% of the adsorbed ^{13}CO . The NMR also found that the remaining ^{13}CO was proportionately distributed among the two T_1 types. Recall that infrared results predict that the surface sites would isotopically scramble within hours upon warming. Thus, it could not be demonstrated experimentally that the species with the shorter T_1 was exclusively removed during the exchange. However, the agreement between the amount of ^{13}CO removed and the amount of ^{13}CO originally in the shorter T_1 group strongly suggests that the CO adsorbed as dicarbonyls has the shorter T_1 's. A fresh sample was chosen for the exchange study because the ratio of species with different T_1 's was more pronounced than in the aged samples and thus made it easier to assign the amount exchanged to a specific group.

Finally, consider the distribution between the T_1 group as a function of the overall CO-to-Rh ratio. A freshly prepared sample with an overall CO-to-Rh ratio of 0.82 had 34% of the ^{13}C in a short T_1 state and 66% in the longer T_1 state. The aged sample had a higher ratio of CO-to-Rh at 1.04, and the T_1 distribution changed from 34:66 to 42:58. Since the aged sample actually has more CO on the surface and not just a redistribution of CO, it is not possible to calculate individual CO/Rh ratios for the two T_1 groups. However, assuming that the two T_1 groups are Rh dicarbonyls and CO on Rh rafts, it is possible to calculate the consequences of pairing these species to the two T_1 groups. Assigning the longer T_1 species to the dicarbonyl requires that at least 36% of the Rh on the fresh sample and at least 12% of the Rh on

the aged sample be inactive. Assigning the shorter T_1 species to the dicarbonyl requires that at least 14% of the Rh on the fresh sample be inactive, but all of the Rh on the aged sample may be active. The hydrogen uptake and the degree of dispersion of Rh measured in other studies (16,18), indicates that the latter assignment is correct, consistent with previous arguments.

C. Molecular Motions of CO Adsorbed on Rh

The two ^{13}C NMR lineshapes of adsorbed CO in Figure 5 are radically different from the rigid chemical shift powder patterns of the model compounds, such as the $\text{Rh}_2\text{Cl}_2(\text{CO})_4$ spectrum in Figure 1 or the $\text{Rh}_6(\text{CO})_{16}$ spectrum of Reference 31. The spectra of the adsorbed CO broaden when the sample is cooled from 300 K to 80 K, as shown in Figures 2(a) and 2(b), indicating that at 300 K the spectrum is narrowed by molecular motions at frequencies greater than or equal to the NMR linewidth, i.e., a few KHz. The residual broadening at 80 K is probably the result of heteronuclear interactions with ^{27}Al and ^1H and the heterogeneity of the adsorbed states. Since the ^{13}C NMR spectrum does not broaden when the CO pressure is reduced from 50 to 10^{-6} Torr, the major averaging mechanism is not rapid exchange with the gas phase, i.e., $\text{CO(g)} \rightleftharpoons \text{CO(ads)}$. Rather, the narrowing of the spectra in Figure 5 is due to motion localized at the individual adsorption sites.

The possible localized motions of adsorbed CO are different on the Rh dicarbonyl site compared to the Rh raft sites. The motions predicted to be in the frequency range of interest are reorientation about the axis bisecting the OC-Rh-CO angle of the dicarbonyl and

surface diffusion of CO from site to site within the Rh raft boundaries. The characteristic effects on the chemical shift powder pattern of rotations and site exchange have been studied previously (40,41). Spiess (40) has shown that when molecules exchange between equivalent sites at correlation times on the order of the chemical shift anisotropy, the axisymmetric powder pattern retains the full anisotropy but decreases in intensity at the extreme frequencies of the tensor and increases in the frequency range between the perpendicular tensor component and the isotropic frequency. For an illustration of the effects of site exchange on a rigid NMR lineshape, see Figure 4 of Reference 40. Reorientation about a rotation axis has a distinctly different effect on the NMR lineshape. For intermediate correlation times, Sillescu (41) has shown that random reorientation about a rotation axis causes the observed observed anisotropy of the NMR lineshape to collapse as the correlation time decreases. As opposed to exchange between sites, this rotation causes no new structure to develop in the lineshape. This is the case illustrated in Figures 1 to 3 of Reference 41. For rapid molecular reorientation, both rotation and site exchange cause the line to collapse to a Lorentzian curve; thus, in this limit it is not possible to identify the type of motion present in the sample.

The ^{13}C NMR spectrum assigned to the dicarbonyl surface species, Figure 5(a) has been fit with a Lorentzian curve with a linewidth of 1.85 KHz. Fitting a Gaussian curve to these data results in a mean square deviation three times that of the Lorentzian fit. The noise level in the spectrum does not permit an accurate determination of the

ratio of the fourth moment to the second moment squared, which is usually used to differentiate between the two characteristic lineshapes (42). The Lorentzian shape of the spectrum in Figure 5(a) indicates that the narrowing of the spectrum is principally the result of motional averaging, as opposed to homogeneous broadening responsible for Gaussian curves (42). The ratio of the Lorentzian linewidth to the anisotropy of the ^{13}C NMR spectrum of the model compound $\text{Rh}_2\text{Cl}_2(\text{CO})_4$ is about 0.3. For this narrowing there still exist subtle differences in the lineshapes caused by the effects of the rotation and site exchange models; however, the high noise level prohibits any such differentiation. The most probable motion for the dicarbonyl species is reorientation of the two CO molecules about an axis perpendicular to the Al_2O_3 surface. In this limit of extensive motional averaging, the linewidth is determined by spin-spin relaxation processes and the inverse halfwidth is T_2 (42). The correlation time for the reorientation is much shorter than T_2 , thus $\tau < 0.5$ msec.

Thus, the ^{13}C NMR spectrum indicates that the single Rh atom is present on the Al_2O_3 surface such that the CO groups and the Rh atom itself are relatively free to rotate to new orientations. In the rhodium carbonyl compounds where the Rh atom forms multiple bonds with the complex, e.g., two Rh-Cl bonds in $\text{Rh}_2\text{Cl}_2(\text{CO})_4$ and four Rh-Rh bonds in $\text{Rh}_6(\text{CO})_{16}$, the ^{13}C NMR powder pattern shows no evidence of motions on the order of a few KHz. As the carbonyls of the $\text{Rh}(\text{CO})_2$ site are relatively unrestricted to reorient, it implies that the bonding of the Rh atom to the Al_2O_3 is more axially symmetric than in the model compounds. Possible models for this situation would be a Rh atom bonded to the support through a single bond, such as to an oxygen atom, or a

Rh atom physisorbed on the Al_2O_3 such that the weak bonding does not orient the Rh-CO bonds.

The ^{13}C NMR lineshape assigned to the CO adsorbed on the Rh rafts, Figure 5(b), is the superposition of a powder pattern for the linear species (three components near 80, -305 and -315 ppm) and a powder pattern for the bridged species (two components at about -102 and -296 ppm) which would result in five structural features, assuming that none are coincident. Figure 5(b) has definite features at about -190, -250, and -300 ppm. The structure at -250 and -300 ppm may be assigned to the perpendicular components of the two overlapping chemical shift tensors, but the peak at -190 ppm is too far upfield to be a principal component of either of the tensors. Rather, the peak at about -190 ppm, close to the isotropic frequency of the linearly adsorbed CO, is characteristic of the effects of CO exchanging between sites on the Rh raft. Also, there is observable intensity over the entire range of the predicted anisotropy, 100 to -300 ppm, as expected by the site site-exchange motional model. The features at 80, 4, and -385 ppm are probably not real since they are comparable to the noise level and are accompanied by negative peaks in the other complementary computed lineshape of Figure 5(a). Spectrum 5(b) does not allow a calculation of the rate of diffusion and activation energy for surface diffusion of CO on the Rh raft. The diffusion rate may be accurately computed only after a separation of the individual ^{13}C NMR spectra of the linear and bridged states and after the sources of the other broadening are quantified.

D. Distribution of Rh Atoms on Al₂O₃

The T₁ results for the aged 2.2% Rh on Al₂O₃ sample indicate that the CO is distributed on the surface as 42% bonded as dicarbonyls (species I) and 58% adsorbed on the Rh rafts. The isotropic chemical shift of the ¹³C NMR spectrum of the CO on the Rh rafts indicates that for this sample the ratio of linear to bridged states is 66 to 34. The overall CO-to-Rh ratio of 1.04 requires that for every 104 adsorbed CO molecules, there are 100 Rh atoms. The 44 CO molecules adsorbed as dicarbonyls are bonded to 22 Rh atoms, or 22% of the Rh on the Al₂O₃. The configuration of the Rh rafts may be determined by assuming a stoichiometry for the Rh-CO bonding on the rafts. If one assumes that a Rh atom linearly bonded to a CO makes no other bonds to CO molecules, the 60 CO molecules on the raft (40 linear and 20 bridged) will require 80 Rh atoms (40 + 40). The local ratio of CO to Rh atoms on the raft for this model is 60/80 = 0.75. It has been shown recently by low energy electron diffraction (43) that at full CO coverage on Rh (111) at temperatures of about 180 K, the ratio of CO to surface Rh atoms is 0.75. This model for the CO on the raft yields an overall CO-to-Rh ratio of 1.03, which is very close to the observed ratio of 1.04. However, the CO-to-Rh ratio of Reference 43 was measured at pressures less than 10⁻⁶ Torr. It is possible that the CO coverage on the Rh (111) would increase at pressures on the order of 50 Torr.

It is possible that some of the raft Rh atoms make multiple bonds to the adsorbed CO. The extreme case is to assume that the raft has only 40 Rh atoms involved in the bonding to the adsorbed CO, and the

bridged CO simply fills the voids between the linear Rh-(CO) sites as is observed in most rhodium carbonyl complexes (28,37-39). In this case, to satisfy the CO-to-Rh ratio of 1.04, 38 of the 100 Rh atoms (38%) must be unavailable for CO adsorption. The H₂ uptake on a freshly reduced 2.2% Rh on Al₂O₃ sample is only about 0.9, compared to values as high as 1.16 reported for Rh on Al₂O₃ samples (18), indicating that some of the Rh is inactive. The uninvolved Rh atoms may be the result of incomplete reduction of the RhCl₃, Rh atoms buried under the surface Rh atoms in the rafts, or Rh atoms trapped in pores rendered inaccessible during the reduction/outgassing procedure. D. J. C. Yates, *et al.* (18) do not report any infrared absorption in the 1870 cm⁻¹ range for the adsorption of CO on a 1% Rh on Al₂O₃ sample where the Rh rafts are entirely two-dimensional, or "ultradispersed," as determined by hydrogen uptake and electron microscopy. This suggests that the presence of a bridged bonded state of CO indicates that the Rh raft is three-dimensional, thus covering a percentage of the Rh atoms. Thus, the actual structure of the Rh rafts on the 2.2% Rh on Al₂O₃ samples studied here is probably partially two-dimensional with some three-dimensional portions.

E. Estimation of Infrared Absorption Coefficients for ¹³CO on Rh

The absolute populations of the three adsorbed states of CO on 2.2% Rh on Al₂O₃ as determined by ¹³C NMR may be used to calibrate the infrared absorption intensities. Using the analysis based on the chemical shift data described earlier, the CO adsorbed on the freshly prepared 2.2% Rh on Al₂O₃ sample with an overall CO-to-Rh ratio of 0.82 was distributed as 34% dicarbonyls, 44% linear states, and 22% bridged

states. Unfortunately, it was not possible to obtain an infrared spectrum of the 13-month-old sample after aging. Although the peaks of the infrared spectrum overlap slightly, as shown in Figure 5 of Reference 14, the individual intensities may be obtained by assuming that the large peaks at 2056 and 1987 cm^{-1} (the symmetric and antisymmetric stretches of $\text{Rh}(\text{CO})_2$) are symmetric about their respective maxima so that the valley between these peaks may be artificially created and subtracted from the peak at 2024 cm^{-1} (the linear species). The background due to the ^{12}CO impurity was estimated from other studies. The molar integrated intensity of each peak, A , is given by the following equation (1):

$$A = \frac{2.303}{c\ell} \int \log_{10} \left(\frac{I_0}{I} \right) dv$$

where c is the molar concentration of the substrate computed from the ^{13}C NMR data, ℓ is the path length through the sample, and the integration is over the full width of the infrared peak. For this particular sample at 300 K under an equilibrium 90% ^{13}CO pressure of 50 Torr, the molar integrated infrared intensities are 74, 128, 26, and 85 (cm^{-1} $(\text{mole}^{-1})^{10^6}$) $\pm 10\%$ for the symmetric and antisymmetric stretches of the dicarbonyl, the linear state, and the bridged state, respectively. The molar intensity for CO(g) is only 5.4×10^6 (44). This dramatic increase in the infrared absorption by CO upon bonding to the surface has been reported previously by Seanor and Amberg (44). By measuring the amount of CO adsorbed with a quartz spring microbalance, they

calculated molar integrated intensities of 60 and 27 (cm) (mole^{-1}) (10^6) for CO chemisorbed on Pt on SiO_2 at 2100 and 2095 cm^{-1} , respectively. These infrared intensities chemisorbed CO are also very comparable to those of many metal carbonyls (45).

The molar integrated intensities reported here are for only one loading of Rh on Al_2O_3 at one coverage of CO. Recent infrared studies indicate that these values change as a function of loading in the range 0.2% to 10% Rh by weight on Al_2O_3 (46). UPS studies have shown that as the loading of Pd on a carbon substrate increases, the Pd cluster properties change from atomic to metallic behavior, which results in changes in the CO bonding to the Pd rafts (47). It is conceivable that the Rh rafts on Al_2O_3 may vary similarly with increased metal loading. In addition, preliminary ^{13}C NMR results suggest that at constant Rh loading, the molar integrated intensities of the adsorbed CO are inhomogeneous, varying as much as a factor of five for the dicarbonyl sites (48).

Further combined infrared and NMR studies as a function of ^{13}CO coverage and Rh loading are needed. It will also be possible to calculate the molar intensities for ^{12}CO adsorbed on Rh by measuring the site distributions of ^{13}CO by NMR and then measuring the infrared spectrum of ^{12}CO adsorbed on an identical sample. Calibration over the complete adsorption isotherm would be extremely useful in future sample characterization since the infrared spectra are relatively easier and faster to obtain than are NMR spectra.

F. Evidence for Isolated Rh Atoms on Al_2O_3

The doublet in the infrared spectrum of CO adsorbed on Rh at 2101 cm^{-1} and 2032 cm^{-1} has been assigned to two ^{12}CO molecules adsorbed to a single Rh atom, based on analogies to the infrared spectra of $\text{Rh}_2\text{Cl}_2(\text{CO})_4$ and $\text{Rh}_2\text{Br}_2(\text{CO})_4$ (13,27,49). This dicarbonyl species is believed to form on either Rh atoms at the edge of the Rh rafts on the Al_2O_3 (18) or at single Rh atoms isolated from the Rh rafts (13,14,17). The cumulative evidence to date in support of the isolated Rh atoms is the following:

- (1) The absorption at 2101 cm^{-1} and 2032 cm^{-1} do not shift to higher wavenumbers as the coverage of CO increases, as do the bands due to the linear and bridged CO species adsorbed on Rh rafts (13,14). Thus, intermolecular CO-CO interactions at the dicarbonyl sites, through metal and through space, do not increase with CO coverage, indicating that these sites are isolated.
- (2) The catalytic decomposition of H_2CO on Rh dispersed on Al_2O_3 forms primarily $\text{Rh}(\text{CO})\text{H}_2$ and not $\text{Rh}(\text{CO})_2$ (20). However, the $\text{Rh}(\text{CO})_2\text{H}$ species forms from $\text{Rh}(\text{CO})\text{H}_2$ readily upon subsequent exposure to CO(g) . If the dicarbonyl site were on the edge of a raft, surface diffusion would allow the dicarbonyl to form from the migration of CO(ads) from the decomposition of H_2CO on other Rh sites of the rafts. Since it does not, it suggests that the Rh atoms are isolated from the rafts.
- (3) The exchange of $^{12}\text{CO(g)}$ with ^{13}CO adsorbed on the Rh dicarbonyl sites at 200 K without the exchange of the ^{13}CO on the rafts

suggest spatial isolation of the Rh atoms (15).

(4) The ^{13}C spin-lattice relaxation times of the adsorbed ^{13}CO are an order of magnitude different for the ^{13}CO on the Rh dicarbonyl sites compared to the ^{13}CO on the rafts. Such a difference in T_1 's is possible only for ^{13}CO on Rh atoms isolated from the ^{13}CO on the Rh rafts.

Thus, the results from infrared spectroscopy, H_2CO adsorption, selective exchange and ^{13}C NMR support the conclusion that isolated Rh atoms exist on the Al_2O_3 surface. Knözinger, et al. have made an isotopic infrared study of the adsorption of $\text{Rh}_6(\text{CO})_{16}$ onto ligand ligand-modified silica substrates (50). The $\text{Rh}_6(\text{CO})_{16}$ decomposes upon adsorption to form $\text{Rh}(\text{CO})_2$ groups as evidenced by only a doublet in the initial infrared spectrum. Based on the results of partial isotopic exchange of $^{13}\text{CO(g)}$ and $^{12}\text{CO(ads)}$ and the absence of linear and bridged species at high CO coverages, Knözinger et al. concluded that the dicarbonyl groups are isolated from each other.

V. CONCLUSIONS

^{13}C NMR has been combined with infrared spectroscopy to characterize the adsorbed states of CO on Rh dispersed on Al_2O_3 . The ^{13}CO is adsorbed on the dispersed Rh in two groups, characterized by ^{13}C T_1 's an order of magnitude different. With respect to the states of adsorbed ^{13}CO identified by previous infrared studies (13-18), the two T_1 groups are interpreted to be ^{13}CO adsorbed on isolated Rh atoms as a dicarbonyl and ^{13}CO adsorbed on Rh rafts. Combining the T_1 data with the isotropic chemical shifts of the lineshapes, the ^{13}CO site

distributions (dicarbonyl: linear: bridged) were found to be 42:38:20 for an aged 2.2% Rh on Al_2O_3 sample and 34:44:22 on a freshly prepared 2.2% Rh on Al_2O_3 sample. These site distributions may then be used to calculate the molar integrated intensities of the infrared spectra. The ^{13}C NMR may now be used directly to observe changes in the CO distribution caused by various surface treatments or indirectly by calibrating the infrared spectra of model samples.

The mobility of the adsorbed CO may also be obtained through NMR studies. This study has suggested two distinct motions of CO adsorbed on the surface. The CO adsorbed as a dicarbonyl is reorienting at the rate of a few KHz at 300 K, probably rotating about an axis bisecting the OC-Rh-CO angle. The CO on the Rh raft is exchanging between sites within the raft also at a rate on the order of a few KHz. Further quantification of these rates can provide information on the bonding of the Rh to the support and the degree of surface diffusion involved in the various reaction mechanisms of adsorbed CO. For example, Campbell and White have proposed that at temperatures near 330 K, CO may react with O_2 over polycrystalline Rh via either Langmuir-Hinshelwood or Eley-Rideal mechanisms, where the later involves a mobile two-dimensional gaseous CO state (51).

The interpretation of the ^{13}C NMR results is being examined further by NMR studies such as magic-angle sample-spinning techniques (52) to resolve the isotropic chemical shifts of the three species and isolation of the spectra as a function of temperature to determine accurately the activation energies for local motions. In addition, the

substrate may be modified to produce predictable changes in the relative amounts of isolated and raft Rh atoms, such as increasing the Rh loading on the Al_2O_3 .

The introductory ^{13}C NMR investigation of the CO adsorbed on the Rh on Al_2O_3 system has provided the necessary background to understand the more complicated changes observed at elevated temperatures and in the presence of other molecules such as O_2 or H_2 . We are currently undertaking the combined infrared and NMR studies of such systems.

VI. ACKNOWLEDGMENTS

The authors gratefully acknowledge support from the Office of Naval Research under contracts N00014-77-F-0008 and N00014-75-C-0960. We thank Professor G. R. Rossman for his generosity in allowing us to use his infrared spectrometer and G. W. Brudvig for measuring the electron paramagnetic resonance spectrum. Helpful comments and discussions were offered by S. I. Chan, W. H. Weinberg, and R. R. Cavanagh.

References

1. L. H. Little, Infrared Spectra of Adsorbed Species (Academic Press, London, 1966).
2. M. L. Hair, Infrared Spectroscopy in Surface Chemistry (Marcel Dekker, New York, 1967).
3. W. H. Weinberg, Ann. Rev. Phys. Chem. 29, 115 (1978).
4. R. W. Vaughan, Ann. Rev. Phys. Chem. 29, 397 (1978).
5. M. Mehring, High Resolution NMR Spectroscopy in Solids, Vol. 11 of NMR: Basic Principles and Progress (Springer-Verlag, New York, 1976).
6. U. Haeberlen, High Resolution NMR in Solids: Selective Averaging, Adv. Mag. Resonance Suppl. 1 (Academic Press, New York, 1976).
7. E. G. Derouane, J. Fraissard, J. J. Fripiat, and W. E. E. Stone, Catalysis Reviews 7, 121 (1972).
8. H. Pfeifer, NMR: Basic Principles and Progress 7 (Springer-Verlag, New York, 1972), p. 53.
9. T. M. Duncan, J. T. Yates, Jr., and R. W. Vaughan, J. Chem. Phys. 71, 3129 (1979).
10. J. B. Stothers, Carbon-13 NMR Spectroscopy (Academic Press, New York, 1972).
11. G. C. Levy, ed. Topics in Carbon-13 NMR Spectroscopy, Vol. 1 (Wiley, New York, 1974).
12. K. F. Lau and R. W. Vaughan, Chem. Phys. Lett. 33, 550 (1975).
13. A. C. Yang and C. W. Garland, J. Phys. Chem. 61, 1504 (1957).
14. J. T. Yates, Jr., T. M. Duncan, S. D. Worley, and R. W. Vaughan, J. Chem. Phys. 70, 1219 (1979).
15. J. T. Yates, Jr., T. M. Duncan, and R. W. Vaughan, J. Chem. Phys. 71, 3908 (1979).

16. M. Primet, J. Chem. Soc. Far. Trans. I, 74, 2570 (1978).
17. H. C. Yao and W. G. Rothschild, J. Chem. Phys. 68, 4774 (1978).
18. D. J. C. Yates, L. L. Murrell, and E. B. Prestridge, J. Catal. 57, 41 (1979).
19. R. M. Kroeker, W. C. Kaska, and P. K. Hansma, J. Catal. 57, 72 (1979).
20. J. T. Yates, Jr., S. D. Worley, T. M. Duncan, and R. W. Vaughan, J. Chem. Phys. 70, 1225 (1979).
21. H. Arai and H. Tominaga, J. Catal. 43, 131 (1976).
22. R. W. Vaughan, D. D. Elleman, L. M. Stacy, W. K. Rhim, and J. W. Lee, Rev. Sci. Instrum. 43, 1356 (1972).
23. (a) H. Y. Carr and E. M. Purcell, Phys. Rev. 94, 630 (1954).
(b) R. L. Vold, J. S. Waugh, M. P. Klein, and D. E. Phelps, J. Chem. Phys. 48, 3831 (1968).
24. H. S. Gutowsky, R. L. Vold, and E. J. Weld, J. Chem. Phys. 43, 4107 (1965).
25. S. A. Al'tshuler and B. M. Kozyrev, Electron Paramagnetic Resonance in Compounds of Transition Elements, 2nd ed., Eng. Trans. from Russian (John Wiley and Sons, New York, 1974), pp. 336-344.
26. J. B. Peri, J. Phys. Chem. 70, 1482 (1966).
27. C. W. Garland and J. R. Wilt, J. Chem. Phys. 36, 1094 (1962).
28. P. Chini, S. Martinengo, D. J. A. McCaffrey, and B. T. Heaton, J. C. S. Chem. Comm. 310 (1974).
29. N. Bloembergen and J. A. Rowland, Acta Metall. 1, 731 (1953).
30. H. W. Spiess, R. Grosescu, U. Haeberlen, Chem. Phys. 6, 226 (1974).
31. J. W. Gleeson and R. W. Vaughan, to be published.
32. The authors had previously reported low temperature $^{12}\text{CO}/^{13}\text{CO}$ exchange data with ambiguous results in the 1900 cm^{-1} region, suggesting a possible exchange of the bridged specie. Further infrared studies have confirmed that the effect was due to a shift in the background spectrum and not exchange.

33. T. M. Duncan, J. T. Yates, Jr., R. W. Vaughan (unpublished).
34. A. Abragam, The Principles of Nuclear Magnetism (Oxford University Press, London, 1961) Chapter IX.
35. Reference 34, Chapter VI.
36. A. A. V. Gibson and T. A. Scott, J. Mag. Resonance 27, 29 (1977).
37. B. T. Heaton, A. D. C. Towl, P. Chini, A. Fumagalli, D. J. A. McCaffrey, and S. Martinengo, J. C. S. Chem. Comm. 523 (1975).
38. J. Evans, B. F. G. Johnson, J. Lewis, J. R. Norton, and F. A. Cotton, J. C. S. Chem. Comm. 807 (1973).
39. J. Evans, B. F. G. Johnson, J. Lewis, and J. R. Norton, J. C. S. Chem. Comm. 79 (1973).
40. H. W. Spiess, Chem. Phys. 6, 217 (1974).
41. H. Sillescu, J. Chem. Phys. 54, 2110 (1971).
42. Reference 34, Chapter IV.
43. P. A. Thiel, E. D. Williams, J. T. Yates, Jr. and W. H. Weinberg, Surf. Sci. 84, 54 (1979).
44. D. A. Seanor and C. H. Amberg, J. Chem. Phys. 42, 2967 (1965).
45. T. L. Brown and D. J. Dahrenbourg, Inorg. Chem. 6, 971 (1967).
46. R. R. Cavanagh and J. T. Yates, Jr., to be published.
47. M. Grunze, Chem. Phys. Lett. 58, 409 (1978).
48. T. M. Duncan, PhD Thesis, California Institute of Technology, 1980.
49. L. F. Dahl, C. Martell, D. L. Wampler, J. Am. Chem. Soc. 83, 1761 (1961).
50. H. Knözinger, E. W. Thornton, and M. Wolf, J. Chem. Soc. Far. Trans. I 75, 1888 (1979).
51. C. T. Campbell and J. M. White, J. Catal. 54, 289 (1978).
52. J. Schaefer and E. D. Stejskal, J. Am. Chem. Soc. 98, 1031 (1976).

TABLE I. ^{13}C NMR Shieldings in Rhodium Carbonyl Complexes

Compound	Carbonyl Group (a)	Principal Shielding Tensor Components (b)			Reference
		σ_{11}	σ_{22}	σ_{33}	
CO	gas ^s solid at 4.2 K	-62.	-303.	-303.	-181.3 (c) -181.3 (d) (10) (36)
$\text{Rh}_2\text{C}_2(\text{CO})_4$	Terminal (2)	99.	-299.	-306.	-169. (-186.) (d) -180.4 (28)
$\text{Rh}_6(\text{CO})_{16}$	Bridged (3)	-102.	-296.	-296.	(31)
	Terminal (2)	80.	-305.	-315.	-231.3 -231.5 -180.0 -180.1 (37)
$[\text{Rh}_{12}(\text{CO})_{30}]^2-$	Bridged (2)	-	-	-	-211.5 (28)
	Bridged (3)	-	-	-	-237.4 (28)
	Terminal (2)	-	-	-	-186.3 (28)
	Terminal (2)	-	-	-	-186.1 (28)
	Terminal (2)	-	-	-	-183.4 (28)
$\text{Rh}_4(\text{CO})_{12}$	Bridged (2)	-	-	-	-228.8 (38)
	Terminal (3)	-	-	-	-183.4 (38)
	Terminal (2)	-	-	-	-181.8 (38)
	Terminal (2)	-	-	-	-175.5 (38)
$\text{Rh}_2(\text{h}^5-\text{C}_5\text{H}_5)_2(\text{CO})_3$	Bridged (2)	-	-	-	-231.8 (39)
	Terminal (1)	-	-	-	-191.8 (39)

(a) Numbers in parentheses are the number of CO molecules at a single Rh atom for the terminals, or the number of Rh atoms involved in the bridged states.

(b) ppm, relative to tetramethylsilane, (TMS)

(c) Ref. 36 reported only the chemical shift anisotropy, $\sigma_{11} - \sigma_{33} = 365$. The principal component values were computed by assuming an isotropic shift of -181.3 ppm. The anisotropy is believed to be averaged by rapid librational modes at 4.2 K. The computed static anisotropy is 406 ± 30 ppm.

(d) Value in parentheses is the computed center of mass, rather than the isotropic value from the lineshape fit.

FIGURE CAPTIONS

Figure 1. ^{13}C NMR spectrum at 300 K of $\text{Rh}_2\text{Cl}_2(\text{CO})_4$ enriched to 20% ^{13}C . 6.89 ppm per data point. See Table I for the fitted chemical shift tensor components.

Figure 2. ^{13}C NMR spectra of (a) a 2.2% Rh on Al_2O_3 sample with ~50 Torr of ^{13}CO at 300 K; (b) same sample, cooled to 80 K after reducing the CO pressure to 0.02 Torr; and (c) model carbonyl compound $\text{Rh}_2\text{Cl}_2(\text{CO})_4$, from Figure 1, added for comparison. All spectra taken with $\tau = 0.5$ msec, 6.89 ppm per point.

Figure 3. Observed magnetization versus τ , the delay between the 180° and 90° pulses, of ^{13}CO on 2.2% Rh on Al_2O_3 . The CO(ads)-to-Rh ratio for this sample was 1.04. Pulse sequences repeated were every 0.4 sec.

Figure 4. ^{13}C NMR spectra of ^{13}CO adsorbed on 2.2% Rh on Al_2O_3 ($\text{CO/Rh} = 1.04$), with τ at (a) 0.5 msec, (b) 8.0 msec, (c) 30.0 msec, and (d) 50 msec.

Figure 5. ^{13}C NMR spectra of ^{13}CO adsorbed on 2.2% Rh on Al_2O_3 generated by decomposing the spectra taken as a function of τ , based on relative proportions computed from the T_1 distribution. The spin-lattice relaxation times of the two basis spectra are (a) 5.6 msec and (b) 64 msec.

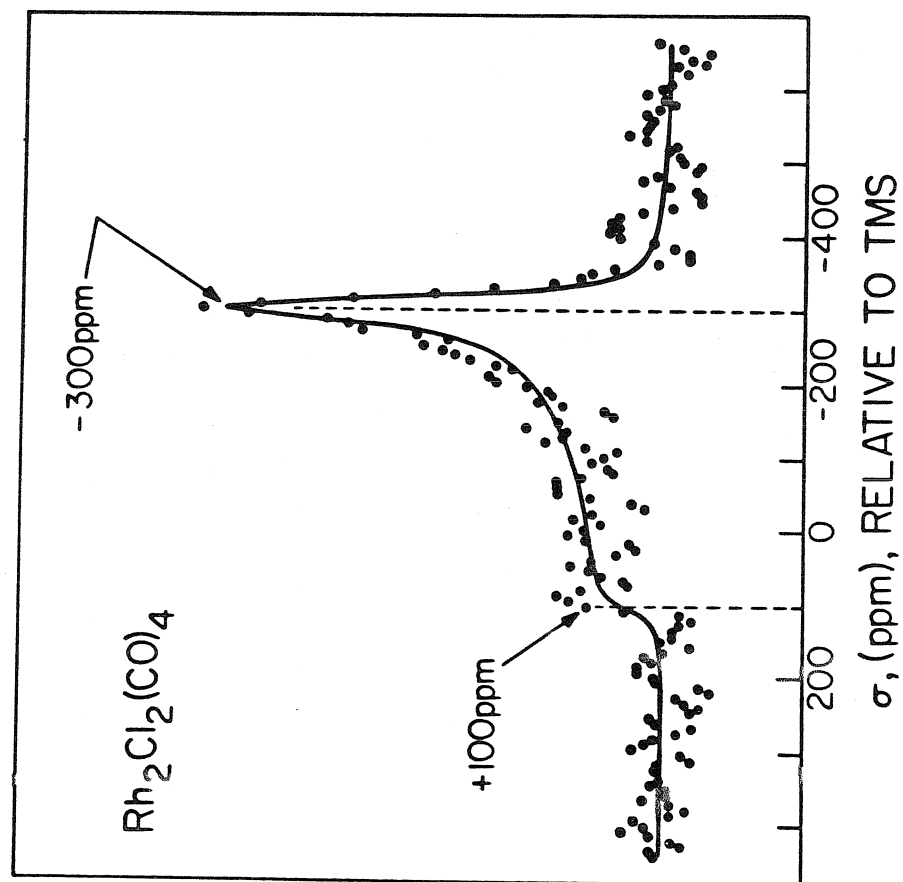


Figure 1

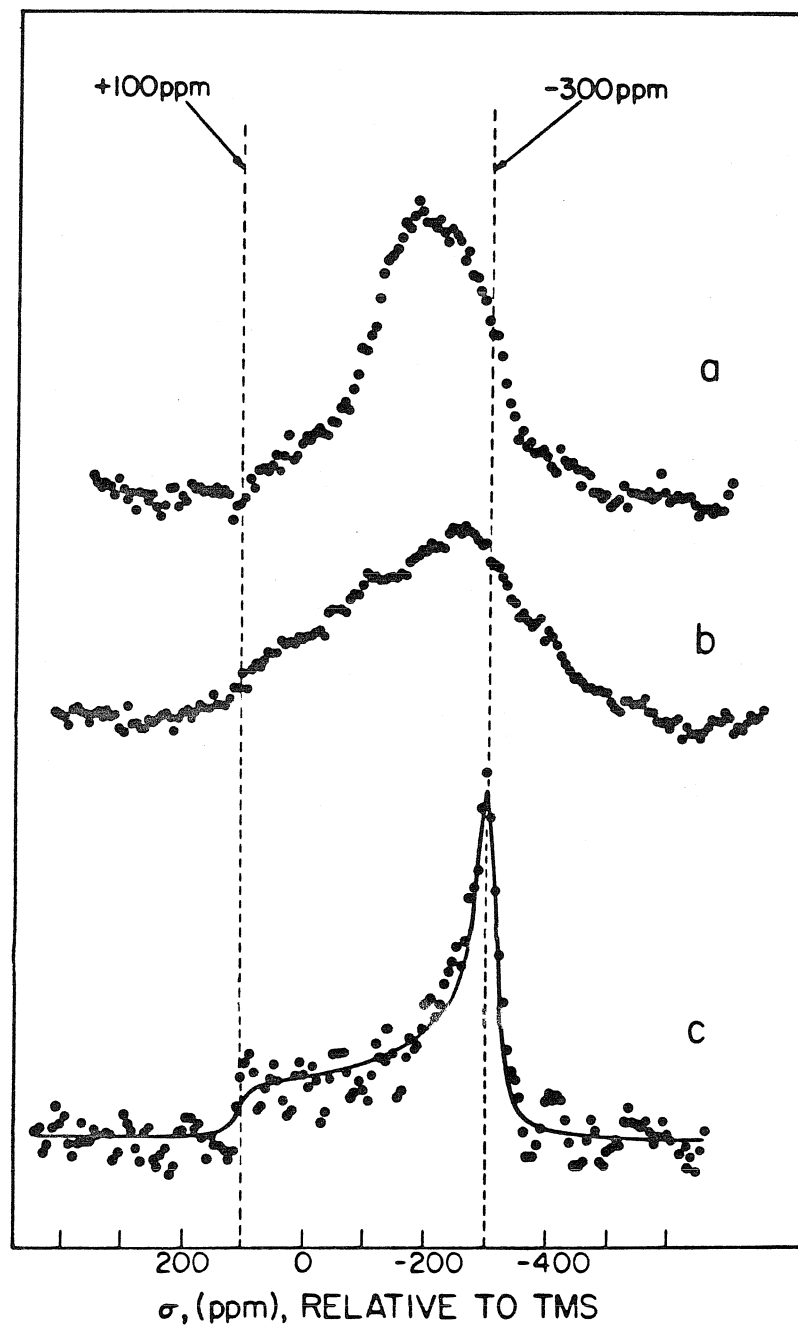


Figure 2

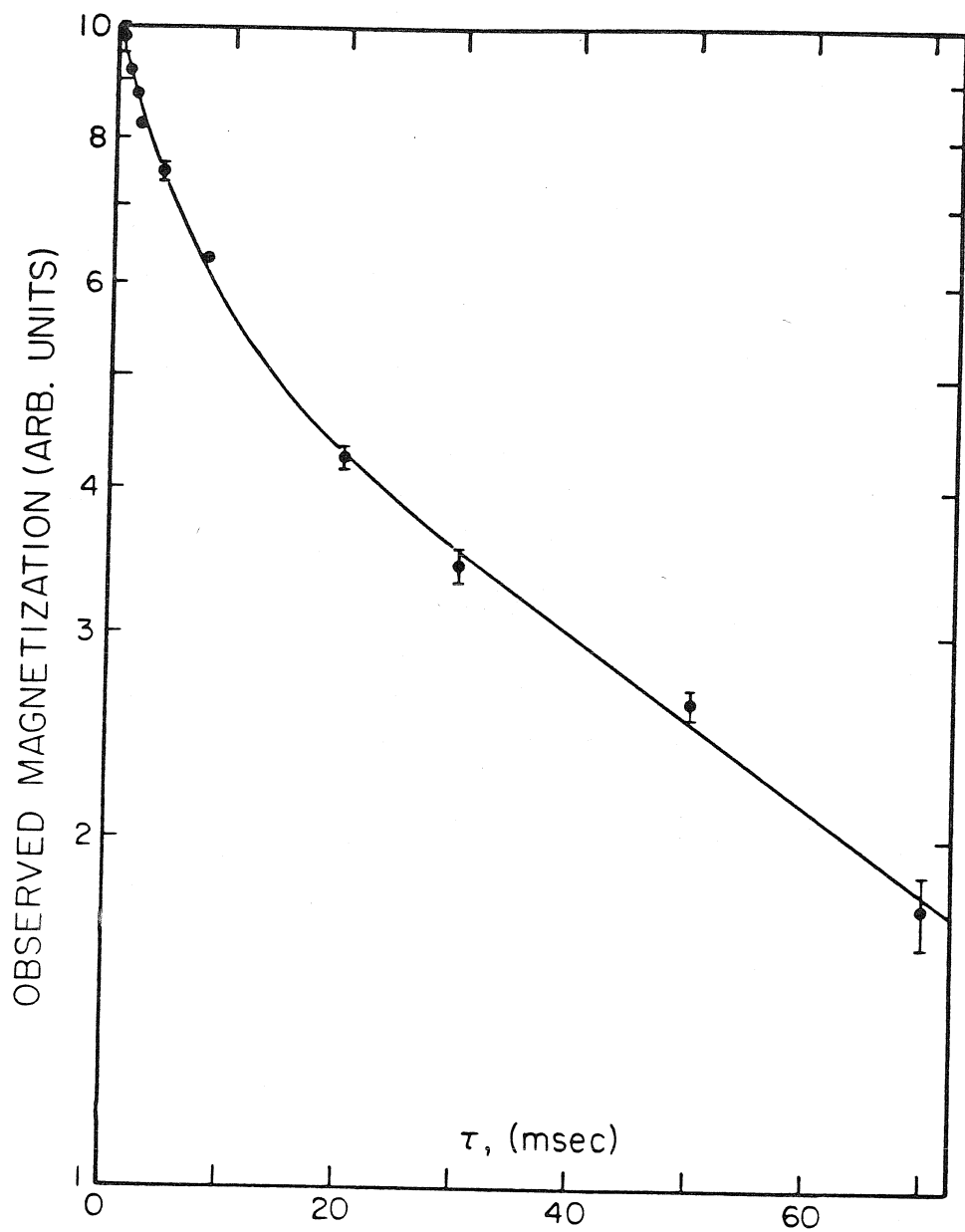


Figure 3

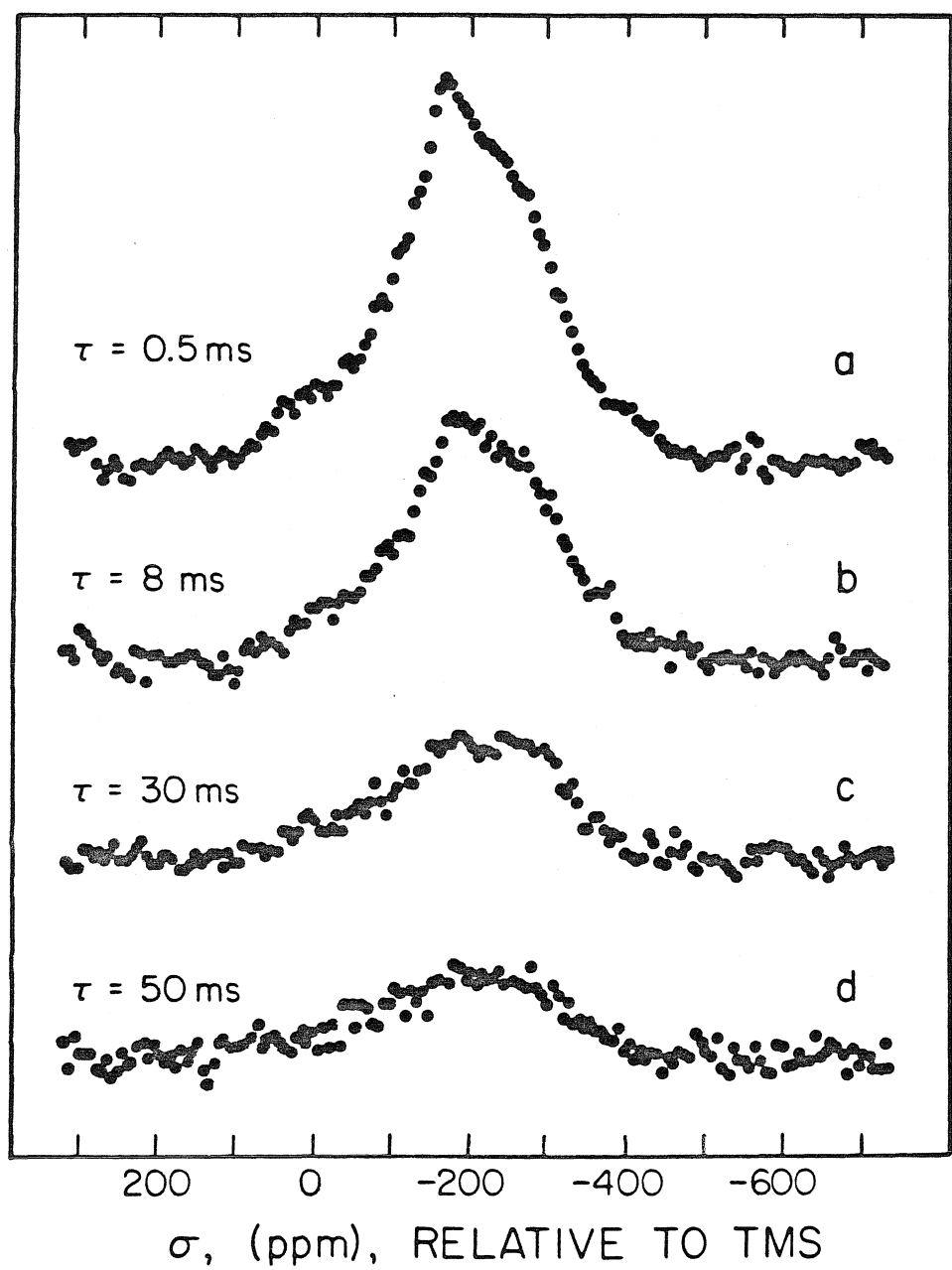


Figure 4

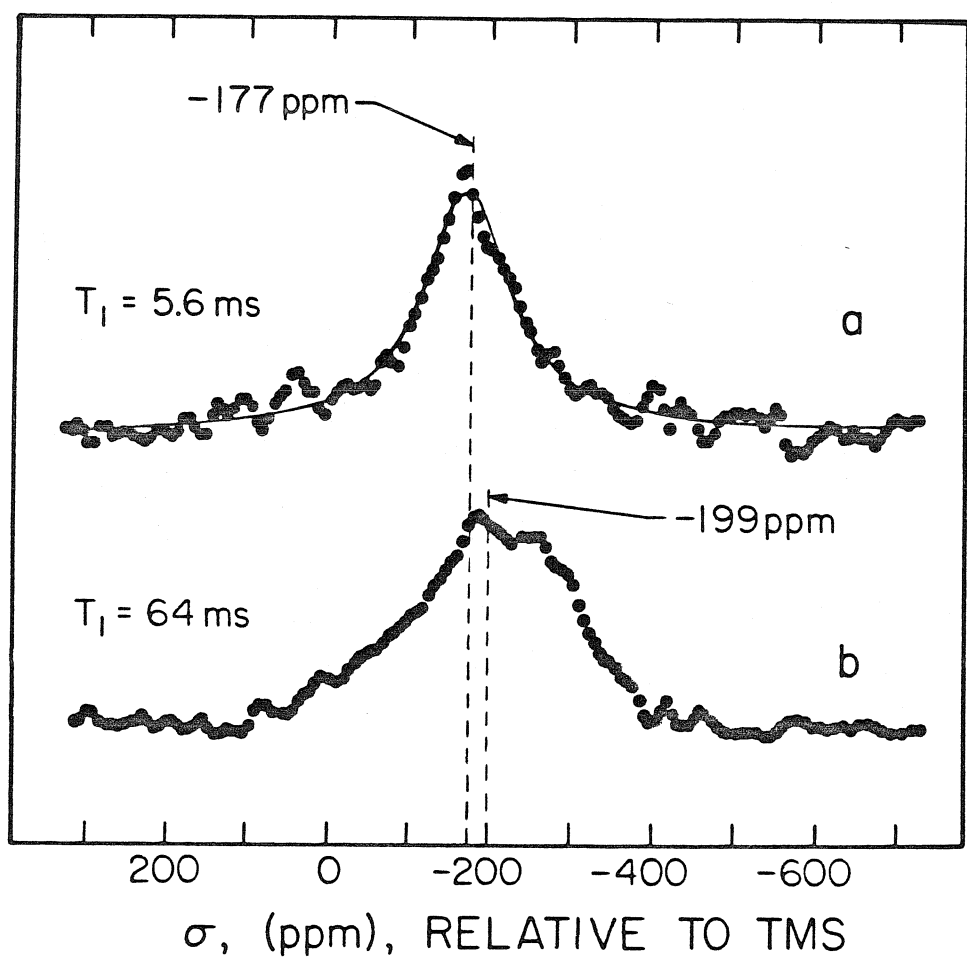


Figure 5

CHAPTER VI

AN INFRARED SPECTROSCOPIC STUDY
OF THE ADSORPTION OF FORMIC ACID
ON AMMONIUM-Y AND ULTRASTABLE HYDROGEN-Y ZEOLITES

(Chapter VI is essentially an article by T. M. Duncan and R. W. Vaughan entitled "An Infrared Spectroscopic Study of the Adsorption of Formic Acid on Ammonium-Y and Ultrastable H-Y Zeolites." This article has been submitted for publication in the Journal of Catalysis.)

Abstract

The adsorption of formic acid on an ammonium-Y ($\text{NH}_4\text{-Y}$) zeolite and an ultrastable hydrogen-Y (H-Y) zeolite has been studied with transmission infrared spectroscopy. The formic acid is determined to be chemically adsorbed on both zeolites as bidentate formate ions and as covalently bonded unidentate formate species. Assuming uniform infrared extinction coefficients for the two adsorbed formates, the $\text{NH}_4\text{-Y}$ zeolite has comparable amounts of each surface species. The ultrastable H-Y zeolite, which has enhanced catalytic properties, adsorbs the formic acid primarily as bidentate formate ions. It is suggested that the nonframework aluminum cations in the ultrastable H-Y zeolite act as adsorption sites for the formate ions.

I. INTRODUCTION

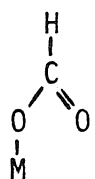
Formic acid decomposes catalytically by dehydration to H_2O and CO or by dehydrogenation to H_2 and CO_2 depending on the nature of the catalyst (1,2). Metals, such as Cu or Ni, catalyze primarily the dehydrogenation reaction. On metal oxides both reactions may occur to some degree. However, on aluminas and silicas the dehydration reaction dominates (2).

We present here a study of the adsorption of formic acid on two zeolites: an ammonium-Y (NH_4 -Y) and an ultrastable hydrogen-Y (H-Y) zeolite. The decomposition of submonolayer coverages of formic acid on these zeolites yields almost exclusively CO and H_2O . Both zeolites have the faujasite-type structure containing nearly spherical cavities 12 \AA^0 in diameter interconnected by 8 to 9 \AA^0 openings (3). The ultrastable H-Y is the "deep-bed" calcination product of the NH_4 -Y zeolite at about 775 K (4). Although derived from the NH_4 -Y zeolite, the ultrastable H-Y zeolite is quite different, possessing increased catalytic properties, increased thermal stability, and increased resistance to acid decomposition (5). It is proposed that the increased stability is the result of the removal of a portion of the tetrahedrally coordinated framework aluminum atoms, yielding cationic aluminum species with charges ranging from 1 to 3 (6). Specifically, it is suggested that the decomposition of the NH_4 -Y to the ultrastable H-Y zeolite creates 9 to 15 aluminum cations per unit cell (6). This is consistent with ammonia adsorption studies on the ultrastable H-Y zeolite which indicate the presence of 12 new Brönsted acid sites per unit cell (6). However, although it is generally accepted that chemical analysis combined with X-ray

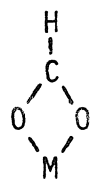
diffraction of the zeolite suggest an aluminum-deficient structure, the nature of the nonframework aluminum and the defect site is still quite uncertain (7).

The adsorbed state of formic acid on metal oxides has been studied by various spectroscopies, primarily by transmission infrared techniques (8,9,10,11). Other techniques include reflectance infrared (12), inelastic electron tunneling spectroscopy (IETS) (13,14), and nuclear magnetic resonance methods (11,15). It is the general conclusion that the formic acid chemisorbs onto metal oxides via the loss of the acidic proton. The formate ion is then bonded to the substrate through one or both of the oxygen atoms. However, there is some discussion regarding the role of the formate ion in the decomposition reaction. Some studies indicate that the rate-determining step for the reaction on alumina is the direct decomposition of the formate ion (9), whereas others maintain that the formate ions first desorb from the alumina as formic acid and then react with surface protons (10).

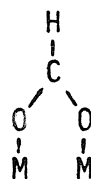
The adsorbed state of the formate ion is important in either the direct-decomposition or the desorption-and-decomposition reaction paths. The state of the formate ion may be described by any one, or a combination, of the species shown below.



I



II



III

The unidentate formate structure (species I) is bonded through a single

oxygen atom, as in formic acid and formate esters. The bidentate and bridging bidentate structures (species II and III) may occur in both symmetrical and unsymmetrical forms, depending on the metal ion lattice spacings. Infrared studies on formate salts suggest that the formate bonding is determined by the ionic radius of the metal atom (16), the electronegativity of the metal (17), or both properties plus the mass of the metal atom (18).

Because of the lack of periodicity and low concentrations of the formate ions on the polycrystalline zeolite samples, it is not feasible to determine directly the structure of the adsorbate by various diffraction methods (19). It is, therefore, necessary to examine other quantities which are sensitive to the molecular geometry and then, through analogy with known structures, determine the state of the adsorbed species. In the paper we will examine one such property, the vibrational spectra of the adsorbed formic acid, with transmission infrared spectroscopy. To aid in the assignment of the infrared bands, we will compare the spectra of the normal formic acid and the ^{13}C -enriched compound to observe the isotopic frequency shifts. In an accompanying paper, we measure another property, the chemical shift tensor, with nuclear magnetic resonance techniques (15).

II. EXPERIMENTAL PROCEDURE

The ammonium-Y ($\text{NH}_4\text{-Y}$) zeolite, unit cell formula $\text{Na}_2(\text{NH}_4)_{48}(\text{AlO}_2)_{50}(\text{SiO}_2)_{142} \cdot 26\text{H}_2\text{O}$, was prepared by ion exchange with a sodium-Y zeolite. This $\text{NH}_4\text{-Y}$ zeolite was calcined at 775 K to yield a "deep bed" product, the ultrastable hydrogen-Y (H-Y) zeolite, with unit cell formula $\text{Na}_2\text{H}_{48}(\text{AlO}_2)_{50}(\text{SiO}_2)_{142} \cdot 26\text{H}_2\text{O}$ (4).

The zeolites were outgassed and dosed with formic acid in a sample cell described previously (3), which was designed for transmission infrared spectroscopy through powdered substrates. It was not feasible to spray a water/acetone suspension of the zeolite onto the hot CaF_2 -windowed flange, as has been done for alumina samples (20,21). Rather, a thin layer was deposited onto the CaF_2 window by sifting the zeolite through a 100-mesh sieve (0.147 mm openings). The surface density of the sifted zeolite powders was typically 4 to 5 mg/cm^2 . Taking care not to disturb the zeolite film, the cell is assembled, evacuated, and heated, with the CaF_2 flange supported horizontally. After cooling, the zeolite layer adheres to the CaF_2 window and the cell may be rotated to a vertical position to be placed in the infrared beam without loss of material. However, such deposits are not so rugged as the sprayed crusts and still require gentle handling.

The zeolites were outgassed on an ion-pumped all-metal vacuum system described previously (21). The samples were warmed at a rate of about 1 K/min while being pumped continuously. The $\text{NH}_4\text{-Y}$ zeolite was outgassed at 395 K for 3 hours, sufficiently cool to ensure that the ammonium ions do not decompose (22). The ultrastable H-Y zeolite was first re-calcined in a furnace at 775 K for 6 hours, cooled to about 450 K, and then sifted onto the CaF_2 flange while still warm. The cell was then assembled and the ultrastable H-Y zeolite was outgassed at 500 K for 3 hours. The typical background pressure of the cooled, outgassed substrate was 10^{-6} Torr.

The BET surface area measurements and the formic acid adsorptions

were carried out on a liquid nitrogen-trapped diffusion-pumped glass vacuum system. The nitrogen BET surface areas of the zeolites are $459 \pm 10 \text{ m}^2/\text{g}$ and $515 \pm 10 \text{ m}^2/\text{g}$ for the $\text{NH}_4\text{-Y}$ and the ultrastable H-Y, respectively, representing monolayers of about 63 and 84 nitrogen molecules per unit cell. The formic acid adsorption isotherms for both zeolites, shown in Figure 1, reveal monolayer coverages of 75 and 56 formic acid molecules per unit cell, or 5.7×10^{14} and 5.5×10^{14} molecules/cm², for the $\text{NH}_4\text{-Y}$ and the ultrastable H-Y zeolites, respectively. The formic acid was adsorbed from the gas phase. The predetermined pressure of the vapor to be adsorbed was calculated from the monomer/dimer equilibrium data of Coolidge (23). The continuous uptake of formic acid by the $\text{NH}_4\text{-Y}$ zeolite for P/P_0 greater than 0.22 suggests that the zeolite is decomposing under acid attack. The ultrastable H-Y exhibits no such degradation in the pressures studied ($P/P_0 < 0.5$). For coverages less than 40 molecules per unit cell, the equilibrium pressure of the formic acid was less than 0.1 Torr, below the range of the Wallace and Tiernan gauge used in the adsorption studies. A mass spectrometric analysis of the formic acid desorption products from a submonolayer coverage on the ultrastable H-Y at 525 K revealed that the carbon was evolved as 98.5% CO and 1.5% CO_2 with no trace on any residual formic acid detected.

The infrared spectra were measured at submonolayer coverages of formic acid adsorbed on the zeolites. In this range, though there were subtle changes in relative peak intensities, no new features developed at higher coverages. For each zeolite, we report here the spectra of two typical coverages. Specifically, the $\text{NH}_4\text{-Y}$ zeolite sample contained

about 20 molecules per unit cell. The formic acid coverage on the $\text{NH}_4\text{-Y}$ zeolite is well below the levels which caused structural degradation of the zeolite. The ratio of hydrogen ions formed during the adsorption to the number of ammonium ions is still low enough to allow the zeolitic framework to remain intact (24). The ultrastable H-Y sample contained about 17 formic acid molecules per unit cell.

The transmission-infrared spectra were measured with a Perkin-Elmer Model 180 spectrometer, operated in the double-beam mode. The resolution in the 1800 to 1200 cm^{-1} region was set at 2.1 cm^{-1} . The frequencies were calibrated with liquid films of the formic acid isotopes.

The ^{12}C formic acid was treated with anhydrous CuSO_4 to remove any water. The isotopically enriched formic acid (91.2% ^{13}C), obtained from Merck Isotopes, was used without further purification.

III. RESULTS

For comparison, the spectral features of the two formic acid isotopes are listed in Table I. The samples were prepared by filling an empty infrared cell to the saturation pressure of formic acid, thus forming a liquid film on the CaF_2 windows. The band assignments in Table I were determined previously through an analysis of the isotopic shifts of the various deuterated forms of formic acid relative to the normal compound (25). The asymmetric vibration of the molecule (C=O stretch) exhibits the most pronounced effect upon the substitution of ^{13}C , decreasing by about 41 cm^{-1} . The symmetric vibration (C-O stretch) is somewhat less perturbed, decreasing by only 9 cm^{-1} .

The infrared spectra at 295 K of the outgassed $\text{NH}_4\text{-Y}$ and the ultrastable H-Y zeolites are shown in Figure 2. The surface coverages

on the CaF_2 windows were 3.8 and 4.6 mg/cm^2 for the $\text{NH}_4\text{-Y}$ and the ultrastable H-Y zeolites, respectively, for the two spectra shown. The spectral features of the $\text{NH}_4\text{-Y}$ zeolite at 1470 and 1430 cm^{-1} have been identified previously as ν_4 bending vibrations of NH_4^+ ions (22). The peak at 1670 cm^{-1} peak on the $\text{NH}_4\text{-Y}$ zeolite has been assigned to the bending vibration of H_2O , and the peak at 1705 cm^{-1} on the ultrastable H-Y has been associated with H_3O^+ ions (22). The infrared spectral region for both zeolites was about 2000 cm^{-1} to 1000 cm^{-1} . Above this range, 4000 cm^{-1} to 2000 cm^{-1} , there were prohibitively large losses in transmittance due to scattering. Below 1000 cm^{-1} , the spectrum was blacked out by the strong absorbances of the zeolite substrate.

The infrared spectra for formic acid adsorbed on the $\text{NH}_4\text{-Y}$ and ultrastable H-Y zeolites are shown in Figures 3 and 4, respectively. The spectra were obtained by subtracting the appropriate background spectra in Figure 2 from the observed spectra. In both Figures 3 and 4, spectrum (a) is the normal formic acid, and spectrum (b) is the 91% ^{13}C -enriched compound. The wavenumber markers are included only as references and are not to be taken literally as the exact assignments of the broad peaks and sidebands. Although each spectrum is composed of a number of overlapping bands, it is possible to identify the peaks due to carbon-oxygen stretches or carbon-hydrogen bands by comparison with the isotopically shifted spectrum. The shifts indicated in Figures 3 and 4 were determined by assuming that if

the intensity at a specific frequency decreased upon the substitution of ^{13}C for ^{12}C , the intensity shifted to a lower frequency, but not more than about 40 cm^{-1} for peaks in the range 1800 to 1500 cm^{-1} , and not more than about 10 cm^{-1} for peaks in the range 1500 to 1200 cm^{-1} . This analysis is rather straightforward in the ultrastable H-Y spectra, but it is slightly more arbitrary for the $\text{NH}_4\text{-Y}$ case. For example, in Figure 3, the structure at 1734 cm^{-1} of spectrum 3(a) has shifted in spectrum 3(b). Using the above guidelines, we propose that the peak has shifted to about 1698 cm^{-1} , a 34 cm^{-1} decrease, and has not shifted to about 1642 cm^{-1} , a decrease of 92 cm^{-1} .

IV. DISCUSSION

Upon isotopic substitution of ^{13}C -enriched formic acid, almost all of the peaks in the spectra of Figures 3 and 4 shift to lower frequencies. In addition, all the high frequency peaks (1750 to 1500 cm^{-1}) have corresponding peaks within 40 cm^{-1} and all the lower frequency peaks (1450 to 1200 cm^{-1}) have corresponding peaks within about 10 cm^{-1} . This is consistent with the observed isotopic shifts of formic acid. Thus, almost all of the features observed in the range 1800 to 1200 cm^{-1} of the infrared spectra of the adsorbed formic acid can be attributed to either carbon-oxygen stretches or carbon-hydrogen bending modes. The other unshifting

peaks can also be assigned to surface formate structures on the basis of their location, as will be discussed later. To interpret the positions of the infrared bands, the spectra of the formate ion in various configurations, as well as adsorbed on surfaces, will be discussed.

The relative positions of the symmetric and asymmetric stretches in the formate structure are indicative of the molecular geometry. For the covalently bonded unidentate structures of formic acid and methyl formate, the two bands are separated by 635 and 560 cm^{-1} , respectively. Upon transformation to the bidentate structure of formate salts, the carbon-oxygen double bond is weakened and the carbon-oxygen single bond is strengthened. Consequently, the separation between the two bands for typical formate salts is decreased to about 230 cm^{-1} . The infrared absorbances for some representative formate structures are given in Table II.

The correlation between the shifts in the infrared bands and the structure of the formate group has been invoked in previous vibrational studies to differentiate between chemically and physically adsorbed formic acid. Table III contains the vibrational spectra of formic acid adsorbed on Al_2O_3 and other surfaces. This is by no means a comprehensive review, but rather a representative survey of previous studies to demonstrate the trends of the observed frequencies. In general, the surface formate ion has an asymmetric stretch in the range 1590 to 1625 cm^{-1} and a symmetric stretch in the range 1360 to 1468 cm^{-1} . These frequencies are in good agreement with those of the formate salts, such as the compounds listed in Table II. On the basis of the similarities with the infrared spectra of

formate ions in metal salts, it has been proposed that the formate ion is adsorbed on the surface as symmetric bidentate structures (19).

When there is only a slight perturbation in the asymmetric band, it is usually proposed that the formic acid is physically adsorbed on the surface (8,11,14). This is most likely the case for formic acid adsorbed on Al_2O_3 at 77 K, which converts to the chemisorbed formate ion upon warming to room temperature (14). However, we propose that in the case of formic acid adsorbed on SiO_2 (11) and the Na-Y zeolite (8) at room temperature, another interpretation of the small shift in the asymmetric frequency is possible. That is, the acid may be dissociatively adsorbed on the surface in a covalently bonded unidentate structure. This is supported by a proton nuclear magnetic resonance study of the formic acid adsorbed on SiO_2 which detected only the carbonyl proton (11). It is probable that the acidic proton had dissociated from the acid and had bonded to the SiO_2 surface. Thus, if the proton were still bonded to the acid it would probably appear in the NMR spectrum, whereas if the proton had bonded to the surface, the spectrum would be extremely broadened and thus not be observed. The formate group could be bonded to the surface through a single oxygen atom to a Si or Al atom of the substrate. In this configuration, one would expect that the asymmetric band of the formic acid at 1743 cm^{-1} would be decreased only slightly, as in the case of methyl formate. Thus, we maintain that there is equal evidence for the unidentate structure as well as physically adsorbed formic acid. However, when the vibrational spectra show no evidence of formic acid OH stretches at about 3580 cm^{-1} or OH bends at about 1218 cm^{-1} , the unidentate structure is strongly implied.

The infrared spectra of formic acid adsorbed on the $\text{NH}_4\text{-Y}$ and the ultrastable H-Y zeolites have peaks extending from the physically adsorbed (or unidentate) region (about 1720 cm^{-1}) to the chemisorbed formate ion region (about 1590 cm^{-1}). The spectrum of the formic acid adsorbed on the ultrastable H-Y zeolite affords the more straightforward analysis. The most intense peaks at 1610 and 1385 cm^{-1} are assigned to the asymmetric and symmetric stretches of the formate ion, consistent with the assignments in Table III. These bands are in close agreement with those of aluminum formate, listed in Table II. Since there was no evidence of OH bending modes of the formic acid molecule and the adsorption isotherm suggests that the formic acid chemisorbs to the surface, the peaks at 1760 and 1718 cm^{-1} are interpreted to be the asymmetric and symmetric stretches of two unidentate formate structures. The corresponding symmetric stretches of these species are probably combined in the side peak at 1336 cm^{-1} , although it is at a higher frequency than would be expected. The 1416 cm^{-1} side peak is interpreted as the CH bend of all the adsorbed formate species.

The spectrum of the formic acid adsorbed on the $\text{NH}_4\text{-Y}$ zeolite is more complex and does not immediately suggest an obvious assignment of the various peaks. However, it is possible to compare the general shape of the spectrum to that of the ultrastable H-Y sample. In the region of the asymmetric stretch the maximum intensity has shifted from 1610 cm^{-1} to higher frequencies, near 1694 and 1734 cm^{-1} . Simultaneously, the maximum intensity in the symmetric stretch region has shifted to a lower frequency, from 1385 to 1292 cm^{-1} . Thus, assuming that the extinction coefficients

of each peak do not change radically from the ultrastable H-Y to the NH_4 -Y zeolite, the infrared spectra suggest that the NH_4 -Y sample contains a larger percentage of unidentate formate groups.

The new peaks that appear in the spectrum of the formic acid adsorbed on the NH_4 -Y sample are tentatively interpreted as follows. The minimum at 1762 cm^{-1} may be only the initial slope of a large dip in the background spectrum caused by the loss of NH_4^+ ions upon the adsorption of formic acid. The 1534 and 1454 cm^{-1} peaks involve the carbon atom since they are shifted upon isotopic substitution. These bands do not have analogies in any of the formate compounds although it is possible that the band at 1454 cm^{-1} is related to the 1468 cm^{-1} band observed for formic acid on Al_2O_3 (13,14).

V. CONCLUSIONS

Vibrational spectra observed by transmission infrared spectroscopy and adsorption isotherms suggest that formic acid chemically adsorbs on the surface of the NH_4 -Y and ultrastable H-Y zeolites in at least two configurations. These two structures have been interpreted to be a covalently bonded unidentate formate group and as a formate ion. Based on the position of the bands assigned to the formate ion and the agreement with the bands of aluminum formate, it is likely that the formate ion has a bidentate structure. It was not possible to determine if the formate ion is adsorbed as a bidentate or bridging-bidentate species. The presence of the unidentate formate group, as opposed to physically adsorbed formic acid, is supported by the adsorption isotherms and the lack of any OH bending vibrations in the infrared spectra. The unidentate structure is probably covalently bonded, similar to ester compounds, to

account for the position of the infrared bands near 1734 and 1694 cm^{-1} . The frequencies of the asymmetric stretches of unidentate salts are generally not this high (27), whereas unidentate-type esters such as methyl formate are all within this range. Although there is no direct experimental evidence to suggest it, the unidentate species would be more likely to form at the Si atoms of the zeolite since the aluminum formate is known to have a bidentate structure (27).

The adsorption of formic acid is markedly different on the $\text{NH}_4\text{-Y}$ and ultrastable H-Y zeolites. As revealed by the infrared spectra, the formic acid is adsorbed on the ultrastable H-Y zeolite primarily as formate ions, whereas on the $\text{NH}_4\text{-Y}$ zeolite, the unidentate species appears to be slightly in the majority. Both zeolites have the faujasite structure and there is no infrared evidence of surface hydroxyl groups on either zeolite. However, the ultrastable H-Y zeolite is suggested to contain a number of non-framework aluminum ions in the supercages (6). Therefore it is likely that the increased proportion of formate ions on the ultrastable H-Y zeolite is due to the presence of the aluminum ions which act as adsorption sites for the formic acid. Further studies are required to determine if these sites are responsible for the enhanced catalytic properties of the ultrastable H-Y zeolite.

These conclusions will be further examined in an accompanying paper (15), in which nuclear magnetic resonance techniques are applied to study the state of the adsorbed formic acid molecule, the nature of the adsorption site, and the relative populations of these sites.

VI. ACKNOWLEDGMENTS

The authors gratefully acknowledge support from the Office of Naval Research under contract N00014-75-C-0960. We thank Professor George R. Rossman for his kindness in allowing us to use his infrared spectrometer and Dr. G. T. Kerr of Mobil Oil Research and Development for supplying the zeolite samples. Professor W. H. Weinberg and Professor S. I. Chan offered helpful discussions and suggestions on the manuscript.

References

1. P. Mars, J. J. F. Scholten, and P. Zweitering, *Adv. Catal.* 14, 35 (1963).
2. J. M. Trillo, G. Munuera, and J. M. Cridao, *Catal. Rev.* 7, 51 (1973).
3. P. B. Venuto and P. S. Landis, *Adv. Catal.* 18, 259 (1968).
4. (a) G. T. Kerr, *Adv. in Chem. Series* 121, 219 (1973);
(b) C. V. McDaniel and P. K. Maher, Molecular Sieves, Soc. of the Chem. Industry, London, 1967, p. 86.
5. M. L. Poutsma, Zeolite Chemistry and Catalysis, J. A. Rabo, ed., ACS Monograph 171, 1976, p. 437.
6. G. T. Kerr, *J. Catalysis* 15, 200 (1969).
7. J. V. Smith, Zeolite Chemistry and Catalysis, J. A. Rabo, ed., ACS Monograph 171, 1976, p. 56.
8. A. Bielanski and J. Datka, *J. Catalysis* 32, 183 (1974).
9. J. J. F. Scholten, P. Mars, P. G. Menon, and R. Van Hardeveld, *Proc. Intern. Cong. Catalysis*, 3rd, Amsterdam, 1964, p. 881.
10. Y. Noto, K. Fukuda, T. Onishi, and K. Tamari, *Trans. Far. Soc.* 63, 2300 (1967).
11. K. Hirota, K. Fueki, K. Shindo, and Y. Nakai, *Bull. Chem. Soc. Japan* 32, 1261 (1959).
12. M. Ito and W. Suetaka, *J. Phys. Chem.* 79, 1190 (1975).
13. B. F. Lewis, M. Mosesman, and W. H. Weinberg, *Surface Sci.* 41, 142 (1974).
14. O. I. Shklyarevskii, A. A. Lysykh, and I. K. Yanson, *Sov. J. Low. Temp. Phys.* 2, 328 (1976).

15. T. M. Duncan and R. W. Vaughan, *J. Catalysis*, submitted.
16. R. Theimer and O. Theimer, *Monatsh.* 81, 313 (1950).
17. B. Ellis and H. Pyszora, *Nature* 181, 181 (1958).
18. R. E. Kagarise, *J. Phys. Chem.* 59, 271 (1955).
19. J. T. Hall and P. K. Hansma, *Surface Sci.* 76, 61 (1978).
20. R. G. Greenler, *J. Chem. Phys.* 37, 2094 (1962).
21. J. T. Yates, Jr., T. M. Duncan, S. D. Worley, and R. W. Vaughan, *J. Chem. Phys.* 70, 1219 (1979).
22. J. B. Uytterhoeven, L. G. Christner, and W. K. Hall, *J. Phys. Chem.* 69, 2117 (1965).
23. A. S. Coolidge, *J. Amer. Chem. Soc.* 50, 2166 (1928).
24. C. V. McDaniel and P. K. Maher, Zeolite Chemistry and Catalysis, J. A. Rabo, ed., ACS Monograph 171, 1976, p. 296.
25. R. C. Millikan and K. S. Pitzer, *J. Chem. Phys.* 27, 1305 (1957).
26. A. R. Katritzky, J. M. Lagowski, and J. A. T. Beard, *Spectrochim. Acta* 16, 964 (1960).
27. J. D. Donaldson, J. F. Knifton, J. O'Donoghue, and S. D. Ross, *Spectrochim. Acta* 20, 847 (1964).

TABLE I

Vibrational Spectra^(a) of H¹²COOH and H¹³COOH^(b)

<u>Assignment</u> ^(c)	<u>H¹²COOH</u>	<u>H¹³COOH</u>	<u>Δv</u>
O-H stretch	3580	3580	0
C-H stretch	{ 2943 2938 }	{ 2934 2927 }	{ -9 -11 }
C=O stretch	{ 1746 1736 }	{ 1705 1694 }	{ -41 -42 }
C-O stretch	1106	1097	-9
C-H bend	1362	1351	-11
O-H bend	1218	1206	-12

(a) all frequencies in wavenumbers, cm⁻¹

(b) monomer form of the acid in a liquid film.

(c) based on band assignments in Reference 25.

TABLE II
Vibrational Spectra of Formate Compounds^(a)

<u>Compound</u>	<u>$\nu(C=O)$</u>	<u>$\nu(C-O)$</u>	<u>$\delta(CH)$</u>	<u>Reference</u>
HCOOH	1741	1106	1362	This work
HCOOCH ₃ ^(b)	1722	1162	1377	26
Na(HCO ₂)	1592	1364	1381	27
NH ₄ (HCO ₂)	1592	1364	1406	27
Al(HCO ₂) ₃	1613	{ 1387 1368 }	{ 1420 1406 }	27

(a) all frequencies in wavenumbers, cm^{-1}

(b) HCOOCH₃ in CHCl₃ solution

TABLE III.
Representative Vibrational Band Positions for Adsorbed Formic Acid

Substrate	Vibrational Band Assignments (a)			Measurement Technique	Reference
	C=O Stretch	C-O Stretch	CH Bend		
Al Metal	1590	1360	-	Reflectance Infrared	12
Al ₂ O ₃	1597	1377	-	Transmission Infrared	20
Al ₂ O ₃	1600	1380	-	Transmission Infrared	9
Al ₂ O ₃	1625	1390	1407	Transmission Infrared	10
Al ₂ O ₃	1620	1344	1402	Transmission Infrared	11
Na-Y Zeolite	-	1385	-	Transmission Infrared	8
Al ₂ O ₃	1621	1468	1390	IETS	13
Al ₂ O ₃	1620	1468	1390	IETS	14
		1320			
B. Physically Adsorbed Formic Acid					
Al ₂ O ₃ at 77 K	1700	1250	1390	IETS	14
SiO ₂	1714	960	-	Transmission Infrared	11
Na-Y Zeolite	1720	-	-	Transmission Infrared	8

(a) a11 frequencies in cm^{-1}

Figure Captions

Figure 1. Adsorption isotherms for formic acid on the $\text{NH}_4\text{-Y}$ (\square) and the ultrastable H-Y (Δ) zeolites at 297 K.

Figure 2. Background infrared spectra for the $\text{NH}_4\text{-Y}$ and ultrastable H-Y zeolites.

Figure 3. Background-corrected infrared spectra of formic acid ((a) H^{12}COOH and (b) H^{13}COOH) adsorbed on the $\text{NH}_4\text{-Y}$ zeolite at 295 K.

Figure 4. Background-corrected infrared spectra of formic acid ((a) H^{12}COOH and (b) H^{13}COOH) adsorbed on the ultrastable H-Y zeolite.

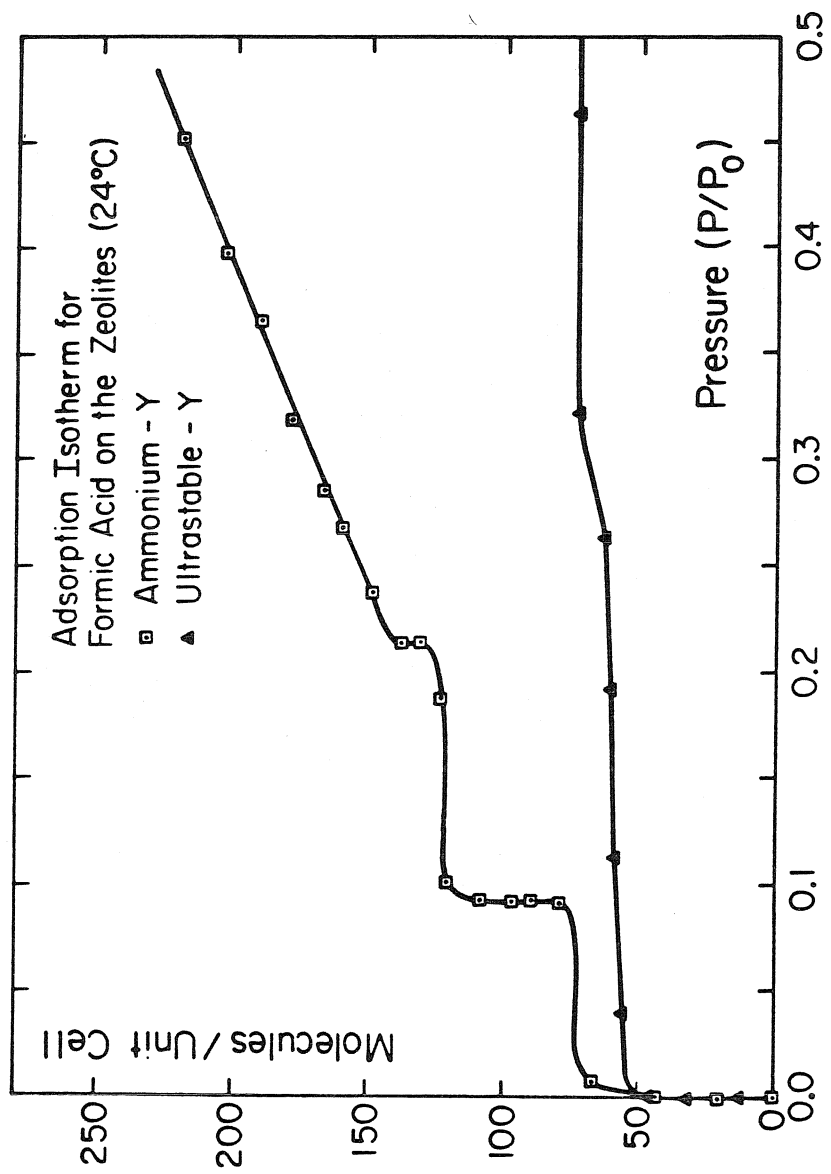


Figure 1

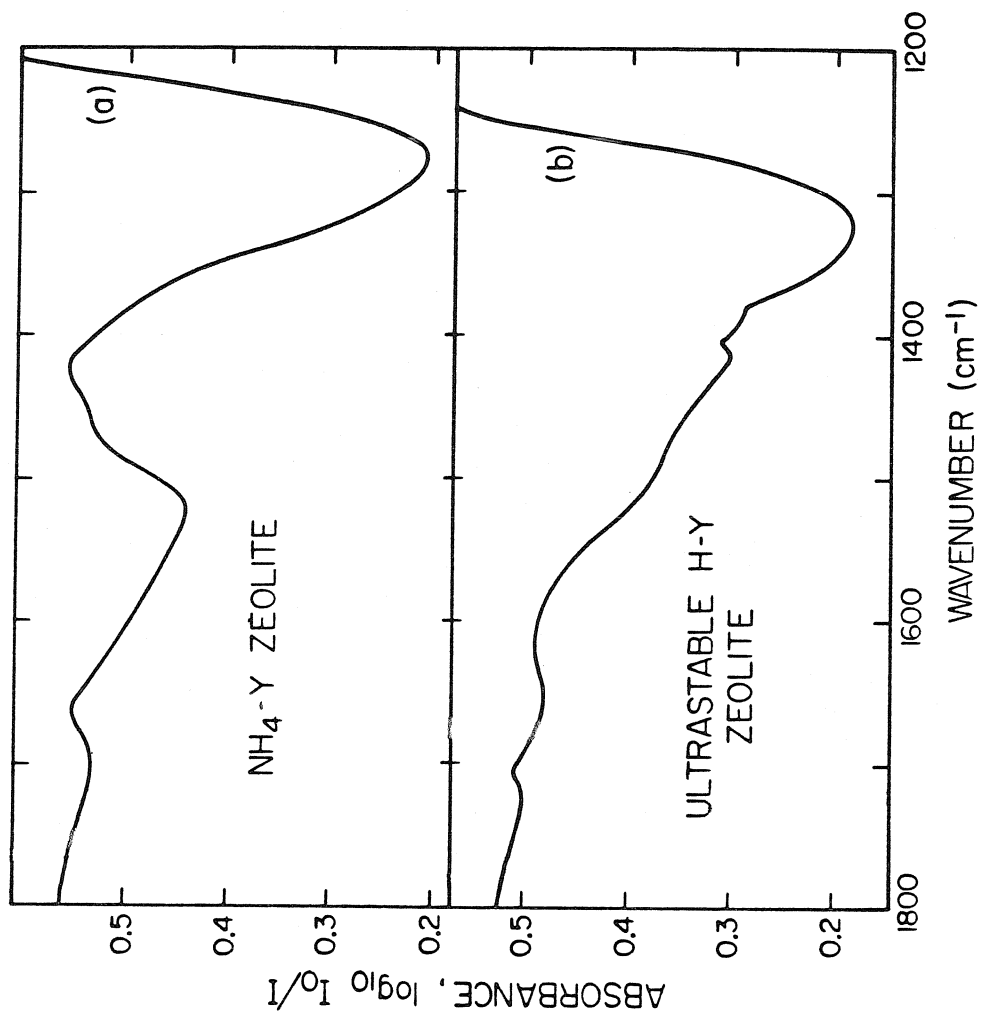


Figure 2

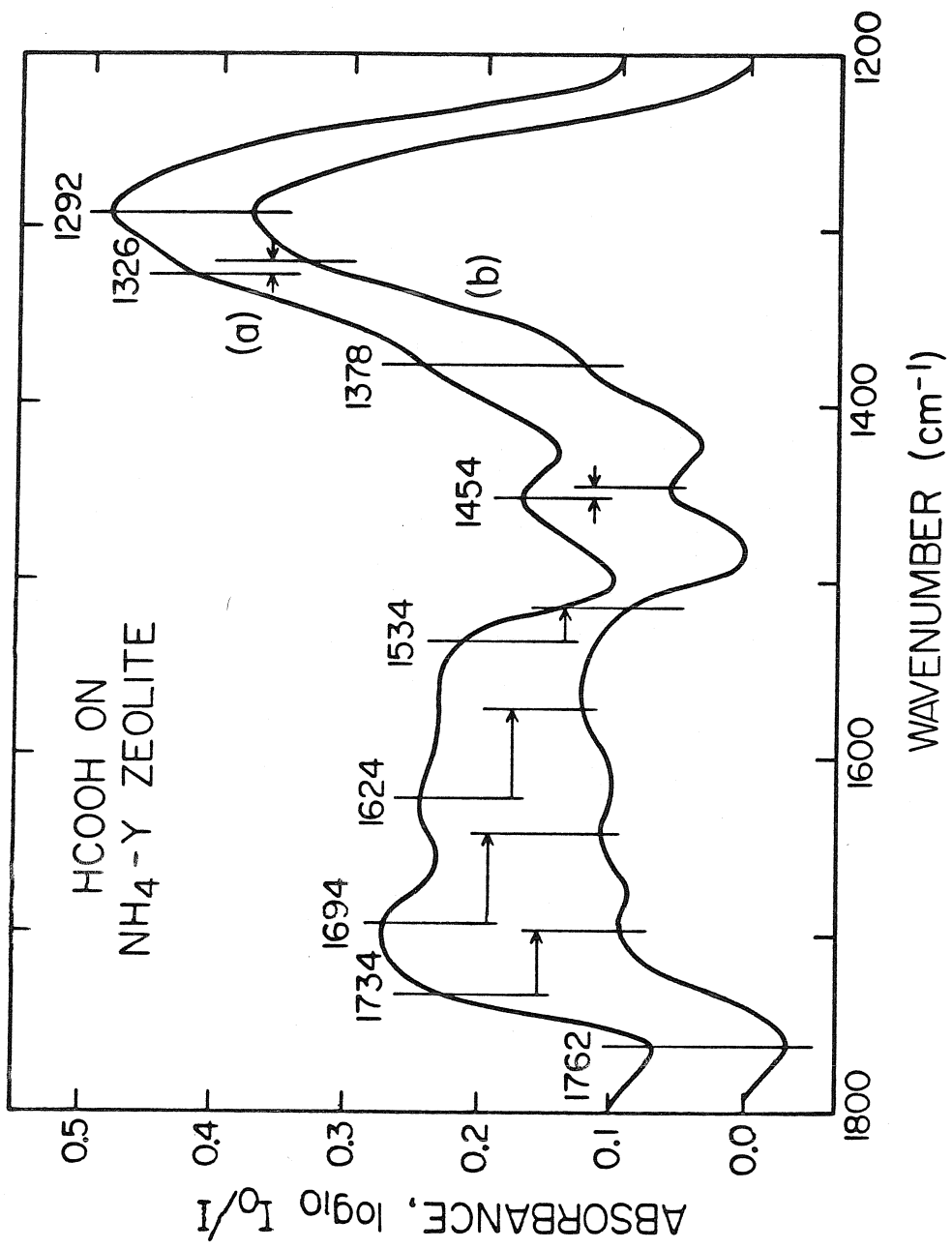


Figure 3

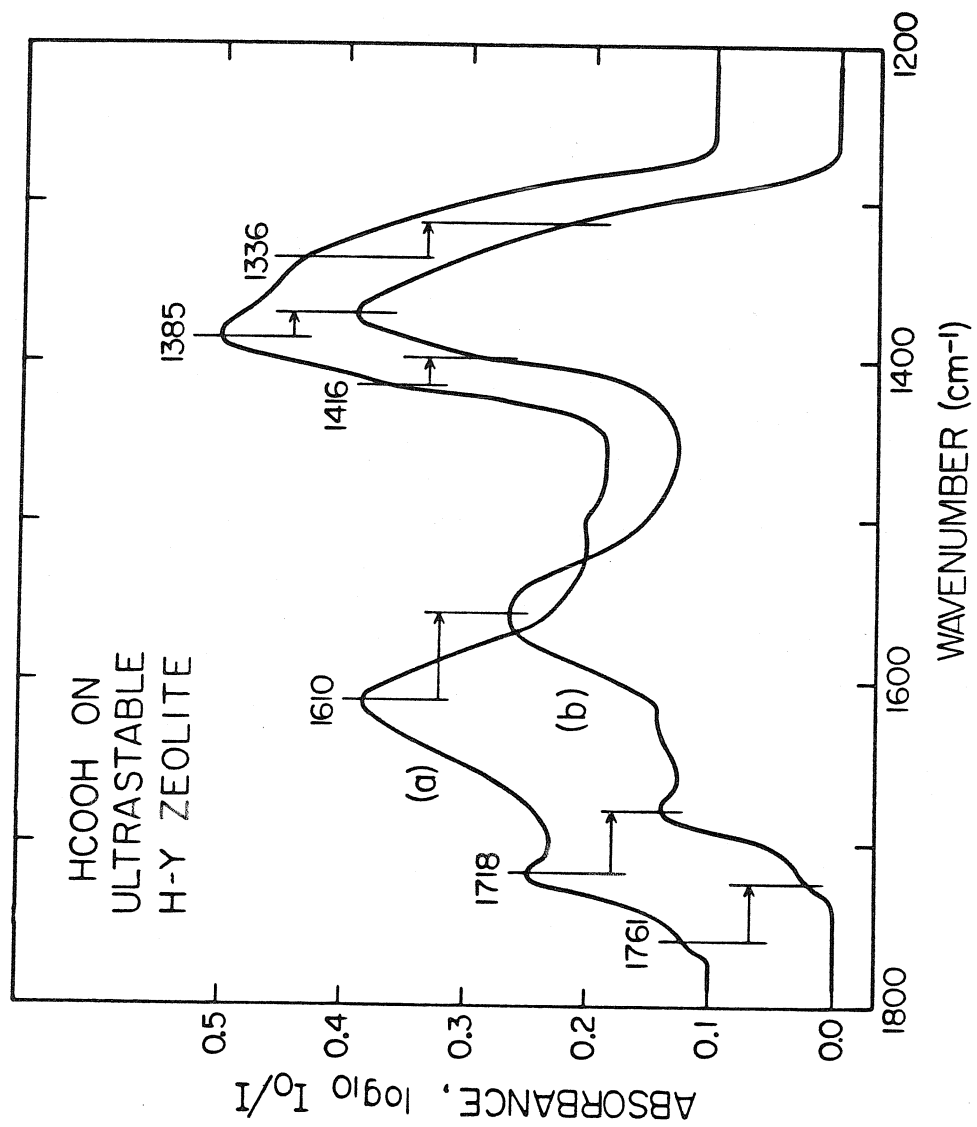


Figure 4

CHAPTER VII

A SOLID STATE NUCLEAR MAGNETIC RESONANCE STUDY
OF THE ADSORPTION OF FORMIC ACID
ON AMMONIUM-Y AND ULTRASTABLE HYDROGEN-Y ZEOLITES

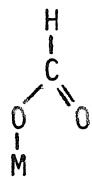
(Chapter VII is essentially an article by T. M. Duncan and R. W. Vaughan entitled "A Solid State Nuclear Magnetic Resonance Study of the Adsorption of Formic Acid on Ammonium-Y and Ultrastable Hydrogen-Y Zeolites." This article has been submitted for publication in the Journal of Catalysis.)

Abstract

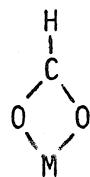
A solid state nuclear magnetic resonance (NMR) study of the adsorption of formic acid on ammonium-Y ($\text{NH}_4\text{-Y}$) and ultrastable hydrogen-Y (H-Y) zeolites confirms the results of a previously reported infrared study and provides a further description of the adsorbed states. The formic acid is adsorbed on the $\text{NH}_4\text{-Y}$ and ultrastable H-Y zeolites in two different forms; as a unidentate formate ligand and as a bidentate formate species, as determined by the symmetry of the chemical shift powder patterns. Cross-polarization techniques exploit the differences in ^{13}C - ^1H dipolar couplings to separate the two groups. The ratio of unidentate to bidentate species is about 52:48 on the $\text{NH}_4\text{-Y}$ zeolite and about 83:17 on the ultrastable H-Y zeolite. The strength of the ^{13}C - ^{27}Al dipolar interaction suggests that the formate ions are directly bonded to the Al atoms of the zeolites. The carbonyl hydrogen, observed by dipolar-difference NMR techniques, is more acidic than that of formic acid, suggesting that the hydrogen is relatively more reactive.

I. INTRODUCTION

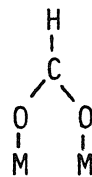
The adsorption of formic acid on ammonium-Y ($\text{NH}_4\text{-Y}$) and ultrastable hydrogen-Y (H-Y) zeolites has been studied recently by transmission infrared spectroscopy (1). A brief review of the adsorption of formic acid on metal oxides as well as a description of the two zeolites has been discussed previously (1). From the results of the adsorption isotherm and the position of the infrared bands, it was determined that the formic acid was chemically adsorbed on the zeolites as both unidentate formate ligands (species I) and bidentate formate species. Through analogies with other studies of adsorbed formic acid and the infrared spectrum of aluminum formate, it was suggested that the formate ion was bonded to the surface as a bidentate group (species II or III). The infrared spectra



I



II



III

indicated that the $\text{NH}_4\text{-Y}$ sample had a nearly even distribution of the two surface species, whereas the formic acid adsorbed on the ultrastable H-Y sample was present primarily as the formate ion. It has been proposed that the decomposition of the adsorbed formate group is the rate-determining step in the catalytic reaction of formic acid to yield carbon monoxide and water (2). Since the ultrastable H-Y zeolite is more active

catalytically than the $\text{NH}_4\text{-Y}$ zeolite, the distribution of the surface states of the formic acid has important implications in the role of the configuration of the adsorbed species.

We present here a solid-state nuclear magnetic resonance (NMR) study of the adsorption of formic acid on $\text{NH}_4\text{-Y}$ and ultrastable H-Y zeolites. The application of NMR techniques to the study of adsorbed species has been discussed in several reviews (3,4,5). Although there have been numerous NMR studies of physically adsorbed hydrocarbons, there have been relatively few applications to the study of chemically adsorbed species. Examples of chemically adsorbed systems include the study of benzene on charcoal and silica gel (6), carbon dioxide on molecular sieves (7), and carbon monoxide on rhodium on alumina (8). One difficulty with NMR studies of chemisorbed molecules is the extremely weak NMR signals of such dilute systems, which is further complicated by excessive broadening. To date, most studies on physically adsorbed molecules have concentrated on the spin-lattice relaxation times and the isotropic frequency of the resonance. This study will concentrate more on the anisotropic chemical shift tensor and the dipolar interaction of the ^{13}C nuclei with neighboring nuclei, two quantities which are averaged-out in physically adsorbed systems. These quantities will be used to determine the geometry of the adsorbed state, the degree of motion on the surface and the nature of the adsorption site on the substrate.

This study will utilize several high-resolution NMR pulse sequences (9,10,11), including spin-decoupling (12), cross-polarization (12,13), dipolar-modulation (14), and dipolar-difference (15) techniques to enhance the NMR signals and remove the extraneous broadening. The analysis will

be based primarily on ^{13}C NMR spectra. The ^{13}C nuclei are a dilute spin system in the zeolite and interact only through other spin systems or the lattice; thus, there is no broadening from homonuclear interactions. The ^{13}C chemical shifts are much larger than those of ^1H nuclei, which allows an interpretation of the spectra even in the presence of substantial broadening. The ^1H spectrum of the carbonyl proton of formic acid will be measured also as a cross-reference on the environment of the adsorbed species.

The NMR pulse techniques will be used to measure the chemical shift tensor, the dipolar interactions with ^1H and ^{27}Al nuclei, and the various relaxation times of the ^{13}C nuclei of the adsorbed formic acid. The center of mass of the chemical shift tensor (the isotropic value observed in physically adsorbed samples) reflects the general character of the chemistry of the molecular species; that is, the isotropic chemical shift readily distinguishes between fundamentally different carbon compounds such as carbonyl, aliphatic, and aromatic groups. However, the isotropic value is not a good indicator of subtle chemical differences within a subgroup such as the formate compounds (16). Rather, the changes in bonding geometry are better reflected by the anisotropy of the chemical shift tensor. In general, within a subgroup the isotropic value indicates the average electron density at the ^{13}C nucleus, whereas the full tensor is sensitive to changes in the angular distribution and symmetry of the electron density.

The interaction of the ^{13}C nuclei with neighboring dipoles can be used to determine average internuclear distances and the extent of

motional averaging. The ^{13}C nuclei are most strongly coupled to the nuclei of the directly bonded hydrogen atoms. Thus, it is possible to apply cross-polarization techniques to study the strength of the coupling (13) and to enhance the ^{13}C NMR spectrum (12). The interaction may be quantified further by the dipolar-modulation experiment (14). Finally, the dipolar interaction may be used to isolate the ^1H NMR spectrum of the carbonyl proton from the broad, diffuse lineshape of the other protons of the sample (15). The extent of the ^{27}Al broadening of the ^{13}C NMR spectrum provides an estimate of the ^{13}C - ^{27}Al internuclear distance and, thus, information on the adsorption site of the formic acid.

The three time constants measured in this study are the spin-lattice relaxation time (T_1), the transverse relaxation time (T_2), and the time constant for the coupling between the ^{13}C and ^1H spin baths (T_{IS}). The T_1 is the time constant for the rate that the perturbed magnetization returns to equilibrium with the external magnetic field. In samples with relatively high paramagnetic impurity levels, as is the case with the two zeolites studied here, the T_1 of a chemisorbed species cannot be used to determine the nature of the motion on the surface or the cross-relaxation rate with neighboring spins. However, in some cases the T_1 may be used to differentiate between various adsorbed states by the nature of the coupling to the paramagnetic centers (8). T_2 is essentially the lifetime of the state, which is often limited by motions of the molecule or motions of nearby unpaired electrons of paramagnetic centers. T_{IS} is measured by the rate at which the magnetization is transferred between the ^{13}C and the ^1H spin systems and may be used to calculate the strength of the

dipolar interaction.

II. EXPERIMENTAL PROCEDURE

A. Sample Description and Preparation

The ammonium-Y ($\text{NH}_4\text{-Y}$) zeolite, unit cell formula $\text{Na}_2(\text{NH}_4)_{48}(\text{AlO}_2)_{50}(\text{SiO}_2)_{142} \cdot 26\text{H}_2\text{O}$, was prepared by ion exchange with a sodium-Y zeolite. This $\text{NH}_4\text{-Y}$ zeolite was calcined at 775 K to yield a "deep bed" product, an ultrastable hydrogen-Y (H-Y) zeolite, with unit cell formula $\text{Na}_2\text{H}_{48}(\text{AlO}_2)_{50}(\text{SiO}_2)_{142} \cdot 26\text{H}_2\text{O}$ (17). The zeolites contain 780 ± 10 ppm Fe and 12 ± 2 ppm Mn, as determined by atomic absorption. The electron paramagnetic spectrum of the zeolites at 8 K and the microwave frequency at 9.25 GHz show a sharp transition at $g = 4.4$ and a multiplet of about 6 transitions ranging from $g = 2.2$ to 1.9. The sharp line at $g = 4.4$ is typical of Fe^{++} in silica-aluminas, whereas the multiplet at about $g = 2.0$ is indicative of Mn^{++} (18). The sharpness of the transitions indicates that the paramagnetic centers are atomically dispersed in the zeolites and not clustered in metallic particles.

The zeolite samples were outgassed with a liquid nitrogen-trapped diffusion pump to pressures of about 5×10^{-5} Torr by heating for 3 hours: the $\text{NH}_4\text{-Y}$ zeolite at 385 K and the ultrastable H-Y at 800 K. The nitrogen BET surface areas of the zeolites are $459 \pm 10 \text{ m}^2/\text{g}$ and $515 \pm 10 \text{ m}^2/\text{g}$ for the $\text{NH}_4\text{-Y}$ and the ultrastable H-Y, respectively, representing monolayers of about 63 and 84 nitrogen molecules per unit cell. The formic acid adsorption isotherms for both zeolites, measured previously (1), reveal monolayer coverages of 75 and 56 formic acid molecules per unit for the

$\text{NH}_4\text{-Y}$ and the ultrastable H-Y , respectively. A submonolayer of isotopically enriched (91.2% ^{13}C) formic acid was deposited on the outgassed $\text{NH}_4\text{-Y}$ and ultrastable H-Y zeolites by condensation from the gas phase. The predetermined pressure of the vapor to be deposited was calculated from the monomer/dimer equilibrium data of Coolidge (19).

This NMR study was performed on two samples of zeolites with submonolayer coverages of formic acid. Quantitatively, one sample consisted of 0.120 g of $\text{NH}_4\text{-Y}$ zeolite loaded with 1.81×10^{-4} moles (9.9×10^{20} ^{13}C nuclei), a coverage of 24.9 molecules of formic acid per unit cell of zeolite. The second sample was 0.121 g of ultrastable H-Y zeolite dosed with 1.86×10^{-4} moles (1.02×10^{20} ^{13}C nuclei) of formic acid, a coverage of 18.5 molecules of formic acid per unit cell. We are confident that the structural integrity of the $\text{NH}_4\text{-Y}$ zeolite is maintained under this light loading of the acid. The acid coverage is significantly below the point where the anomalies occur in the adsorption isotherm and the ratio of hydrogen ions to ammonium ions is low, an important criterion for zeolite stability (20).

The ^{13}C NMR spectra of the reference compounds were obtained from enriched samples of formic acid, ammonium formate, and calcium formate. The formic acid sample was 20% ^{13}C -enriched, prepared by diluting the 91.2% stock with natural abundance formic acid. The ammonium formate sample (12% ^{13}C -enriched) was prepared by neutralizing the formic acid with ammonium formate and then vacuum-desiccating to remove the residual water and ammonia. The calcium formate reference, previously examined elsewhere (14), contained 6% ^{13}C and was doped with Mn^{++} to lower spin-

lattice relaxation times.

B. NMR Spectrometer and Pulse Sequences

The Fourier transform ^{13}C and ^1H NMR spectra were measured on a double-resonance multiple-pulse spectrometer (21,22). The 1.32 Tesla Varian magnet is stabilized to about 1 ppm with an external ^{19}F pulsed field-frequency lock. The data were taken with a single coil (5 mm diameter) double-resonance probe tuned for ^1H resonance at 56.4 MHz and ^{13}C resonance at 14.2 MHz (22). Temperatures were regulated by a dewared nitrogen flow system.

The ^{13}C NMR spectra in this study were obtained by Fourier transforming the signals observed with three techniques: the $180^\circ-\tau-90^\circ$ (23), $^{13}\text{C}-^1\text{H}$ cross-polarization (12), and $^{13}\text{C}-^1\text{H}$ dipolar-modulation (14) experiments. The ^1H spectrum of the carbonyl proton was observed by the $^{13}\text{C}-^1\text{H}$ dipolar-difference experiment (15). These four pulse sequences are diagrammed in Figure 1. The intensities and lineshapes of the NMR spectra as a function of the various parameters of each pulse sequence can be used to describe the adsorbed state and the local environment of the formic acid. The main features of each of the pulse schemes will be discussed here only briefly. More extensive discussions may be found in the reviews mentioned earlier (9,10,11).

The $180^\circ-\tau-90^\circ$ pulse sequence provides a quantitative measure of the number of ^{13}C nuclei in the sample; provided that $T_1 \gg \tau$, the sequence is repeated only after waiting a period of at least five T_1 's, and the proton irradiation is sufficiently intense to decouple the $^{13}\text{C}-^1\text{H}$ spins. The criterion for heteronuclear decoupling is that the decoupling field

is greater than both the ^{13}C - ^1H heteronuclear coupling and the ^1H - ^1H homonuclear spin coupling (10); that is, the Larmor frequency of the protons in the decoupling field must be comparable to the spin-flip rate of the protons caused by both the ^{13}C and other protons. The Larmor frequency of the protons in a holding field of 16 G is 68 KHz. The ^{13}C - ^1H coupling for a bond length of 1.09 \AA^0 is less than 45 KHz at the most intense orientation and averages less than 11 KHz. The square root of the second moment of the ^1H spectrum of either the $\text{NH}_4\text{-Y}$ of ultrastable H-Y zeolites is only about 5.2 KHz at 295 K. Thus, 16 G is sufficient to assure reliable ^{13}C spin counts for the adsorbed formic acid. The intensity of the observed magnetization as a function of τ , the delay between the 180° and 90° pulses, may be used to calculate the T_1 of the ^{13}C nuclei (23). The 180° - τ - 90° sequence is alternated with a single 90° pulse, and the successive free induction decays are alternately added and subtracted. This add-subtract mode removes instrumental artifacts during the period immediately after the 90° pulse.

The ^{13}C - ^1H cross-polarization experiment yields enhanced ^{13}C spectra and quantifies the strength of the heteronuclear interaction by measuring the rate of transfer of magnetization between the two spin systems (12). In general, it is not possible to calibrate the intensity of the signal from the cross-polarization experiment for an inhomogeneous system, such as the formic acid adsorbed on the zeolites, without a knowledge of the distribution of bond lengths and the degree of motional averaging. The cross-polarization process will selectively emphasize the signal from ^{13}C nuclei with stronger couplings to the ^1H nuclei. The stronger couplings

may be the result of more ^1H spins in the immediate environment (within about 5 Å), $^{13}\text{C}-^1\text{H}$ bonds at select orientations to the external magnetic field (the interaction is proportional to $(3 \cos^2 \theta - 1)$, where θ is the angle between the internuclear bond and the external field), or the $^{13}\text{C}-^1\text{H}$ bond is not being averaged by motion. For $^{13}\text{C}-^1\text{H}$ internuclear bonds at orientations where the heteronuclear dipolar coupling is weak (i.e., near 55°), the ^{13}C magnetization must be produced by transfer from intramolecular protons, or $^{13}\text{C}-^{13}\text{C}$ homonuclear spin transfer. Both processes are slow and require longer ^{13}C locking fields. Thus, it is not feasible to calculate a priori the intensity of the ^{13}C cross-polarization spectra. It is, however, possible to compare relative single intensities from one sample as a function of the experimental parameters.

The Hartmann-Hahn (24) condition for cross-polarization ($\gamma_{\text{H}}^{\text{H}} \text{H} = \gamma_{\text{C}}^{\text{H}} \text{c}$, where γ is the gyromagnetic ratio and H is the applied magnetic field) was satisfied with fields of 8.6 G at the proton frequency and 34 G at the carbon frequency. The proton decoupling was 8 G for the reference compounds and 16 G for the formic acid adsorbed on the zeolites. To effect a maximum magnetization transfer, cross-polarization times ranged from 0.1 msec, for the ammonium formate at 295 K, to 8.0 msec for calcium formate at 125 K.

The better signal-to-noise ratios of the ^{13}C spectra from the cross-polarization experiment make it feasible to perform more demanding experiments such as studying the shape and intensity as a function of the cross-polarization time, the echo time, or the dipolar evolution time (14). As described earlier, the intensity of the magnetization as a function of the cross-polarization time is a measure of the strength of the coupling of

the ^{13}C spins to the ^1H spins. The signal intensity as a function of the echo time is used to calculate the transverse relaxation rate, T_2 .

The ^{13}C - ^1H dipolar-modulation experiment (14,25) is a variation of the cross-polarization scheme, such that immediately after the ^{13}C spin-locking pulse, a series of eight-pulse cycles (26) are applied to decouple the proton homonuclear interaction while allowing the ^{13}C - ^1H coupling to remain although it is decreased by a scaling factor of about 0.6.

Immediately after the eight-pulse cycles, the ^1H decoupling pulse is turned on, which conversely decouples the ^{13}C - ^1H interaction but not the ^1H - ^1H coupling. For ^{13}C - ^1H systems with very weak or no couplings, the dipolar-modulated spectra will be similar to the cross-polarization spectra. However, for stronger ^{13}C - ^1H couplings, the ^{13}C magnetization will oscillate during the eight-pulse sequence at a frequency proportional to the ^{13}C - ^1H coupling. Thus, the extent of the modulation of the ^{13}C magnetization observed after echo as a function of the duration of the dipolar-modulation sequence is determined by the strength of the ^{13}C - ^1H coupling. With this technique it is possible in some cases to orient the chemical shift principal axis system in the molecular coordinate system by the rate of modulation of different portions of the ^{13}C powder pattern (14,25). Also, the area of the ^{13}C spectrum will oscillate at a frequency proportional to the average ^{13}C - ^1H coupling in the sample, thus allowing one to calculate the average ^{13}C - ^1H bond lengths.

The isolated ^1H chemical shift spectrum of the carbonyl hydrogen of the absorbed formic acid may be observed with the dipolar-difference experiment (15). In the dipolar-difference experiment, the homonuclear-

decoupled ^1H spectrum is observed alternately in two environments: first, using the eight-pulse cycle (26) to remove the ^1H - ^1H interactions, and second, simultaneously irradiating the proton spins with the eight-pulse cycle while irradiating the ^{13}C nuclei to remove the heteronuclear dipolar coupling to the protons (27). Thus, the first cycle will yield chemical shift spectra from all protons except those directly bonded to ^{13}C nuclei, which will be dipolar broadened into the baseline. In the second cycle, this heteronuclear dipolar broadening is removed and all the protons are observed. Alternately adding and subtracting these two signals yields only the spectrum of the protons directly bonded to the ^{13}C nuclei.

The lines through the spectra were obtained by a nonlinear least-squares fit of a theoretical chemical shift powder pattern (28). The spectra of the reference formates and the 180° - τ - 90° spectra were convoluted with a Lorentzian broadening function, whereas the cross-polarization spectra were convoluted with a Gaussian broadening function.

III. RESULTS

A. ^{13}C NMR Spectra of Formate Compounds

The anisotropy and resolution of the structure of the ^{13}C NMR spectra of formic acid, ammonium formate, and calcium formate both increased as the temperature of the sample was lowered. This suggests that there are molecular motions in the crystals which are being quenched at lower temperatures. The motions are probably small anisotropic waggings or rockings which cause a local averaging in the ^{13}C NMR powder patterns. In each case, the spectra were recorded at the lowest temperatures experimentally feasible, restricted by the limitations of the equipment and the

temperature dependence of the spin-lattice relaxation times.

The ^{13}C NMR spectra of the reference formates shown in Figure 2 were obtained by $^{13}\text{C}-^1\text{H}$ cross-polarization and then observing the free induction decay immediately after the ^{13}C spin-locking pulse, while decoupling the protons with 8 G. The principal components of the chemical shift tensors are reported in Table I. The features in the spectrum for formic acid at 125 K, Figure 2(a), suggest three principal components of the chemical shift tensor, but the data do not fit a theoretical powder pattern lineshape. A least-squares fit, shown by the solid line, follows the upfield component at -92 ppm but clearly misses the downfield shoulder. If the three principal components are fixed at the approximate locations of the shoulders, the computed intensities at the center and downfield components are in error, as shown by the dotted line. The distortion from the theoretical lineshape is probably the result of motion as well as an angular dependence of the $^{13}\text{C}-^1\text{H}$ cross-polarization rate in a polycrystalline sample. The spectrum in Figure 2(a), obtained by cross-polarizing for 8 msec, is less distorted than the spectra that result with only 0.5 msec of $^{13}\text{C}-^1\text{H}$ spin contacting or at higher temperatures.

The spectrum for ammonium formate shown in Figure 2(b) is the result of cross-polarizing for 0.1 msec at 185 K. At about 195 K, the proton T_1 's lengthened from a few msec to over 10 sec, which indicates that the major relaxation process had halted, probably the rapid reorientation of the ammonium ion. The proton T_1 's continue to increase at temperatures below 185 K, which prohibited extended averaging.

The calcium formate ^{13}C NMR spectrum exhibited the most pronounced motional effects of the formates studied. The apparent chemical shift anisotropy increases from about 100 ppm at 295 K to 136 ppm at 125 K. The spectrum shown in Figure 2(c) was obtained by cross-polarizing for 8.0 msec at 125 K. A previous ^{13}C NMR study of a calcium formate single crystal detected two distinct sets of chemical shift components for the crystallographically inequivalent formate ions (16). The resolution in the powder pattern of Figure 2(c) is not sufficient to resolve the two spectra, which are separated by only 5, 3, and 0 ppm at the three principal components.

B. Formic Acid Adsorbed on Zeolites

1. ^{13}C T_1 Measurements

The logarithm of the calibrated amplitude of the observed ^{13}C magnetization versus the delay between the 180° and 90° pulses is plotted in Figure 3. If the recovery of the longitudinal magnetization was described by a single T_1 , the data would lie on a straight line when plotted as in Figure 3. The curves through these data, however, can be fit with the sum of two exponentials:

$$\text{HCOOH on NH}_4\text{-Y: } M(\tau) = 8.8 \times 10^{19} (0.35e^{-\tau/2.6} + 0.65e^{-\tau/82}) \quad (1)$$

$$\text{HCOOH on ultrastable H-Y: } M(\tau) = 5.2 \times 10^{19} (0.25e^{-\tau/4.4} + 0.75e^{-\tau/71}) \quad (2)$$

where τ is in msec. Thus, this suggests that of the $8.8 \times 10^{19} \text{ }^{13}\text{C}$ nuclei on the $\text{NH}_4\text{-Y}$ zeolite, 35% relax with an average T_1 of about 2.6 msec and 65% relax with an average T_1 of 82 msec. On the ultrastable H-Y zeolite, the $5.2 \times 10^{19} \text{ }^{13}\text{C}$ nuclei detected are distributed as 25% which relax

with an average T_1 of 4.4 msec and 75% with an average T_1 of 71 msec. The centers of mass and the linewidths did not change significantly as τ was lengthened. However, the extremely weak signals for long τ values caused large experimental error limits, as much as 20 ppm for delays longer than 10 msec.

The lineshapes for two representative ^{13}C NMR spectra resulting from the 180° - τ - 90° sequence for formic acid adsorbed on the $\text{NH}_4\text{-Y}$ and the ultrastable H-Y zeolites at 295 K are shown in Figure 4. These lineshapes are for short delays, $\tau=0.5$ msec, thus the two T_1 groups are overlapped in each spectrum. Although the linewidths are comparable to those of the reference formates, the spectral structures at the principal components of the chemical shift tensor are not as well resolved. The centers of mass of the ^{13}C lineshapes of the adsorbed formic acid are -164 ppm and -165 ppm, relative to TMS, for the $\text{NH}_4\text{-Y}$ and the ultrastable H-Y substrates, respectively. This is within experimental error of pure formic acid: -163 ppm. Although these lines were fit with the same chemical shift regression analysis applied to the reference formates, the computed components are not as well defined and thus are rather ambiguous. The lineshape analysis data are reported in Table II.

The quantitative data of the 180° - τ - 90° experiment do not account for all of the ^{13}C originally deposited on the zeolites. The magnetization extrapolated to $\tau = 0$ accounts for only 89% and 51% of the formic acid on the $\text{NH}_4\text{-Y}$ and the ultrastable H-Y zeolites, respectively. A portion of the spins (less than about 3%) may be undetectable because the formate molecules are adsorbed within a critical radius of a paramagnetic impurity

(about 7 Å). The NMR signal from these species is extremely broad and would not be observed (35). The T_1 data and the spectra in Figure 4 were obtained after the zeolites had been loaded with the formic acid and stored at 273 K for four weeks. Figure 5 shows the spectra obtained for the ultrastable H-Y sample after an additional seven months at 273 K. The intensity of the broad line centered at -165 ppm has significantly decreased and there is a sharp feature at -180 ppm. This sharp line remains even when the proton decoupling is not applied, indicating that for this species, the coupling to the protons is less than its linewidth, 150 Hz. Since the isotropic chemical shift of pure CO is -181 ppm (34) and CO is the principal reaction product for formic acid on these zeolites, we attribute the sharp peak to physically adsorbed CO. Thus, at the time of the T_1 measurement, the formic acid had partially reacted to CO, which desorbed into the dead volume above the NMR sample, resulting in a reduced ^{13}C spin count.

2. Cross-polarization Experiments

The ^{13}C NMR signal intensity of the adsorbed formic acid as a function of the cross-polarization time is shown in Figure 6. The maximum magnetization for both zeolite samples was attained at approximately 0.6 msec. These data were also measured when the samples were four weeks old, the same time as the T_1 data in Figure 3. However, the signal from the ultrastable H-Y sample is greater than the signal from the $\text{NH}_4\text{-Y}$ sample, although it was a factor of 1.7 less in the $180^\circ\text{-}\tau\text{-}90^\circ$ experiment. In general, the maximum obtainable signal enhancement for the ^{13}C - ^1H cross-polarization is a factor of 4, provided that there is an infinite

proton spin bath relative to the ^{13}C spins and the ^{13}C and ^1H T_1 's are long compared to the time constant of the heteronuclear interaction, T_{IS} . The ratios of the heat capacities of the ^1H and ^{13}C baths are 120:1 and 30:1 for the $\text{NH}_4\text{-Y}$ and ultrastable H-Y zeolites, respectively, sufficient to approximate an infinite bath of ^1H spins. The maximum enhancements measured for the adsorbed formic acid are factors of 1.9 and 3.2 for the formic acid adsorbed on the $\text{NH}_4\text{-Y}$ and ultrastable H-Y samples, respectively. Thus, the ultrastable H-Y sample has an effective $^{13}\text{C}-^1\text{H}$ magnetization transfer, but the $\text{NH}_4\text{-Y}$ sample is considerably below the theoretical maximum.

The data in Figure 6 may be interpreted with the following thermodynamic model. The ^{13}C magnetization increases via transfer of magnetization from the ^1H spins. The rate of transfer is proportional to the difference in the spin-temperature between the two baths and is determined by the rate constant T_{IS}^{-1} . The ^{13}C magnetization decays by two processes: directly, by relaxation with the lattice, and indirectly, by transfer of magnetization back to the proton bath which, in turn, is directly relaxing with the lattice. Solving the coupled differential equations for the rate of change of the magnetization of the two spin systems and taking the limit of an infinite ^1H bath relative to the ^{13}C bath yields equation (3).

$$M_{xp}(t_{xp}) = \alpha_{xp} M_0 \frac{\gamma_H}{\gamma_C} \left[\frac{T_{1C}T_{1H}}{\frac{T_{1C}T_{1H}}{T_{IS}T_{1H}} + T_{IS} - T_{IS}T_{1C}} \right] \cdot \left[e^{-t_{xp}/T_{1H}} - \left(e^{-t_{xp}/T_{IS}} \right) \left(e^{-t_{xp}/T_{1C}} \right) \right] \quad (3)$$

Thus, the observed ^{13}C magnetization, M_{xp} , a function of the cross-polarization time, t_{xp} , grows exponentially with rate constant $(T_{IS}^{-1} + T_{1C}^{-1})$

and then decreases exponentially with rate constant T_{1H}^{-1} . The maximum enhancement of the magnetization relative to M_0 is determined by the product of three prefactors: a term containing the three rate constants (which is about 1.0), the ratio of the gyromagnetic ratios γ_H/γ_C (which is 4.0), and an arbitrary normalization factor, α_{xp} . In general, α_{xp} is the fraction of the ^{13}C nuclei susceptible to the cross-polarization process before the magnetizations decay in the respective holding fields. The physical interpretation of the factor will be discussed later. T_{1C} and T_{1H} , the relaxation times in the respective holding fields, are determined experimentally. The data for formic acid on the $\text{NH}_4\text{-Y}$ zeolite in Figure 6 are fit with $T_{IS} = 0.23$ msec, $T_{1H} = 5.6$ msec, and $T_{1C} = 3.0$ msec. The formic acid on the ultrastable H-Y sample is characterized by a shorter T_{IS} , 0.16 msec, indicating a stronger $^{13}C-^1H$ coupling, $T_{1H} = 16$ msec and $T_{1C} = 5.0$ msec. These values of T_{IS} are similar to those of the reference formates. The lines are relatively insensitive to the value of T_{1C} . The α_{xp} fractions are 0.52 and 0.83 for the $\text{NH}_4\text{-Y}$ and ultrastable H-Y samples, respectively.

Typical spectra obtained by observing the proton-decoupled free-induction decays immediately after the ^{13}C holding pulses are shown in Figure 7. Although the signal-to-noise ratio is considerably better than that of the $180^\circ-\tau-90^\circ$ experiment, the chemical shift components are again not resolved. Compared to the spectra from the $180^\circ-\tau-90^\circ$ experiment, the lineshapes from the cross-polarization experiments are about 25% and 7% broader for the $\text{NH}_4\text{-Y}$ and the ultrastable H-Y samples, respectively. The broader spectra are the result of the cross-polarization process emphasizing the signal from adsorbed species with broader lineshapes. In general, the

more stationary ^{13}C nuclei will have stronger $^{13}\text{C}-^1\text{H}$ couplings and thus will be enhanced more. The internuclear cross-polarization process for rapidly reorienting $^{13}\text{C}-^1\text{H}$ systems will be ineffective and these ^{13}C nuclei will be polarized only through $^{13}\text{C}-^{13}\text{C}$ homonuclear transfers or intramolecular $^{13}\text{C}-^1\text{H}$ couplings. Such processes would require about 5 to 10 msec of cross-polarization, as is necessary for the rapidly tumbling adamantane molecules at 295 K. For the adsorbed formic acid molecules, such long transfers are not possible since the magnetization in the holding fields decays before the process would be complete. Thus, the lineshapes in Figure 7 are primarily due to adsorbed formic acid molecules with nearly rigid $^{13}\text{C}-^1\text{H}$ bond systems.

The spectrum from the $\text{NH}_4\text{-Y}$ sample broadens the most compared to the $180^\circ\text{-}\tau\text{-}90^\circ$ spectrum, indicating that it contains a larger percentage of reorienting adsorbed species. The ultrastable H-Y sample has a much smaller change in linewidth. This is consistent with the enhancement factor of 3.2 which suggests that a larger percentage of the formic acid on the ultrastable H-Y sample is rigidly bonded to the substrate.

The center of mass frequencies of the cross-polarized spectra at 295 K are 17 and 15 ppm upfield from the $180^\circ\text{-}\tau\text{-}90^\circ$ spectra for the $\text{NH}_4\text{-Y}$ and the ultrastable H-Y zeolites, respectively. This also indicates that the cross-polarization technique is emphasizing a specific subgroup of the total lineshape. The isotropic frequencies on both samples at 295 K do not change as a function of the cross-polarization time for the range reported in Figure 6.

The cross-polarization spectra broaden and the isotropic frequencies move almost back to that of the $180^\circ\text{-}\tau\text{-}90^\circ$ spectra as the temperature is

lowered, as seen in Figure 7. In addition, the general shapes of the spectra change, which is best visualized for the formic acid adsorbed on the $\text{NH}_4\text{-Y}$ zeolite. The frequency at which the maximum intensity occurs shifts from the downfield side (i.e., the more negative side) of the isotropic frequency to the upfield side as the temperature is decreased. Spectra were measured at several intermediate temperatures, and it was observed that this shift is a gradual process. The lineshape parameters for the spectra in Figure 7 are given in Table II.

The logarithm of the spectral area as a function of the delay from the end of the ^{13}C cross-polarization holding pulse to the echo for the formic acid adsorbed on the zeolites at 295 K is plotted in Figure 8. For each zeolite sample, the data decay with a single transverse relaxation time, T_2 . The values of T_2 are 2.5 and 3.1 msec for the formic acid adsorbed on the $\text{NH}_4\text{-Y}$ and the ultrastable H-Y zeolites, respectively. The center of mass frequencies and the linewidths of the spectra do not vary, within experimental limits, as a function of the echo time.

3. Dipolar-Modulation Experiments

The heteronuclear dipolar-modulation experiments were preformed on the formic acid adsorbed on the $\text{NH}_4\text{-Y}$ zeolite at both 295 K and 125 K. The ^{13}C magnetization was first prepared by cross-polarization for 1.0 msec. Recall from previous results that the cross-polarization process will enhance selectively the more rigidly adsorbed formic acid molecules. The NMR signal was observed as an echo 1.2 msec after the end of the ^{13}C spin-locking pulse. Since the ^{13}C NMR spectra from the previous experiments do

not have well-resolved structure at the principal chemical shift components, it is not possible to assign the modulations in the lineshapes to distinct molecular orientations as was previously done with benzene and calcium formate (14,25). However, the variation of the spectral area as a function of the number of ^1H eight-pulse cycles (the dipolar-modulation time, see Figure 1) yields an average dipolar interaction and, thus, information on the average ^{13}C - ^1H bond length and the extent of motional averaging (14). The spectral areas versus the dipolar-modulation time are shown in Figure 9. The spectral area of the adsorbed formic acid initially decreases at a rate comparable to that of calcium formate. Also note that the areas of the ^{13}C NMR spectra of calcium formate and benzene exhibit a damped oscillation about zero as predicted, but the spectral areas of adsorbed formic acid remain positive and do not oscillate.

4. Dipolar-Difference Experiment

The dehydration of formic acid requires necessarily the cleavage of the carbon-hydrogen bond. Thus, the ionic character of the carbonyl hydrogen attached to the adsorbed formate species, relative to formic acid, is of interest in the decomposition reaction. The average electron distribution of the hydrogen atom may be determined by measuring its chemical shift properties.

The linewidth of the homonuclear-decoupled ^1H NMR spectrum of the $\text{NH}_4\text{-Y}$ zeolite at 295 K is about 26 ppm, as measured by the eight-pulse cycle. This broad Gaussian line is the sum of spectra from the hydrogens of the ammonium ions, the crystalline water, and the hydrogen bonded to the

carbon of the adsorbed formic acid. The dipolar-difference experiment eliminates the extraneous hydrogen signals and observes only the spectrum of the carbonyl hydrogen, approximately 3% of the total spectral intensity.

The ^1H NMR spectrum of the carbonyl hydrogen measured by the dipolar-difference experiment at 295 K for the formic acid adsorbed on the $\text{NH}_4\text{-Y}$ zeolite is shown in Figure 10. It is similar to the ^{13}C NMR spectra in that it lacks any sharp structure but, in contrast, is much narrower, only 6.0 ppm wide at half-maximum intensity. The center of mass frequency for the spectrum is at about -12.3 ppm, relative to TMS. Though this experiment may not be calibrated *a priori* for an unknown system, the spectrum intensity indicates that the number of hydrogen species is on the order of the number of formate species.

IV. DISCUSSION

A. The Nature of the Adsorption of Formic Acid

A previous infrared study of the adsorption of formic acid on the $\text{NH}_4\text{-Y}$ and ultrastable H-Y zeolites concluded that the acid was chemically adsorbed on the surfaces (1). Although the infrared spectra contained bands often attributed to physically adsorbed formic acid (36,37), there was no evidence of OH bending modes, and the adsorption isotherm indicated that the submonolayer was chemisorbed. The positions of the infrared bands were interpreted to be formic acid adsorbed as unidentate groups. As will be shown, the NMR data confirm that the formic acid is chemically adsorbed on both zeolites.

The ^{13}C NMR linewidths of the adsorbed formic acid are comparable to that of the solid reference formates. In general, the linewidth of the NMR spectrum of an adsorbed species may be the result of a number of interactions including paramagnetic broadening, heteronuclear dipolar broadening (from nuclei other than ^1H), spatial susceptibility inhomogeneities, and chemical shift anisotropy. These interactions have been discussed at length elsewhere (5,38). The dipolar interactions are the result of the molecular surroundings, such as the framework atoms of the zeolite supercage. The chemical shift broadening is an individual effect, determined by the electron distribution localized at the nucleus of interest.

Of the possible interactions, all but the chemical shift anisotropy can be eliminated by considering the ^1H spectrum of the carbonyl proton. If the other effects were the major causes of the ^{13}C NMR linewidth, the ^1H NMR spectrum would also be subjected to these effects and thus would be comparably broadened. However, the linewidth of the ^1H line is only 6 ppm, which places an approximate upper limit on the residual broadening of the ^{13}C NMR spectra.

Thus, the widths of the ^{13}C spectra are due primarily to chemical shift anisotropy. Such anisotropies are observed only in chemically adsorbed states. (However, there may still exist local motions at a site, as will be discussed later.) If a portion of the formic acid was physically adsorbed on the zeolite, the ^{13}C NMR line would contain an extremely narrowed component, as was observed for the CO decomposition product in Figure 5. Thus, all of the formic acid on the $\text{NH}_4\text{-Y}$ and ultrastable H-Y zeolites is chemically adsorbed.

B. Spin-lattice Relaxation Times of Adsorbed Formic Acid

In many solids, particularly for ^1H spin systems, the homonuclear spin-spin coupling is much stronger than the spin-lattice coupling. Thus, the macroscopic magnetization decays uniformly and exponentially with time constant T_1 . However, in dilute spin systems, the internuclear coupling is weak and each spin relaxes independently. For a homogeneous dilute system, the spins may still have a single T_1 since the spins are relaxing independently, but identically. However, if each spin should relax differently because of different local environments (e.g., paramagnetic impurities or nearby heteronuclear spins) or different motional properties, there would be a distribution of relaxation times in the sample. Such T_1 distributions are present in solid $\text{C}_6\text{H}_6\text{CF}_3$ because of an angular dependence of the heteronuclear coupling (39) and in CO on Rh on Al_2O_3 due to adsorption site heterogeneity (8).

The ^{13}C T_1 data of the formic acid adsorbed on the zeolites may be interpreted by assuming that the formic acid has adsorbed in two states, each described by a different T_1 . The relative proportions of the two states are given by the pre-exponential factors in equations (1) and (2). Both T_1 's on either zeolite are extremely short and are typical of relaxation by a paramagnetic center. This is to be expected with the high Fe^{++} and Mn^{++} content of the samples. It is possible that the two T_1 groups represent chemically different formate species on the surface or that the T_1 distribution is the result of an inhomogeneous distribution of separations between the ^{13}C nuclei and the paramagnetic centers. The change in distributions between the short and long T_1 's from the $\text{NH}_4\text{-Y}$ to the

ultrastable H-Y samples (35:65 to 25:75) may be rationalized with either model. The infrared data suggest that the ultrastable H-Y zeolite contains a greater percentage of formate ions than the $\text{NH}_4\text{-Y}$ sample (1). In this model, the longer T_1 group would be assigned to the formate ion and the shorter T_1 group to the unidentate structure. On the other hand, the transformation of the $\text{NH}_4\text{-Y}$ zeolite to the ultrastable H-Y zeolite could have redistributed the paramagnetic centers and thus changed the distribution of T_1 's.

The spectra from the T_1 experiment associated with the data points in Figure 3 did not change in width or isotropic frequency as τ was increased. However, the signal-to-noise ratios for the spectra with τ longer than about 10 msec became quite poor. Thus, if any subtle change in either quantity did occur, it would be difficult to detect. Recall that the isotropic chemical shifts for the entire range of formates do not vary more than about 8 ppm. Thus, although the T_1 data suggest a heterogeneity of surface states, it cannot be determined if the sites with different T_1 's are chemically distinct.

C. Cross-polarization Experiments

The cross-polarization experiments also indicate that the formic acid is inhomogeneously adsorbed on the zeolites although in this case the basis for the differences may be unambiguously determined. The molecules are differentiated by the rate in which they cross-polarize, that is, by the strength of the dipolar coupling. The spectra shown in Figure 7(a) and 7(c), observed after 1.0 msec of cross-polarization at 295 K, contain primarily contributions from only those $^{13}\text{C}-^1\text{H}$ systems with semi-rigid

internuclear bonds. Those systems averaged by reorientations faster than the heteronuclear coupling (about 5 KHz) would require more than 5 msec to complete an intramolecular cross-polarization.

On the ultrastable H-Y zeolite, the intensity of cross-polarized ^{13}C NMR signal was a factor of 3.2 greater than the signal from the $180^\circ - \tau - 90^\circ$ experiment. The $\text{NH}_4\text{-Y}$ sample was enhanced by only a factor of 1.9. These data may be interpreted by assuming that the surface contains two types of species: those that may be enhanced by the cross-polarization process by the theoretical maximum (a factor of 4) and those that are not cross-polarized in 1.0 msec. For the ultrastable H-Y sample, this assumption is probably realistic since the infrared spectrum of the adsorbed formic acid suggests that there are only two types of surface structures (1). However, the formic acid on the $\text{NH}_4\text{-Y}$ zeolite exists in several different states, which probably have a distribution of heteronuclear dipolar couplings and thus the assumption is a more arbitrary distinction (1). With this assumption, the intensities of the cross-polarization spectra indicate that the distribution between the two groups is 52:48 on the $\text{NH}_4\text{-Y}$ zeolite and 83:17 on the ultrastable H-Y zeolite. In order to interpret the two types of species, the chemical shift data must be considered.

D. The Relation of Chemical Shift Data to Formate Structures

The formate group bonds in a range of configurations from the ester-like unidentate compounds (species I) covalently bonded through a single oxygen atom, to the bidentate structure where the formate ion is chelated about one or more metal ions (species II and III). The structural parameters of a few compounds are listed in Table IB. One index of the

bonding of the formate group is the ratio of the two carbon-oxygen bond lengths. This ratio ranges from 1.12 for methyl formate to about 1.00 for calcium formate.

The chemical shift information for these formate compounds is presented in Table IA. The isotropic chemical shifts of the compounds, σ , does not correlate with the geometry of the formate group. This was first observed by Ackerman, et al. in a study of the two crystallographically distinct forms of calcium formate (16). The overall anisotropy, $\sigma_{33} - \sigma_{11}$, tends to decrease as R_2/R_1 decreases, but the scatter in the correlation is extremely large. There is, however, a very good correlation between the position of the central principal component, σ_{22} , and the ratio of the carbon-oxygen bond lengths. As the bond lengths become more symmetric, σ_{22} moves from the upfield side of the powder pattern to the downfield side. This is reflected in the ratio of the difference between the upfield component and the central component, $\sigma_{22} - \sigma_{11}$, to the overall anisotropy, $\sigma_{33} - \sigma_{11}$. This ratio ranges from 0.20 for methyl formate ($R_2/R_1 = 1.12$) to 0.66 for calcium formate ($R_2/R_1 = 1.00$). Thus, in general, for bidentate formate ions $(\sigma_{22} - \sigma_{11})/(\sigma_{33} - \sigma_{11})$ is on the order of 0.6, and for ester-like formate groups the ratio is closer to 0.3. As this correlation is based on relatively few data points, the relation between these two parameters does not permit a reliable calculation of the R_2/R_1 from the chemical shift components, only the general trend.

E. The Molecular Structure of the Adsorbed Formic Acid

The relation between the ^{13}C chemical shift components and the

symmetry of the formate group may be used to determine the state of the adsorbed formic acid. The chemical shift components are meaningful only in ^{13}C powder patterns without appreciable motional averaging. The spectra from the $180^\circ-\tau-90^\circ$ experiment at 295 K, which contain motionally averaged contributions, are not applicable. However, the cross-polarization experiment observes selectively the more rigid species for short cross-polarization times, i.e., about 1.0 msec. Thus, the rigid components of the $180^\circ-\tau-90^\circ$ spectra at 295 K in Figure 4, isolated by the cross-polarization technique, are shown in Figure 7. The values of the ratio $(\sigma_{22} - \sigma_{11})/(\sigma_{33} - \sigma_{11})$ for the cross-polarized spectra at 295 K for the formic acid adsorbed on the $\text{NH}_4\text{-Y}$ and ultrastable H-Y zeolites are 0.69 and 0.58, respectively. These relatively high values of this ratio argue that this species is a semi-rigidly bonded formate ion, with approximately symmetric carbon-oxygen bond lengths. Furthermore, the degree of enhancement of the cross-polarization technique, discussed earlier, indicates that the formate ion species comprises 52% and 83% of the formic acid adsorbed on the $\text{NH}_4\text{-Y}$ and ultrastable H-Y zeolites, respectively.

When the cross-polarization experiment is repeated at reduced temperatures, the central component of the powder patterns shifts from the downfield side to the upfield side, as mentioned earlier. Thus, the ratio $(\sigma_{22} - \sigma_{11})/(\sigma_{33} - \sigma_{11})$ changes from 0.69 to 0.41 on the $\text{NH}_4\text{-Y}$ sample and from 0.58 to 0.33 on the ultrastable H-Y sample. These transitions may be attributed in part to a quenching of the motions responsible for the averaging of the other species at room temperature. If the motionally averaged group had a $(\sigma_{22} - \sigma_{11})/(\sigma_{33} - \sigma_{11})$ ratio on the order of the

unidentate formate groups, about 0.20, the incorporation of this species into the powder pattern would lower the average ratio. However, on both samples the added contributions from this species do not account for the large decreases in the ratios. For example, if 83% of the formic acid on the ultrastable H-Y zeolite is adsorbed as formate ions, the contribution from the remaining 17% is not sufficient to cause $(\sigma_{22} - \sigma_{11})/(\sigma_{33} - \sigma_{11})$ to decrease from 0.58 to 0.33. One interpretation of the large change is that upon cooling to temperatures below 150 K, some of the surface formate structures convert from ionicly bound bidentate groups to unidentate structures. This interpretation is supported by the fact that upon cooling, the isotropic chemical shift does not return to the value measured by the $180^0 - \tau - 90^0$ experiment. However, because of the lack of pronounced features in the powder patterns, the fitted chemical shift components may be somewhat arbitrary, that is, changing any of the components by 10% will not cause a large change in the error of the fitted spectrum. Thus, there may be errors as great as 10% in the computed ratios and the incorporation of the unidentate species may actually be sufficient to explain the shifts.

Regardless of the exact ratios, there is a definite change in the symmetries of the cross-polarization spectra upon cooling from 295 K to below 150 K. This transition is probably due to the addition of the unidentate groups which have become more rigid at the lower temperatures. There may also be some conversion of bidentate ions to unidentate groups although this interpretation will require further study.

The assignment of the cross-polarization data to unidentate and bidentate structures on the surface is in agreement with the results of an infrared study (1). The approximate distributions between the two groups (52:48 on the $\text{NH}_4\text{-Y}$ zeolite and 83:17 on the ultrastable H-Y zeolite) also agree with the qualitative distributions based on the relative intensities of the infrared spectra peaks.

F. The Nature of the Bidentate Formate Ion Surface Species

As discussed in the Introduction, the ultrastable H-Y zeolite is catalytically more active than the $\text{NH}_4\text{-Y}$ zeolite. The infrared spectra and the NMR data indicate that there is an increased percentage of the formate ions on the ultrastable H-Y surface. Thus, if the direct decomposition of the formate ion is the rate-determining step in the dehydration reaction to CO and H_2O (2), the structure of the adsorbed state is of interest. By isolating the ^{13}C NMR signal of the formate ion with the cross-polarization process at 295 K, it is possible to determine the adsorption site, the ^{13}C - ^1H bond characteristics, and the ionic character of the carbonyl hydrogen.

In the presence of proton-decoupling, the main sources of broadening of the ^{13}C NMR spectra are chemical inhomogeneity of the species, vibrational motion, lifetime broadening, and dipolar broadening from the ^{27}Al . The full widths at half-maximum of the Gaussian broadening functions convoluted with the chemical shift powder pattern of the cross-polarization spectra at 295 K, spectra 7(a) and 7(b), are 124 and 142 ppm for the $\text{NH}_4\text{-Y}$ and ultrastable H-Y samples, respectively. The second moments for these broadening functions are 0.67 G^2 and 0.88 G^2 , respectively. The

contributions due to chemical inhomogeneities and librational motions are estimated from the broadening in the reference formates, which is about 0.08 G². The lifetime broadenings, computed from the T₂'s, are 0.14 G² for the NH₄-Y and 0.09 G² for the ultrastable H-Y samples. The remainder of the broadening is attributed to the ¹³C-²⁷Al dipolar interaction. The second moment of this interaction may be calculated from the Van Vleck equation for heteronuclear broadening shown below (40).

$$\langle \Delta^2 \omega \rangle_{IS} = \frac{1}{3} \gamma_s^2 \hbar^2 s(s+1) \frac{1}{N} \sum_{j,k} \frac{(1 - 3\cos^2 \theta_{jk})}{r_{jk}^6} \quad (4)$$

In equation 4, the second moment of the ¹³C spectrum due to ²⁷Al is determined by the gyromagnetic ratio of ²⁷Al, 6.97 x 10³ rad G⁻¹ sec⁻¹; \hbar , 1.05 x 10⁻³ G Å³ sec; the spin of the ²⁷Al nucleus, S = 5/2, and the ¹³C-²⁷Al internuclear vector of length r at an angle θ with the external magnetic field. The sum is over all ¹³C and ²⁷Al spins in the sample, normalized by N, the number of ¹³C spins. For a polycrystalline sample, the spherical average of the angular dependence is 4/5. For a formate ion bonded to an Al ion, the bidentate would be similar to the Na, Ca, and Sr salts, and the ¹³C-²⁷Al internuclear distance is 2.75 Å. With this configuration, equation 4 yields a second moment of 0.29 G². The contribution from Al atoms in the surrounding zeolite framework, not directly bonded to the formate ion, is estimated to be about 0.15 G². Thus, the ¹³C-²⁷Al broadening is calculated to be 0.44 G² for a formate ion directly bonded to the Al atom and 0.15 G² when bonded to a Si atom.

However, this interaction will increase if the ²⁷Al nuclei are in a non-

Zeeman state; that is, it is possible that large electrostatic field gradients at the zeolite surface determine the orientation of the quadrupolar ^{27}Al rather than the external magnetic field. It has been observed that for amorphous aluminas, the ^{27}Al $1/2 \longleftrightarrow -1/2$ transition vanishes in samples with BET surface areas greater than about $100 \text{ m}^2\text{g}^{-1}$, indicating that the ^{27}Al nuclear alignment is determined by local electrostatic fields (41). In the case of spin 1/2 - spin 7/2 systems if the spin 7/2 is in a non-Zeeman state, the second moment may increase by as much as a factor of 1.8 (42). Similarly, it has been shown that the non-Zeeman state of ^{27}Al (spin 5/2) may also result in as much as a factor of 1.8 increase in the second moment of the ^{13}C lineshape (43). Thus, the total second moment, including the librational contribution, is about 0.52 to 0.87 G^2 for the formate ion bonded directly to the Al atom and about 0.23 to 0.35 G^2 for the formate ion bonded to a Si atom. The second moments of the observed broadenings of the chemical shift powder patterns, minus the lifetime contributions are 0.53 G^2 for the $\text{NH}_4\text{-Y}$ sample and 0.79 G^2 for the ultra-stable H-Y sample. Thus, the residual dipolar broadening indicates that the formate ion is bonded to the Al ions.

The dipolar-modulation data for the formate ion in the $\text{NH}_4\text{-Y}$ zeolite, shown in Figure 9, indicate that the $^{13}\text{C}-^1\text{H}$ coupling is similar to that of calcium formate. The initial decrease of the spectral area for both calcium formate and the surface formate ion is less than predicted for a bond length of 1.09 \AA , shown by the dotted line in Figure 9. The bond length in calcium formate measured by X-ray diffraction is 1.09^0 \AA . The slower decrease in the oscillation of the spectral area compared to the

theoretical rate has been attributed to librational motions in the calcium formate (14,25). We propose that the adsorbed formate ion internuclear bond length is also 1.09 \AA^0 and is undergoing motions similar to those in calcium formate. Also, as the dipolar-modulation time is increased, the area of the adsorbed formic acid spectra do not decrease below zero, contrary to the data of calcium formate and solid benzene. It is suggested that although the direct ^1H - ^1H coupling is suppressed by the eight-pulse cycles, the ^1H nuclei are still coupled through the ^{27}Al nuclei. Thus, after about 0.1 msec, the ^1H - ^{27}Al - ^1H spin diffusion has destroyed some of the phase coherence in the experiment.

The dipolar-difference experiment selectively observes the ^1H bonded to the ^{13}C nuclei where the internuclear bond is rigid. Thus, the ^1H spectrum in Figure 10 is the carbonyl proton of the formate ion on the $\text{NH}_4\text{-Y}$ zeolite at 295 K. As was discussed earlier, the ionic character of this proton is of importance to dehydration reaction mechanisms. The isotropic chemical shift of this spectrum, -12.3 ppm relative to TMS, is similar to that of formate salts. It has been reported previously that the equivalent protons in calcium formate and ammonium formate have isotropic chemical shifts of -10.9 ppm and -12.8 ppm, whereas formic acid is further upfield, at -9.2 ppm (15). The downfield shift of the chemical shift of the carbonyl hydrogen suggests that the hydrogen has acquired a more acidic nature. Thus, the hydrogen may be more susceptible to nucleophilic attack, or it may more readily shift to electron-rich centers.

V. CONCLUSIONS

The results of solid state NMR experiments have determined that formic acid is chemically adsorbed on the $\text{NH}_4\text{-Y}$ and ultrastable H-Y zeolites in two states, differentiated by the strength of the $^{13}\text{C}-^1\text{H}$ dipolar coupling. The difference in heteronuclear couplings is attributed to differences in motional properties. Based on the symmetry of the chemical shift tensors, the more rigidly adsorbed state is interpreted to be a bidentate formate ion. The other surface species becomes rigid at temperatures below 150 K. Changes in the chemical shift tensor upon cooling indicate that this other species is a unidentate formate group. From the enhancements obtained by the cross-polarization technique, relative to the $180^\circ\text{-}\tau\text{-}90^\circ$ experiment, it is determined that the ratio of bidentate to unidentate groups is 52:48 on the $\text{NH}_4\text{-Y}$ zeolite and 83:17 on the ultrastable H-Y zeolite. These values are for loadings of about 0.3 monolayer on both the $\text{NH}_4\text{-Y}$ and ultrastable H-Y zeolites. These results are in agreement with the qualitative interpretations of a previous infrared study of similar loadings of formic acid on the two zeolites (1).

The ^{13}C NMR spectrum of the formate ion may be selectively observed by the cross-polarization technique at 295 K. The magnitude of the broadening in the spectrum that is attributed to ^{27}Al dipolar interactions indicates that on both zeolites, the formate ion is bonded to Al atoms in the zeolite supercages. The initial behavior of the dipolar-modulation data for the adsorbed formate ion are similar to that of calcium formate. These data are interpreted as a $^{13}\text{C}-^1\text{H}$ bond of 1.09 \AA^0 in a librational

motion comparable to that of calcium formate. The isotropic chemical shift of the carbonyl hydrogen of the surface formate ion is similar to those of other bidentate salts, rather than formic acid. The more acidic nature of this hydrogen may be involved in the cleavage of the carbon-hydrogen bond. The center of mass of the bidentate formate ion is much lower than other formate salts, by at least 15 ppm. Though this may have implications in the state of the ion, the complex combination of paramagnetic and diamagnetic contributions does not allow an interpretation of the ionic state of the carbon atom.

The motional averaging of the unidentate is most likely a reorientation at the adsorption site, such as rotation about the zeolite-oxygen bond or the carbon-oxygen bond. It is conceivable that the different bonding to the zeolite surface is the result of formic acid bonding to Si atoms.

The distribution of adsorbed states of formic acid on the two zeolites suggests that the ultrastable H-Y zeolite has more Al sites available for adsorption. In addition, the ^{13}C - ^{27}Al dipolar interaction of the formate ions on the ultrastable H-Y zeolite is stronger as evidenced by the second moments of the broadenings, 0.79 G^2 compared to 0.53 G^2 . The increased number of Al atoms with stronger couplings to formate groups is consistent with the proposal that the thermal decomposition of $\text{NH}_4\text{-Y}$ to ultrastable H-Y creates 9 to 15 nonframework Al ions in the zeolite supercages (17).

VI. ACKNOWLEDGEMENTS

This work was supported in part by the Office of Naval Research, under contract N00014-75-0960. The authors wish to thank J. A. Reimer for obtaining the dipolar-modulation and dipolar-difference spectra, G. W. Brudvig for measuring the electron paramagnetic spectra of the zeolites, and Dr. G.T. Kerr of Mobil Oil Research and Development for supplying the zeolite samples. We also are indebted to Professor S. I. Chan for helpful discussions and comments.

References

1. T. M. Duncan and R. W. Vaughan, *J. Catalysis*, submitted.
2. J. J. F. Scholten, P. Mars, P. G. Menon, and R. Van Hardeveld, *Proc. Intern. Cong. Catalysis*, 3rd, Amsterdam, 1964, p. 881.
3. E. G. Derouane, J. Fraissard, J. J. Fripiat and W. E. E. Stone, *Catalysis Reviews* 7, 121 (1972).
4. H. Pfeifer, Nuclear Magnetic Resonance, Vol. 7, P. Diehl, E. Fluck and R. Kosfeld, Eds., (Springer-Verlag, New York, 1972), p. 55.
5. K. J. Packer, *Progr. NMR Spectroscopy* 3, 81 (1967).
6. S. Kaplan, H. A. Resing and J. S. Waugh, *J. Chem. Phys.* 59, 5681 (1973).
7. E. O. Stejskal, J. Schaefer, J. M. S. Henis and M. K. Tripoli, *J. Chem. Phys.* 61, 2351 (1974).
8. T. M. Duncan, J. T. Yates, Jr., and R. W. Vaughan, *J. Chem. Phys.*, Submitted
9. R. W. Vaughan, *Ann. Rev. Phys. Chem.* 29, 397 (1978).
10. M. Mehring, High Resolution NMR Spectroscopy in Solids, (Springer-Verlag, New York, 1976).
11. U. Haeberlin, High Resolution NMR in Solids - Selective Averaging, (Academic Press, New York, 1976).
12. (a) A. Pines, M. G. Gibby and J. S. Waugh, *J. Chem. Phys.* 56, 1776 (1972);
(b) A. Pines, M. G. Gibby, and J. S. Waugh, *J. Chem. Phys.* 59, 569 (1973).
13. D. E. Demco, J. Tegenfeldt, and J. S. Waugh, *Phys. Rev. B* 11,

4133 (1975).

14. (a) M. E. Stoll, A. J. Vega and R. W. Vaughan, *J. Chem. Phys.* 65, 4093 (1976);
(b) M. E. Stoll, A. J. Vega and R. W. Vaughan, *XIXth Congress Ampere*, Heidelberg, 1976.
15. J. A. Reimer and R. W. Vaughan, *Chem. Phys. Lett.* 63, 163 (1979).
16. J. L. Ackerman, J. Tegenfeldt, and J. S. Waugh, *J. Amer. Chem. Soc.* 96, 6843 (1974).
17. (a) G. T. Kerr, *J. Catalysis* 15, 200 (1969); (b) G. T. Kerr, *Adv. in Chem. Series* 121, 219 (1973); (c) C. V. McDaniel and P. K. Maher, Molecular Sieves, (Soc. Chem. Industry, London, 1967) p. 186.
18. S. A. Al'tshuler and B. M. Kozyrev, Electron Paramagnetic Resonance in Compounds of Transition Elements, 2nd ed., Eng. Trans. from Russian, (Wiley, New York, 1974).
19. A. S. Coolidge, *J. Amer. Chem. Soc.* 50, 2166 (1928).
20. C. V. McDaniel and P. K. Maher, Zeolite Chemistry and Catalysis, J. A. Rabo, ed., ACS Monograph 171, Washington, D. C., 1976, p. 296.
21. R. W. Vaughan, D. D. Elleman, L. M. Stacey, W. K. Rhim, and J. W. Lee, *Rev. Sci. Inst.* 43, 1356 (1972).
22. M. E. Stoll, A. J. Vega and R. W. Vaughan, *Rev. Sci. Inst.* 48, 800 (1977).
23. (a) H. Y. Carr and E. M. Purcell, *Phys. Rev.* 94, 630 (1954);
(b) R. L. Vold, J. S. Waugh, M. P. Klein, and D. E. Phelps, *J. Chem. Phys.* 48, 3831 (1968).

24. S. R. Hartmann and E. L. Hahn, Phys. Rev. 128, 2042 (1962).
25. M. E. Stoll, Ph.D. Thesis, Caltech, 1977.
26. W-K. Rhim, D. D. Elleman, L. B. Schreiber and R. W. Vaughan, J. Chem. Phys. 60, 1595 (1974).
27. M. Mehring, A. Pines, W-K. Rhim and J. S. Waugh, J. Chem. Phys. 54, 3239 (1971).
28. N. Bloembergen and J. A. Rowland, Acta Metall. 1, 731 (1953).
29. A. Pines, M. G. Gibby, J. S. Waugh, Chem. Phys. Lett. 15, 373 (1972).
30. J. M. O'Gorman, W. Shand, Jr., and V. Schomaker, J. Amer. Chem. Soc. 72, 4222 (1950).
31. R. G. Lerner, B. P. Dailey, and J. P. Friend, J. Chem. Phys. 26, 680 (1957).
32. I. Nahringbauer, Acta Cryst. B 24, 565 (1968).
33. I. Nitta and K. Osaki, X-Rays 5, 37 (1948); ref. in Structural Reports 11, 556 (1948).
34. J. B. Stothers, Carbon-13 NMR Spectroscopy, (Academic Press, New York, 1972).
35. A. Abragam, The Principles of Nuclear Magnetism, (Oxford University Press, London, 1961), Chap. IX
36. A. Bielanski and J. Datka, J. Catalysis 32, 183 (1974).
37. K. Hirota, K. Fueki, K. Shindo and Y. Nakai, Bull. Chem. Soc. Japan, 32, 1261 (1959).
38. M. D. Sefcik, J. Schaeffer and E. O. Stejskal, Molecular Sieves-II, J. R. Katzer, ed. ACS Symposium Series 40, Washington, D. C. 1977,

p. 344.

39. J. E. Anderson and W. P. Slichter, J. Chem. Phys. 43, 433 (1965).
40. Reference 35, Chapter IV.
41. (a) D. E. O'Reilly, J. Chem. Phys. 28, 1263 (1958); (b) D. E. O'Reilly, Adv. in Catalysis 12, 31 (1960).
42. D. L. Vanderhart, H. S. Gutowsky, T. C. Farrar, J. Amer. Chem. Soc. 89, 5056 (1967).
43. D. L. Vanderhart, private communication.

TABLE I
13C Chemical Shift Parameters

Compound	Temperature (K)	Principal Components (a)			σ	$\sigma_{33}-\sigma_{11}$	$\frac{\sigma_{22}-\sigma_{11}}{\sigma_{33}-\sigma_{11}}$	Reference
		σ_{11}	σ_{22}	σ_{33}				
HCOOCH_3 (b)	87	-107	-136	-253	-165	146	0.20	29
HCOOH (c)	125	-92	-162	-252	-169	160	0.44	This Work
$(\text{NH}_4)\text{HCO}_2$	185	-99	-168	-225	-164	126	0.55	This Work
$\text{Ca}(\text{HCO}_2)_2$	125	-96	-186	-235	-172	139	0.66	This Work

B. Structure					
Compound	C-O Bond Lengths (Å)		R_2/R_1	Method	Reference
	R_1	R_2			
HCOOCH_3	1.22 ± 0.03	1.37 ± 0.04	1.12	electron diffraction	30
HCOOH	1.245 ± 0.002	1.312 ± 0.002	1.05	isotopic microwave	31
$(\text{NH}_4)\text{HCO}_2$	1.237 ± 0.007	1.246 ± 0.007	1.01	X-ray diffraction	32
$\text{Ca}(\text{HCO}_2)_2$ (d)	1.25 ± 0.03	1.25 ± 0.03	1.00	X-ray diffraction	33
	1.24 ± 0.03	1.25 ± 0.03	1.01		

(a) in ppm, relative to tetramethylsilane (TMS)

(b) data converted from original reference using $\sigma(\text{C}_6\text{H}_6) = -128.7$ ppm, relative to TMS

(c) principal components estimated from data, rather than computed lineshape.

(d) two crystallographically distinct formate groups.

TABLE II
 ^{13}C Spectral Parameters of Adsorbed Formic Acid

Spectrum	Experiment	Temperature (K)	Linewidth (a)	Principal Components (b)			$\frac{\sigma_{22}-\sigma_{11}}{\sigma_{33}-\sigma_{11}}$	δ
				σ_{11}	σ_{22}	σ_{33}		
A. HCOOH on the $\text{NH}_4\text{-Y}$ Zeolite								
4 (a)	180°-τ-90°	295	60	-153	-168	-172	-164	0.79
7 (a)	Cross-Polarization	295	75	-129	-151	-161	-147	0.69
7 (b)	Cross-Polarization	150	111	-95	-152	-233	-160	0.41
B. HCOOH on the Ultrastable H-Y Zeolite								
4 (b)	180°-τ-90°	295	98	-112	-176	-206	-165	0.68
7 (c)	Cross-Polarization	295	105	-95	-155	-199	-150	0.58
7 (d)	Cross-Polarization	115	144	-98	-145	-240	-161	0.33
							116	116

(a) Full width at half-maximum, in ppm
 (b) in ppm, relative to TMS
 (c) Isotropic frequency of the lineshape, relative to TMS
 (d) Linewidth of the Gaussian broadening function convoluted into the powder pattern, in ppm
 (e) Spectrum convoluted with a Lorentzian broadening function

TABLE III.
Representative Vibrational Band Positions for Adsorbed Formic Acid

Substrate	Vibrational Band Assignments (a)			Measurement Technique	Reference
	C=O Stretch	C-O Stretch	CH Bend		
Al Metal	1590	1360	-	Reflectance Infrared	12
Al ₂ O ₃	1597	1377	-	Transmission Infrared	20
Al ₂ O ₃	1600	1380	-	Transmission Infrared	9
Al ₂ O ₃	1625	1390	1407	Transmission Infrared	10
Al ₂ O ₃	1620	1344	1402	Transmission Infrared	11
Na-Y Zeolite	-	1385	-	Transmission Infrared	8
Al ₂ O ₃	1621	1468	1390	IETS	13
Al ₂ O ₃	1620	1468	1390	IETS	14
		1320			
B. Physically Adsorbed Formic Acid					
Al ₂ O ₃ at 77 K	1700	1250	1390	IETS	14
SiO ₂	1714	960	-	Transmission Infrared	11
Na-Y Zeolite	1720	-	-	Transmission Infrared	8

(a) all frequencies in cm^{-1}

FIGURE CAPTIONS

Figure 1. Schematic representations of the NMR pulse schemes used in this study. The abscissa for these representations is time and the pulses are indicated by rectangular boxes of arbitrary height. The observed magnetization is indicated by the dotted lines. The ^{13}C and ^1H pulse schemes are started simultaneously. In the 180° - τ - 90° and dipolar-difference sequences, the ^{13}C A and B modes are alternately applied and the NMR signal is alternately added and subtracted.

Figure 2. ^{13}C NMR spectra of reference formates measured by ^{13}C - ^1H cross-polarization. (a) Formic acid at 125 K, (b) ammonium formate at 185 K and (c) calcium formate at 125 K. The abscissa scale is 3.44 ppm per point in all spectra. Frequencies are relative to tetramethylsilane (TMS).

Figure 3. Amplitude of the observed ^{13}C magnetization versus τ , the delay between the 180° and 90° pulses, for formic acid adsorbed on the $\text{NH}_4\text{-Y}$ (\square) and the ultrastable H-Y (Δ) zeolites at 295 K. Absolute counts for the ^{13}C nuclei were calibrated with an enriched adamantane sample. The proton-decoupling was set at 16 G.

Figure 4. ^{13}C NMR spectra of formic acid adsorbed on (a) the $\text{NH}_4\text{-Y}$ zeolite (130,000 averages) and (b) the ultrastable H-Y zeolite (66,000 averages), as measured by the 180° - τ - 90° experiment at 295 K. In both spectra, $\tau = 0.5$ msec and

proton decoupling was at 16 G.

Figure 5. ^{13}C NMR spectra of the ultrastable H-Y zeolite dosed with formic acid, eight months later, with (a) 16 G proton decoupling and (b) no decoupling. Both spectra are the result of about 66,000 averages of the $180^\circ-\tau-90^\circ$ sequence with $\tau = 0.5$ msec at 295 K.

Figure 6. The amplitude of the observed ^{13}C magnetization versus the length of the cross-polarization process for formic acid adsorbed on the $\text{NH}_4\text{-Y}$ (□) and the ultrastable H-Y (△) zeolites at 295 K. The proton decoupling was set at 16 G.

Figure 7. ^{13}C NMR spectra of adsorbed formic acid as a function of temperature, measured by the cross-polarization scheme. The data were recorded immediately after 1.0 msec of cross-polarization with 16 G of proton decoupling. The spectra are formic acid adsorbed on the $\text{NH}_4\text{-Y}$ zeolite at (a) 295 K and at 155 K; and the ultrastable H-Y zeolite at (c) 295 K and at 115 K. Each spectrum is the accumulation of about 66,000 averages.

Figure 8. The amplitude of the observed ^{13}C magnetization versus the delay to the echo in the cross-polarization sequence for formic acid adsorbed on the $\text{NH}_4\text{-Y}$ zeolite (□) and the ultrastable H-Y zeolite (△) at 295 K. Proton decoupling pulses of 16 G were applied immediately after the ^{13}C spin-locking pulses.

Figure 9. Spectral areas versus the dipolar-modulation time for formic acid adsorbed on the $\text{NH}_4\text{-Y}$ zeolite at 295 K (\square) and at 125 K (Δ). For comparison, we also plot the data for benzene at 185 K (\diamond) and calcium formate at 295 K (\circ) reported by Stoll, et al. (14,25). Theoretical curves are for a rigid $^{13}\text{C}-^1\text{H}$ bond length of 1.09 Å (dotted line), a rigid bond at 1.19 Å (dashed line), and for a 1.09 Å bond averaged by rotation in a plane (dashes and dots).

Figure 10. Proton spectrum of the carbonyl hydrogen of formic acid adsorbed on the $\text{NH}_4\text{-Y}$ zeolite at 295 K, obtained with about 8,000 averages of the dipolar-difference experiment.

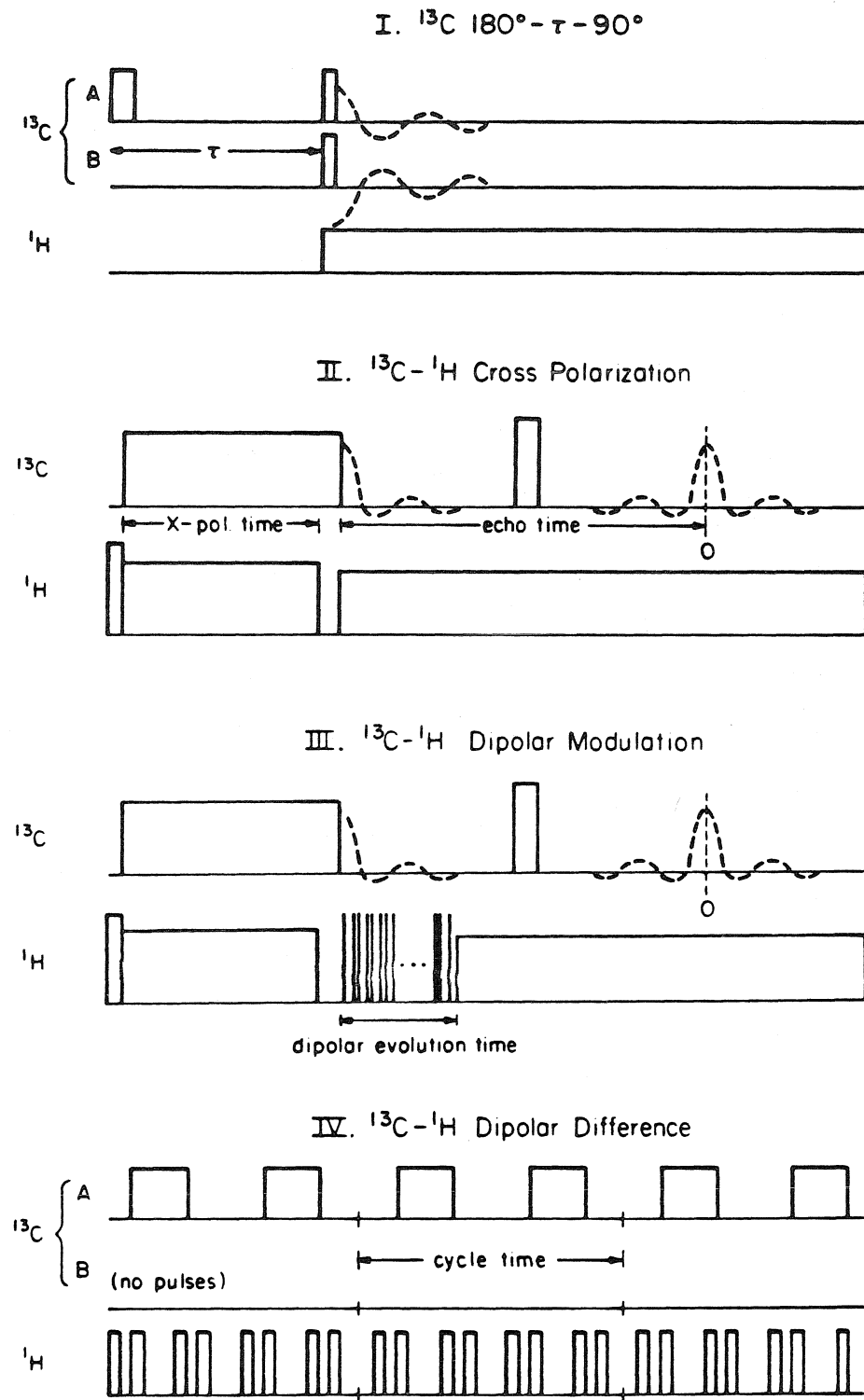


Figure 1.

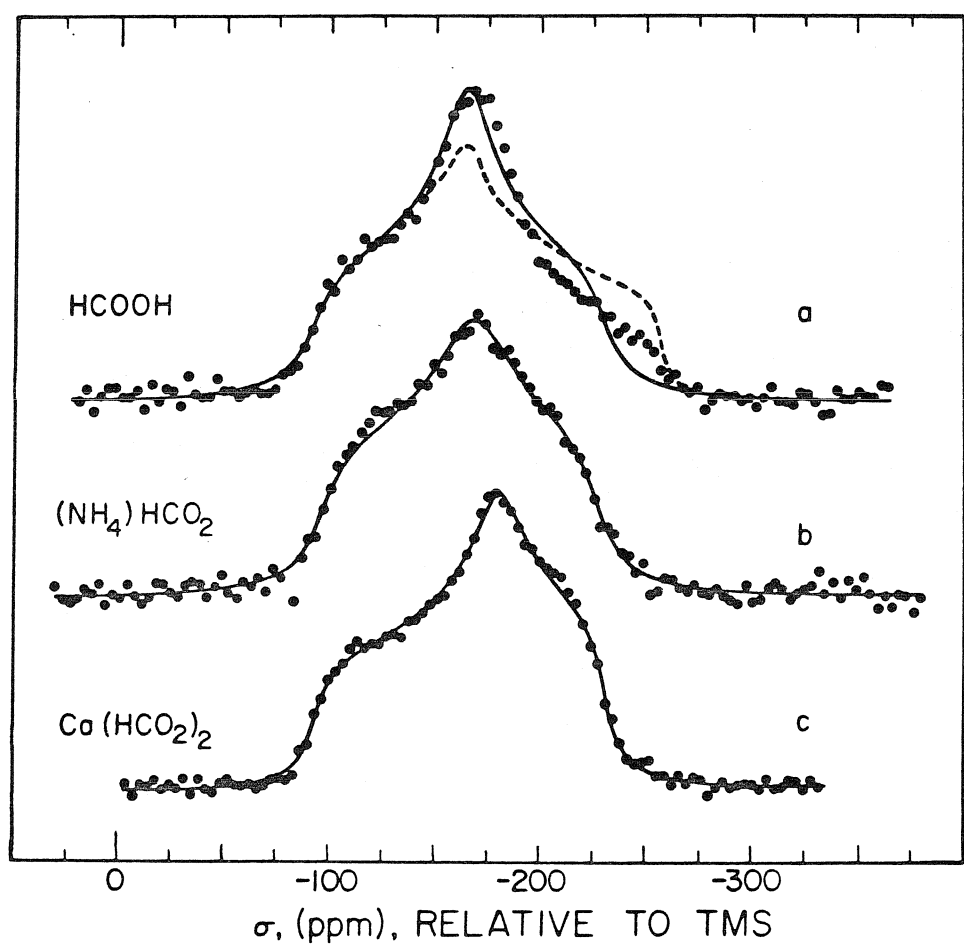


Figure 2.

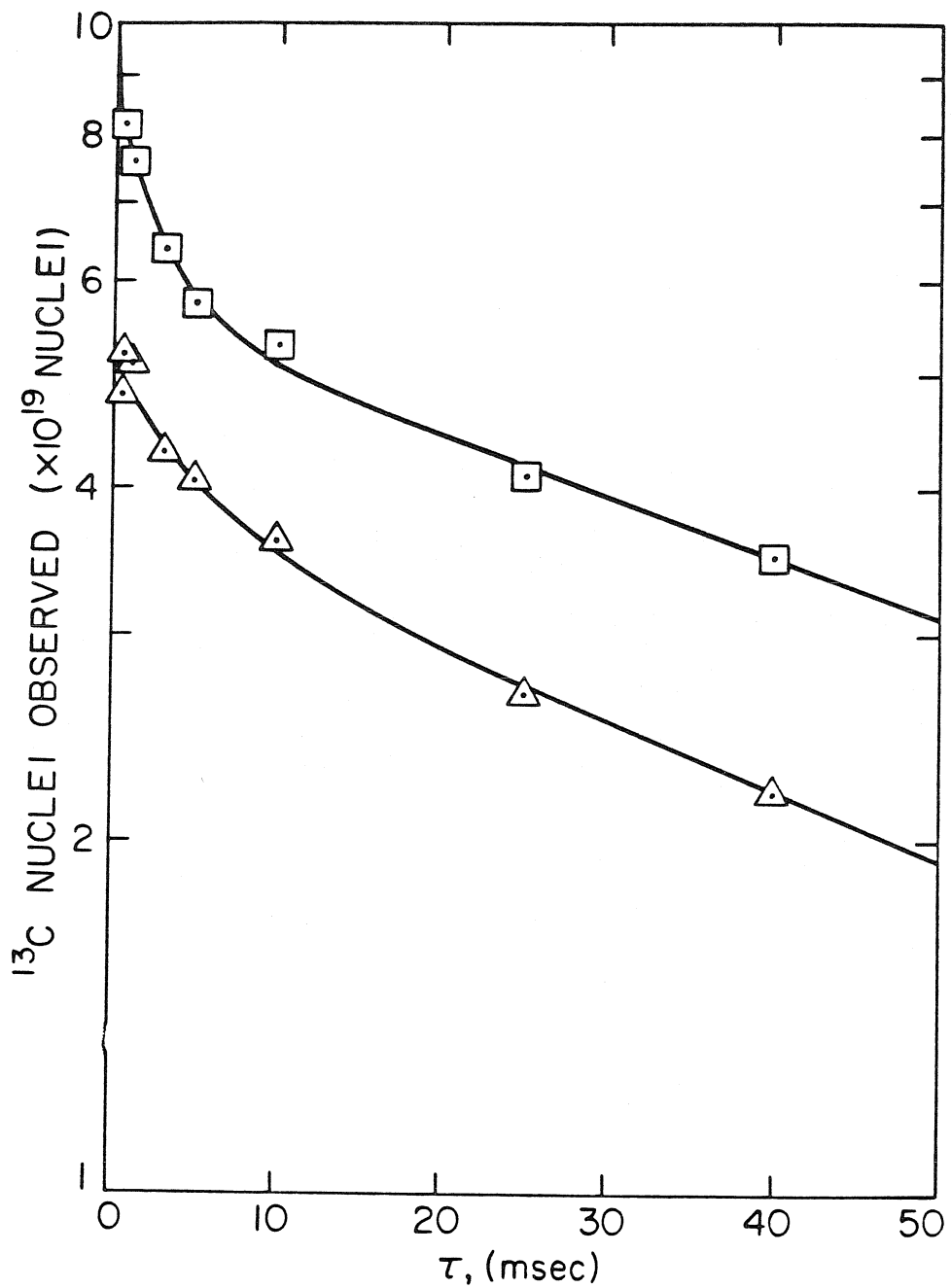


Figure 3.

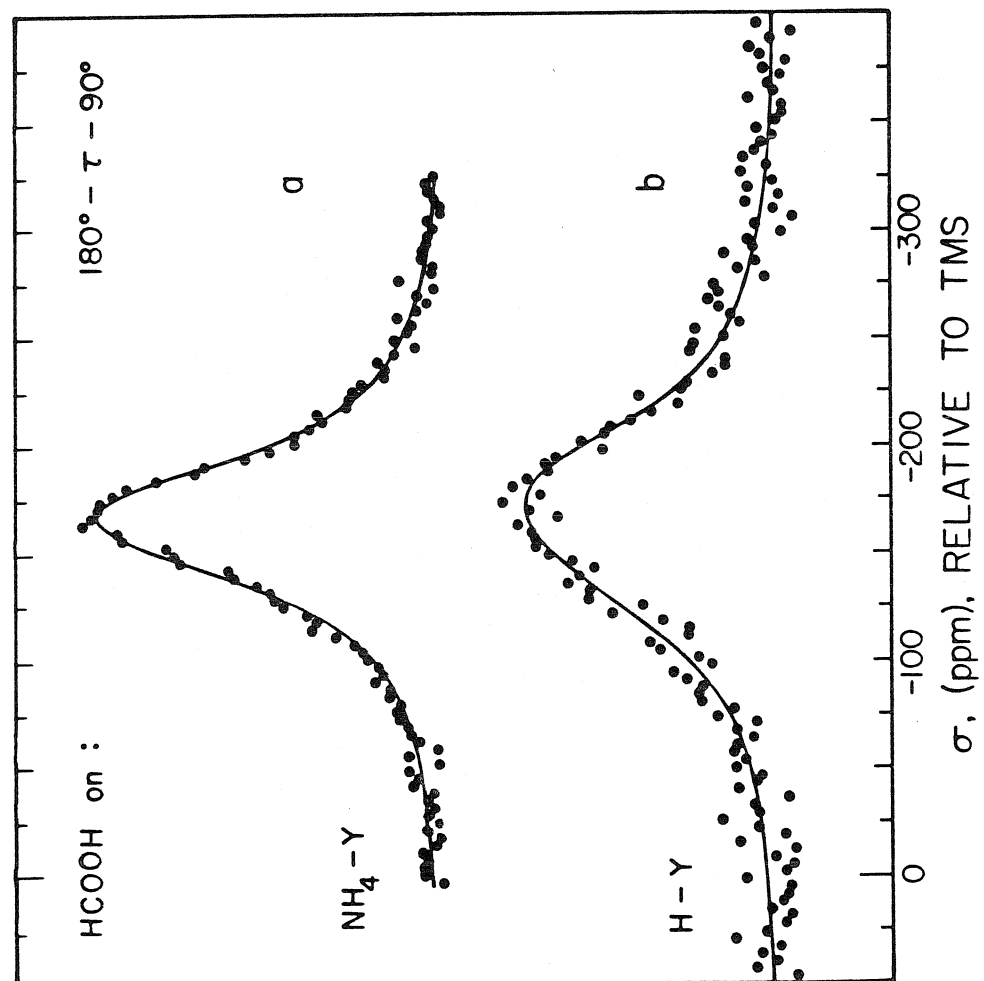


Figure 4.

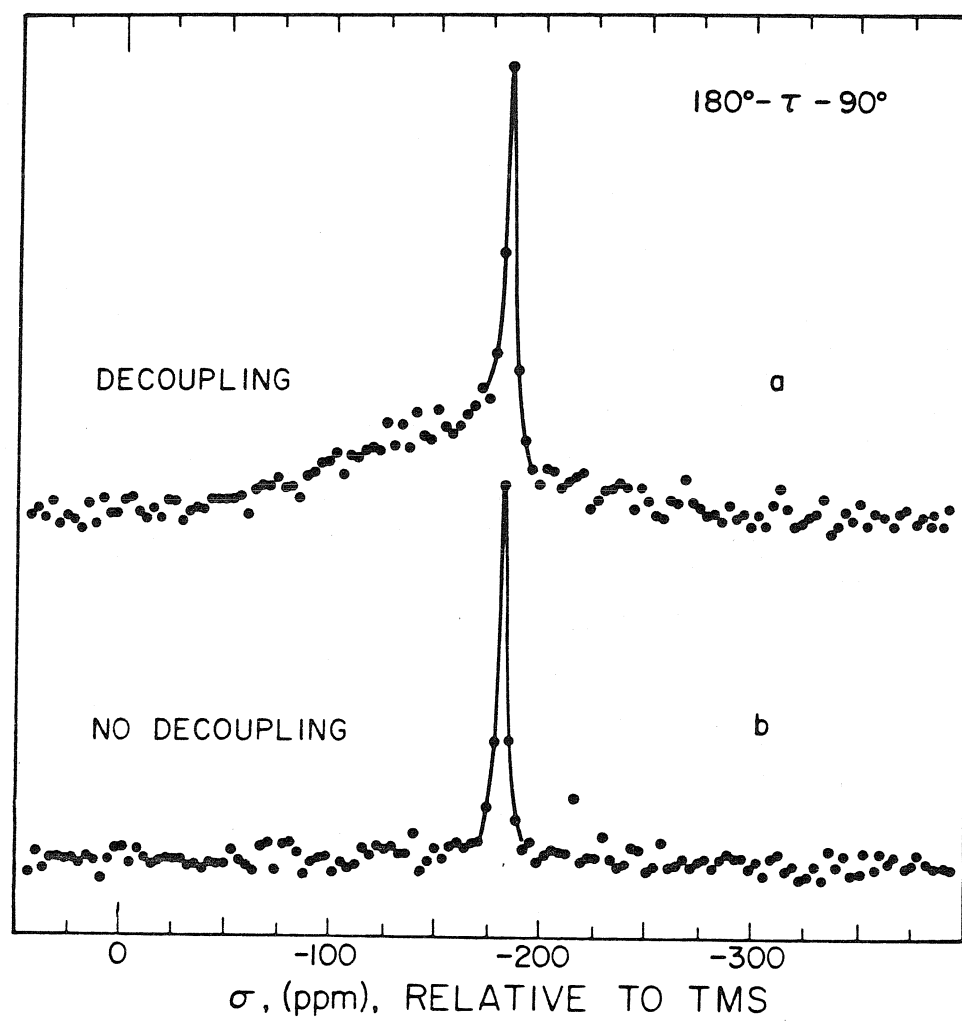


Figure 5.

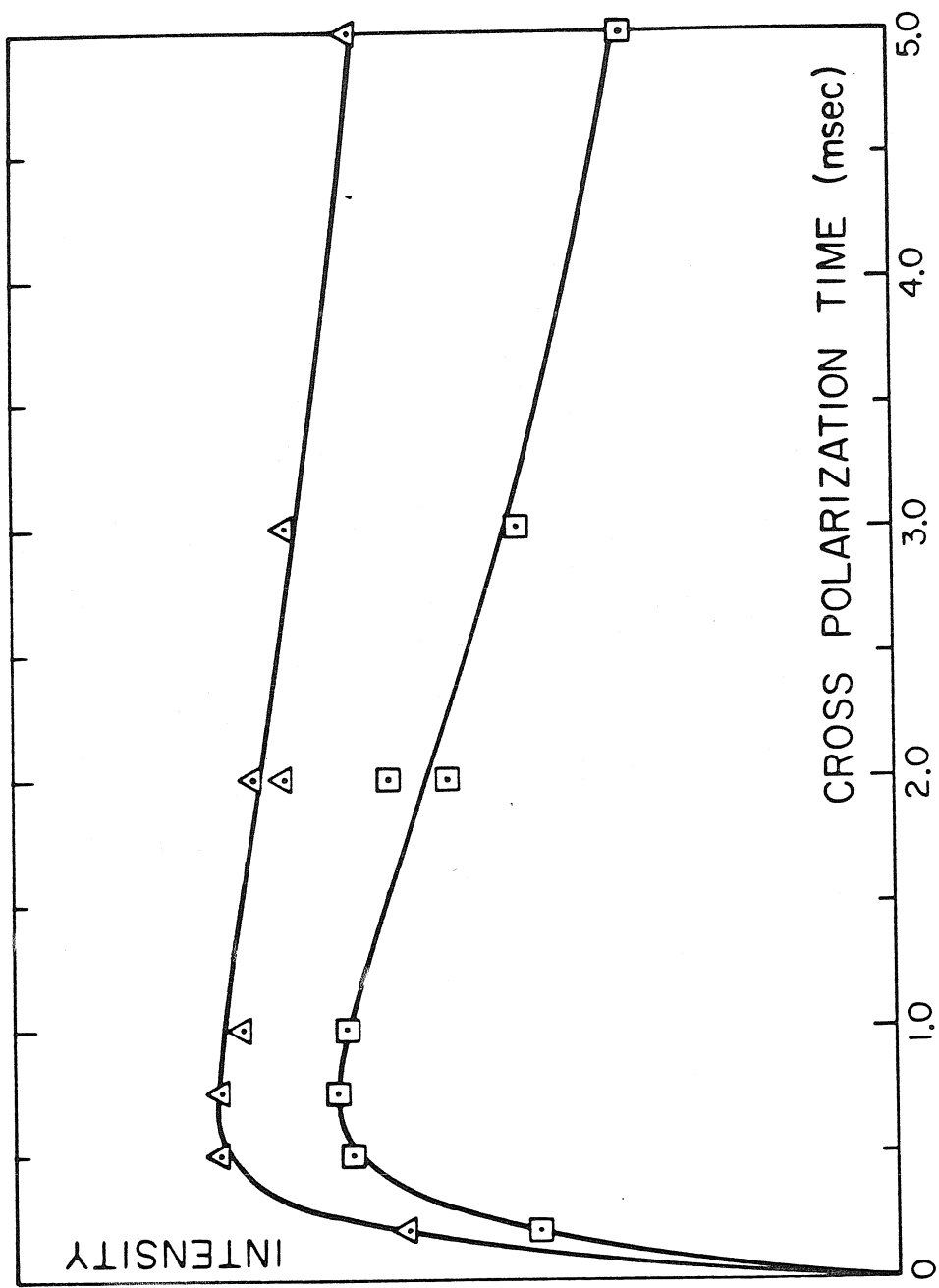


Figure 6.

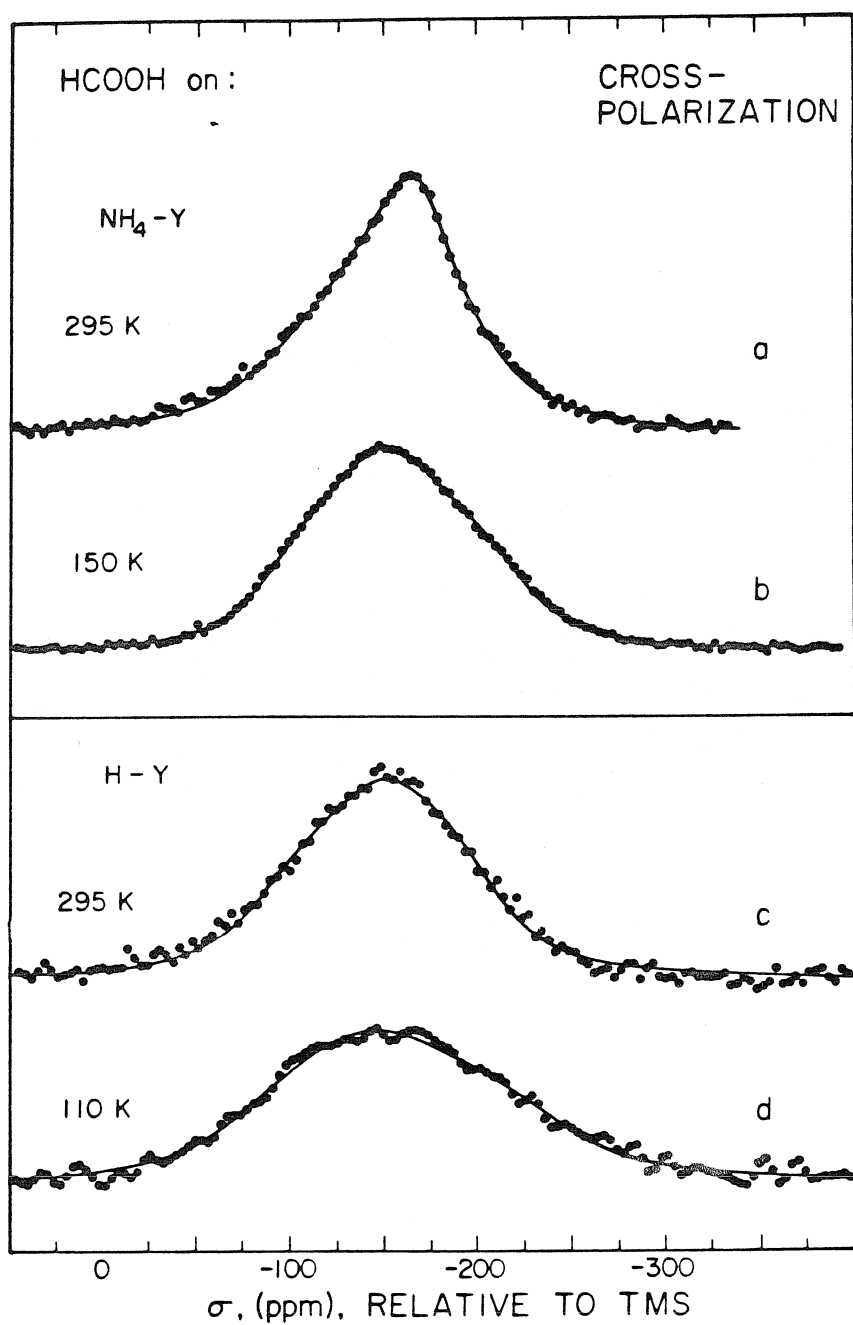


Figure 7.

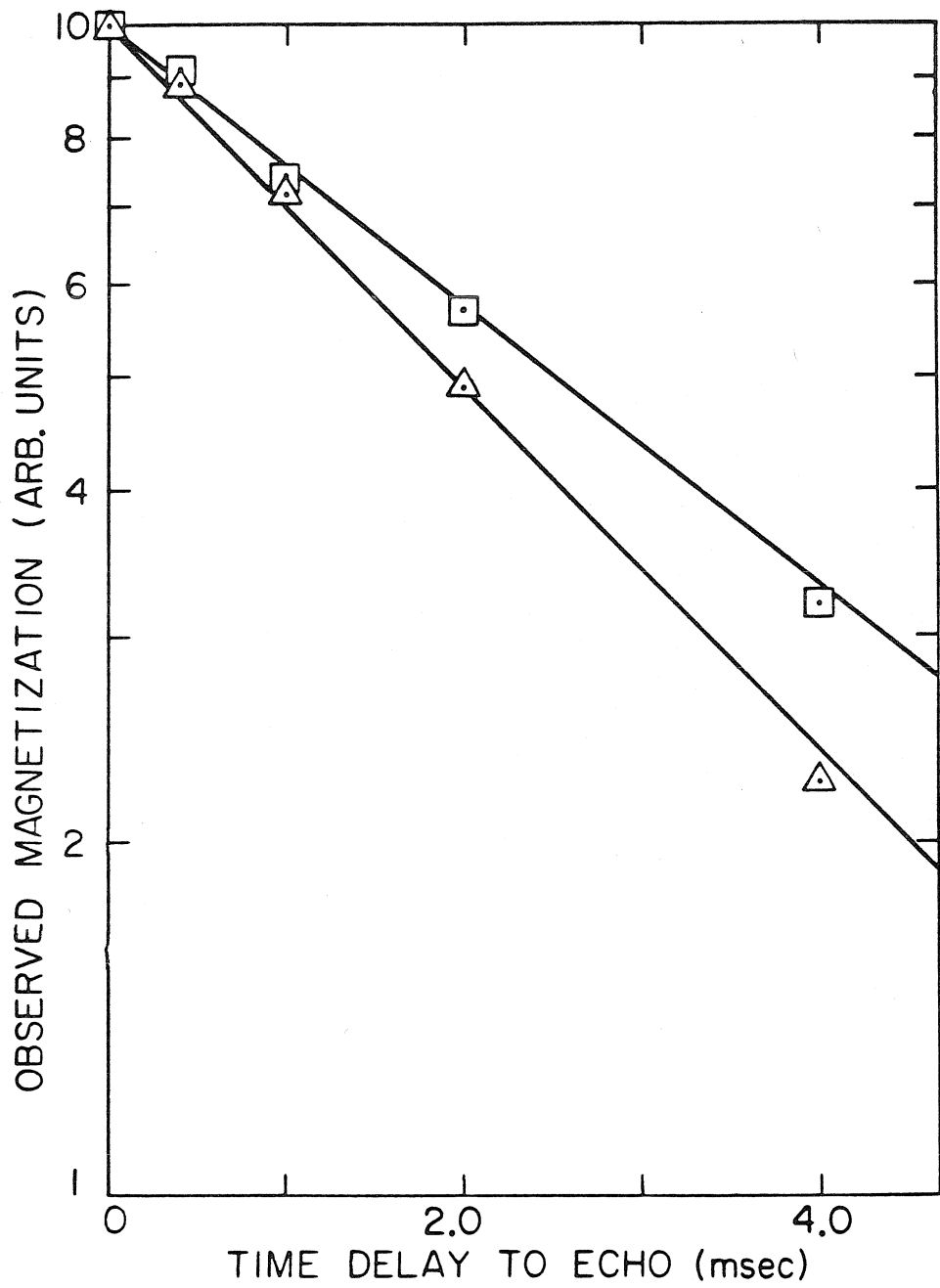


Figure 8.

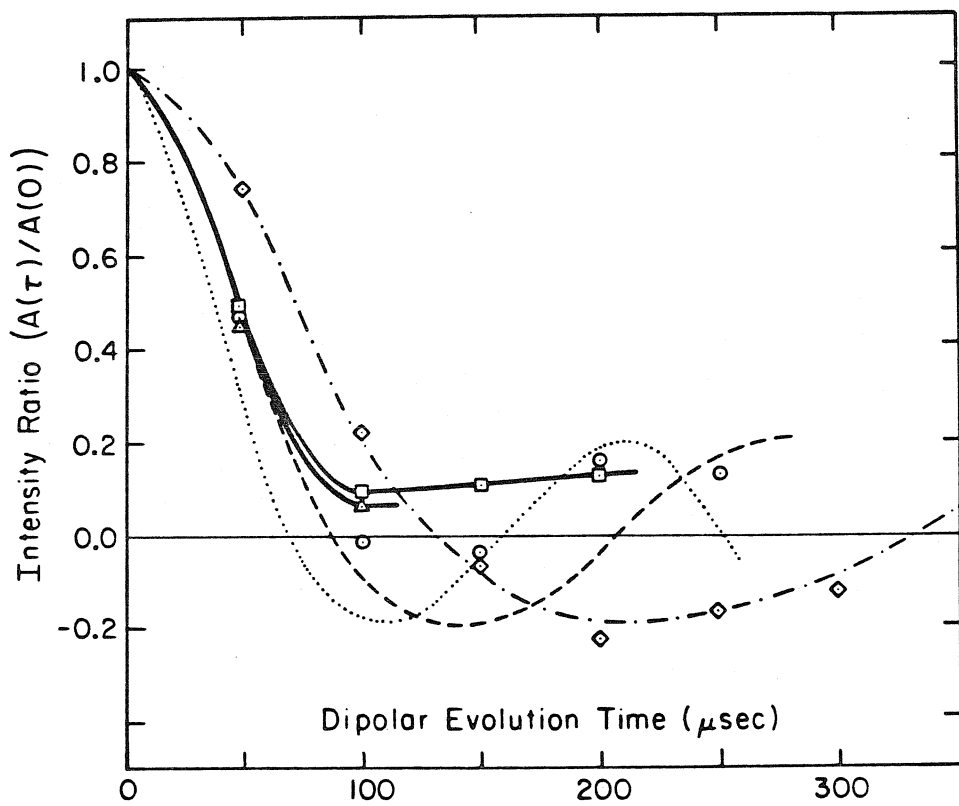


Figure 9.

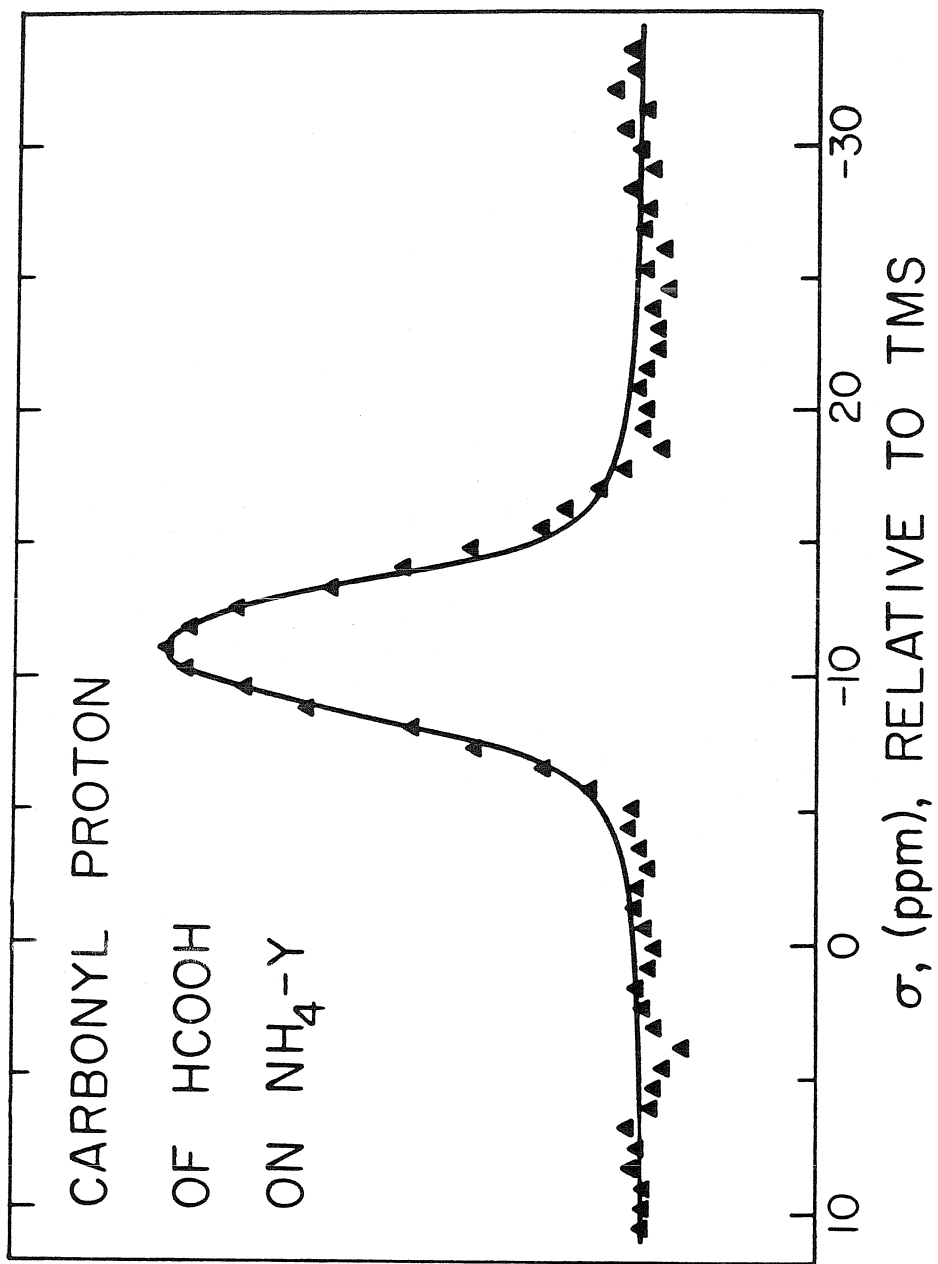


Figure 10.

CHAPTER VIII

Conclusions

For the two catalytic systems studied in this thesis, the combined results of infrared and NMR spectroscopic techniques have, to a degree, succeeded in describing the three features listed in the Introduction; i.e. the structure of the adsorbed species, the nature of the adsorption site, and the motional properties of the adsorbed molecule. The conclusions regarding the nature of the adsorbed states of CO on Rh dispersed on Al_2O_3 and formic acid on Y zeolites have been summarized at the end of each chapter, particularly chapters V and VII, respectively. Rather, this chapter will discuss the application of the combination of the infrared and NMR techniques to the study of molecules adsorbed on catalytic surfaces.

The more conventional infrared technique is relatively simple to apply and analyze. Typically, each infrared scan requires about 20 minutes. The characteristic positions and the adequate separations of the absorbance peaks allow straightforward analyses and interpretations. The recent introduction of commercial Fourier transform spectrometers will provide increased resolution through extensive signal averaging, in addition to the advantage of an internally calibrated frequency (1). Plus, since the individual Fourier transform infrared spectra may be obtained in less than one minute, it is possible to monitor surface processes in progress, such as adsorption or isotopic exchange.

However, the infrared technique is limited in several aspects. For small molecules with carbonyl components, such as CO and formic acid, the infrared spectrum is strong and relatively simple. However, for larger molecules, such as butenes, aromatics, or polymers, the spectra are much more complex and difficult to analyze. The effects of the

interaction of one portion of the molecule with the surface may be lost in the numerous other peaks of the spectrum. Plus, in general, the more complex molecule is more likely to yield a greater number of surface states. Quantitative analysis with infrared spectra is not possible since the relative infrared intensities of the various species are not proportional to the relative populations of the surface states. The infrared spectrum may be calibrated, as with gravimetric techniques (2) or with NMR (3), but the calibration may change upon reaction of the surface, as is shown in Appendix A of this thesis. The presence of certain species which are important in the methanation reaction may be difficult or impossible to observe with infrared techniques. Examples include surface carbides, M-C, which have metal-carbon stretches below 1000 cm^{-1} , the lower limit of the spectrum of oxide-supported catalysts, or surface methyl groups, M-CH₃, which may have weak bands that are overwhelmed by other species.

However, many of these difficulties may be solved by combining the results of infrared techniques with those of solid-state NMR. The NMR signal will observe all ¹³C nuclei on a surface sample, provided that the necessary considerations have been given to relaxation times and dipolar broadening. However, the NMR spectra of the chemically adsorbed species will at least overlap, if not coincide. However, the infrared technique may be used to place a lower limit on the number of different surface groups. With this in mind, the NMR spectrum may be deconvoluted based on differences in relaxation times (3) or dipolar couplings (4), or isotopic chemical shifts. The deconvoluted spectra may then be analyzed for the symmetry, motional properties, and electronic nature

of the adsorbed species.

Whereas the carbonyl groups are the easiest to detect and analyze with infrared techniques, the aliphatic compounds are the best suited to double-resonance multiple-pulse NMR studies. The NMR parameters such as the chemical shift anisotropy and center of mass are relatively insensitive to the state of the CO molecule. But small changes in hydrocarbon bondings and carbon hybridization result in readily detectable changes in the NMR spectra. The ^{13}C and ^1H spin baths allow one to apply a large number of multiple-pulse schemes to remove and/or quantify the heteronuclear dipolar interactions. Plus, comparing and contrasting the ^{13}C and ^1H NMR spectra provides a valuable cross-check on the surface environment and the state of the adsorbed molecule.

For complex molecules, the NMR spectrum of only one nuclear site may be obtained by enriching only that atom with ^{13}C . Thus, even for molecules with as many as 10 carbon atoms, the extraneous ^{13}C signal due to naturally occurring ^{13}C , will be only about 10%. Successive NMR experiments with different ^{13}C -enriched sites on the molecule would yield a complete description of the adsorbed state.

However, even in the absence of dipolar broadening, the NMR spectrum may still be quite complex, due to the overlapping chemical shift powder patterns of several surface complexes. In this case, it more important to simply tabulate the number of different surface species. The broadening due to the chemical shift anisotropy may be removed by spinning the sample at the "magic angle" relative to the external magnetic field (i.e. $(3\cos^2\theta - 1) = 0$, or $\theta = 54.7^\circ$) (5). For samples spinning at rates comparable to the individual NMR linewidths, the powder patterns

will collapse to several sharp lines centered at their respective isotropic chemical shifts. Each sharp line indicates a distinct species, the population of which is proportional to the intensity of the line.

To further quantify the catalytic system, it is also possible to obtain the NMR spectra of the substrate. Recently, the state of oxide-supported vanadium and platinum in catalysts taken from commercial reactors have been analyzed with NMR (6). The recent advances in NMR interferometry have made it possible to examine the state of quadrupolar nuclei, such as ^{27}Al , even in the presence of large electrostatic field gradients (7). Thus, it is possible to study directly the active site and observe the electronic changes upon the adsorption of molecules.

Currently, the principal problems with NMR studies of surface adsorbed species are that NMR is relatively difficult and time consuming. Both problems are being dealt with by the recent availability of high-field commercial spectrometers. The spectra reported in this thesis were taken at 1.32 Tesla and required a minimum of 8 hours each to accumulate. The 6.3 Tesla superconducting magnets yield a proportional increase in the intensity of the NMR signal and thus, a factor of almost 25 improvement in the amount of time necessary to obtain comparable spectra. In addition, other changes in instrumentation, made with the application of catalytic studies specifically in mind, will further improve the sensitivity. Examples include quadrature-phase detection, increasing the length of the sampling windows of the analog-to-digital converter, faster cycling times on the computer, and improved amplifiers and gating networks to reduce the critical ring-down time of the free

induction decays of the extremely broad lines.

In the early 1950's, the introduction of liquid-line NMR into analytical laboratories made it possible to complete structural analyses of unknown compounds in a matter of hours instead of the weeks required for chemical analysis. A solid-state NMR study of an unknown surface species currently requires weeks and even months to complete. However, since in many cases there may be no other method to obtain such an analysis, solid-state NMR should prove to be a viable and promising tool for the investigation of catalytic systems.

References

1. For example, see R. Bouwman and I.L.C. Fretiks, *Appl. Surf. Sci.* 4, 11 (1980).
2. D. A. Seanor and C. H. Amberg, *Rev. Sci. Instrum.* 34, 917 (1963).
3. This thesis, chapter V
4. This thesis, chapter VII
5. (a) E.R. Andrew, *Prog. Nucl. Magnetic Resonance Spect.* 8, 1 (1971);
(b) E.O. Stejskal, J. Schaefer, J.S. Waugh, *J. Mag. Resonance* 28, 105 (1972); (c) L.M. Ryan, R.E. Taylor, A.J. Paff, and B.C. Gerstein, *J. Chem. Phys.* 72, 508 (1980).
6. (a) B. Silbernagel, *J. Catalysis* 56, 315 (1979);
(b) G.J. den Otter and F.M. Dautzenberg, *J. Catalysis* 53, 116 (1978).
7. (a) M. Polak and R.W. Vaughan *Phys. Rev. Lett.* 39, 1677 (1977);
(b) M. Polak and R.W. Vaughan *J. Chem. Phys.* 69, 3232 (1978).

APPENDIX A

Combined NMR and Infrared Studies
of CO on Rh dispersed on Al_2O_3 :
Desorption and Elevated Temperature Experiments

Introduction

The investigation of the adsorption of CO on Rh dispersed on Al_2O_3 with combined NMR and infrared techniques described in chapters II through V of this thesis have been extended to characterize the system after various treatments. Specifically, the catalytic system was subjected to prolonged desorption and elevated temperatures and then analyzed with both spectroscopic techniques. The results, though preliminary, suggest that the adsorbed CO has a large distribution of infrared molar absorbance coefficients, and/or the existence of surface species not detected by the infrared technique.

Experimental Procedure

The preparation and characterization of the 2.2% by weight Rh on Al_2O_3 substrate, the combined NMR/infrared sample cell, the ion-pumped metal vacuum system, and the description and operation of the infrared and NMR spectrometers have been described in chapters II through V of this thesis. The ^{13}C NMR spectra were obtained with the $180^\circ-\tau-90^\circ$ experiment with $\tau = 0.5$ msec.

ResultsA. Desorption and Re-adsorption Experiments

A freshly prepared 2.2% Rh on Al_2O_3 substrate was exposed to about 50 Torr of 91.2% ^{13}C enriched CO. The infrared and NMR spectra of this sample (spectra (a) of Figures 1 and 2, respectively) are similar to those previously reported. The infrared spectrum reveals the presence of the three surface states; the isolated dicarbonyl (2049 cm^{-1} and 1987 cm^{-1}), the linearly-bonded state (2020 cm^{-1}) and the bridged-bonded state

(1830 cm^{-1}). The rotational spectrum of $^{13}\text{CO(g)}$ is also seen as wiggles over the range of about 2150 cm^{-1} to 2000 cm^{-1} . After about 50 days of continuous evacuation with a 20 liter sec^{-1} ion pump, the equilibrium pressure of CO was reduced to 3×10^{-7} Torr. Spectra (b) of Figures 1 and 2 are the infrared and NMR results after the evacuation, respectively. Whereas the infrared spectrum decreased uniformly by 85%, the ^{13}C NMR spectrum was reduced by only 15%, as seen by the difference spectrum, Figure 2(a-b). Upon subsequent re-exposure to about 50 Torr of ^{13}CO , spectra (c) of Figures 1 and 2 were observed. Both the infrared and the NMR spectra have returned to their original intensities. The infrared spectrum shows evidence of some surface reconstruction. The linear state (2020 cm^{-1}) is more intense and the dicarbonyl peaks are slightly reduced in intensity. This desorption and re-adsorption experiment was repeated with a second sample, with about 23 days of evacuation, and similar spectra were observed.

B. Elevated Temperatures Experiments

The ^{13}CO on Rh dispersed on Al_2O_3 sample from the previous experiment was heated to elevated temperatures in the presence of about 50 Torr of ^{13}CO , cooled to 295 K and then examined with the infrared and NMR spectroscopic techniques. First, the combined NMR/infrared cell was held at 425 K for 3 hours. The resulting spectra, (d) of Figures 1 and 3, at first inspection, appear to reveal contradictory conclusions. The infrared spectrum has a loss of intensity in the dicarbonyl bands (2049 cm^{-1} and 1987 cm^{-1}), an increase in the linear species (2020 cm^{-1}) and little or no change in the bridged state (1830 cm^{-1}). The ^{13}C NMR spectrum, however, has increased in intensity, indicating that the heating process has

resulted in the adsorption of more ^{13}C species on the dispersed Rh substrate. Recall that whereas the infrared technique is not quantitative due to the distribution of molar absorbances, infrared-active species, and absorbances below the range of the spectrum, 1000 cm^{-1} , the intensity of the NMR spectrum is directly proportional to the number of observed ^{13}C nuclei. Proper calibrations have been taken to ensure that all the ^{13}C nuclei are observed.

The infrared and NMR components of the cell were separated by collapsing the copper section of the NMR tube to form an ultrahigh vacuum cold weld seal. The results of the remaining experiments will therefore be monitored with only the ^{13}C NMR spectroscopy. The NMR tube was then re-heated to 425 K for 24 hours, cooled to 295 K and measured with NMR. The ^{13}C NMR spectrum is reported in Figure 3(e). The intensity has increased further as best seen in the difference spectrum, 3(e-c).

Finally, the NMR tube was heated to 525 K for 12 hours, and recooled. The ^{13}C NMR spectrum at 300 K, shown in Figure 4, has changed dramatically. The sharp line, centered at -121 ppm, has narrowed from about 200 ppm to only 3 ppm. The isotropic chemical shift of CO_2 is -124.2 ppm (1). Thus, the narrow line suggests that the CO has either disproportionated or reacted with surface hydroxyls to form CO_2 via $\text{CO} + 2(\text{OH}) \rightarrow \text{H}_2\text{O} + \text{CO}_2$. While the tip of the NMR sample was being held at 525 K, a clear liquid (probably H_2O) condensed at the cold end of the tube. If this narrow line is indeed physically adsorbed CO_2 , cooling the sample to 80 K should condense the CO_2 and the ^{13}C NMR spectrum would broaden to the anisotropic chemical shift powder pattern ($\sigma_{11} = \sigma_{22} = \sim 100 \text{ ppm}$, $\sigma_{33} = \sim 175 \text{ ppm}$) (2). However, the broadened lineshape in Figure 4 is not a powder pattern. Rather, it is the combination of two

Lorentzian lineshapes, a narrow peak centered at -58 ppm and a broad line centered at -177 ppm. The relative intensities of the two peaks is 25% narrow and 75% broad line. Thus, the narrow NMR line at 300 K may be physically adsorbed CO_2 , or result of rapid interconversion between two surface states with NMR centers of mass of -58 ppm and -177 ppm. The weak intensity of the line at 300 K suggests that it is physically adsorbed CO_2 . The centers of mass of the two lines at 80 K may be used to propose possible surface species. In general, compounds with carbon-oxygen single bonds, $\text{R}_3\text{C-OR}$ range from -64 to -92 ppm (1). Compounds with aryl C-O groups range from -150 to -176 ppm and carboxylic acids RCOOH may vary from -166 to -182 ppm (1).

DISCUSSION

A. Desorption and Re-Adsorption Spectra

The differences in the infrared and NMR sample sizes and geometries could account for some, but not all, of the apparent discrepancies between the infrared and NMR spectra after prolonged evacuation. The infrared sample is a very thin crust about 1 mm thick, whereas the NMR plug in the bottom of the NMR tube is a cylinder 13 mm long and about 8.5 mm in diameter. Thus, the equilibrium pressure inside the NMR plug pores may be greater than the measured pressure of 3×10^{-7} Torr. However, it has been shown that reducing the pressure from 50 Torr to about 0.01 Torr results in more than a 15% loss in the infrared spectrum, as seen in Figures 2 and 5 of chapter II of this thesis. Thus, artifacts due to differences in sample geometries can account for the discrepancy between the amounts lost from the infrared and NMR spectra only if the pressure within the Al_2O_3 pores of the NMR plug are on the order of 0.01 Torr. However, since the sample is about 80% voids, as determined from the

bulk density, and the mean pore diameter is about 550 Å, a pressure gradient of 0.01 Torr to 3×10^{-7} Torr is inconceivable.

At least two models may be proposed to explain the fact that upon desorption, the infrared spectral intensity decreased by 85% and the ^{13}C NMR intensity decreased by only 15%. If one assumes that the infrared molar absorbances for a specific surface state are uniform throughout the sample, the data suggest that the infrared spectroscopy is observing only about 20% of the surface species. That is, there exists on the surface a state that comprises 80% of the surface ^{13}C that does not desorb upon extended evacuation. Thus the desorption of 85% of the 20% of the sites observed by infrared results in about 15% loss of the total surface species, as observed by the ^{13}C NMR. The most likely possibility for this infrared-unobserved surface state would be a surface carbide formed by the dissociation of CO at a Rh site. It has recently been proposed that the Rh^0 must be first oxidized by the dissociation of CO before it may adsorb any undissociated CO (3). However, such an interpretation has two problems. First, the ^{13}C NMR experiments in chapter V have assigned all of the NMR intensity to infrared-observed species. No new surface states were observed. Second, one would expect that such a carbide species would not readily exchange with CO(g) . However, as seen in chapter V, 33% of the surface species exchanged at 200 K. Further exchange studies at 295 K have shown that in one hour, all but about 5% of the $^{13}\text{CO(ads)}$ is exchanged with $^{12}\text{CO(g)}$, as measured with ^{13}C NMR spin counting. Thus, the existence of a carbide species seems unlikely.

A second model for the desorption results suggests that for each surface CO species, there exists a distribution of infrared molar

absorbance coefficients. Thus, if the extended evacuation of the surface removed selectively the species with the stronger infrared absorbances, the decrease in the infrared spectrum would be artificially enhanced. It has been demonstrated recently that as the loading of Rh on Al_2O_3 is increased from 0.1% to 10%, the infrared molar absorbances of the dicarbonyl species decreases by about a factor of 3 (4). To explain the discrepancy between the infrared and NMR spectra reported here, the molar infrared absorbances would have to vary by over one order of magnitude.

Further analysis with the NMR technique, such as measuring the T_1 distribution after heating, or using magic angle sample spinning to search for unknown species, should resolve this question.

B. Elevated Temperatures Experiments

The results of heating the 2.2% Rh on Al_2O_3 substrate to 425 K in the presence of about 50 Torr can also be explained by the distribution of infrared molar absorbances, though by no means is this currently the only explanation. Heating the catalyst caused the ^{13}C NMR spectrum to increase in intensity. The difference spectrum Figure 3(d-c), centered at -176 ppm, is nearly identical to spectrum 5(a) of chapter V of this thesis, which was assigned to ^{13}CO adsorbed on isolated Rh atoms as dicarbonyls. Thus, the ^{13}C NMR data suggest that the heating caused the migration of Rh atoms from the Rh rafts which then formed isolated Rh dicarbonyl species. However, at the same time, the infrared spectrum intensity of the dicarbonyl bands decreased. It is therefore proposed that heating the sample to 425 K in the presence of CO(g) caused the nature of the isolated site to change, thus resulting in reduced infrared molar absorbances. Further studies, such as T_1 measurements and heating

to 425 K in vacuo would test this hypothesis.

The results of heating to 525 K in about 50 Torr of ^{13}CO are the most difficult to explain. Presently, it seems that the heating caused the chemically adsorbed CO to react, thus forming physically adsorbed CO_2 . However, upon cooling the sample to 80 K, the CO_2 adsorbs on the Rh on Al_2O_3 substrate in a state that is rapidly interconverting between two forms, reflected by the two Lorentzian lines in the ^{13}C NMR spectrum at -58 and -177 ppm, with a center of mass at -147 ppm. This interconversion may involve interactions with local hydroxyl groups of the Al_2O_3 . Further studies, with both NMR and infrared techniques at cryogenic temperatures with $^{13}\text{CO}_2$, should resolve this question.

CONCLUSIONS

The results of NMR and infrared investigation of desorption and treatment at elevated temperatures, when considered separately, yield incomplete or erroneous conclusions. However, the combined results may be analyzed to suggest a finite number of models which may then be tested.

Though still inconclusive, the data suggest that the infrared molar absorbances of the adsorbed CO may vary by over one order of magnitude. This possibility suggests that infrared studies alone to determine the surface concentrations after various treatments may indicate wrong conclusions, as in the case of heating the sample to 425 K.

ACKNOWLEDGEMENTS

This work was supported in part by the Office of Naval Research under contract N00014-75-C0960. I wish to thank Professor George R. Rossman for the use of the infrared spectrometer and Dr. John T. Yates, Jr. for

suggestions and discussions of these results.

References

1. J. B. Stothers, Carbon-13 NMR Spectroscopy, (Academic Press, New York, 1972).
2. These values are estimated from the chemical shift of CS_2 ; $\sigma_{11} = \sigma_{22} = -119$ ppm, $\sigma_{33} = -195$ ppm, $\sigma_{\text{ave}} = -144$ ppm; A. Pines, W.K. Rhim, J.S. Waugh, J. Chem. Phys. 54, 5438 (1971).
3. M. Primet, J. Chem. Soc. Faraday Trans. I 74, 2570 (1978).
4. R. R. Cavanagh and J. T. Yates, Jr., private communication.

Figure Captions

Figure 1. Infrared spectra at 295 K of ^{13}CO adsorbed on 2.2% Rh on Al_2O_3 after various treatments. (a) A freshly prepared substrate after exposure to about 50 Torr of ^{13}CO . (b) The same sample, after continuous evacuation at 295 K with an ion pump for about 50 days to 3×10^{-7} Torr. (c) The redevelopment of the spectrum upon re-exposing the evacuated sample to about 50 Torr of ^{13}CO . (d) The same sample, at 295 K, after 3 hours at 425 K in the presence of 50 Torr ^{13}CO .

Figure 2. ^{13}C NMR spectra at 295 K of CO on 2.2% Rh on Al_2O_3 after the same treatments described in Figure 1. A fresh substrate was exposed to about 50 Torr of ^{13}CO (a); evacuated to 3×10^{-7} Torr (b); and then re-exposed to about 50 Torr of ^{13}CO . (c). Spectrum (a-b) is the difference between spectra (a) and (b).

Figure 3. ^{13}C NMR spectra at 295 K of ^{13}CO on 2.2% Rh on Al_2O_3 after warming to 425 K for 3 hours (d) and for 24 hours (e) in the presence of about 50 Torr ^{13}CO . Spectrum (c), from Figure 2, is added for comparison. The two lower spectra are the differences observed after warming.

Figure 4. ^{13}C NMR spectra at 300 K and 80 K of a 2.2% Rh on Al_2O_3 substrate after 24 hours at 525 K in the presence of about 50 Torr of ^{13}CO . The insert in the upper corner is an expansion of the peak at 300 K.

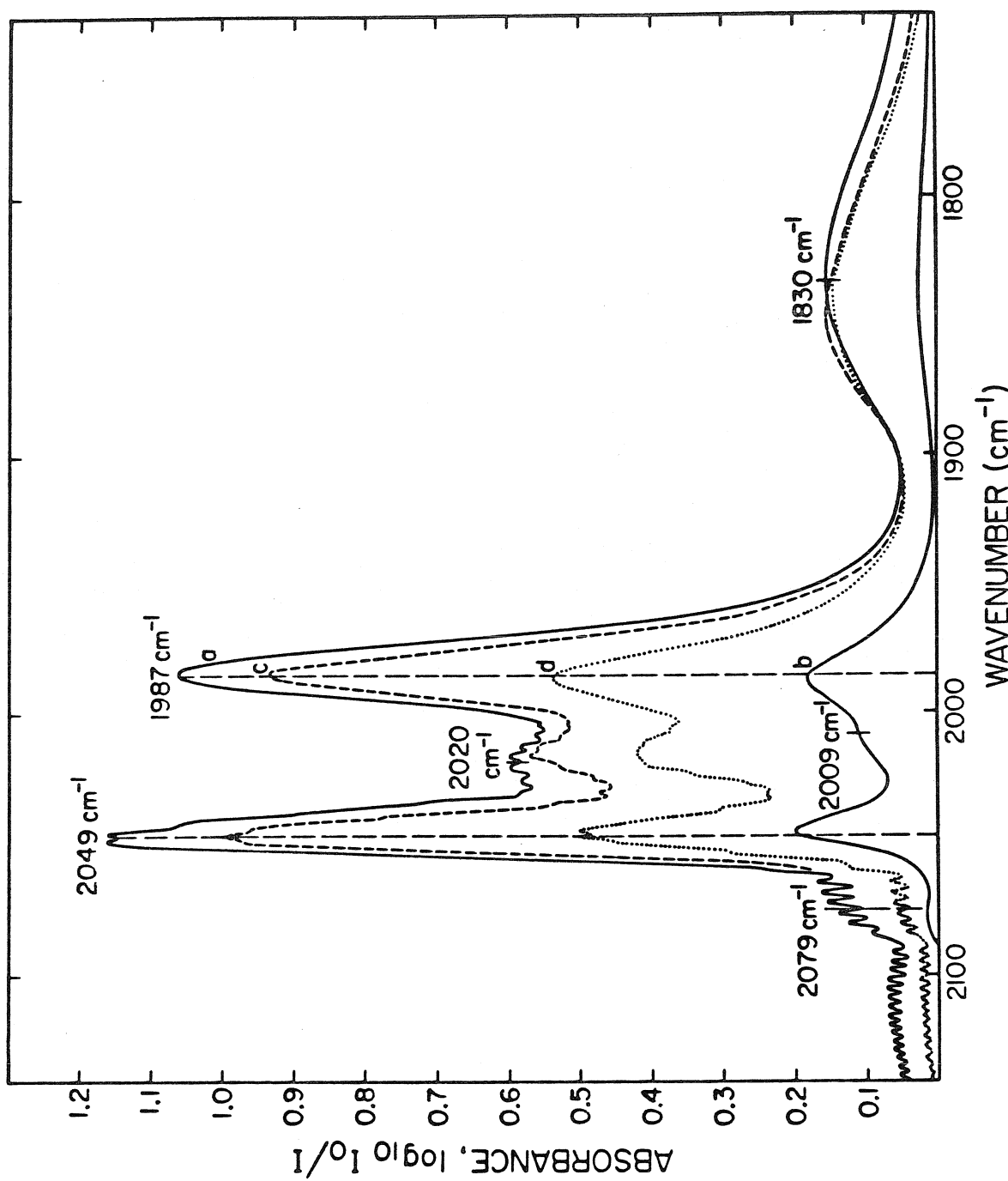


Figure 1.

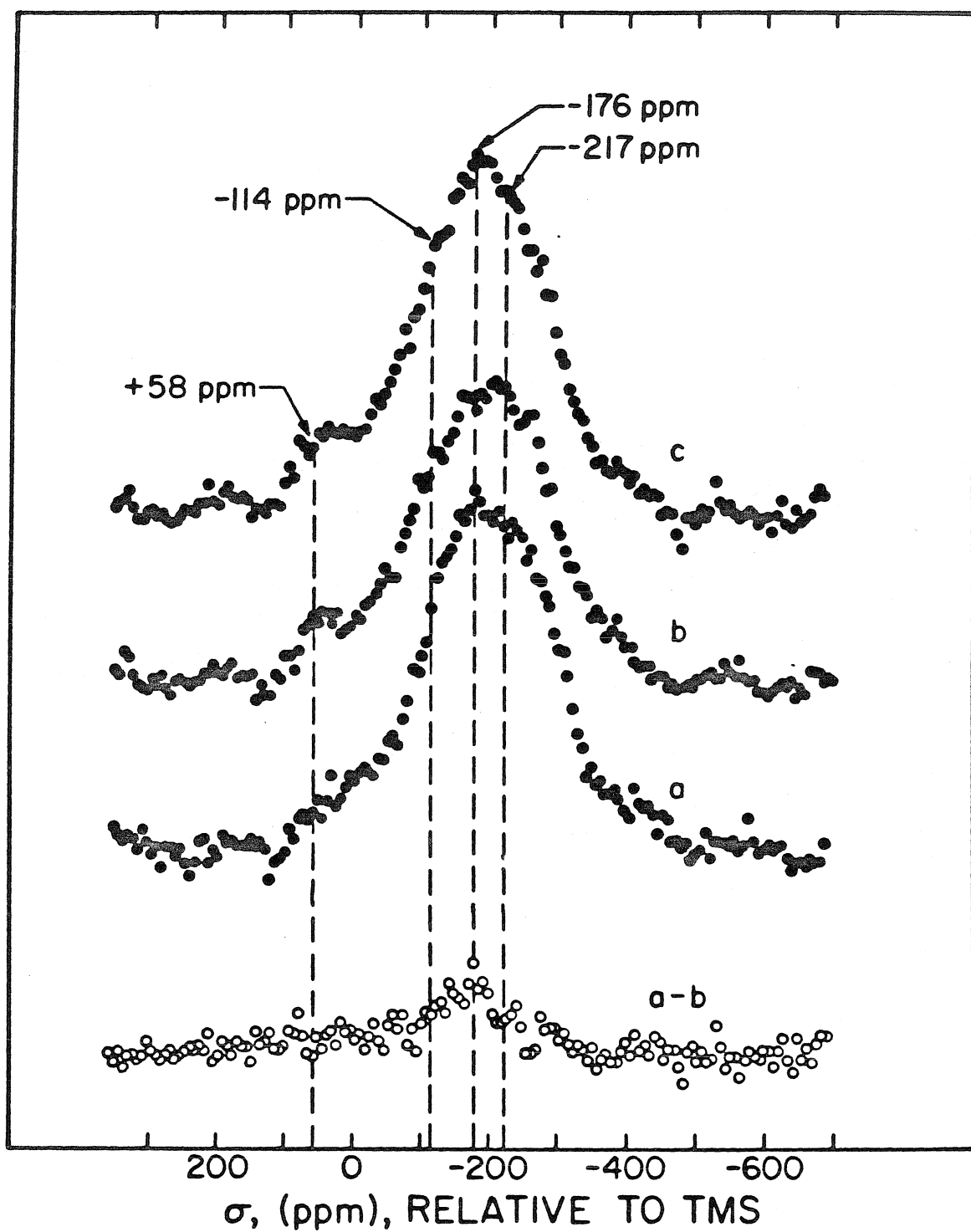


Figure 2.

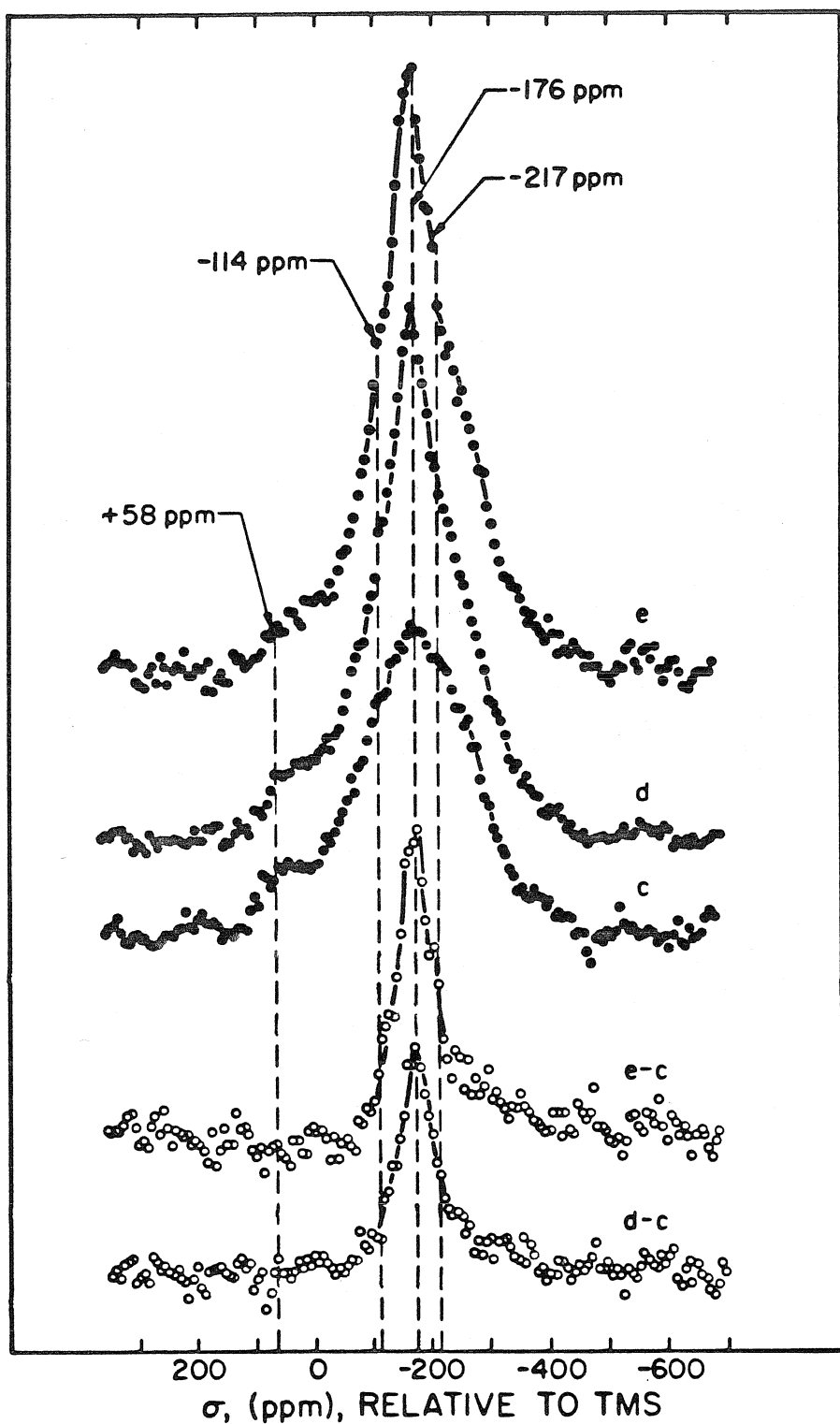


Figure 3.

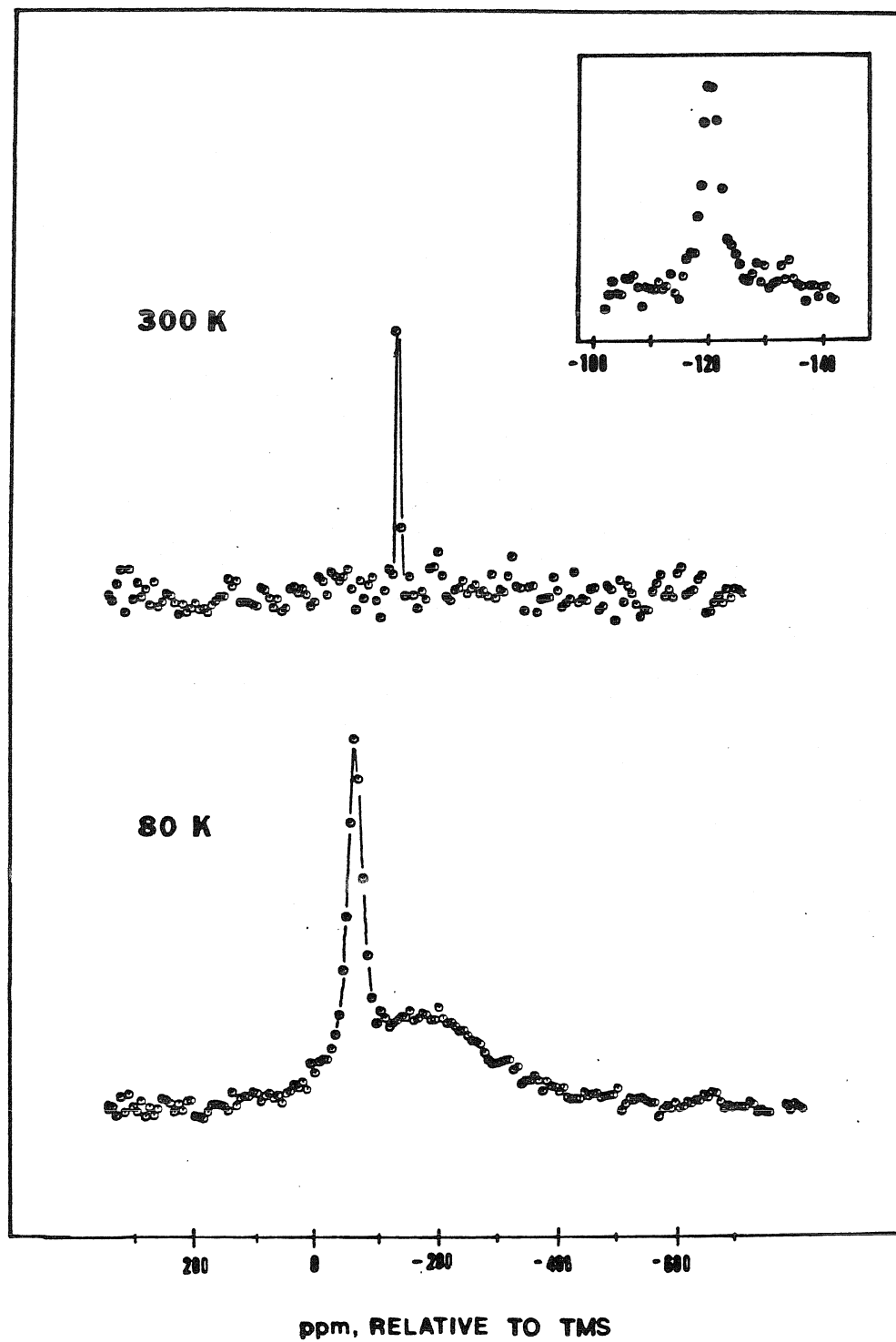


Figure 4.